Effect of Centrifugal Stiffening on Natural Frequencies of Aircraft Wings During Rapid Roll Maneuvers

Revati R. Deshpande

Thesis submitted to the Faculty of the

Virginia Polytechnic Institute and State University

in partial fulfillment of the requirements for the degree of

Masters of Science

in

Aerospace Engineering

Rakesh K. Kapania, Chair

Mayuresh J. Patil

Saad A. Ragab

Dec 11, 2017

Blacksburg, Virginia

Keywords: Centrifugal Stiffening, Rotating beam, Natural Frequencies

Effect of Centrifugal Stiffening on Natural Frequencies of Aircraft Wings During Rapid Roll Maneuvers

Revati R. Deshpande

(ABSTRACT)

The rolling of an aircraft about its fuselage produces centrifugal forces which affect the stiffness of the wings. A number of previous studies explain the effect of centrifugal stiffening in rotating beams and consequently on the frequencies of the beam. Multiple cases of the rotating beam are explored in this thesis to investigate effects of mass distribution and boundary conditions on the frequencies of centrifugally stiffened beams. It is found that for a uniform beam with all degrees of freedom free on both ends, the rigid modes of the beam are affected and are no longer zero when it is stiffened from centrifugal forces. This thesis aims to set up a model to investigate the stiffening effects using the mAEWing2 aircraft. A preliminary analysis is done for the mAEWing2 aircraft and the roll rate, control surface deflection and angle of attack are identified as the parameters to be studied. For a given angle of attack and control surface deflection, the centrifugal forces in the aircraft in steady roll are determined using trim analysis. These are used to pre-stress the model for modal analysis. It is found that in mAEWing2 aircraft in steady roll maneuvers, the centrifugal stiffening effect on the natural frequencies is not significant. It emphasizes the need to conduct a sensitivity analysis to include centrifugal stiffening in the dynamic analysis while designing an aircraft. This, along with some de-stiffening due to gravity loads might be important for the future N+3 aircraft with their high aspect ratio large wingspans.

Effect of Centrifugal Stiffening on Natural Frequencies of Aircraft Wings During Rapid Roll Maneuvers

Revati R. Deshpande

(GENERAL AUDIENCE ABSTRACT)

Structural analysis is mainly concerned with determining the behavior of a structure when subjected to a disturbance. The natural response of a structure to some disturbance is termed as free vibration of the structure. The term vibration describes repetitive motion that can be observed in a structure and is influenced by its material and structural properties. These vibrations may cause fatigue in the structure and the performance of the structure may be adversely affected. Consequently it becomes necessary to study and eliminate these vibrations.

The vibration characteristics of a system are described by its natural frequencies and mode shapes. Natural frequencies of a structure are the frequencies at which the structure naturally tends to vibrate if it is subjected to a disturbance. The deformed shape of the structure vibrating at one of its specific natural frequencies of vibration is termed its normal mode shape.

In the case of a rotating beam, the centrifugal force acts axially along the length of the beam. When the rotating beam deflects upwards, the centrifugal force creates a downward bending moment, reducing its net deflection. The ratio of force to displacement increases, increasing the stiffness of the rotating beam. This effect is called the stiffening effect.

There is a large volume of literature that presents the effect of stiffening on the natural frequencies of a rotating beam model, for various boundary conditions. Such a stiffening analysis has also been done for the blades of a turbine and turbo fans. In addition, there are models available for analyzing the aerodynamic model of an aircraft in roll, considering stability derivatives of the aircraft. However, there are gaps in the available literature in analyzing an aircraft in roll from the perspective of structural analysis. The rolling of an aircraft about its fuselage produces centrifugal forces which affect the stiffness of the wings.

A number of previous studies explain the effect of centrifugal stiffening in rotating beams and consequently on the frequencies of the beam. Multiple cases of the rotating beam are explored in this thesis to investigate effects of mass distribution and boundary conditions on the frequencies of centrifugally stiffened beams. It is found that for a uniform beam with all degrees of freedom free on both ends, the rigid modes of the beam are affected and are no longer zero when it is stiffened from centrifugal forces. This further motivates the need for investigating the effect of centrifugal stiffening in spinning spacecraft and aircraft in rapid roll maneuvers.

This thesis further aims to set up a model to investigate the stiffening effects using the mAEWing2 aircraft. A preliminary analysis is done for the mAEWing2 aircraft and the roll rate, control surface deflection and angle of attack are identified as the parameters to be studied. For a given angle of attack and control surface deflection, the centrifugal forces in the aircraft in steady roll are determined using trim analysis. These are used to pre-stress the model for modal analysis. It is found that in the mAEWing2 aircraft in steady roll maneuvers the stiffening effect on the frequencies is not significant. It emphasizes the need to conduct a sensitivity analysis to include centrifugal stiffening in the dynamic analysis while designing an aircraft. This, along with some de-stiffening due to gravity loads might

be important for the future N+3 aircraft with their high aspect ratio large wingspans.

Acknowledgments

I would like to thank Dr. Kapania for his guidance and advice during the development of this thesis. His continuous support and encouragement have been invaluable. I would also like to thank Dr. Patil and Dr. Ragab for being on my committee.

I would like to thank Dr. Davide, Dr. Jrad and Dr. Zhao for their valuable opinions in this work and for always being available to discuss their insights.

I would also like to take this opportunity to thank all my friends who stood by me and supported me through my graduate studies.

Lastly, I would like to thank my parents and my sister for always being a strong support and always encouraging me in all my endeavors.

Contents

List of Figures

List of Tables

List of Abbreviations

α_i	Southwell's coefficient
η	Non-dimensional angular speed
Ω	Angular speed of rotation
ω_i	Natural frequency of the ith mode
ω_{nr}	Frequency of the non-rotating beam
ϕ_j	amplitude
ρ	Material density of the beam
$_a$	Structural points
$_k$	Aerodynamic points
$_x$	Extra aerodynamic points
A	Cross sectional area
A_{jj}	Aerodynamic influence co-efficient matrix
D_{jk}	Real part of differentiation matrix
E	Modulus of elasticity
F	Generalized forces
I	Area moment of inertia

K	Stiffness matrix
K_{aa}	Structural stiffness matrix
K_D	Differential Stiffness matrix
L	Length of the beam
M	Mass matrix
m	mass
M_{aa}	Structural mass matrix
P	Centrifugal force
P_a	Vector of applied loads
P_k	Forces at aerodynamic grid points
q	Flight dynamic pressure
Q_{aa}	Aerodynamic influence co-efficient matrix in aerodynamic degrees of freedom
Q_{ax}	Forces at structural grid points due to unit deflections at aerodynamic grid points
R	Radius of the wheel
S_{kj}	Integration matrix
t	time
u	Displacements
u_k	Displacement of aerodynamic grid point
V	Free stream velocity

V Volume

W External work potential

w Bending deflection in transverse direction

W^c Virtual work rate of centrifugal force

owTEL1 Outermost Trailing Edge Control Surface on the Left Wing

owTEL2 Second Trailing Edge Control Surface on the Left Wing

owTEL3 Third Trailing Edge Control Surface on the Left Wing

owTEL4 Fourth Trailing Edge Control Surface on the Left Wing

owTER1 Fourth Trailing Edge Control Surface on the Right Wing

owTER2 Third Trailing Edge Control Surface on the Right Wing

owTER3 Second Trailing Edge Control Surface on the Right Wing

owTER4 Outermost Trailing Edge Control Surface on the Right Wing

F-F implies the free free boundary condition

C-F implies the clamped free boundary condition

SWBM is Symmetric Wing Bending Mode

AWBM is Anti-symmetric Wing Bending Mode

SWTM is Symmetric Wing Torsion Mode

AWTM is Anti-symmetric Wing Torsion Mode

CWBTM is Coupled Wing Bending Torsion Mode

Chapter 1

Introduction

With the boom in the demand for affordable air transportation, design of efficient aircraft has become a necessity. Modern aircraft are designed to be highly maneuverable in order to achieve high-performance objectives including low fuel consumption, making them more efficient. Towards this goal, designers have been incorporating thin, large-aspect-ratio wings in the design process.

Aircraft design concepts that take advantage of wing flexibility for improved maneuverability include deflection of the left and right wing control surfaces to produce an aerodynamic moment. Depending on whether the control surfaces are deflected in the same or in the opposite direction, they produce pitching and rolling moments respectively. Structural deflections of lifting surfaces interact with aerodynamic forces to create aeroelastic coupling that can result in fatigue [24]. Aeroelasticity studies the interaction between aerodynamic and structural forces [13]. This interaction in itself explains the need to analyze the stiffening effect during roll maneuvers.

The following two figures illustrate instances where centrifugal stiffening may be expected. The first figure, Figure 1.1a shows Airbus A380 in a coordinated roll and coupled yaw maneuver while executing a right turn. The next figure, Figure 1.1b shows the blades of a wind turbine that are designed by considering the design frequencies that reflect the effect

of centrifugal stiffening.

(a) Airbus A380 Executing a Right Turn

(b) Wind Turbines

When an aircraft banks during a turn, executes a roll maneuver or meets turbulence, the aircraft experiences centrifugal forces. The centrifugal force along with axial component of lift and gravity force, all affect the stiffness of the aircraft wings. These effects are most dominant on the natural frequencies of the aircraft. Thus, this structural analysis reduces to the classical problem of studying the effect of stiffening on natural frequencies of a rotating beam.

The vibrational analysis of a rotating beam is an important subject of study in structural engineering. There are many engineering examples which can be idealized as rotating beams. These include turbine blades, turbo-engine fan blades and helicopter blades. For accurate analysis of structures in their vibrational characteristics *i.e.* natural frequencies and mode shapes, these characteristics should be well identified. When compared to the vibrational characteristics of a non-rotating beam, those of a rotating beam vary significantly. The variation results from the increased stiffness induced from the tensile nature of the axial forces coming from the rotation [39].

As mentioned previously, the computation of natural frequencies and mode shapes are important elements of vibration analysis of rotating beams. Several research groups have addressed this problem using different experimental and analytical approaches [2, 12, 23, 31,

34, 39]. The literature on this topic is vast and continuously expanding. Using traditional methods that are based on the derivation of differential equations and application of appropriate boundary conditions, the free vibration characteristics of uniform rotating beams have been studied by a number of researchers. Some of these researchers have emphasized the practical importance of these studies. Other researchers have restricted themselves solely to rotating cantilever beams since turbine blades and propeller blades are often idealized as rotating cantilever beams [2].

During the historical development of this problem, a number of solution techniques with varying degrees of applicability have been presented. The refinement of formulation techniques led to the development of many studies on the vibration of rotating radial beams having different root offset configurations. This has been set in a variety of contexts ranging from turbo-machinery blades and helicopter blades to gyroscopic instruments and flexible appendages on spinning spacecraft to name a few. Numerous investigators have studied such structures and a variety of methods are proposed [10].

The most simplified representation of a rotating beam is a one-dimensional Euler-Bernoulli beam model. A uniform rotating beam of a doubly symmetric cross section is a special case of the rotating beam where the flapping, *i.e.* out-of-plane, and lead-lagging, *i.e.* in-plane frequencies, are uncoupled. Owing to the centrifugal stiffening effect due to centrifugal tension a change is expected in the natural frequencies [23]. The stiffening effect of centrifugal force on the fundamental frequency is seen more prominently than in the successive modes [33].

The dynamic behavior of a rotating beam is of practical interest since it is possible to develop such a model for several engineering structures. Some examples are steam, and gas

turbine blades, helicopter blades and wind turbine blades. Sometimes tip masses are added to such rotating structures to enhance their functional properties [3]. At times, rotating beams are directly used as simple models for propellers, turbine blades and satellite booms [20]. Hence, the determination of the dynamic response of rotating beams *i.e.* mode shapes and natural frequencies is an important prerequisite for the design of helicopter and turbomachinery blades.

Several studies have been directed to the evaluation of natural frequencies of rotating structural elements such as space frames, windmill rotors, aircraft propellers, turbine blades etc.

1.1 Objective

With this background, we investigate whether the effect of rolling maneuver will cause a significant centrifugal stiffening in the aircraft wings. If natural frequencies for these stiffened frequencies are determined, direct effects of increasing the roll rate are reflected in the natural frequencies.

This study hopes to understand the effect of centrifugal stiffening on the rolling aircraft. Further, the necessity to include this analysis in the preliminary designing process is evaluated.

With the problem thus defined, the following objectives are outlined for this thesis:

- To study centrifugally stiffened beams and investigate the effect of rotation speed, mass distribution and boundary conditions on the frequencies of centrifugally stiffened beams.

- To investigate centrifugal stiffening in mAEWing2 aircraft during rapid roll maneuvers and its effect on natural frequencies.
- To determine the influence of roll rates on the centrifugal stiffening effect.

1.2 Motivation

Ample amount of literature is available for studying the aerodynamics of an aircraft in maneuvers, however there are some gaps when it comes to analyzing the structural model and vibration response of an aircraft in maneuver [8, 24, 25, 27]. This thesis attempts to build a model that can be used to evaluate the structural stability of an aircraft during roll maneuvers. The model used for analysis is mAEWing2, an aircraft designed and developed as a part of the Performance Adaptive Aeroelastic Wing (PAAW) project.

1.3 Thesis Structure

The development of this thesis is presented through seven chapters. Chapter 1 lays out the background for the thesis and outlines the objectives of this thesis. The need for such a structural analysis is discussed. Chapter 2 discusses the work previously done in the field, including the classical problem of a rotating cantilever beam and its natural frequencies, the roll coupling problem and the stiffening of blades in turbines and helicopter blades. Chapter 3 is dedicated to explaining the theory of centrifugal stiffening and the determining of the natural frequencies of a continuous system, both of which are topics related to the theme of this thesis. Chapter 4 explains the method implemented to achieve the objectives outlined based on literature review and theory. Chapter 5 explains the models used for analysis in this study, a rotating beam model and the mAEWing2 model. Chapter 6 discusses the results

obtained from this analysis and Chapter 7 summarizes the work done in this thesis. The Figure 1.2 gives an overview of the work presented in all seven chapters.

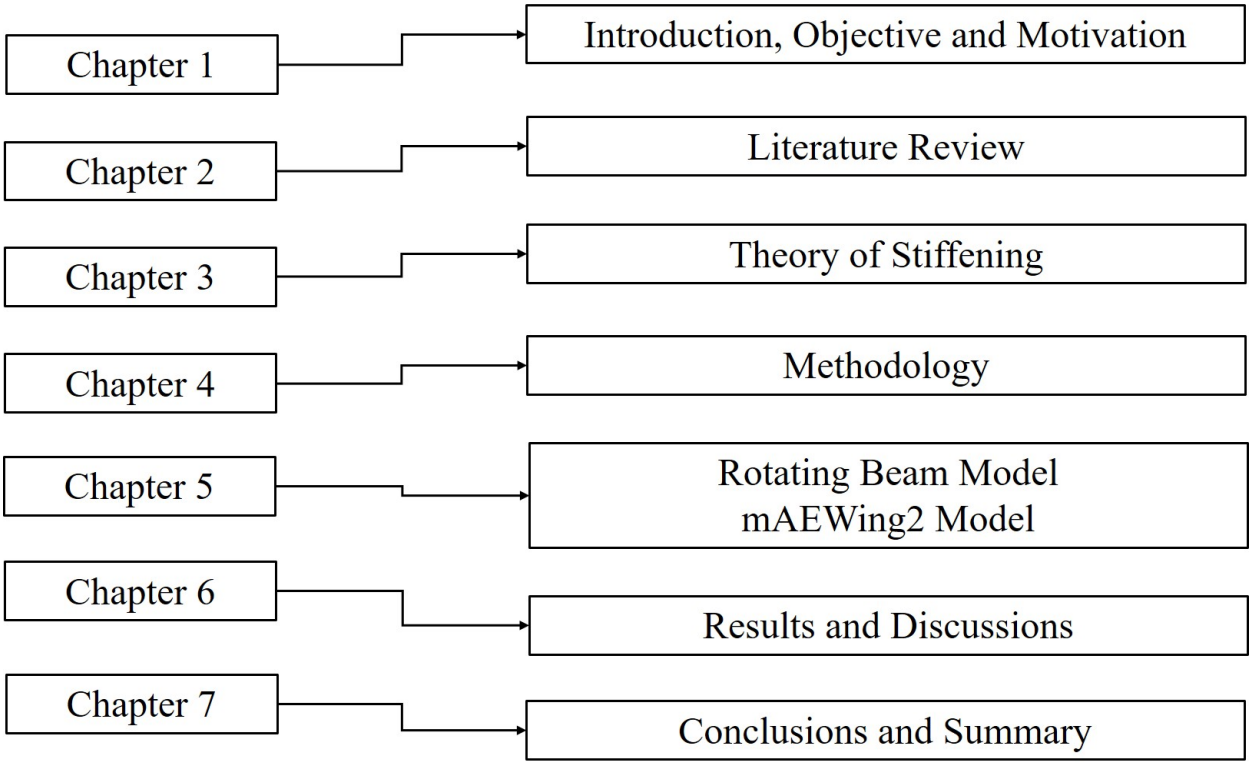

Figure 1.2: An Overview of the Chapters in this Thesis

Chapter 2

Review of Literature

The problem of rotating beams is a classical problem and there has been a significant amount of work done on determining the effect of centrifugal stiffening on the natural frequencies of rotating beams. In addition, significant amount of work has also been done to understand the nature of roll maneuvers of an aircraft under diverse flight conditions. However, the gaps between the aerodynamics of these maneuvers and the stiffening of the wings during these maneuvers needs to be bridged. In achieving the objectives of this thesis of modeling the aircraft wing to study the centrifugal stiffening produced and to study the influence of control parameters like angle of attack, control surface deflection on these effects, the literature already available has been very instrumental. The literature review is also presented in parts, viz:

- Rotating Beams
- Stiffening in Turbine Blades
- The Roll Maneuver

2.1 Rotating Beams

One of the first known work on rotating beams was presented by Southwell and Gough [34]. The natural frequencies determined from the Southwell equation given in this paper

have been used as benchmark results for most successive works. Their work was based on Rayleigh's theorem. This work was further extended by Liebers [19] and Theodorsen [36]. They predicted the natural frequencies of a rotating cantilever beam but modifications were required in order to plot the mode shapes. Schilhansl [31] used the linear partial differential equation governing the bending motions of the rotating beam and solved them using the Ritz method to obtain equations for mode shapes and natural frequencies.

A few years later Sharma [33] discussed the stiffening effect of centrifugal force on the fundamental frequency of rotating slender beams under the effect of coupled aerodynamic effects. This work discussed slender beam analysis of a turbine blade. The coupling between the elastic axis and the line of center of gravity was taken into account and the assumption that the elastic axis and the line of centers coincide was removed. The coupling between bending and torsional deflections was also taken into account. The Rayleigh's Quotient method was used to derive the solution of the governing equation. This work further studied the effect of hub radius and blade length for a given rotation speed. They concluded that for a given speed the fundamental frequency and the highest critical speed are affected by the blade length.

Hibbit [11] explained the effect of follower forces by demonstrating that the changes in stiffness matrix were observed in the form of load matrix. The follower forces discussed in this work included surface pressure, centrifugal load, frictional drag and cable loads. Fox and Burdess [7] used the Galerkin procedure to solve the governing differential equation of rotating beams and studied the out-of-plane vibrations of the rotating beam problem. Hodges and Rutkowski [14] solved the governing differential equation of a rotating beam using finite element method of variable order. To overcome the computational disadvantages in using the finite element method of variable order Hodges [12] suggested the use of orthogonal shape

functions. Wright et al. [38] presented an analytical solution to the mode shape equation obtained from the governing differential equation for cantilever beam attached to a rotating hub.

Bhat [3] predicted the natural frequencies and mode shapes of a rotating beam with tip mass by using beam characteristic orthogonal polynomials as the basis functions in the Rayleigh Ritz method. These orthogonal polynomials were generated using the Gram-Schimdt process. The advantage of using orthogonal polynomials over arbitrary polynomials was the lack of numerical difficulties while computing higher natural frequencies of any order. However, this work presented only the transverse vibrations of a rotating beam and did not consider the coupling between transverse and in-plane vibrations and the inclusion of shear deformations.

Chandrashekhara et al. [5] presented exact solutions for the free vibrations of symmetrically laminated composite rotating beams. They considered first order shear deformation and rotary inertia in the governing equations of the composite rotating beams. The solution thus obtained was applicable to arbitrary boundary conditions.

Later, Naguleswaran [23] described the lateral vibrations of an Euler-Bernoulli beam attached radially to the outside of a rotating hub. The principal axis of the beam was assumed to be parallel to the axis of rotation because of which the in-plane and the out-of-plane vibrations were uncoupled. The equations of motion were derived assuming equilibrium of the forces and moments as opposed to using the energy method. To solve the equations of motion, the Frobenius method was used. The general solution was expressed as the superposition of four linearly independent polynomials. The roots of the equation were determined by a numerical procedure based on the initial trial and error method. They concluded

that it was possible to obtain the in-plane frequencies of a rotating beam from out-of-plane frequencies of the rotating beam when the rotation speed was known.

Yoo and Shin [39] derived the equations of motion of a rotating beam based on a new dynamic modeling method for considering stretching and bending, coupled through gyroscopic terms. They used the Rayleigh-Ritz method to approximate the hybrid set of variables. Using the quadratic form of strain energy, they obtained the generalized inertia forces. By linearizing the generalized inertia forces, the equations of motion were derived. They concluded that the coupling effect became negligible as the slenderness ratio increased. They also showed the influence of these coupling terms on the eigenvalues and the effect of high rotating speeds on the mode shapes.

Hashemi et al. [10] proposed a new dynamic finite element formulation using trigonometric shape functions which was used to develop the frequency dependent element stiffness matrix which has both mass and stiffness properties. They used a bisection method based on Sturm sequence root counting technique to find the flexural natural frequencies.

Banerjee [2] started from the governing equations for cantilever beam rotating with uniform angular velocity and used the Frobenius method (power solution technique) to solve the differential equation and obtain the expressions for the slope, moment and shear force. A power series solution was assumed for the governing differential equation. The dynamic stiffness which related the amplitude of a harmonically varying force to the corresponding displacement was obtained by imposing the boundary conditions for a free-free and clamped-free beam. Substituting the appropriate boundary conditions and writing the force and moment expressions in matrix form resulted in a vector of constants that could be eliminated so that the force-displacement relation gave the dynamic stiffness matrix. The Wittrick-

William algorithm was used to obtain the natural frequencies from the dynamic stiffness matrix. This algorithm did not give the numerical values of the natural frequencies directly, but it gave the number of frequencies existing under the trial natural frequency. By choosing successive trial frequencies and setting the required accuracy, this algorithm helps to bracket any desired natural frequency. This method did not consider the pre-twist of the beam, the coupling between the in-plane and out-of-plane transverse deflections and the coupling between the bending and torsion motions.

Later Lin and Hsiao [20] considered the Timoshenko beam theory instead of the Euler-Bernoulli theory, and used the power series solution to derive the eigenvalue problem for computing natural frequencies of a rotating beam. They also studied the effect of Coriolis forces on a rotating beam and concluded that the effect of Coriolis forces on the natural frequencies of the rotating Timoshenko beam were negligible when the beam is linear elastic and the steady state axial strain is small.

Labuschagne et al. [17] developed three models of cantilever beams. They used the Euler-Bernoulli beam theory for the first model, Timoshenko beam theory for the second model and 2-dimensional elasticity model for the third model. They used natural frequencies for bench-marking, and found that for lower modes, there was very little difference in the solutions i.e. difference between the frequencies of Euler-Bernoulli and Timoshenko beams was within 0.1%.

2.2 Stiffening in Turbine Blades

Park et al. [26] investigated the variations in natural frequencies using a systematic formulation of the turbine blade system. They reduced the complex turbine blade system to a constrained multi-body system with rigid bodies connected through beam elements. With the comparison from results for natural frequencies at different operating speeds, the maximum variation in the natural frequencies from the natural frequency at zero rotation speed was observed. Consequently they proposed an increase in the design natural frequency to reflect these observations.

Li et al. [18] used the Rayleigh Energy Method to derive the equations of motion of the blade including and the axial force. The Figure 2.1 shows a line diagram of the wind turbine blade.

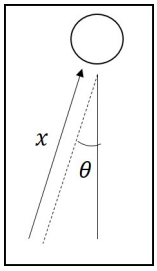

Figure 2.1: Wind Turbine Blade

The centrifugal force in the blade of a turbine rotating with angular speed ω is given by the following equation:

$$T(x) = \frac{1}{2}m\Omega^2(L_B^2 + 2L_BL_R - 2L_RL_x - x^2) \tag{2.1}$$

The gravity component acting axially along the blade varies with Θ, the angle of rotation where $\Theta = \Omega t$ at any time instant t. The component of gravity along the blade is given by

G_{xl} in (2.2)

$$G_{1l} = mg(L_B - x)\cos(\Omega t) \tag{2.2}$$

The net axial forces in the blade under consideration is given in equations (2.3) (**??**) (**??**)

$$N_1(x) = T(x) + G_{1l} \tag{2.3}$$

Using this net axial force to update the stiffness matrix, the frequencies can be calculated using:

$$|\bar{K} - \omega^2 M| = 0 \tag{2.4}$$

where $\bar{K} = K + K_G$

K = stiffness matrix of the blade

K_G = Geometric-stiffness matrix from the axial force

The frequencies calculated using this equation reflect the stiffening.

A centrifugal stiffening co-efficient was introduced to quantitatively study the relation between the centrifugal stiffening effect and the rotating speed. Further, a fundamental frequency correction formula was also suggested.

2.3 The Roll Maneuver Problem

Phillips [27] was one of the first people to work on stability of aircraft under roll maneuvers. He published a NASA technical note in 1948 which is now considered a classic and is still fundamental in the evaluation of the stability of steady rolling motion. Even though the results published were approximate, they are still considered to be a benchmark case for validating different novel models that are built. Phillips [27] work discussed the effects of

rolling on the stability of the aircraft. The work considered an aerodynamic model equivalent of the single degree of freedom system to calculate the pitching and yawing frequencies of a non-rolling and rolling aircraft. The model was allowed longitudinal and directional *i.e.* pitching and yawing motions respectively, and the roll rates were kept constant. The equations of motion were derived for the pitching and yawing motions. The undamped natural frequencies were calculated and expressed as ratios of the pitching and yawing frequencies to the steady rolling frequency. Thus, by changing the roll rate, the effects on the pitching and yawing frequency were analyzed. It is important to note that the frequencies were uncoupled. Though this study provided an in-depth study of the effect on frequencies, it considered the effects only in the aerodynamic environment. There were no structural models used in this study.

Hacker and Oprişiu [8] addressed the gaps in the problem of roll stability. They addressed the inertia-roll coupling cross coupling and the effect of controls that actually produce roll maneuver.

Niedenfuhr [25] addressed the dynamic couplings between rigid and flexible aircraft introduced due to rapid steady roll. They showed that rotating elastic systems exhibit several types of instabilities and sub-harmonic responses.

Based on this literature survey, this work aims to tie all these works together and produce a work that attempts to understand the structural changes that occur due to the stiffening during the roll maneuvers. In order to achieve this, it is envisioned to model the aircraft analogous to the rotating cantilever beam. The following chapter will discuss some key concepts required for this study.

Chapter 3

Theory of Centrifugal Stiffening

While solving the problems of complex structures under different sets of loads, the solution is often governed by ordinary or partial differential equations. A key feature of the approximate methods used to solve these differential equations is to convert the ordinary or partial differential equation into a set of linear or nonlinear algebraic equations which can be reduced to the form $Ku = F$. Here, K is called the stiffness matrix, u is the vector of generalized co-ordinates and F is the vector of generalized forces. The concept of stiffening refers to the change in the stiffness matrix as a result of applied forces and the resulting displacements. To understand the nature of these forces and the implications of the perturbations in stiffness matrix because of these forces, it is necessary to start right from their definitions.

An integral part of the methodology is to work with the natural frequencies of a continuous system which is pre-stressed. The later part of this chapter will deal with determining the natural frequencies of a continuous system.

3.1 Types of Forces

Based on the gradient of the potential energy, forces may be classified as conservative or non-conservative in nature. A system is said to be conservative when both the external

and internal forces are derivable from a potential; the force is equal to the gradient of the potential energy with respect to the generalized variables. Thus, in the case of an elastic system, the internal forces may be derivable from the potential. Depending on the nature of the external loads, the system will then be labeled as conservative or non-conservative: when the external force F can be derived from the external work potential W by differentiating with respect to the state variables,

$$F = \frac{dW}{du_i} \tag{3.1}$$

the system is conservative. Non-conservative forces cannot be derived from the work potential. When the forces depend on the displacements of the body on which they act, they are called follower forces. They occur frequently in the analysis of structures. In most cases consideration of the dependency between the force and the resulting displacement is essential for accurate solutions. Common solution techniques, like eigenvalue problem for dynamic analysis or buckling analysis requires the development of the tangent stiffness matrix as a result of using the principle of virtual work. Using the principle of virtual work results in a modification in the stiffness matrix, and resulting matrix is called the tangent stiffness matrix. The follower forces are known to contribute to the stiffness matrix [11]. This leads us to discuss the stiffness matrix in further details.

3.2 Stiffness Matrix

The stiffness matrix of a system can be decomposed into three components:

1. Elastic stiffness: The elastic stiffness is that stiffness which depends only on the material and the geometry of the structure.

2. Geometric stiffness: The stress stiffness depends on the internal stresses in the struc-

ture. This stiffness is most prominently observed in guitar strings. To change the pitch of the guitar, the tension in the stress is changed, which changes the internal stresses in the string. For a rotating blade, the stress is mostly tension and the stress stiffness increases with increasing revolutions per minute (rpm), with the same effect as increasing the tension in guitar string.

For a given force, $F(u, \lambda)$, where u is the displacement of the structure on which force F acts and λ is some externally prescribed force parameter. Then equation (3.2) gives the stiffness called the geometric stiffness.

$$dF = \frac{\partial F}{\partial u}du + \frac{\partial F}{\partial \lambda}d\lambda \tag{3.2}$$

$$Q = \frac{\partial F}{\partial u} \tag{3.3}$$

Clearly, this is a preload stiffness (it is non-zero only if the force is non-zero) and is relevant only to non-linear analysis or linear analysis of preloaded systems. Thus, one of the most defining feature of the non-conservative force is that it contributes the load stiffness to the tangent stiffness matrix.

3.3 Natural Frequencies of a Continuous System

In a continuous system, the distribution of mass and other properties is considered to be continuous. The governing equation of a beam with Modulus of Elasticity E, and material density ρ is:

$$\frac{\partial^2}{\partial x^2}(EI\frac{\partial^2 w}{\partial x^2}) + m\ddot{w} = 0 \tag{3.4}$$

where x is a point along the length of the beam and w is the transverse deflection.

For constant EI in equation (3.4)

$$EI\frac{\partial^4 w}{\partial x^4} + m\ddot{w} = 0 \tag{3.5}$$

Assume the solution of the nature: $w(x,t) = \bar{w}(x)e^{iwt}$, we get:

$$EI\frac{\partial^4 \bar{w}(x)}{\partial x^4}e^{iwt} - w^2 m\bar{w}(x)e^{iwt} = 0 \tag{3.6}$$

$$EI\frac{\partial^4 \bar{w}(x)}{\partial x^4} - w^2 m\bar{w}(x) = 0 \tag{3.7}$$

The solution to the above differential equation is of the form: $\bar{w}(x) = e^{px}$

Substituting in the equation (3.7)

$$p^4 e^{px} - \frac{m\omega^2}{EI}e^{px} = 0 \implies p^4 = \frac{m\omega^2}{EI} \tag{3.8}$$

If $p^4 = \lambda^4$ then $\lambda = (\frac{m\omega^2}{EI})^{\frac{1}{4}}$ and $p = \lambda, -\lambda, i\lambda, -i\lambda$

The solution of equation (3.7) is given by:

$$w(x) = G_1 e^{\lambda x} + G_2 e^{-\lambda x} + G_3 e^{i\lambda x} + G_4 e^{-i\lambda x} \tag{3.9}$$

$$w(x) = C_1 \sinh(\lambda x) + C_2 \cosh(\lambda x) + C_3 \sin(\lambda x) + C_4 \cos(\lambda x) \tag{3.10}$$

where $G_1, G_2, G_3, G_4, C_1, C_2, C_3, C_4$ are the constants. Hence we need four boundary conditions to find the deflections and the natural frequencies. Since we consider the problem of the rotating cantilever beam, the beam will be fixed at $x = 0$ and free at $x = L$

Boundary conditions: At the fixed end $x = 0$: $w = 0$ and $\partial w(x)/\partial x = 0$

At the free end $x = L$: $EI\partial^2 w/\partial x^2 = 0$ and $EI\partial^3 w/\partial x^3 = 0$

Applying boundary conditions, $w(0) = 0$ and $\partial w(x)/\partial x = 0$, gives $C_2 + C_4 = 0$ and $C_1 + C_3 = 0$

The solution can be rewritten as:

$$w(x) = C_1(\sinh(\lambda x) - \sin(\lambda x)) + C_2(\cosh(\lambda x) - \cos(\lambda x)) \tag{3.11}$$

Applying the other two boundary conditions gives:

$$\begin{bmatrix} \sinh(\lambda L) + \sin(\lambda L) & \cosh(\lambda L) + \cos(\lambda L) \\ \cosh(\lambda L) + \cos(\lambda L) & \sinh(\lambda L) - \sin(\lambda L) \end{bmatrix} \begin{bmatrix} C_1 \\ C_2 \end{bmatrix} = \begin{bmatrix} 0 \\ 0 \end{bmatrix} \tag{3.12}$$

or $1 + \cosh \lambda L \cos \lambda L = 0$

Solving the equation numerically,

$\lambda L = 1.875104, 4.694091$ and 7.48547

Using the second set of boundary conditions,

$$C_2 = -C_1 \frac{\cosh(\lambda L) + \cos(\lambda L)}{\sinh(\lambda L) - \sin(\lambda L)}$$

$$w(x) = C_1[\sinh(\lambda x) - \sin(\lambda x)] - \frac{\cosh(\lambda L) + \cos(\lambda L)}{\sinh(\lambda L) - \sin(\lambda L)}[\cosh(\lambda x) - \cos(\lambda x)]$$

The first three natural frequencies are given by

$\omega_1 = (1.8751)^2\sqrt{\frac{EI}{mL^4}}$

$\omega_2 = (4.6940)^2\sqrt{\frac{EI}{mL^4}}$

$\omega_3 = (7.8547)^2\sqrt{\frac{EI}{mL^4}}$

It is frequently required to find the vibration characteristics of a small vibrations of rotating machinery. For those parts of the machinery which are rotating, the centrifugal load acts as the preload. The eigenvalue analysis of the small vibrations about this preloaded state should include the centrifugal load stiffness for accurate predictions. The centrifugal stiffness is easy to develop [11]. The axis of rotation is defined a point with co-ordinates P_i with unit vector along the axis. Then the virtual work rate of the centrifugal load is

$$\delta W^c = \int_V f_i \delta u_i dV \tag{3.13}$$

$$= \int_V \rho\Omega^2((x_i - P_i) - (x_j - P_j)a_j a_i)\delta u_i dV$$

where ρ is the mass density of the material

Ω is the angular speed of the machine

x_i is the current position of a material point.

For a rotating blade, the load stiffness can either increase or decrease the frequencies depending on how the blade deforms. Two cases are discussed below:

Case I: Assume the rotor is rotating in the horizontal plane. The deflection of the beam is vertical. The centrifugal force is still acting in the horizontal direction. The blade tends to deflect upwards when rotating. Thus, the centrifugal force starts acting at a different height above the hub of the blade. This creates a bending moment which tries to bend the blade downwards i.e. increasing the stiffness of the blade.

Case II: Assume the rotor is rotating in the horizontal plane. The beam now moves in the tangential direction but stays in the same horizontal plane. The centrifugal force is now acting radially away from the blade of the hub, and that force is trying to bend the blade

further downwards in the tangential direction. i.e. it decreases the stiffness of the blade. One reason for the blade to bend tangentially would be when the rotor is accelerating or decelerating, and the blades either lag behind or get in front of the position of the hub. The two cases discuss about the geomeric stiffness due to centrifugal force.

The literature review answers most of the questions about how the centrifugal force acting axially affects the lagging frequencies proportional to the square of the rotating speed. However, it generates an equal number of questions about the implications of these results. There are a large number of systems with rotating parts which are reduced to a beam for structural analysis. Depending on the application and the force systems, it is possible that the rotation of the beam does not oppose its bending, similar to Case II and instead enhances it. In this case, the centrifugal force will further reduce the frequencies, instead of increasing them, and pose a greater threat in terms of structural stability (if they are underestimated). In the typical case of a rotating beam, it is seen that the natural frequencies of a rotating cantilever beam are higher as compared to that of the non - rotating cantilever beam.

In either case, it is important to understand the exact implication of what stiffening does to a beam. The stress stiffness and load stiffness, both, not only depend on the speed of rotation, but are also proportional to the square of the speed of rotation. These effects can be large. In the case of a long blade with a rigid hub, the potential decrease in stiffness is more significant. For such a system with long blades and rigid hub of rotors, it is very common for the vibration frequency of different vibration modes to increase, decrease or stay the same as the RPM varies.

Consideration of gravity and aerodynamic forces are also equally essential in the calculations of these frequencies. But these are all theories with respect to analysis of turbine

blades, or small rotating parts of any machinery.

Based on this understanding of the theory of centrifugal stiffening, there has been a lot of work done to understand the vibrations of blades of helicopters and turbines [18, 26, 32]. However, the problem of a rolling aircraft has never been looked at in the same light. A lot of research has been done on the stability analysis of aircraft [8, 24, 25, 27]. But there is a gap in the work done on the vibrational analysis of an aircraft in roll maneuver. When an aircraft banks during roll, or executing a turn there is a difference in the lift forces on either wing of the aircraft and it can be considered analogous to a cantilever beam rotating about a rigid hub i.e. fuselage, albeit with lower rotational speeds. A centrifugal stiffening effect, similar to what is seen in a rotating beam can be expected.

Chapter 4

Methodology

With the background of the problem established, understanding of the theory, and the objectives clearly outlined, a three part methodology is proposed to solve the problem and achieve the objectives. The objectives of this thesis are reiterated here.

- To study centrifugally stiffened beams and investigate the effect of rotation speed, mass distribution and boundary conditions on the frequencies of centrifugally stiffened beams.
- To investigate centrifugal stiffening in mAEWing2 aircraft during rapid roll maneuvers and its effect on natural frequencies.
- To determine the influence of roll rates on the centrifugal stiffening effect.

It is hoped that the proposed method remains coherent with the objectives as well as the philosophy which helped develop the problem in the first place, that of research through development. With the understanding that an axial force will always affect the natural frequencies of a beam, it was proposed to make the rotating cantilever beam model as the starting point for the present work. This thesis further attempts to extend this model by introducing geometric non-linearities and investigate the possibility of observing a similar effect in aircraft, when the aircraft banks during a turn, experiences roll during turbulence or attempts a rapid roll maneuver. The aircraft under consideration is the mAEWing2 aircraft.

Thus, the rolling of the aircraft maybe considered analogous to the rotating of the cantilever beam with the fuselage acting as the hub.

For smaller and less complex systems, it is easy to observe and quantify the effects of non-conservative loads and their contribution in the form geometric stiffness to the tangent stiffness matrix. However, for larger and more complex systems, it is often required to use software - commercial or in house developed - to observe these effects. In this report, to study the effects of the non-conservative forces on the stiffness of the wings of the mAEWing2 aircraft during roll, the natural frequencies will be determined using the modified stiffness matrix and compared to the natural frequencies of the unstressed aircraft.

4.1 Method

The work has been divided into three parts. The flowchart in Figure 4.1 explains the four parts of this work, and shows how they help achieve the objectives outlined at the outset of this work.

4.1.1 Part 1: Literature Review

This is the first part of the thesis which includes a review of the work that has been done in studying the rotating beam problem and the different methods used to solve the problem. It includes studying how the problem is developed and semi-analytical solutions used to solve the problem.

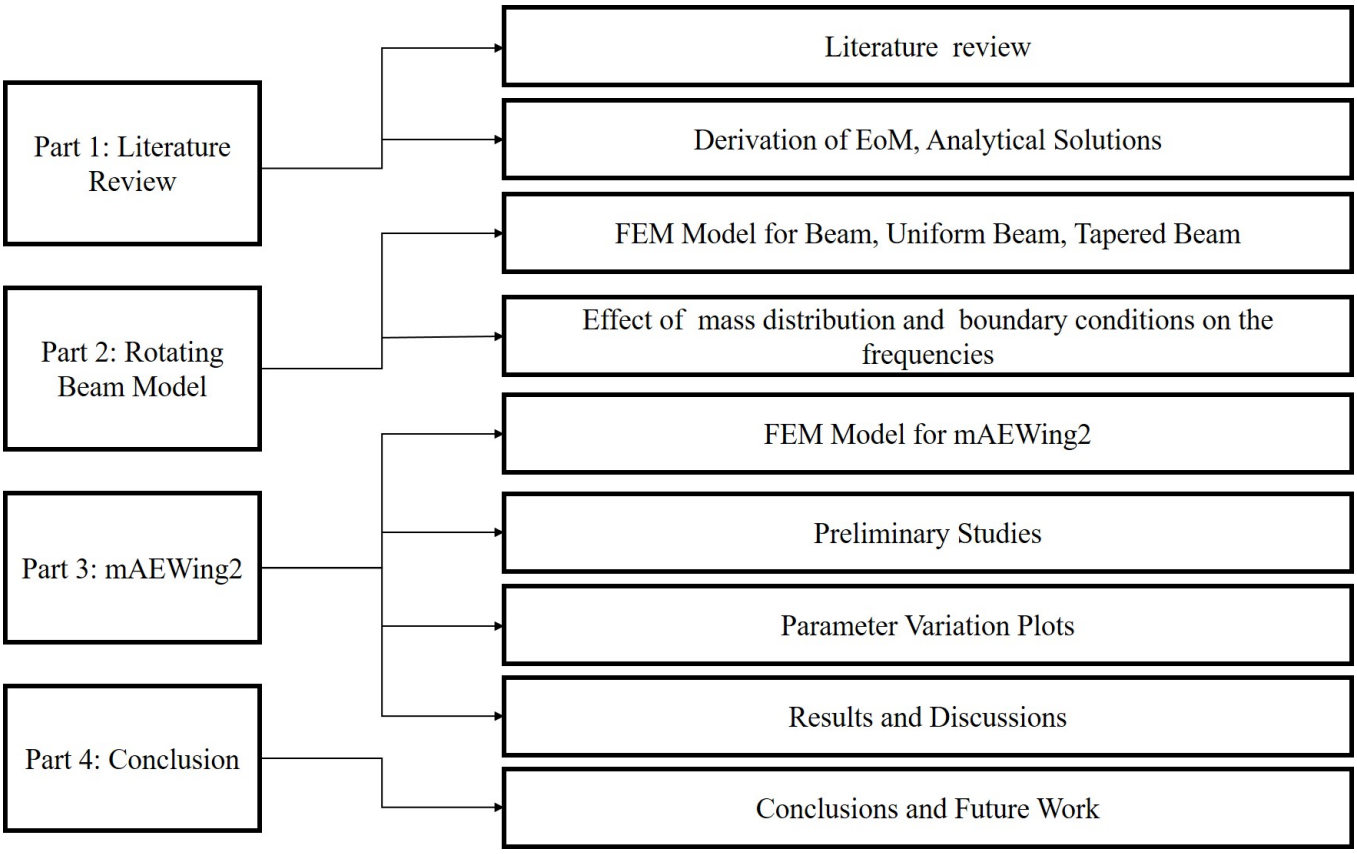

Figure 4.1: The Four Parts of this Thesis

4.1.2 Part 2: Rotating Beam Model

The aim of this part of the methodology is to study the rotating cantilever beam model. This includes studying the effect of varying speeds on the natural frequencies. It also includes studying the effect of other parameters like mass distribution and taper ratio. To achieve this, a finite element model of a beam is set up, the details of which are discussed in the next chapter.

The finite element model of the beam is set up using the commercial software MSC Nastran and Patran. To validate this model, the natural frequencies of this model were calculated using the SOL103, Normal Modes Analysis (the working of this solver is explained at the

end of this chapter) available in MSC Nastran, and the first three natural frequencies for the transverse vibration were compared with those obtained using analytical methods. Chapter 6 will discuss in detail the results of this comparative study.

Further, to study the natural frequencies of the pre-stressed beam, the cantilever beam model is stressed using rotor dynamics tools available in Nastran. These tools allow the user to define the direction and magnitude of the rotation vector. The Linear Static Solver in Nastran, SOL 101 is used to analyze this stressed beam at equilibrium. This helps in determining the forces acting on the beam. By pre-stressing the beam using these forces, the Sol 103 is called to obtain the natural frequencies for the pre-stressed beam.

The next step is to validate this pre-stressed model. The equations of motion are derived using force and moment equilibrium. The resulting partial differential equations can be solved by explaining the separation of variables technique. As is evident from the literature survey, solving this partial differential equation in space is in itself a very difficult and computationally expensive task. From [37] the transverse and in-plane frequencies were calculated. By comparing the results obtained analytically with those published by Naguleswaran [23] the analytical model is validated. The results from the analytical model are now used to validate the finite element beam model set up in Nastran. The flowcharts in Figure 4.2 and Figure 4.3 summarize the method explained above.

Once the finite element beam model is validated, geometrical complexities are introduced in the model in the form of a taper ratio, a tip mass, and composite material properties. These beams are then pre-stressed for different speeds, and subjected to a similar solution as outlined in the flowchart in Figure 4.5. The details of the model are discussed in Chapter 5 and the results are discussed in Chapter 6.

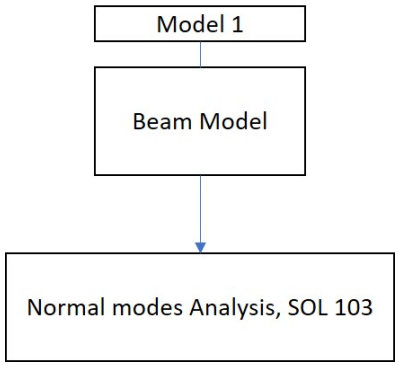

Figure 4.2: Procedure to Determine Normal Modes of an Unstressed Beam

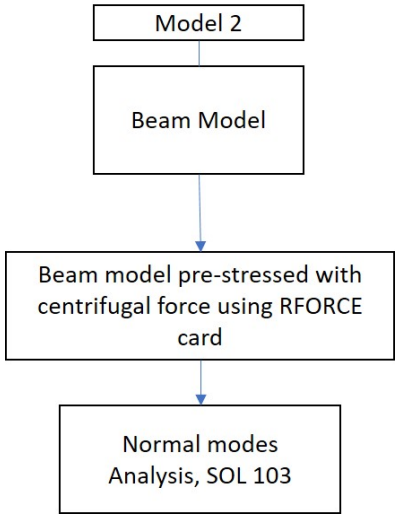

Figure 4.3: Procedure to Determine Normal Modes of a Pre-stressed Beam

Executing this first part of the methodology helps in achieving the first objective of this thesis. It also helps in validating the analysis method set up, to be used for the following part of the methodology.

4.1.3 Part 3: mAEWing2 Model

The next step in the methodology is to set up the model for mAEWing2, the aircraft under consideration. The structural and aerodynamic model of mAEWing2 is discussed in detail in Chapter 5. The aircraft is subjected to different roll rates, and the pre-stressed model of the

aircraft is used for SOL 103 to determine the natural frequencies. Here, the Static Aeroelastic Solution, SOL 144 (the working of this solver is explained at the end of this chapter), is used to calculate the forces acting on the aircraft during the roll maneuvers. The aircraft is subjected to different roll rates using the deflection of the outermost control surface. The SOL144 gives the resultant of the aerodynamic and structural forces, alongwith the axial component of the centrifugal force and gravity acting on the nodes during the maneuver, and hence helps in observing the effect of centrifugal forces on the natural frequencies of the aircraft. The results are discussed in Chapter 6. The flowchart in Figure 4.5 summarizes the procedure explained above.

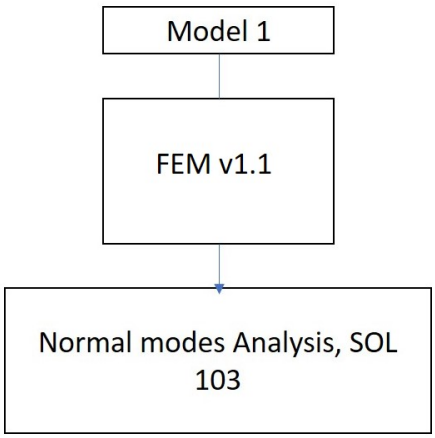

Figure 4.4: Procedure to Determine Normal Modes of an Unstressed mAEWing2 Aircraft

This step of the procedure helps in achieving the second objective of the thesis.

4.1.4 Part 4: Results and Conclusion

This part deals with all the result cases and a comparison of the results obtained from the previous two methods explained in Part 2 and Part 3. The conclusions that are drawn from the result tables will help determine the need to include the effects of centrifugal stiffening on the natural frequency among other things. The results will be discussed in Chapter 6.

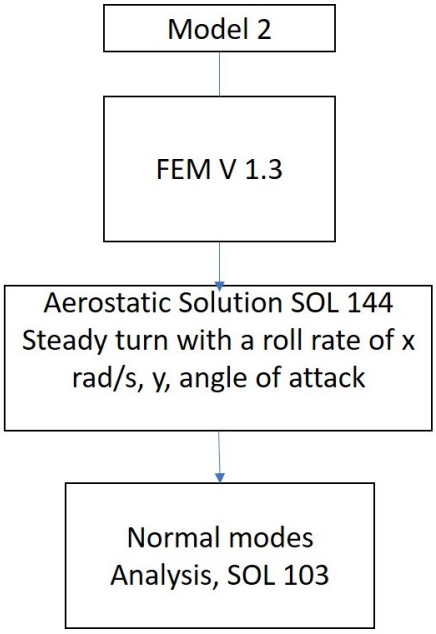

Figure 4.5: Procedure to Determine Normal Modes of a Pre-stressed mAEWing2 Aircraft

The following section discusses the different solvers available in Nastran [4, 29, 30] which will be used in this thesis.

4.2 Nastran Solution Sequences:

4.2.1 SOL103, Normal Modes Analysis

There are many reasons to compute the natural frequencies and mode shapes of a structure, all of which are based on the fact that real eigenvalue analysis is the basis for many types of dynamic response analysis. Natural frequencies and mode shapes are functions of structural properties and boundary conditions. If the structural properties change, the natural frequencies change, but the mode shapes may or may not get significantly affected. But the boundary conditions will most certainly affect the mode shapes.

Consider the reduced form of the equation of motion of a structure with M denoting the mass matrix, u denoting the displacement and K denoting the stiffness. The dot indicates derivative with respect to time.

$$[M]\{\ddot{u}\} + [K][u] = 0 \tag{4.1}$$

For the equation of undamped free vibration, assuming a harmonic solution of the form

$$\{u\} = \{\phi\}\, sin\omega t \tag{4.2}$$

Differentiating twice with respect to time and substituting in the equation of motion.

$$-\omega^2[M]\{\phi\}\sin\omega t + [K]\{\phi\}\sin\omega t = 0 \tag{4.3}$$

This results in the eigenvalue problem (4.4):

$$([K] - \omega^2[M])\{\phi\} = 0 \tag{4.4}$$

This equation, which is the eigenvalue problem, is an algebraic expression with many forms in linear matrix algebra.

$$|[K] - \omega^2[M]| \neq 0 \Rightarrow \{\phi\} = 0 \Rightarrow Trivial\ solution$$

$$|[K] - \omega^2[M]| = 0 \Rightarrow \{\phi\} \neq 0 \Rightarrow Non - trivial\ solution$$

$$\Rightarrow |[K] - \omega^2[M]| = 0$$

$$\Rightarrow |[K] - \lambda[M]| = 0\ where\ \lambda = \omega^2$$

The determinant is zero only at a set of discrete eigenvalues λ_i *or* ω_i^2. The eigenvectors computed in Nastran are computed are extracted using the following extraction method:

- Inverse Power Method (INV) : Often referred to as the inverse iteration method with sweeping. This method finds one eigenvalue and eigenvector at a time, starting with the lowest value. Each value is found using an iterative process. There is a possibility of missing the modes, and hence is unreliable.

- Enhanced Inverse Power Method (SINV) : This method is similar to INV, but uses Sturm Sequence logic to ensure that all modes in the desired range are found. This method is a recommended solution, when the model is small to medium sized.

- Lanczos Method : This method computes accurately predicts the eigenvalues and highly recommended for medium to large scaled models. For the model considered in this study, mAEWing2 aircraft, this method is used for extracting the eigenvalues.

The i^{th} eigenvector is related to the i^{th} natural frequency:

$$f_i = \frac{\omega_i}{2\pi} \quad and \quad \omega_i = \sqrt{\lambda_i} \tag{4.5}$$

The number of eigenvalues possible is equal to the number of degrees of freedom that have mass or the number of dynamic degrees of freedom. The mode shapes obtained here are relative quantities. The relation between structural loading and the natural frequencies that determine the absolute magnitude of the dynamic response. The results presented in this thesis are normalized with mass i.e. the eigenvectors are scaled to result in a unit value of generalized mass:

$$\{\phi_j\}^T [M] \{\phi_j\} = 1 \tag{4.6}$$

For the normal modes analysis of a pre-loaded structure, the eigenvalue problem corresponding to the pre-stiffened structures is:

$$(-\omega^2[M] + ([K] + [K]_D))\{\phi\} = \{0\} \tag{4.7}$$

$[K]_D$ is the differential stiffness matrix resulting from the load. The entire procedure of computing the eigenvalues remains the same.

When a structure is not fully constrained, it is possible for the structure to displace as a rigid body. Associated with every possible component of rigid body motion is one natural frequency which is zero. These are called the rigid body modes. Rigid body modes are useful in conducting dynamic analyses of unconstrained structures, such as aircraft and satellites.

4.2.2 SOL144, Static Aeroelastic Analysis

The aerodynamic load redistribution and consequent internal structural load and stress redistributions are of concern to the structural analyst. Static aeroleastic problems deal with the interaction of aerodynamic and structural forces on a flexible vehicle that result in redistribution of the aerodynamic loading as a function of airspeed. The structural stiffness, mass, damping matrices required by the aeroelastic analysis are generated by Nastran from the user input of geometric, structural, inertial and damping data, for subsequent use in the various aeroelastic analyses. The matrices of aerodynamic influence co-efficients are computed from the data describing the geometry of the aerodynamic finite elements. Aerodynamic grid points for the aerodynamic model are independent of the location of the structural grid points. A subsonic theory, doublet-lattice method, which can account for the interaction between multiple lifting surfaces and bodies, is used for the aerodynamic modeling of this

model. Nastran has an automated interpolation procedure to relate the aerodynamic and structural degrees of freedom. Splining techniques for lines and surfaces are used to generate the transformation matrix to transform deflections at structural grid points to deflections at aerodynamic grid points. The structural load distribution on an elastic vehicle is determined by solving the equations for static equilibrium. The solution results in aerodynamic stability derivatives like the lift and moment curve slopes and the lift and moment co-efficients due to the control surface deflections. From among the trim variables like angle of attack, control surface deflection, pitch, roll, yaw rates as well as aerodynamic and structural loads, structural deflections and element stresses, it is possible to determine some when the others are known. The following equations are the equations used for static aeroelastic analysis.

$$Q_{aa} = [G_{ka}]^T [W_{kk}][S_{kj}][A_{jj}]^{-1}[D_{jk}][G_{ka}] \tag{4.8}$$

$$Q_{ax} = [G_{ka}]^T [W_{kk}][S_{kj}][A_{jj}]^{-1}[D_{jx}] \tag{4.9}$$

$$[K_{aa} - \bar{q}Q_{aa}]\{u_a\} + [M_{aa}]\{\ddot{u_a}\} = \bar{q}[Q_{ax}]\{u_x\} + \{P_a\} \tag{4.10}$$

These equations are used to determine the stability derivatives. They can further be used to compute the roll rates and the corresponding control surface deflections, when the flight conditions are known.

Chapter 5

Rotating Beam Model

Following the discussion in section 4.1.1 of the Chapter 4, the detailed analytical and finite element models of a rotating cantilever beam are discussed in this chapter. The expressions for the natural frequencies are determined analytically for the rotating cantilever beam. Along with the analytical solution for a rotating cantilever beam the different result cases considered are explained here.

5.1 Analytical Model:

A rotating cantilever beam model is considered for analysis in this study. In the body axis system, the length of the beam is along the X-axis and it rotates in the $X-Y$ plane, i.e. about the Z-axis. The beam is fixed to a rotor which is at the origin of the co-ordinate system and the radius of the hub is assumed to be negligible. These assumptions are done in order to simplify the modeling and computational process and focus on studying the effects of the centrifugal force. The beam has homogeneous and isotropic material properties. Table 5.1 shows the material properties of the beam. The beam also has a slender shape so that shear and rotary effects are ignored. The cross-section of the beam is rectangular. The geometric properties of the beam are shown in Table 5.2. The flapping vibrations are defined in the $X-Z$ plane, and the lead-lag vibrations in the $X-Y$ plane. The beam rotates with an angular velocity of Ω about the Z-axis. The entire setup is shown in Figure 5.1 and Figure

5.2 shows the forces acting on an element of the beam.

Table 5.1: Material Properties

Material	Al 7075-T6
Modulus of Elasticity	71.1 GPa
Poisson's Ratio	0.33
Density	2810 kg/m^3

Table 5.2: Geometrical Properties

Length	10 m
Cross section	0.2x0.1 m
Area	0.02m^2
I_x	6.66667E-05
I_y	1.66667E-05

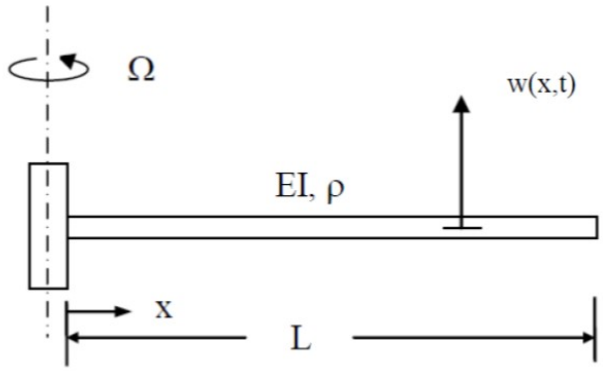

Figure 5.1: Rotating Beam Setup

5.1.1 Equation of Motion for a Beam with a Compressive Force

Considering the force equilibrium in equation (5.1),

$$-(V+dV)+fdx+V+(P+dP)\sin(\theta+d\theta)-P\sin\theta=\rho Adx\frac{\partial^2 w}{\partial t^2} \tag{5.1}$$

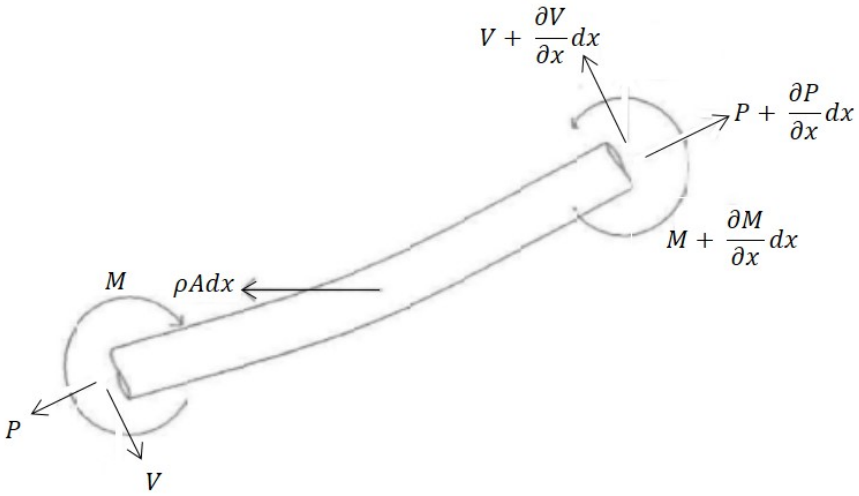

Figure 5.2: Forces Acting on an Element of the Beam

For moment equilibrium,

$$(M + dM) - (V + dV)dx + f dx\frac{dx}{2} - M = 0 \tag{5.2}$$

or

$$V = \frac{dM}{dx} \tag{(5.2(a))}$$

For very small deflections, $\sin\Theta = \Theta$ where $\Theta = \theta + d\theta$

$$\theta + \frac{\partial\theta}{\partial x}dx = \frac{\partial w}{\partial x} + \frac{\partial^2 w}{\partial x^2}dx \tag{5.3}$$

Substituting the above equation in (5.1)

$$-(\frac{dM}{dx} + \frac{d^2M}{dx^2}) + f dx + \frac{dM}{dx} + P\theta + dP\theta - P\theta = \rho A dx\frac{\partial^2 w}{\partial t^2} \tag{5.4}$$

Not considering higher powers of the derivative,

$$-fdx + \frac{d^2M}{dx^2} - dP(\frac{\partial^2 w}{\partial x^2}dx + \frac{\partial w}{\partial x}) + \rho A dx \frac{d^2w}{dt^2} = 0 \tag{5.5}$$

For free vibrations, $f = 0$ Rearranging the terms and substituting $M = EI\frac{\partial^2 w}{\partial x^2}$

$$\frac{\partial^2}{\partial x^2}(EI\frac{\partial^2 w}{\partial x^2}) - P\frac{\partial^2 w}{\partial x^2} + \rho A\frac{\partial^2 w}{\partial t^2} = 0 \tag{5.6}$$

For constant material properties,

$$EI\frac{\partial^4 w}{\partial x^4} - \frac{\partial}{\partial x}P\frac{\partial w}{\partial x} + \rho A\frac{\partial^2 w}{\partial t^2} = 0 \tag{5.7}$$

5.1.2 Expression for the Centrifugal Force

Consider an element of the beam of length dx at length x from the root and mass dm

$$dm = \rho dV \tag{5.8}$$

where dV is elemental volume

$$dm = \rho A dx \tag{5.9}$$

The centrifugal force, which is given by mv^2r, will be:

$$dP = dm\Omega^2 x \tag{5.10}$$

$$dP = \Omega^2 \rho A x dx \tag{5.11}$$

Integrating equation (5.11) over the length of the beam,

$$\int_0^L dP = \int_x^L \Omega^2 x \rho A dx \tag{5.12}$$

Taking out the constants under the integral in equation (5.12),

$$\int_0^L dP = \Omega^2 A \rho \int_x^L x dx \tag{5.13}$$

$$P(x) = \frac{1}{2}\rho A \Omega^2 (L^2 - x^2) \tag{5.14}$$

Substituting in the value for the centrifugal force P which is the axial force from equation (5.14) in (5.7) we get the governing differential equation for the rotating beam:

$$EI\frac{\partial^4 w}{\partial x^4} + \rho\Omega^2 A x \frac{\partial w}{\partial x} - \frac{1}{2}\rho\Omega^2 A(L^2 - x^2)\frac{\partial^2 w}{\partial x^2} + \rho A \frac{\partial^2 w}{\partial t^2} = 0 \tag{5.15}$$

Over the years, there have been multiple ways presented to solve the above non-homogeneous partial differential equation. However, this is a very complex as well as a tedious problem to solve.

To separate the variables in the above equation, it is written without substituting in the expression for P in (5.7):

$$EI\frac{\partial^4 w}{\partial x^4} - \frac{\partial}{\partial x} P \frac{\partial w}{\partial x} + \rho A \frac{\partial^2 w}{\partial t^2} = 0 \tag{5.16}$$

Separating the variables by $w(x,t) = W(x)t(t)$ and the constant set to $\lambda^2\Omega^2$,

$$EI\frac{\partial^4 W}{\partial x^4} - \frac{\partial}{\partial x} P \frac{\partial W}{\partial x} - m\lambda^2\Omega^2 W = 0 \tag{5.17}$$

and

$$\frac{d^2Y}{dt^2} + \lambda^2\Omega^2 Y = 0 \tag{5.18}$$

The equation for the space variable can be solved by multiple approaches. However, because the axial force is not constant, approximate-solution techniques are required. It is possible to use the assumed modes methods, or the power solution technique, each of which is computationally expensive. The boundary conditions used here are those of a cantilever beam, with displacement and slope zero at the clamped end and bending moment and shear force zero at the free end. Further, using Southwell's equation,

$$\omega_i^2 = \omega_{nr}^2 + \alpha_i\Omega^2 \tag{5.19}$$

α_i is the Southwell coefficient given by the following expression

$$\alpha_i = \frac{\int_0^1 m\bar{x}[\int_0^{\bar{x}}(\frac{d\bar{w}_i}{d\bar{x}})^2 d\bar{x}]d\bar{x}}{\int_0^1 m\bar{w}_i^2 d\bar{x}} \tag{5.20}$$

Here $\bar{w}_i = \bar{w}_i(x)$ is the assumed mode shape which satisfies the boundary conditions. From the Southwell plot for $\Omega \to 0$, the fundamental frequency of the clamped-free beam is $3.516\sqrt{EI/mL^4}$ gave the values of the first three fundamental frequencies for the non-dimensional speed $\eta = 0, 1, 3$ where $\eta = \Omega/\sqrt{EI/mL^4}$ [37]. These values are tabulated in Table **??**. These are the frequencies of a rotating beam, determined analytically.

5.2 Finite Element Model:

The finite element model of the rotating cantilever beam was modeled with the help of Patran. The beam was divided into 200 beam elements and 201 nodes. The element type used is CBEAM element. The boundary conditions imposed are:

Table 5.3: Analytical Fequencies of a Rotating Beam

η	Mode No.	Frequency, Hz.	Frequency, Hz.
0	1	$3.516\sqrt{EI/mL^4}$	1.62
	2	$22.035\sqrt{EI/mL^4}$	10.16
	3	$61.697\sqrt{EI/mL^4}$	28.44
1	1	$3.682\sqrt{EI/mL^4}$	1.7
	2	$22.181\sqrt{EI/mL^4}$	10.22
	3	$61.842\sqrt{EI/mL^4}$	28.52
3	1	$4.7973\sqrt{EI/mL^4}$	2.21
	2	$23.32\sqrt{EI/mL^4}$	10.75
	3	$62.985\sqrt{EI/mL^4}$	29.04

- at node 1 : all the six degrees of freedom were constrained

- at nodes 2 to 201 : none of the degrees of freedom were constrained

The RFORCE card from rotordynamics was used to define rotation at the fixed end about the Z-axis. The rotation speed, Ω is determined using the relation in equation (5.21)

$$\Omega = \frac{\eta}{\sqrt{\frac{EI}{mL^4}}} \tag{5.21}$$

where η is the non-dimensional speed. Table 5.4 explains the values of rotation used as input for the values of non-dimensional speed η varying from 0 to 15. In this step, the beam is loaded with centrifugal force. A total of 15 cases are generated, one for each of the 15 speeds considered. This pre-stressed model is then used as the input for the normal modes analysis. The result thus obtained is the mode shapes and frequencies for each of the 15 speeds of rotation. Section 6.1 and 6.2 of Chapter 6 discuss the results in detail. In order to compare the results with the analytical results, the beam is kept fixed at one end and free at the other end.

Table 5.4: Non-dimensional Speeds of Rotation

η	Rotation Speed, rad/sec
1	0.461
2	0.922
3	1.383
4	1.845
5	2.306
6	2.767
7	3.228
8	3.689
9	4.151
10	4.612
11	5.073
12	5.534
13	5.995
14	6.456
15	6.918

In the interest of studying the effect of stiffening on the rigid body modes, a separate case of the free-free boundary condition is also demonstrated. However, it is important to know that this is a purely hypothetical case, since it is not possible to have the free-free boundary condition for a beam that is rotating. For the beam to rotate, it is necessary to have a form of rotor that will provide the beam the necessary rotation. The importance of studying this case lies in observing the effect that the axial force has on the rigid modes of vibration and it may help us understand the results to be expected for unsupported rotating bodies. Figure 5.3 and Figure 5.4 show the finite element models used for analysis in Nastran for the F-F and C-F boundary conditions.

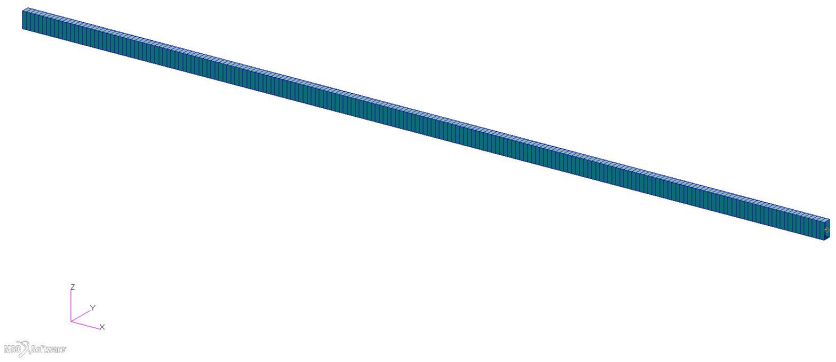

Figure 5.3: F-F Beam

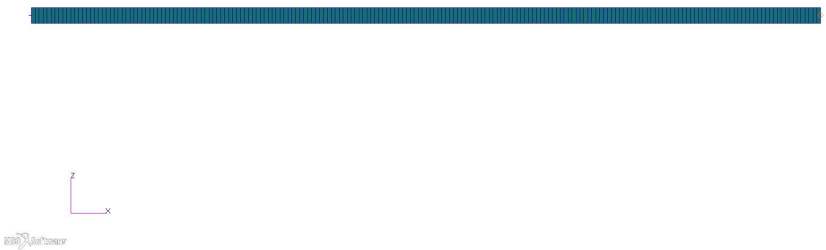

Figure 5.4: C-F Beam

5.3 Tapered Beam

The tapered beam model is a modification of the uniform beam model. The taper ratio used is 0.5. The objective of this analysis is to investigate the effects of taper ratio on the frequencies of the rotating beam. The number of elements is 200 and the number of nodes is 201. The element type used is CBEAM element. It is important to note that the stiffness EI and mass distribution m are no longer constants, but functions of the length of the beam now, which further complicates the analytical model. The result cases discusses will be for

η ranging from 0 to 15, and for the clamped-free boundary condition. Figure 5.5 shows the tapered beam model used for analysis.

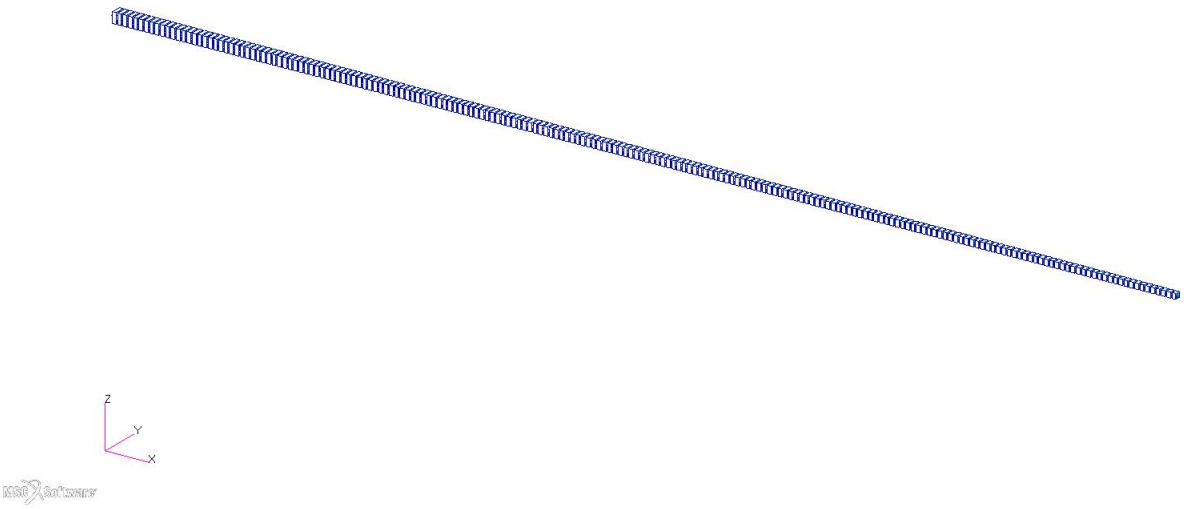

Figure 5.5: Tapered C-F Beam

5.4 Beam with Added Mass

This beam model is a modification of the uniform beam model. A lumped mass is added half way along the length of the beam. The objective of this model is to investigate the effects of lumped masses on the frequencies of a rotating beam. The number of elements is 200 and the number of nodes is 201. The element used is CBEAM type element. The result cases discussed will be for η ranging from 0 to 15, and for the clamped-free boundary condition.

5.5 Result Cases

This section summarizes the result cases for the beam model discussed in the previous section.

5.5.1 Uniform Beam

- Free-free beam vibration
- Free-free beam vibration (η = 1,7,15)
- Clamped-free beam vibration
- Clamped-free beam vibration (η = 1-15)

5.5.2 Tapered Beam

- Clamped-free Non-rotating Tapered Beam
- Clamped-free Rotating Tapered Beam

5.5.3 Beam with Added Mass

- Clamped-free Non-rotating Beam
- Clamped-free Rotating Beam

5.6 mAEWing2 Model

This section discusses the aircraft model that is used in the analysis of this study. However, before the model is discussed, it is important to have a brief introduction of the Performance

Adaptive Aeroelastic Wing (PAAW) project, and the motivation behind the development of this aircraft.

The PAAW project is an initiative by NASA where Virginia Tech and the University of Minnesota have been working in collaboration to design and build the aircraft, respectively. In following a Research Through Development philosophy, three scaled unmanned aircraft would be designed as a part of this project, viz. mAEWing1, mAEWing2 and xAEWing3. For analysis in this report, mAEWing2 is considered.

The mAEWing2 research aircraft is a 14-feet span symmetric aircraft designed to investigate and validate the flexible aircraft dynamic model, MDAO tool and feasibility of wing shape control [28]. The weight of the aircraft is about 33 pounds and the maximum speed it can achieve is 76.5 miles/hr. [41]. Figure 5.6 shows an isometric view of the aircraft and Figure 5.7 shows a CAD model indicating the control surfaces on the wings. There are four control surfaces on the trailing edge of the outer wing and one on the inner wing, which are called the body flaps. Additionally, there is one more control surface on the leading edge of the outer wing. The maximum deflection possible for each of the flaps is 30°.

For executing a roll maneuver, there needs to be a difference in the lift produced on the two wings. Hence, control surface deflections are used to produce the necessary moment to affect the roll. To achieve the objective of investigating the effect of roll rate on the natural frequencies, the other complexities are controlled by using one control surface deflection at one time to produce the necessary roll rate. As such, the results produced here are for the deflection of outermost control surfaces on the left and the right wing.

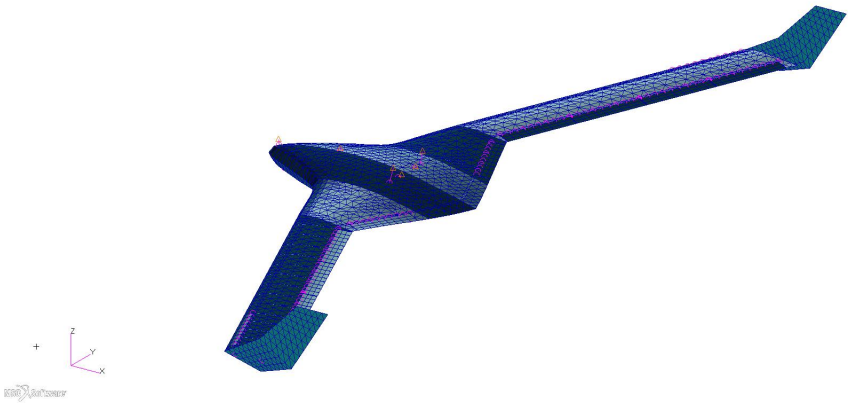

Figure 5.6: mAEWing2 Aircraft Isometric View

Preliminary results from the rotating beam models, which are discussed in detail in the following chapter, showed that lumped masses and modifications in physical properties, broadly modeled as tapered in the case of wings, affect the natural frequencies significantly. Based on these observations, the following four parameters were identified.

- Angle of attack
- Control Surface deflected
- Distribution of lumped masses
- Roll rate

The reason for selecting angle of attack is that it greatly affects the lift produced and hence is a crucial parameter to investigate. The control surface deflection was considered since the location of the deflected surface along the wing will affect the centrifugal force.

This led to the analysis of following cases as a part of the preliminary study.

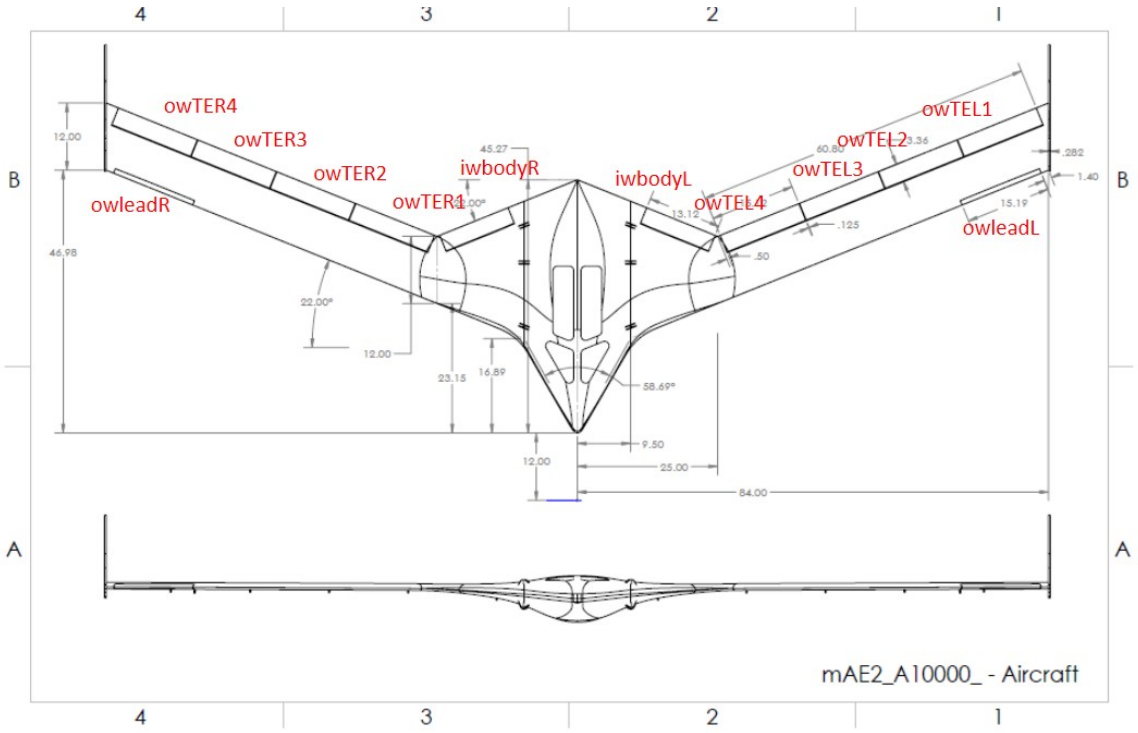

Figure 5.7: CAD Model mAEWing2 Aircraft [41]

Case 1: Roll rate produced by the deflection of Control Surface owTEL4

Case 2: Roll rate produced by the deflection of Control Surface owTEL3

Case 3: Roll rate produced by the deflection of Control Surface owTEL2

Case 4: Roll rate produced by the deflection of Control Surface owTEL1

The results are attached in the appendix section. Based on these results, it can be seen that varying the control surface to be deflected does not affect the roll rate significantly. Hence it is decided to fix the control surface to be deflected to owTEL1.

The next factor was the angle of attack. Preliminary results showed that the angle of attack affected the natural frequencies, and hence was decided to keep it as a crucial parameter.

Results from the rotating beam model show that the roll rate and the distribution of mass, both affect the natural frequencies, hence it was decided to keep them as well.

Thus, the cases for the study are now developed to include:

Case 1: For angle of attack 2° and only the control surface owTEL1 free to deflect, roll rate varying from 0.0 to 1.0 rad/sec using the FEM model v1.1

Case 2: For angle of attack 4° and only the control surface owTEL1 free to deflect, roll rate varying from 0.0 to 1.0 rad/sec using the FEM model v1.1

Case 3: For angle of attack 6° and only the control surface owTEL1 free to deflect, roll rate varying from 0.0 to 1.0 rad/sec using the FEM model v1.1

Case 4: For angle of attack 8° and only the control surface owTEL1 free to deflect, roll rate varying from 0.0 to 1.0 rad/sec using the FEM model v1.1

The results of the above cases are discussed in the next chapter. The approach used is shown in flowchart in Figure 4.5.

Chapter 6

Results

This chapter will discuss all the results from the analyses mentioned in the previous chapters. This chapter is divided into two parts. The first part with sections 6.1 and 6.2 will discuss the results of cases explained in Chapter 5 pertaining to rotating beam models. The second part, with sections 6.3 and 6.4 will discuss the results of cases explained in Section 5.6, pertaining to mAEWing2 aircraft.

6.1 Validation of the Model Set-up

The flowcharts shown in Figures 4.4 and 4.5 explain the procedure employed to determine the frequencies of an aircraft in steady roll, affected due to centrifugal stiffening. To ensure that this procedure will give the correct results, it is necessary to validate this method. To validate this procedure, the rotating beam model explained in Chapter 5 is used. The flowcharts in Figures 4.2 and 4.3 show the same procedure being applied to the rotating beam model. By comparing the results obtained from the model shown in the flowcharts with results published in [23], the model setup in Nastran is validated as shown in Table 5.3 and hence, the procedure is verified. The first three frequencies computed using the analytical model match with an accuracy of 0.1% when compared with [23]. Further, to ensure that higher speeds are not affecting the results, the results are calculated for the first three out-of-plane frequencies for the non-dimensional speed varying from 1 to 15, and

compared with those published in [23]. The results match with an accuracy within 0.6%. With this validation completed, the next cases of the beam, explained in section 5.5 of Chapter 5 are studied.

Table 6.1: Frequencies of a Rotating C-F Uniform Beam for $\eta = 1$ to 15

	Results, Hz			Normalized frequency			Reference Value			Relative Error(%)		
η	ω_1	ω_2	ω_3	Ω_1	Ω_2	Ω_3	$\Omega 1_{ref}$	$\Omega 2_{ref}$	$\Omega 3_{ref}$	e_1	e_2	e_3
1.00	1.71	10.28	28.58	3.70	22.28	61.98	3.68	22.18	61.84	0.57	0.46	0.23
2.00	1.92	10.48	28.78	4.16	22.72	62.41	4.14	22.61	62.27	0.45	0.45	0.23
3.00	2.22	10.80	29.11	4.81	23.42	63.12	4.80	23.32	62.99	0.33	0.42	0.22
4.00	2.58	11.24	29.56	5.60	24.37	64.10	5.59	24.27	63.97	0.24	0.38	0.21
5.00	2.98	11.78	30.13	6.46	25.53	65.34	6.45	25.45	65.21	0.18	0.34	0.20
6.00	3.40	12.40	30.81	7.37	26.89	66.81	7.36	26.81	66.68	0.14	0.31	0.19
7.00	3.83	13.10	31.59	8.31	28.41	68.51	8.30	28.33	68.39	0.11	0.27	0.18
8.00	4.27	13.87	32.47	9.26	30.07	70.41	9.26	30.00	70.29	0.08	0.24	0.17
9.00	4.72	14.68	33.43	10.23	31.84	72.50	10.23	31.77	72.39	0.06	0.21	0.15
10.00	5.17	15.54	34.47	11.21	33.70	74.75	11.20	33.64	74.65	0.05	0.18	0.14
11.00	5.62	16.44	35.58	12.19	35.64	77.16	12.18	35.59	77.06	0.04	0.15	0.13
12.00	6.08	17.36	36.76	13.17	37.65	79.71	13.17	37.60	79.61	0.03	0.13	0.11
13.00	6.53	18.32	37.99	14.16	39.72	82.37	14.16	39.67	82.29	0.02	0.11	0.10
14.00	6.99	19.29	39.27	15.15	41.83	85.14	15.15	41.79	85.07	0.01	0.10	0.09
15.00	7.44	20.28	40.59	16.14	43.98	88.01	16.14	43.94	87.94	0.01	0.08	0.08

**Results in the above column *Results* refers to the frequencies obtained using the Nastran model, which is validated.

6.1.1 Non-rotating F-F Beam

The frequencies for a uniform F-F non-rotating beam are tabulated in Table 6.2. The mode shapes for a non-rotating uniform F-F beam are shown in Figure A.1 and A.2 attached in Appendix A of this report.

Table 6.2: Frequencies of a Non-rotating F-F Beam

Mode No.	Frequency, Hz.
1	0.0000
2	0.0000
3	0.0000
4	0.0001
5	0.0001
6	0.0000
7	5.1911
8	10.3772
9	14.3023
10	28.0172

6.1.2 Rotating F-F Uniform Beam

The frequencies for a uniform F-F beam, rotating at speeds $\eta = 1$, 7 and 15 are tabulated in Tables 6.3. To further understand the relation between the frequencies and the rotating speeds, comparative plots are attached in the following section of this chapter. The mode

Table 6.3: Frequencies of a Rotating F-F Beam for $\eta = 1$, 7, 15

Mode No./*eta*	$\eta = 1$	$\eta = 7$	$\eta = 15$
1	0.2222	1.5564	3.3356
2	0.0008	0.0374	0.1719
3	0.0001	0.0001	0.00
4	0.8148	4.9054	10.2229
5	0.9191	5.9666	12.2536
6	5.4768	12.1225	22.4943
7	10.5337	15.9928	26.3789
8	14.5425	22.5766	37.4406
9	28.2326	34.0089	47.365
10	28.6771	36.7656	55.5265

**All frequencies are in Hz.

shapes for all the above cases of a F-F uniform beam are attached in Appendix A of this report. Figures A.1 to A.2 show the mode shapes of a F-F rotating beam. The mode shapes

for $\eta = 1$ are shown in Figure A.3 and A.4, mode shaped for $\eta = 7$ Figures A.5 and A.6, and mode shapes for $\eta = 15$ in Figures A.7 and A.8.

6.1.3 Non-rotating C-F Beam

The frequencies for a uniform C-F non-rotating uniform beam are tabulated in Table 6.4. To further understand the relation between the frequencies of a uniform beam, tapered beam, and beam with added mass, comparative plots are attached in the following section of this chapter. The mode shapes for a non-rotating uniform C-F beam are shown in Figures A.9 and A.10 in Appendix A of this report.

Table 6.4: Frequencies of a Non-rotating C-F Beam

Mode No.	Frequency, Hz.
1	0.8088
2	1.6173
3	5.0105
4	10.0083
5	13.8808
6	26.8925
7	27.6768
8	43.9030
9	53.4737
10	64.5808

6.1.4 Rotating C-F Uniform Beam

The frequencies for a uniform C-F beam, rotating at speeds ranging form $\eta = 1$ to 15, are tabulated in Tables 6.5 and 6.6. To further understand the relation between the frequencies and the rotating speeds, comparison plots are attached in the Section 6.2 of this chapter. The mode shapes for all the above cases of a C-F uniform beam are attached in Appendix A

Table 6.5: Frequencies of a Uniform Rotating C-F Beam for $\eta = 1$ to 7

Mode No./*eta*	1	2	3	4	5	6	7
1	0.84	0.90	0.99	1.08	1.17	1.26	1.34
2	1.71	1.92	2.22	2.58	2.98	3.40	3.83
3	5.22	5.55	6.05	6.69	7.43	8.24	9.09
4	10.28	10.48	10.80	11.24	11.78	12.40	13.10
5	14.43	14.79	15.38	16.17	17.12	18.21	19.40
6	28.14	28.53	29.11	29.56	30.13	30.81	31.59
7	28.58	28.78	29.17	30.05	31.13	32.39	33.82
8	46.37	46.78	47.46	48.38	49.54	50.91	52.48
9	55.76	55.97	56.31	56.78	57.38	58.11	58.95
10	69.11	69.53	70.22	71.18	72.39	73.83	75.50

**All frequencies are in Hz.

of this report. Figures A.11 through A.39 show the mode shapes of a C-F uniform rotating beam, rotating at speeds $\eta = 1$ to 15.

For the results of the cases explained in Section 5.5.1 the frequencies for non-rotating uniform beams are computed to observe and quantify the changes when the beam is subjected to rotation. They are presented in Tables 6.2 and 6.4. While Table 6.2 presents the frequencies of a F-F uniform beam, Table 6.4 presents the frequencies of a C-F uniform non-rotating beam. In the case of a C-F beam one end is completely fixed and the other end is kept free. It is important to note that the number of rigid body modes in both the cases; the F-F case has first six modes rigid body modes while the C-F case has no rigid body modes.

The mode shapes of the F-F uniform beam are shown in Figure A.1 and the mode shapes of a C-F beam are shown in Figure A.9. On comparing the mode shapes in these two figures it is seen that the first mode of the F-F beam is an in-plane mode and the second mode is an out-of-plane mode *i.e.* the first bending mode of a cantilever beam the frequency for which is 1.6 Hz. Although the case of a uniform F-F rotating beam is considered to be hypothetical,

Table 6.6: Frequencies of a Uniform Rotating C-F Beam for $\eta = 8$ to 15

Mode No./*eta*	8	9	10	11	12	13	14	15
1	1.42	1.49	1.57	1.63	1.70	1.77	1.83	1.89
2	4.27	4.72	5.17	5.62	6.08	6.53	6.99	7.44
3	9.99	10.91	11.85	12.81	13.78	14.75	15.74	16.73
4	13.87	14.68	15.54	16.44	17.36	18.32	19.29	20.28
5	20.69	22.04	23.45	24.90	26.38	27.90	29.44	31.00
6	32.47	33.43	34.47	35.58	36.76	37.99	39.27	40.59
7	35.38	37.05	38.83	40.68	42.60	44.58	46.60	48.67
8	54.23	56.13	58.17	60.33	62.60	64.95	67.38	69.24
9	59.91	60.97	62.14	63.40	64.74	66.17	67.67	69.88
10	77.37	79.43	81.66	84.04	86.56	89.21	91.96	94.81

**All frequencies are in Hz.

it is analyzed since it gives a good idea about the vibrations of a free-free space craft or air vehicle.

The results in Table 6.3 for $\eta = 1$, 7 and 15, respectively, present the in-plane and out-of-plane frequencies for a F-F beam with rotation speeds 0.46 rad/sec, 3.23 rad/sec and 6.92 rad/sec. The most interesting observation of these results is the effect of rotation on the rigid modes of the beam, as seen in the table. For $\eta = 1$ and 7, by comparing the mode shapes in Figures A.3 and A.5, it is seen that the first six modes still appear to be rigid, even if the frequencies are non-zero. The displacements increase with speed of rotation. As explained in Section 4.3.1, Sol103, Normal Modes Analysis, the mode shapes plot in Nastran are relative values that are normalized with mass. Further, they have been plot relative to the model scale. However, while this may discount their magnitudes, it cannot discount the incremental nature.

The first bending mode of the F-F beam is the sixth mode for the F-F beam rotating at $\eta = 1$ and there is an increase in the frequency. When compared with the non rotating F-F

beam case, the first frequency of the F-F beam rotating at $\eta = 1$ shows about 5% increase, the frequency at $\eta = 7$ is greater by about 57.17%, while at $\eta = 15$ is greater by about 76%.

Even though the case of the free-free boundary condition of the beam is studied as a purely hypothetical and academic case, it does have practical implications since aircraft vibrates as free-free structures. However, since for the purpose of analysis, we have considered all, except one degree of freedom fixed for aeroelastic analysis, the same boundary condition is maintained for uniformity and continuity of the problem. The translation in all the three directions and the rotation about the Y-axis and Z-axis is constrained so that only rotation about X-axis i.e. rolling about the the fuselage is possible. This helps in eliminating the complexities of both roll-yaw coupling and the adverse yaw effects, and helps to retain focus on the stiffening effect due to roll.

For the case of C-F rotating beam, the first bending natural frequency for $\eta = 7$ is 57% higher than the first natural frequency of the non rotating C-F beam, while the first bending frequency increases by 75% for $\eta = 15$ compared to the first frequency of the non-rotating C-F beam. For the tenth mode of the C-F rotating beam, the increase between $\eta = 1$ and $\eta = 15$ was only about 27.1%. This also shows that at higher modes, the stiffening effect is not as significant as that for the first mode. Figures 6.4 and 6.5 shows this effect of increase in stiffening due to the increase in rotation speed on the natural frequencies and how it diminishes at higher modes. Tables 6.5 and 6.6 show the frequencies of C-F rotating beams at $\eta = 1$ to 15.

6.1.5 Non-rotating C-F Tapered Beam

The natural frequencies for a uniform C-F non-rotating tapered beam are tabulated in Table 6.7. To further understand the relation between the frequencies of a uniform beam, tapered beam, and beam with added mass, comparative plots are attached in the following section of this chapter. The mode shapes for all the above cases of a C-F tapered beam are attached

Table 6.7: Frequencies of a C-F Non-rotating Tapered Beam

Mode No.	Frequency, Hz.
1	1.0734
2	2.1462
3	4.5341
4	9.0622
5	11.2653
6	21.2797
7	22.4900
8	34.6017
9	42.4206
10	51.2290

in Appendix B of this report. The mode shapes for a non-rotating tapered C-F beam are shown in Figure B.1 and B.2.

6.1.6 Rotating C-F Tapered Beam

The natural frequencies for a uniform C-F tapered beam, rotating at speeds ranging form $\eta =$ 1 to 15, are tabulated in Tables 6.8 and 6.9. To further understand the relation between the frequencies and the rotating speeds, comparative plots are attached in the following section of this chapter. The mode shapes for all the above cases of a C-F tapered beam are attached in Appendix B of this report. Figures B.3 to B.32 show the mode shapes for a rotating C-F tapered beam for speeds $\eta = 1$ to 15.

Table 6.8: Frequencies of a C-F Rotating Tapered Beam for $\eta = 1$ to 7

Mode No./η	1	2	3	4	5	6	7
1.00	1.1026	1.1797	1.2834	1.3967	1.5107	1.6217	1.7283
2.00	2.2098	2.3898	2.6604	2.9944	3.3703	3.7735	4.1943
3.00	4.6318	4.9132	5.3495	5.9051	6.5475	7.2515	7.9987
4.00	9.1230	9.3032	9.5962	9.9920	10.4790	11.0449	11.6777
5.00	11.3732	11.6909	12.2013	12.8806	13.7024	14.6411	15.6741
6.00	21.3920	21.7253	22.2691	23.0075	23.9187	24.5202	25.2119
7.00	22.5489	22.7248	23.0149	23.4147	23.9213	24.9897	26.1921
8.00	34.7163	35.0579	35.6195	36.3901	37.3561	38.5015	39.8094
9.00	42.4795	42.6557	42.9477	43.3530	43.8683	44.4896	45.2121
10.00	51.3451	51.6919	52.2644	53.0549	54.0532	55.2471	56.6232

**All frequencies are in Hz.

For tapered beams, the mass is no longer uniform, and is a function of the length and cross section. It reduces radially outwards. Comparing the frequencies of a uniform non-rotating C-F beam with those of tapered non-rotating C-F beam, the fundamental frequency of in-plane vibrations is 24.7% higher and the first bending frequency is also 24.6% higher. Comparing the frequencies at $\eta = 1$ for the C-F uniform beam and tapered beam, the first and the second natural frequencies are higher by 23% than the respective natural frequencies for the non-rotating beams. Tables 6.8 and 6.9 show the frequencies of rotating tapered C-F beams for $\eta = 1$ to 15.

6.1.7 Non-rotating Beam with Added Mass

The frequencies for a uniform C-F non-rotating beam with added mass are tabulated in Table 6.10. To further understand the relation between the frequencies of a uniform beam, tapered beam, and beam with added mass, comparative plots are attached in the following section of this chapter. The mode shapes for all the above cases of a C-F beam with added mass are attached in Appendix C of this report. The mode shapes for a non-rotating C-F

Table 6.9: Frequencies of a C-F Rotating Tapered Beam for $\eta = 8$ to 15

Mode No./η	8	9	10	11	12	13	14	15
1	1.8303	1.9280	2.0216	2.1116	2.1981	2.2816	2.3623	2.4404
2	4.6267	5.0668	5.5122	5.9613	6.4129	6.8665	7.3215	7.7776
3	8.7766	9.5767	10.3929	11.2213	12.0589	12.9036	13.7540	14.6088
4	12.3666	13.1023	13.8766	14.6829	15.5155	16.3702	17.2430	18.1311
5	16.7826	17.9513	19.1681	20.4234	21.7100	23.0220	24.3548	25.7050
6	25.9862	26.8357	27.7530	28.7312	29.7639	30.8452	31.9697	33.1328
7	27.5094	28.9242	30.4214	31.9882	33.6136	35.2886	37.0055	38.7582
8	41.2631	42.8461	44.5432	46.3402	48.2246	50.1852	52.2123	53.9964
9	46.0309	46.9405	47.9354	49.0099	50.1586	51.3760	52.6569	54.2974
10	58.1676	59.8659	61.7041	63.6687	65.7470	67.9272	70.1986	72.5513

**All frequencies are in Hz.

Table 6.10: Frequencies of a C-F Non-rotating Beam with Added Mass

Mode No.	Frequency, Hz.
1	0.8159
2	1.2847
3	2.0633
4	5.1113
5	10.3475
6	14.3030
7	28.0031
8	28.5185
9	46.2377
10	55.7149

beam with an added mass are shown in Figures C.1 and C.2.

6.1.8 Rotating Beam with Added Mass

The frequencies for a uniform C-F beam with added mass, rotating at speeds ranging form $\eta = 1$ to 15, are tabulated in Tables 6.11 and 6.12. To further understand the relation between the frequencies and the rotating speeds, comparative plots are attached in the following section of this chapter. The mode shapes for all the above cases of a C-F beam with added

mass are attached in Appendix C of this report. Figures C.3 through C.32 show the mode shapes for a rotating C-F beam for speeds $\eta = 1$ to 15. For beam with added mass, a comparison similar to that of the tapered beam shows the in-plane frequency to be higher by about 0.87%, for the non-rotating beam case, while the out-of-plane frequency reduced by 20.4%. With the increase in rotating speed, the percent increase in the frequencies is very small compared to the earlier cases. The reason for this is thought to be the location of the added mass, which is half way along the length of the beam.

Table 6.11: Frequencies of a C-F Rotating Beam with Added Mass for $\eta = 1$ to 7

Mode No./η	1	2	3	4	5	6	7
1.00	0.84	0.90	0.99	1.08	1.17	1.26	1.34
2.00	1.32	1.39	1.47	1.52	1.55	1.57	1.59
3.00	2.10	2.23	2.46	2.77	3.13	3.53	3.95
4.00	5.22	5.55	6.05	6.69	7.43	8.24	9.09
5.00	10.41	10.61	10.93	11.36	11.89	12.51	13.20
6.00	14.43	14.79	15.38	16.17	17.12	18.21	19.40
7.00	28.14	28.53	29.11	29.56	30.13	30.81	31.59
8.00	28.58	28.78	29.17	30.05	31.13	32.39	33.82
9.00	46.37	46.78	47.46	48.38	49.54	50.91	52.48
10.00	55.78	55.99	56.33	56.80	57.40	58.13	58.97

**All frequencies are in Hz.

6.2 Comparison Plots for Beams

Taking into consideration the number of tables and figures generated to demonstrate the results for different cases of beam studied, this section presents the consolidated results. Figure 6.1 shows a comparison of the first ten natural frequencies for non-rotating C-F uniform beam, tapered beam and beam with the added mass. This figure shows the comparison of frequencies for the three types of beams considered for zero rotation speed.

Table 6.12: Frequencies of a C-F Rotating Beam with Added Mass for $\eta = 8$ to 15

Mode No./η	8	9	10	11	12	13	14	15
1.00	1.42	1.49	1.57	1.62	1.62	1.62	1.63	1.63
2.00	1.60	1.61	1.61	1.63	1.70	1.77	1.83	1.89
3.00	4.37	4.81	5.25	5.70	6.15	6.60	7.05	7.51
4.00	9.99	10.91	11.85	12.81	13.78	14.75	15.74	16.73
5.00	13.96	14.77	15.62	16.51	17.43	18.38	19.35	20.34
6.00	20.69	22.04	23.45	24.90	26.38	27.90	29.44	31.00
7.00	32.47	33.43	34.47	35.58	36.76	37.99	39.27	40.59
8.00	35.38	37.05	38.83	40.68	42.60	44.58	46.60	48.67
9.00	54.23	56.13	58.17	60.33	62.60	64.95	67.38	69.26
10.00	59.93	61.00	62.16	63.42	64.76	66.19	67.69	69.88

**All frequencies are in Hz.

Figures 6.2 and 6.3 show the variation of the first four in-plane and transverse natural frequencies with increasing rotation speed for a F-F uniform rotating beam.

Figures 6.4 and 6.5 show the variation of the first four in-plane and transverse natural frequencies with increasing rotation speed for a C-F uniform rotating beam.

Figures 6.6 and 6.7 show the variation of the first four in-plane and transverse natural frequencies with increasing rotation speed for a C-F uniform tapered rotating beam.

Figures 6.8 and 6.9 show the variation of the first four in-plane and transverse natural frequencies with increasing rotation speed for a C-F uniform rotating beam with added mass.

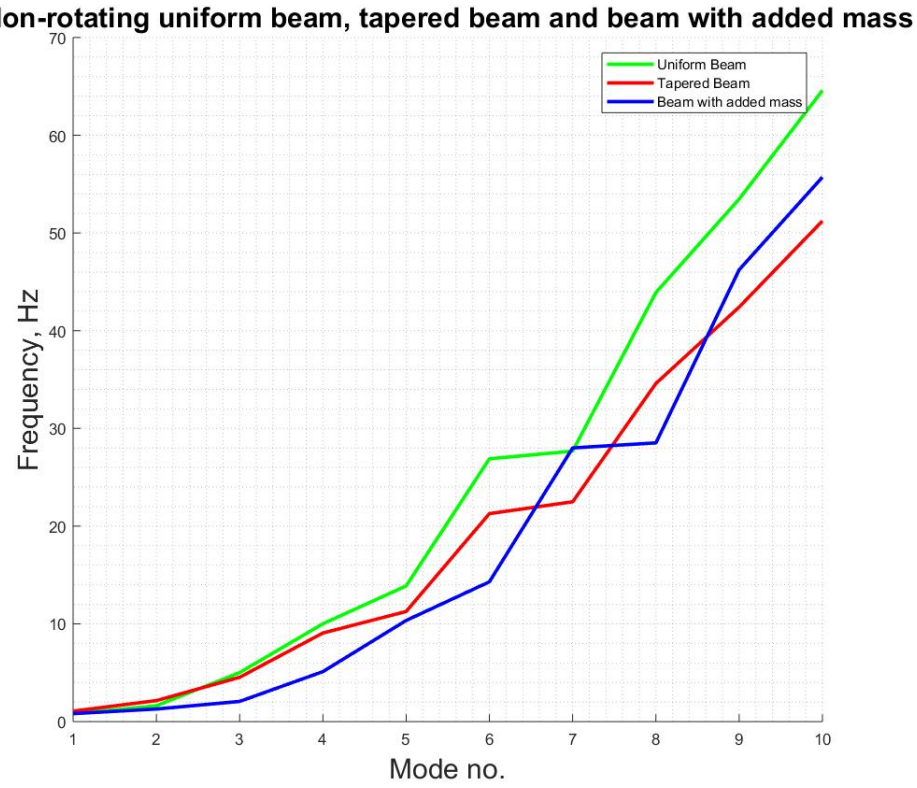

Figure 6.1: Frequencies of C-F Non-rotating Uniform Beam, Tapered Beam and Beam with Added Mass

6.3 mAEWing2: Preliminary results

Table 6.13 shows the results of the preliminary test cases for mAEWing2. These test cases are done to determine the control parameters for this study and to determine the maximum and minimum values. Once these are known, the final test cases are determined by controlling the parameters between their extreme values. The control parameters are the flaps deflected, deflection of the flap, angle of attack and roll rate.

Before discussing the results of all the test cases, it is important to know about the assumptions that are made in this study. All the test cases assumed are for steady roll rates,

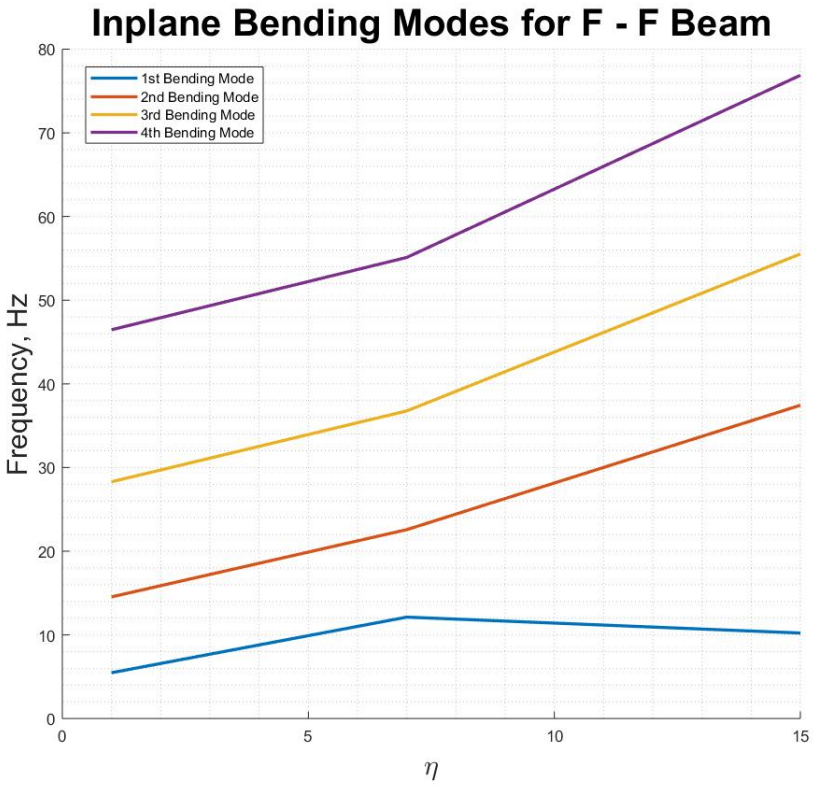

Figure 6.2: Variation of In-plane Natural Frequencies with Rotation Speed of F-F Rotating Uniform Beam

with 0.0 rad/s^2 roll acceleration. There is no coupling between yaw and roll, the model is analyzed considering only rotation about the fuselage, *i.e.* roll as the only unconstrained degree of freedom. Further, only the four trailing edge control surfaces are considered for the analysis, one at a time. The control surface on the left and the right wing are linked in such a way that if the left wing control surface has a downward deflection, the corresponding control surface on the right wing will have an upward deflection of the same magnitude. When the left wing control surface has a downward deflection and the right wing control surface has an upward deflection, that would indicate that the aircraft is banked to the left, or a left roll.

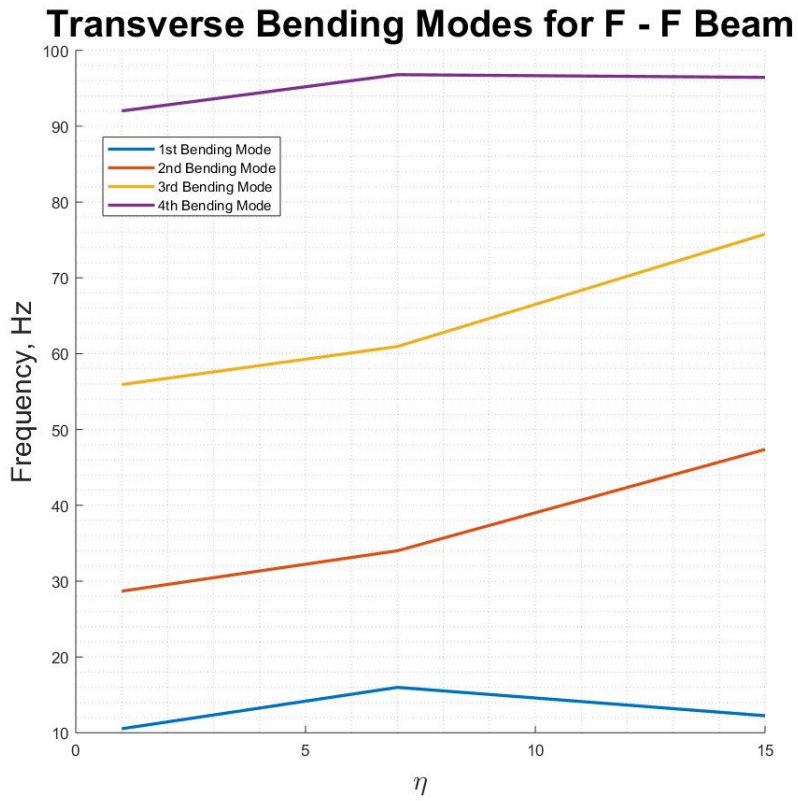

Figure 6.3: Variation of Out-of-plane Natural Frequencies with Rotation Speed of F-F Rotating Uniform Beam

For mAEWing2 aircraft, the maximum allowable flap deflection is 15°. According to FAA regulations, an aircraft the size of mAEWing2 should be able to execute roll from $30°/sec$ to $-30°/sec$ in about 5 seconds and 4 seconds for climb and approach respectively. These values give some idea of the maximum and minimum values of control parameters that should be set for analysis in this study.

From Table 6.13 the roll rate produced by deflection of owTEL1 at 2° AoA is $75.51°/sec$ while the same deflection of owTEL4 at AoA 2° is $-30.82°/sec$. This clearly shows that for the same deflection and angle of attack, owTEL1 would produce a higher roll rate while owTEL4 produces the opposite effect. Hence the further preliminary test cases are studied

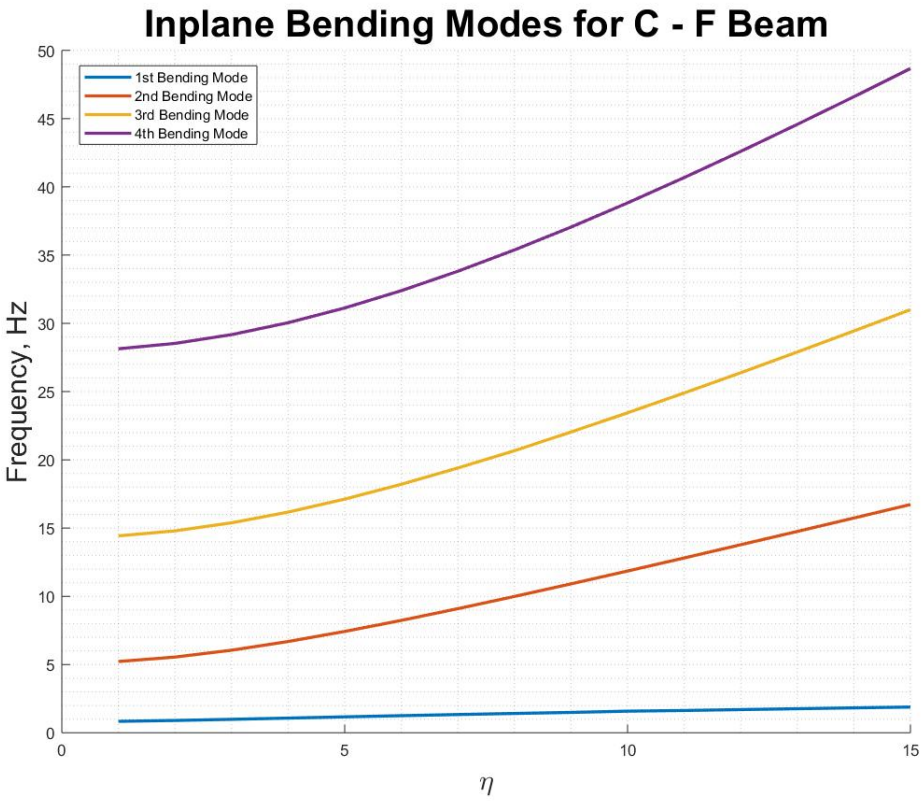

Figure 6.4: Variation in In-plane Natural Frequencies with Rotating Speeds of a C-F Uniform Rotating Beam Rotating at $\eta = 1$ to 15

only for owTEL1 as they make a better case for studying the effect of stiffening.

While for AoA 2° and deflection of 15° for owTEL1 the roll rate produced is $75.51°/sec$, that for AoA 8° is $74.83°/sec$ which is comparable to the roll produced by owTEL1. This seems to indicate that the AoA makes only a very small difference to the roll produced.

The third thing to be observed from Table 6.13 is that a deflection of 15° seems to produce a large roll rate, hence restricting the deflection to a lower angle should be considered. For the same roll rate to be produced, the owTEL4 needs a higher deflection and in the direction opposite to what would be expected for the required turn. For AoA 2° and roll rate of

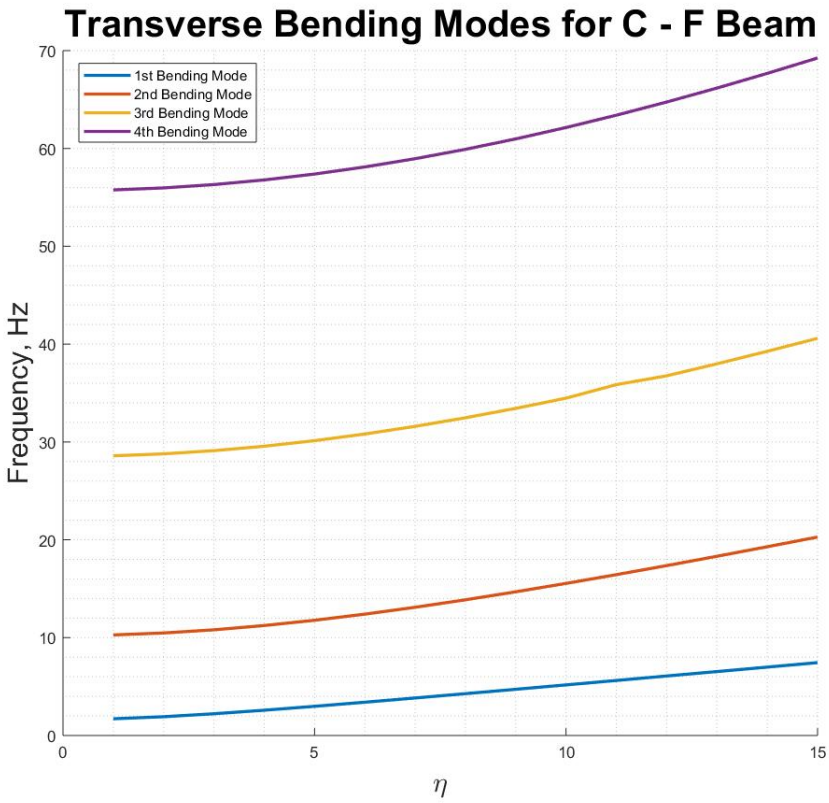

Figure 6.5: Variation in Out-of-plane Natural Frequencies with Rotating Speeds of a C-F Uniform Rotating Beam Rotating at $\eta = 1$ to 15

$1 rad/sec$ which is about $57.29°/sec$, the owTEL4 requires a deflection of 28°, which is higher than the allowable deflection for the flaps of mAEWing2 aircraft.

Based on all these observations, it is decided to keep the deflection restricted to owTEL1, and vary the angle of attack from 2° to 8° in steps of two. Further, the roll rate will be varied from 0 to 1 rad/sec. Also, in considering the impact of boundary conditions on the rigid body modes in stiffening, a test case will be considered for each of the 4 AoAs, for 0.5 rad/sec. All the other results are obtained at the same boundary condition as aeroelastic analysis in order to maintain the continuity in the problem.

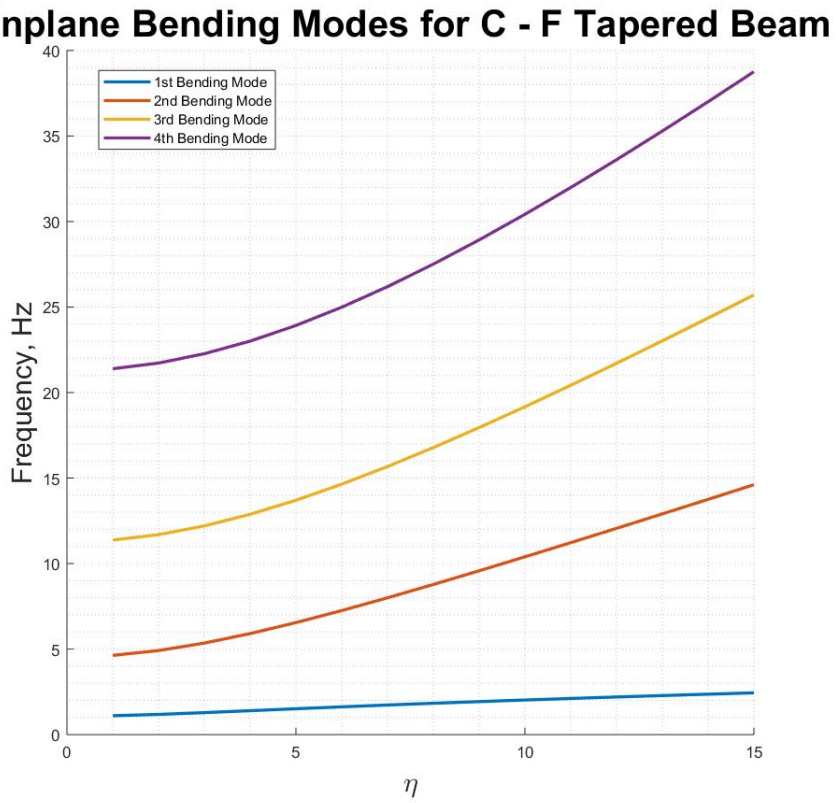

Figure 6.6: Variation in In-plane Natural Frequencies with Rotating Speeds of a C-F Uniform Tapered Rotating Beam Rotating at $\eta = 1$ to 15

6.4 mAEWing2: Final results

6.4.1 Angle of attack 2°, owTEL1 deflected

The frequencies for angle of attack 2°, for different roll rates are tabulated as follows.Table 6.14 shows the natural frequencies of v1.1 mAEWing2 model for zero roll rate and 0.5 rad/sec roll rate, with free-free boundary conditions for the normal modes. Further, Table 6.15 shows the natural frequencies for roll rate 0.0 rad/sec, 0.5 rad/sec and 1.0 rad/sec for FEM v1.1 model for the constrained boundary conditions used in aeroelastic analysis. The mode shapes for v1.1 mAEWing2 for angle of attack 2° and zero roll rate for constrained

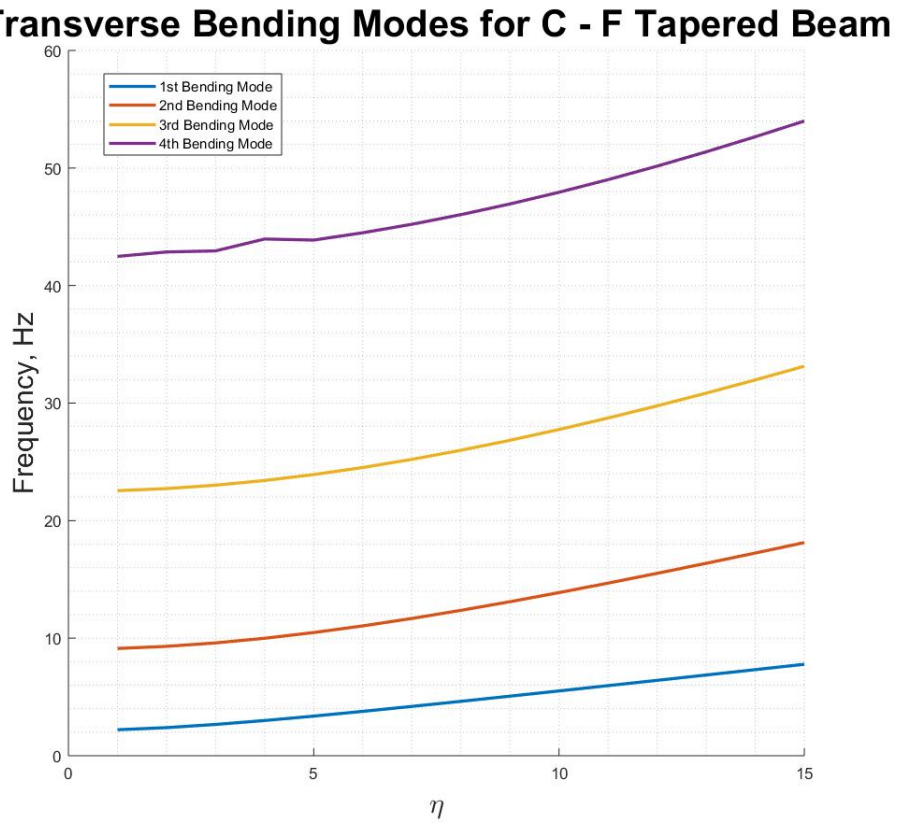

Figure 6.7: Variation in Transverse Natural Frequencies with Rotating Speeds of a C-F Uniform Tapered Rotating Beam Rotating at $\eta = 1$ to 15

vibrations are attached in Appendix D, Figure D.1. Appendix E, Figures E.1 and E.2 have mode shapes for roll rates 0.5 rad/sec (Figure E.1) and 1 rad/sec (Figure E.2) for v1.1 of mAEWing2 for constrained boundary conditions used in aeroelastic analysis.

6.4.2 Angle of attack 4°, owTEL1 deflected

The frequencies for angle of attack 4°, for different roll rates are tabulated as follows. Table 6.16 shows the natural frequencies of v1.1 mAEWing2 model for 0.0 rad/sec roll rate and 0.5 rad/sec roll rate, with free-free boundary conditions for the normal modes. Further, Table 6.17 shows the natural frequencies for roll rate 0.0 rad/sec, 0.5 rad/sec and 1.0 rad/sec for

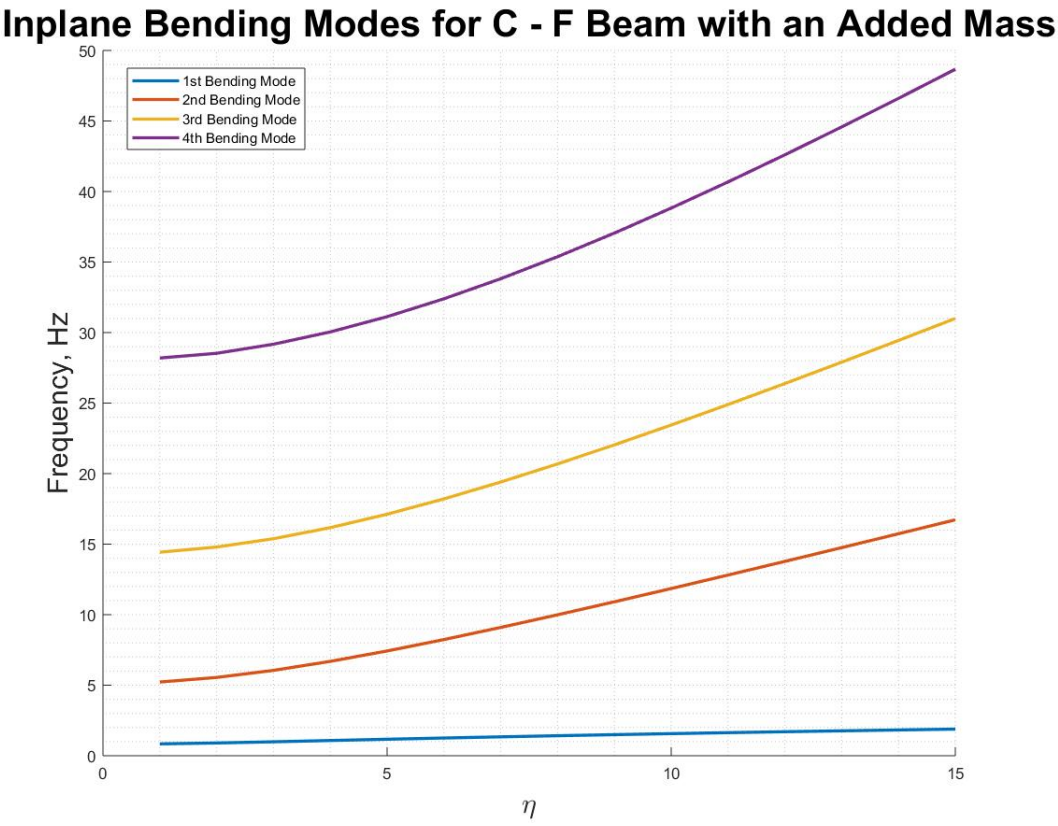

Figure 6.8: Variation in In-plane Natural Frequencies with Rotation Speed of a C-F Uniform Beam with Added Mass Rotating at $\eta = 1$ to 15

FEM v1.1 model for the constrained boundary conditions used in aeroelastic analysis.

The mode shapes for v1.1 mAEWing2 for angle of attack 4° and zero roll rate for constrained boundary conditions are attached in Appendix D, Figure D.2. Appendix E, Figures E.3 and E.4 have mode shapes for roll rates 0.5 rad/sec (Figure E.3) and 1 rad/sec (Figure E.4) for v1.1 of mAEWing2 for constrained boundary conditions used in aeroelastic analysis.

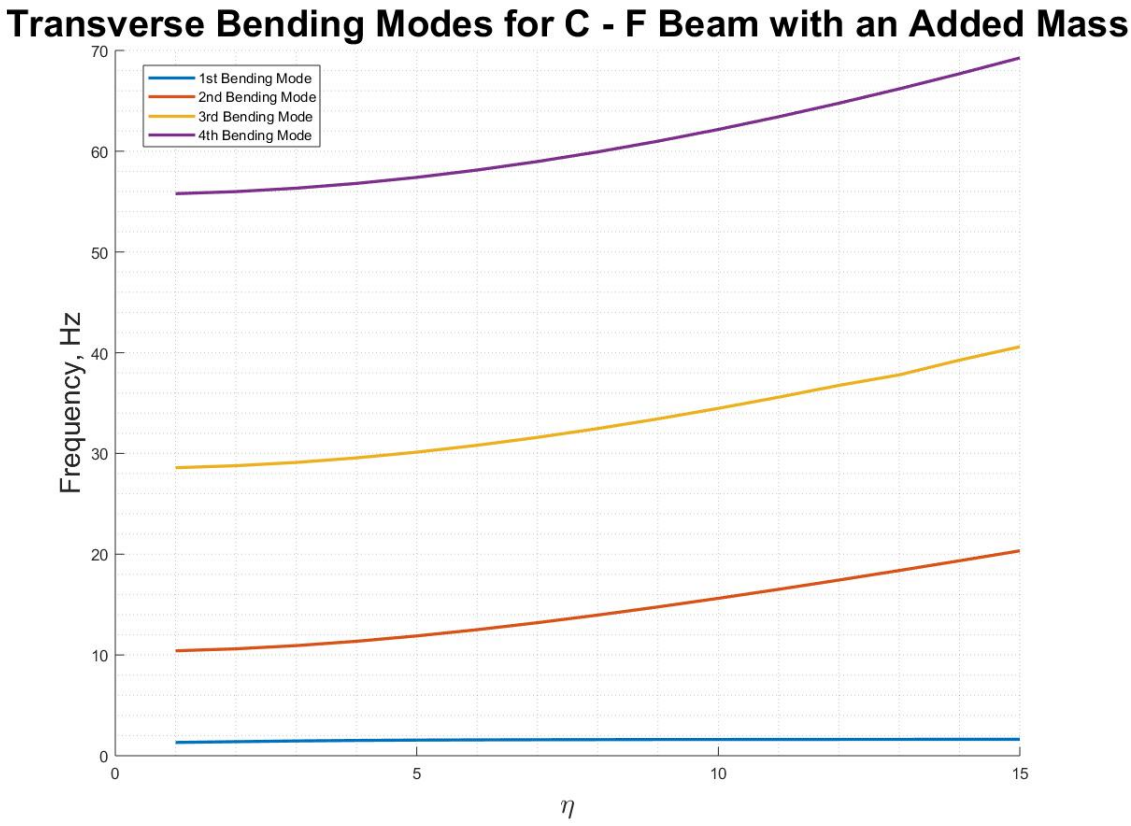

Figure 6.9: Variation in Transverse Natural Frequencies of a C-F Uniform Beam with Added Mass Rotating at $\eta = 1$ to 15

6.4.3 Angle of attack 6°, owTEL1 deflected

The frequencies for angle of attack 6°, for different roll rates are tabulated as follows. Table 6.18 shows the natural frequencies of v1.1 mAEWing2 model for zero roll rate and 0.5 rad/sec roll rate, with free-free boundary conditions for the normal modes. Further, Table 6.19 shows the natural frequencies for roll rate 0.0 rad/sec, 0.5 rad/sec and 1.0 rad/sec for FEM v1.1 model for the constrained boundary conditions used aeroelastic analysis.

The mode shapes for v1.1 mAEWing2 for angle of attack 6° and zero roll rate are attached in Appendix D, Figure D.3 for constrained vibrations. Appendix E, Figures E.5 and E.6 have

Table 6.13: Preliminary Result Cases

Case	Flap Deflected	Flap Deflection (°)	Aoa (°)	Roll (rad/sec)	Roll (°/sec)
1	owTEL1	15.00	2.00	1.32	75.51
2	owTEL1	15.00	8.00	1.31	74.84
3	owTEL1	1.16	2.00	0.10	5.73
4	owTEL1	11.38	2.00	1.00	57.30
5	owTEL1	1.45	8.00	0.10	5.73
6	owTEL1	11.52	8.00	1.00	57.30
7	owTEL4	15.00	2.00	-0.54	-30.82

mode shapes for roll rates 0.5 rad/sec (Figure E.5) and 1 rad/sec (Figure E.6) for v1.1 of mAEWing2 for constrained boundary conditions used in aeroelastic analysis.

6.4.4 Angle of attack 8°, owTEL1 deflected

The frequencies for angle of attack 8°, for different roll rates are tabulated as follows. Table 6.20 shows the natural frequencies of v1.1 mAEWing2 model for zero roll rate and 0.5 rad/sec roll rate for free-free boundary conditions. Further, Table 6.20 shows the natural frequencies for roll rate 0.0 rad/sec and 5.0 rad/sec for FEM v1.1 model for the constrained boundary conditions used in aeroelastic analysis.

The mode shapes for v1.1 mAEWing2 for angle of attack 8° and zero roll rate are attached in Appendix D, Figure D.4 for constrained vibrations. Appendix E, Figures E.7 and E.8 have mode shapes for roll rates 0.5 rad/sec (Figure E.7) and 1 rad/sec (Figure E.8) for v1.1 of mAEWing2 for constrained boundary conditions used in aeroelastic analysis.

Tables 6.14 to 6.21 show the four cases for each angle of attack: 2°, 4°, 6°, and 8°.

Table 6.14: Frequencies of mAEWing2 v1.1 for at 0 and 0.5 rad/sec for Angle of Attack 2° for F-F Vibrations

p rad/sec	0	0.5
p°/sec	0	28.6479
Roll mode	0.0000	0.0000
Yaw mode	0.0000	0.0000
Surge mode	0.0000	0.0000
Heave mode	0.0000	0.0000
Sway mode	0.0000	0.0000
Pitch mode	0.0000	0.3184
1^{st} SWBM	5.5877	5.5843
1^{st} AWBM	8.0017	8.0006
2^{nd} SWBM	18.7890	18.7664
2^{nd} AWBM	21.6824	21.6819
1^{st} AWTM	24.0326	24.0342
1^{st} SWTM	30.2324	30.2207

**All frequencies are in Hz.

As can be seen from the results of FEM v1.1 there is negligible difference in the natural frequencies for roll rates from 0 to 1.0 rad/sec for a given angle of attack, which indicates that there is not considerable stiffening at the examined roll rates. However, for the same roll rate the natural frequency of a given mode increases with the angle of attack. The AoA does seem to make some difference to the fundamental frequencies albeit the effect is gradual and can be considered negligible. On a closer inspection of the mode shapes, it can be seen that the roll rigid mode is considerably affected by the stiffening. However, it should be noted that the significance mentioned here is in purely relative terms, since the absolute effect of stiffening on frequencies is negligible. Other factors, like the symmetric design of the aircraft may also affect the stiffening effect. It is also possible that the component of lift and gravity forces help in reducing the net effect of the centrifugal force.

Table 6.15: Frequencies of mAEWing2 v1.1 for at 0 and 0.5 rad/sec for Angle of Attack 2° for Constrained Vibrations

p rad/sec	0	0.5	1.0
$p°/sec$	0	28.6479	57.296
Roll Mode	0.0000	0.0000	0.0
Yaw Mode	2.0770	2.0770	2.077
$1^{st}SWBM$	2.5531	2.5530	2.5529
$2^{nd}SWBM$	6.1367	6.1366	6.1362
$2^{nd}AWBM$	8.0013	8.0013	8.0013
$1^{st}SWTM$	8.7766	8.7766	8.7766
$2^{nd}CWBTM$	27.7304	27.7299	27.728

**All frequencies are in Hz.

Table 6.16: Frequencies of mAEWing2 v1.1 at 0 and 0.5 rad/sec for Angle of Attack 4° F-F Vibrations

p rad/sec	0	0.5
$p°/sec$	0	28.6479
Roll Mode	0.0000	0.0000
Yaw Mode	0.0000	0.0000
Surge Mode	0.0000	0.0000
Heave Mode	0.0000	0.0000
Sway Mode	0.0000	0.2572
Pitch Mode	0.0000	0.3594
$1^{st}SWBM$	5.5877	5.5789
$1^{st}AWBM$	8.0017	7.9997
$2^{nd}SWBM$	18.7890	18.7621
$2^{nd}AWBM$	21.6824	21.6818
$1^{st}AWTM$	24.0326	23.9911
$1^{st}SWTM$	30.2324	30.1118

**All frequencies are in Hz.

Table 6.17: Frequencies of mAEWing2 v1.1 at 0, 0.5 and 1.0 rad/sec for Angle of Attack 4° for Constrained Vibrations

p rad/sec	0	0.5	1.0
$p°/sec$	0	28.6479	57.296
Roll Mode	0.1969	0.1969	0.197
Yaw Mode	2.0725	2.0722	2.0722
$1^{st}SWBM$	2.5547	2.5531	2.5528
$2^{nd}SWBM$	6.1418	6.1353	6.1342
$2^{nd}AWBM$	8.0003	8.0003	8.0003
$1^{st}ASWTM$	8.7784	8.7762	8.7760
$2^{nd}CWBTM$	27.7678	27.7278	27.724

**All frequencies are in Hz.

Table 6.18: Frequencies of mAEWing2 v1.1 at 0 and 0.5 rad/sec for Angle of Attack 6° for F-F Vibrations

p rad/sec	0	0.5
$p°/sec$	0	28.6479
Roll Mode	0.0000	0.0000
Yaw Mode	0.0000	0.0000
Surge Mode	0.0000	0.0000
Heave Mode	0.0000	0.0000
Sway Mode	0.0000	0.3167
Pitch Mode	0.0000	0.3958
$1^{st}SWBM$	5.5877	5.5438
$1^{st}AWBM$	8.0017	7.9985
$2^{nd}SWBM$	18.7890	18.6923
$2^{nd}AWBM$	21.6824	21.6761
$1^{st}AWTM$	24.0326	23.1266
$1^{st}SWTM$	30.2324	29.5716

**All frequencies are in Hz.

Table 6.19: Frequencies of mAEWing2 v1.1 at 0, 0.5 and 1.0 rad/sec for Angle of Attack 6° for Constrained Vibrations

p rad/sec	0	0.5	1.0
$p°/sec$	0	28.6479	57.296
Roll Mode	0.2376	0.2377	0.23772
Yaw Mode	2.0675	2.0675	2.0674
$1^{st}SWBM$	2.5586	2.5541	2.5493
$2^{nd}SWBM$	6.1540	6.1365	6.1198
$2^{nd}AWBM$	7.9996	7.9993	7.9992
$1^{st}SWTM$	8.7802	8.7762	8.7727
$1^{st}CWBTM$	27.7824	27.7076	27.645

**All frequencies are in Hz.

Table 6.20: Frequencies of mAEWing2 v1.1 at 0 and 0.5 rad/sec for Angle of Attack 8° for F-F Vibrations

p rad/sec	0	0.5
$p°/sec$	0	28.6479
Roll Mode	0.0000	0.0000
Yaw Mode	0.0000	0.0000
Surge Mode	0.0000	0.0000
Heave Mode	0.0000	0.0000
Sway Mode	0.0000	0.3669
Pitch Mode	0.0000	0.4285
$1^{st}SWBM$	5.5877	5.5690
$1^{st}AWBM$	8.0017	7.9977
$2^{nd}SWBM$	18.7890	18.7632
$2^{nd}AWBM$	21.6824	21.6817
$1^{st}AWTM$	24.0326	24.0055
$1^{st}SWTM$	30.2324	30.1941

**All frequencies are in Hz.

Table 6.21: Frequencies of mAEWing2 v1.1 at 0.0 rad/sec, 0.5 rad/sec and 1.0 rad/sec for Angle of Attack 8° for Constrained Vibrations

p rad/sec	0	0.5	1.0
p°/sec	0	28.6479	57.296
Roll Mode	0.2726	0.2726	0.2726
Yaw Mode	2.0628	2.0630	2.063
$1^{st}SWBM$	2.5528	2.5578	2.5578
$2^{nd}SWBM$	6.1315	6.1484	6.1484
$2^{nd}AWBM$	7.9983	7.9985	7.9985
$1^{st}SWTM$	8.7752	8.7789	8.7789
$1^{st}CWBTM$	27.7215	27.7777	27.778

**All frequencies are in Hz.

Chapter 7

Summary and Conclusions

As stated at the start of this thesis, the aim of this thesis is to determine the effects of centrifugal stiffening on the natural frequencies of aircraft in rapid roll maneuvers. The problem of a rotating beam, from which this analysis stems, is a classical problem, as is evident from the literature review in Chapter 2. This includes investigating the modal characteristics like natural frequencies and mode shapes. With this in view, a thorough understanding of the modal analysis of a continuous system is as important as the study of the concept of centrifugal stiffening, discussed in Chapter 3. Based on this study a structured method is employed to analyze the effect of centrifugal stiffening on aircraft in roll maneuver which is explained in Chapter 4. Chapter 5 explains the fem models that are used for the study.

From the discussion of results in Chapter 6, it can be concluded that while the rotation does create stiffening effect in structures, the extent to which it is created is dependent on a number of geometric and operational parameters. In the case of a rotating cantilever beam model, it is seen that the rotational speed as well as the geometric parameters like taper ratio and mass distribution influence the effect of centrifugal stiffening. When compared to the frequencies of a uniform non-rotating cantilever beam, those of a uniform rotating cantilever beam, tapered rotating beam and beam with an added mass, all increase with increasing rotational speeds. The mode shapes are not distinctly affected. The increase in frequencies

of a rotating tapered beam is higher than that of a uniform beam. In beams with added mass, a marginal increase in frequencies is observed with increase in rotation speeds.

In mAEWing2 aircraft, the increase in frequencies observed is negligible for the steady roll maneuver cases studied. In the case of mAEWing2 aircraft, there need to be a number design tests done before considering the effect of stiffening during roll maneuvers. When the frequencies from a stiffening analysis are underestimated, it is suggested to consider the higher values as design values.

In the case of beams as well as mAEWing2, the effect of stiffening on the rigid body modes in the case of free-free vibrations of the structures are also noteworthy.

7.1 Future Scope

These results have answered a lot of questions that were raised at the start of this work, however, they have also generated an equal, if not greater number of questions and paved the way for future work in this field. They have generated a lot more avenues to study, like the effects of stiffening on the buckling strength. It is also important to establish a quantitative study which might be able to establish clear conditions of where underestimation or overestimation of frequencies may be expected.

Bibliography

[1] alephzero (https://physics.stackexchange.com/users/123188/alephzero). Does centrifugal force stiffen a rotating blade? Physics Stack Exchange. URL https://physics.stackexchange.com/q/346207. URL:https://physics.stackexchange.com/q/346207 (version: 2017-07-18).

[2] JR Banerjee. Free Vibration Of Centrifugally Stiffened Uniform And Tapered Beams Using The Dynamic Stiffness Method. *Journal of Sound and Vibration*, 233(5):857–875, 2000.

[3] RB Bhat. Transverse Vibrations Of A Rotating Uniform Cantilever Beam With Tip Mass As Predicted By Using Beam Characteristic Orthogonal Polynomials In The Rayleigh-Ritz Method. *Journal of Sound and Vibration*, 105(2):199–210, 1986.

[4] Ken Blakely. *MSC/NASTRAN Basic Dynamic Analysis: User's Guide, Version 68*. MacNeal-Schwendler, 1993.

[5] K Chandrashekhara, K Krishnamurthy, and Samit Roy. Free Vibration Of Composite Beams Including Rotary Inertia And Shear Deformation. *Composite Structures*, 14(4): 269–279, 1990.

[6] Earl H Dowell, Howard C Curtiss, Robert H Scanlan, and Fernando Sisto. *A Modern Course In Aeroelasticity*, volume 3. Springer, 1989.

[7] CHJ Fox and JS Burdess. The Natural Frequencies Of A Thin Rotating Cantilever With Offset Root. *Journal of Sound and Vibration*, 65(2):151–158, 1979.

[8] T Hacker and C Oprişiu. A Discussion Of The Roll-Coupling Problem. *Progress in aerospace sciences*, 15:151–180, 1974.

[9] S Mohammad Hashemi and Marc J Richard. Free Vibrational Analysis Of Axially Loaded Bending-Torsion Coupled Beams: A Dynamic Finite Element. *Computers & Structures*, 77(6):711–724, 2000.

[10] SM Hashemi, MJ Richard, and G Dhatt. A New Dynamic Finite Element (DFE) Formulation For Lateral Free Vibrations Of Euler–Bernoulli Spinning Beams Using Trigonometric Shape Functions. *Journal of Sound and Vibration*, 220(4):601–624, 1999.

[11] HD Hibbit. Some Follower Forces And Load Stiffness. *International Journal for Numerical Methods in Engineering*, 14(6):937–941, 1979.

[12] Dewey H Hodges. An Approximate Formula For The Fundamental Frequency Of A Uniform Rotating Beam Clamped Off The Axis Of Rotation. *Journal of Sound and Vibration*, 77(1):11–18, 1981.

[13] Dewey H Hodges and G Alvin Pierce. *Introduction To Structural Dynamics And Aeroelasticity*, volume 15. cambridge university press, 2011.

[14] Dewey H Hodges and Michael J Rutkowski. Free-Vibration Analysis Of Rotating Beams By A Variable-Order Finite-Element Method. *American Institute of Aeronautics and Astronautics Journal*, 19:1459–1466, 1981.

[15] DeltaLima (https://physics.stackexchange.com/users/23738/deltalima). Does centrifugal force stiffen a rotating blade? Physics Stack Exchange. URL https://physics.stackexchange.com/q/346170. URL:https://physics.stackexchange.com/q/346170 (version: 2017-07-17).

[16] AMIR Karimi-Nobandegani, S AHMAD Fazelzadeh, and ESMAEAL Ghavanloo. Effect of Uniformly Distributed Tangential Follower Force on the Stability of Rotating Cantilever Tube Conveying Fluid. *Latin American Journal of Solids and Structures*, 13(2): 365–377, 2016.

[17] Anneke Labuschagne, NF Janse van Rensburg, and AJ Van der Merwe. Comparison Of Linear Beam Theories. *Mathematical and Computer Modelling*, 49(1):20–30, 2009.

[18] Jing Li, Jianyun Chen, and Xiaobo Chen. Dynamic Characteristics Analysis Of The Offshore Wind Turbine Blades. *Journal of Marine Science and Application*, 10(1):82, 2011.

[19] Fritz Liebers. Contribution To The Theory Of Propeller Vibrations. 1930.

[20] SC Lin and KM Hsiao. Vibration Analysis Of A Rotating Timoshenko Beam. *Journal of Sound and Vibration*, 240(2):303–322, 2001.

[21] VT Nagaraj. Relationship Between Fundamental Natural Frequency And Maximum Static Deflection For Rotating Timoshenko Beams, 1997.

[22] VT Nagaraj and P Shanthakumar. Rotor Blade Vibrations By The Galerkin Finite Element Method. *Journal of Sound and Vibration*, 43(3):575–577, 1975.

[23] S Naguleswaran. Lateral Vibration Of A Centrifugally Tensioned Uniform Euler-Bernoulli Beam. *Journal of sound and vibration*, 176(5):613–624, 1994.

[24] Nhan T Nguyen and Ilhan Tuzcu. Flight Dynamics Of Flexible Aircraft With Aeroelastic And Inertial Force Interactions. 2009.

[25] FW Niedenfuhr. The Dynamics of Rolling Aircraft. *Journal of the Aerospace Sciences*, 28(2):133–140, 1961.

[26] Jung-Hun Park, Hyun-Yong Park, Seok-Yong Jeong, Sang-Il Lee, Young-Ho Shin, and Jong-Po Park. Linear Vibration Analysis Of Rotating Wind-Turbine Blade. *Current Applied Physics*, 10(2):S332–S334, 2010.

[27] William H Phillips. Effect Of Steady Rolling On Longitudinal And Directional Stability. 1948.

[28] Christopher D Regan. mAEWing2: Conceptual Design and System Test. In *AIAA Atmospheric Flight Mechanics Conference*, page 1391, 2017.

[29] Michael Reymond. *MSC/NASTRAN Quick Reference Guide: Version 68*. MacNeal-Schwendler, 1994.

[30] William P Rodden and Erwin H Johnson. *MSC/NASTRAN Aeroelastic Analysis: User's Guide; Version 68*. MacNeal-Schwendler Corporation, 1994.

[31] M Schilhansl. Bending Frequency Of A Rotating Cantilever Beam. *Journal of Applied Mechanics*, 25(1), 1958.

[32] Edward Seckel. *Stability And Control Of Airplanes And Helicopters*. Academic Press, 2014.

[33] BB Sharma. Stiffening Effect Of Centrifugal Force On Fundamental Frequency Of Coupled Vibration Of A Rotating Slender Beam Under Aerodynamic Couplings. *Indian National Science Academy*, 1972.

[34] Richard V Southwell and Barbara S Gough. *On The Free Transverse Vibrations Of Airscrew Blades*. HM Stationery Office, 1922.

[35] D Storti and Y Aboelnaga. Bending Vibrations Of A Class Of Rotating Beams With Hypergeometric Solutions. *Journal of Applied Mechanics*, 54(2):311–314, 1987.

[36] Theodore Theodorsen. Propeller Vibrations And The Effect Of The Centrifugal Force. 1935.

[37] Lawrence N Virgin. *Vibration Of Axially-Loaded Structures*. Cambridge University Press, 2007.

[38] AD Wright, CE Smith, RW Thresher, and JLC Wang. Vibration Modes Of Centrifugally Stiffened Beams. *Journal of applied mechanics*, 49(1):197–202, 1982.

[39] HH Yoo and SH Shin. Vibration Analysis Of Rotating Cantilever Beams. *Journal of Sound and vibration*, 212(5):807–828, 1998.

[40] Hong Hee Yoo, Jung Hun Park, and Janghyun Park. Vibration Analysis Of Rotating Pre-Twisted Blades. *Computers & Structures*, 79(19):1811–1819, 2001.

[41] Wei Zhao, Mohamed Jrad, Rikin Gupta, and Rakesh K Kapania. Multidisciplinary Design Analysis and Optimization of Performance Adaptive Aeroelastic Wings. In *Proceedings of the AIAA SciTech Conference*, pages 9–13, 2017.

Appendices

Appendix A

A.1 Mode shapes of Non-rotating F-F Uniform Beam

A.2 Mode shapes of Rotating F-F Uniform Beam

A.3 Mode shapes of Non-rotating C-F Uniform Beam

A.4 Mode shapes of Rotating C-F Uniform Beam

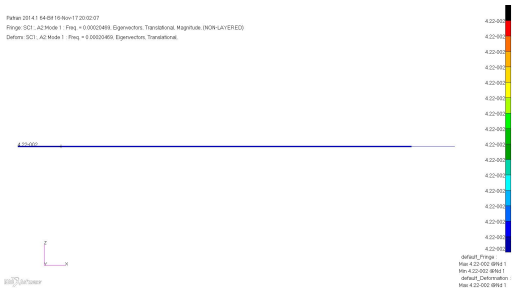

(a) Mode 1

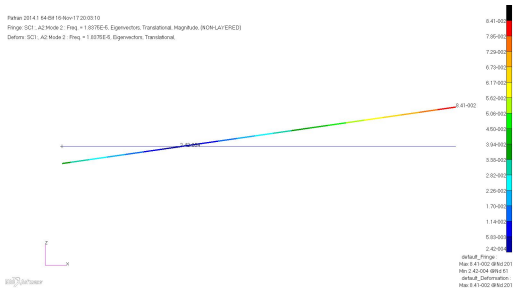

(b) Mode 2

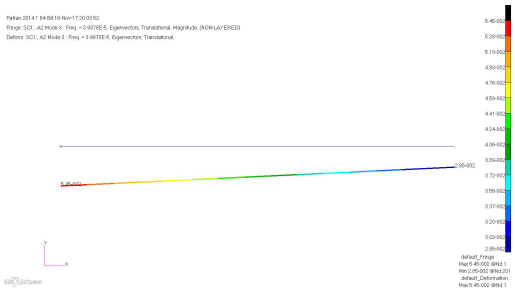

(c) Mode 3

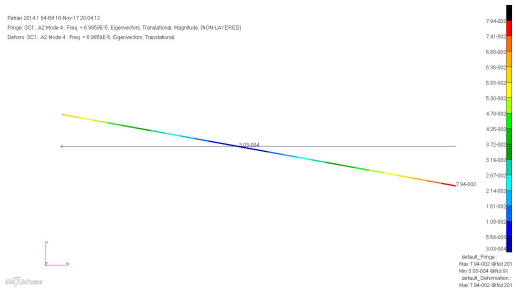

(d) Mode 4

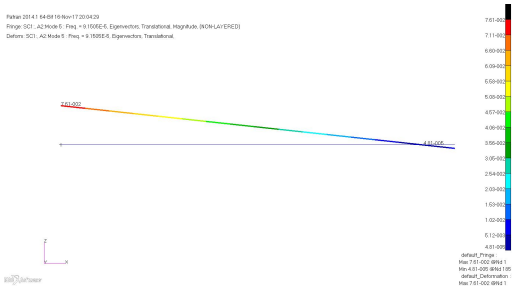

(e) Mode 5

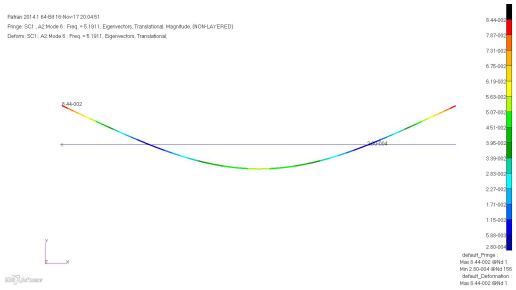

(f) Mode 6

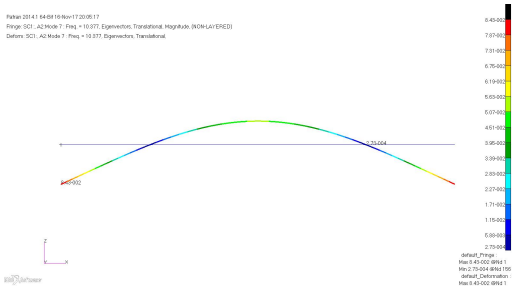

(g) Mode 7

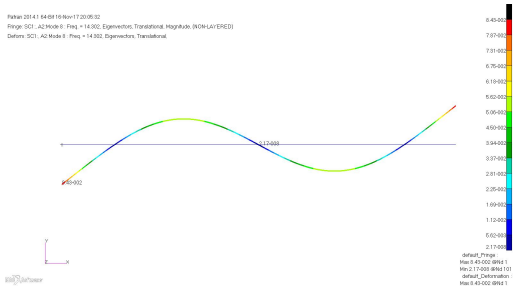

(h) Mode 8

Figure A.1: Mode shapes for the Modes 1 to 8 of a Uniform F-F Beam

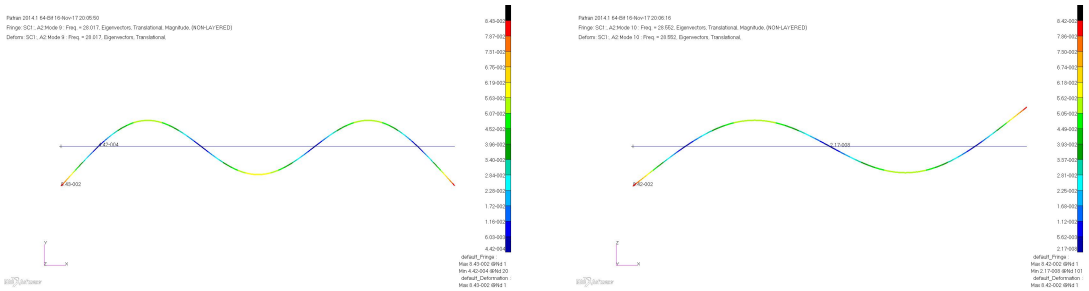

(a) Mode 9

(b) Mode 10

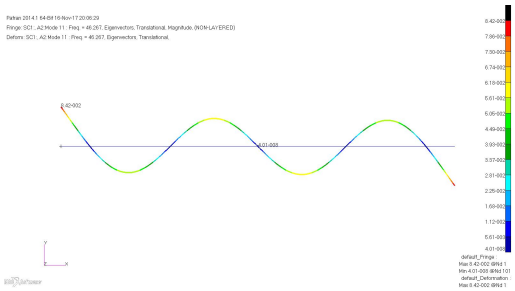

(c) Mode 11

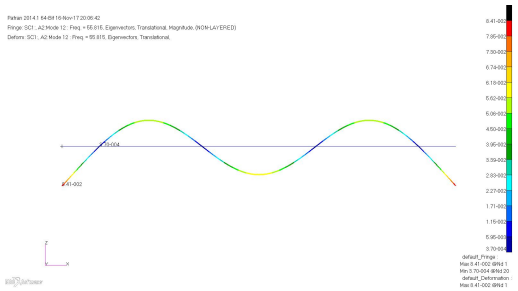

(d) Mode 12

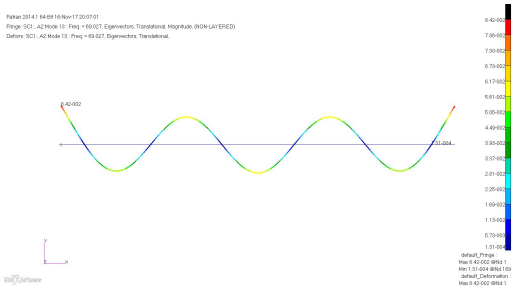

(e) Mode 13

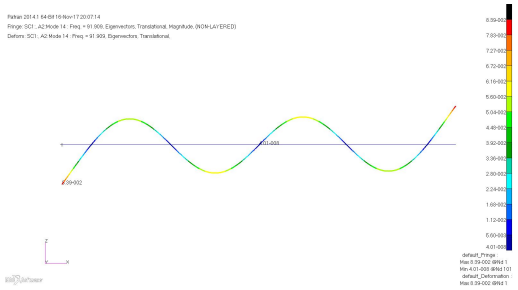

(f) Mode 14

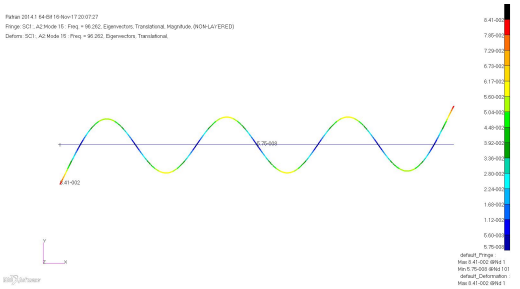

(g) Mode 15

Figure A.2: Mode shapes for the Modes 9 to 15 of a Uniform F-F Beam

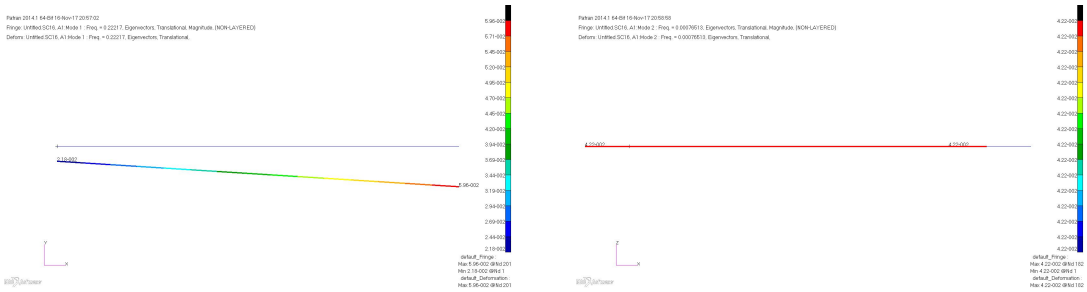

(a) Mode 1

(b) Mode 2

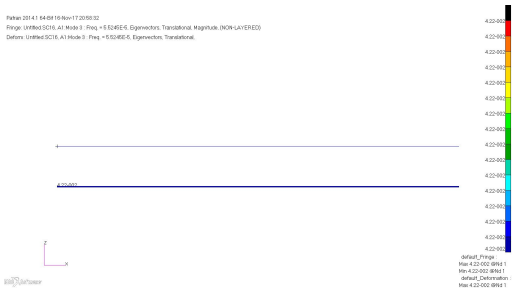

(c) Mode 3

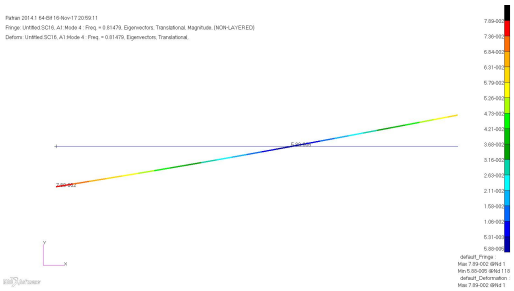

(d) Mode 4

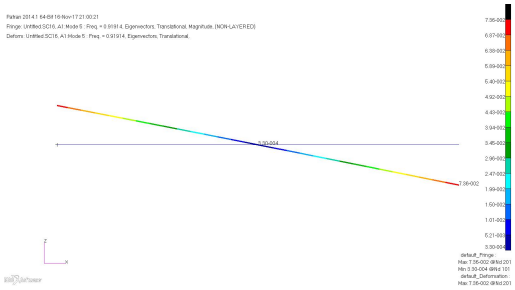

(e) Mode 5

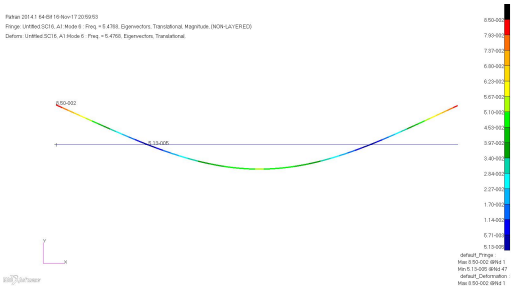

(f) Mode 6

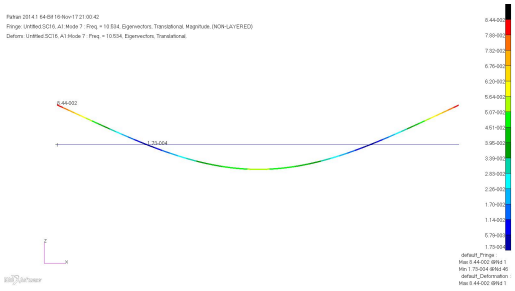

(g) Mode 5

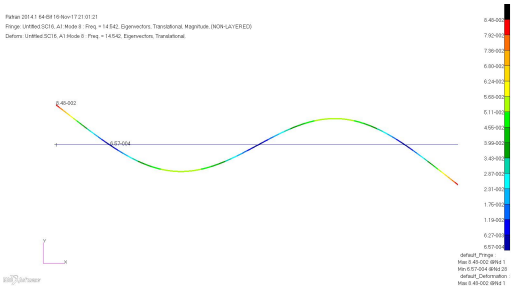

(h) Mode 6

Figure A.3: Mode shapes for the Modes 1 to 8 of a Uniform F-F Rotating Beam with $\eta = 1$

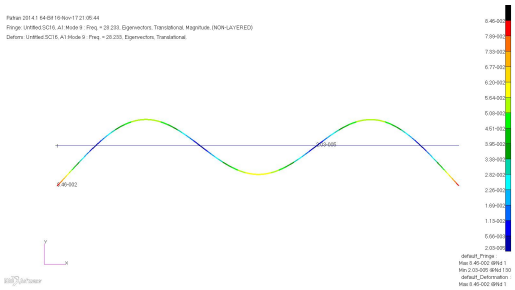

(a) Mode 7

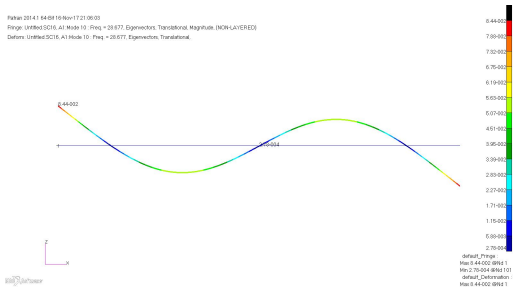

(b) Mode 8

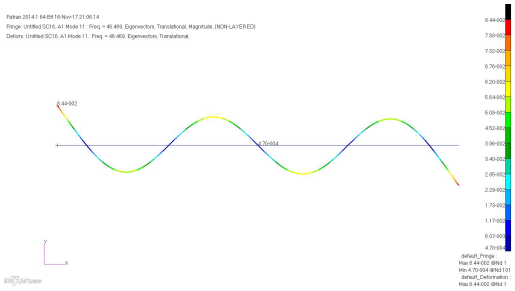

(c) Mode 9

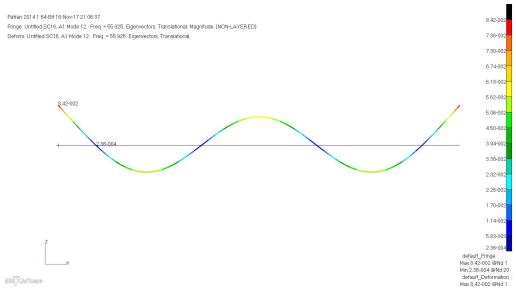

(d) Mode 10

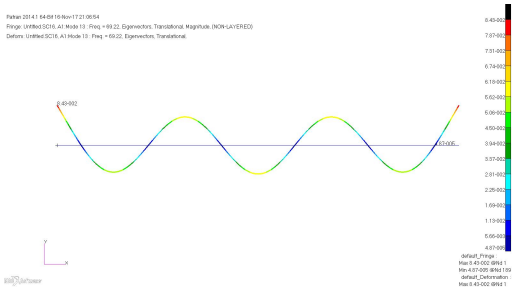

(e) Mode 11

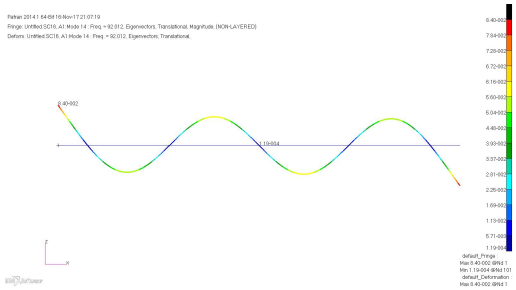

(f) Mode 12

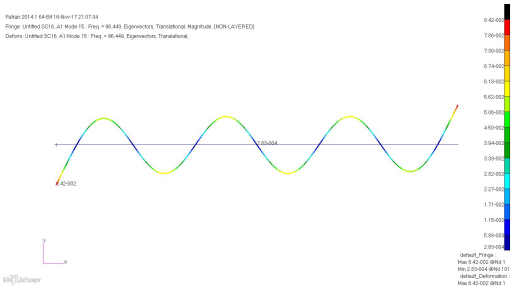

(g) Mode 11

Figure A.4: Mode shapes for the Modes 9 to 15 of a Uniform F-F Rotating Beam with $\eta = 1$

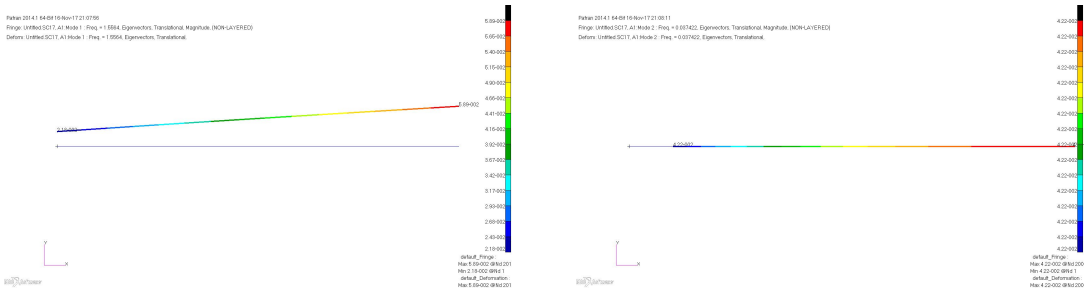

(a) Mode 1

(b) Mode 2

(c) Mode 3

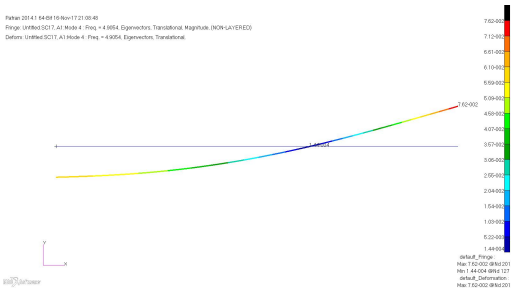

(d) Mode 4

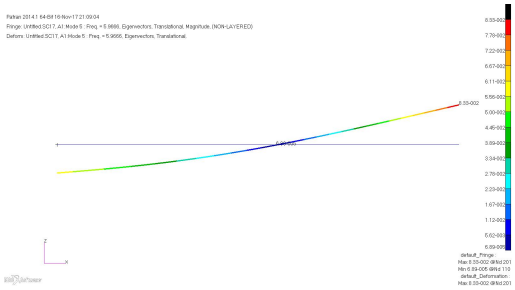

(e) Mode 5

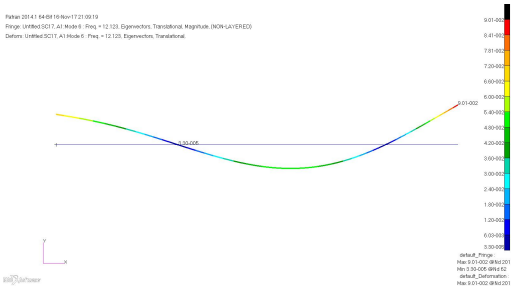

(f) Mode 6

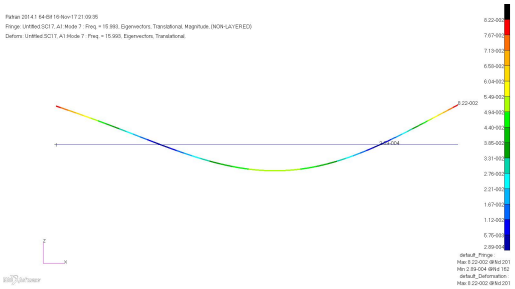

(g) Mode 6

Figure A.5: Mode shapes for the Modes 1 to 7 of a Uniform F-F Rotating Beam with $\eta = 7$

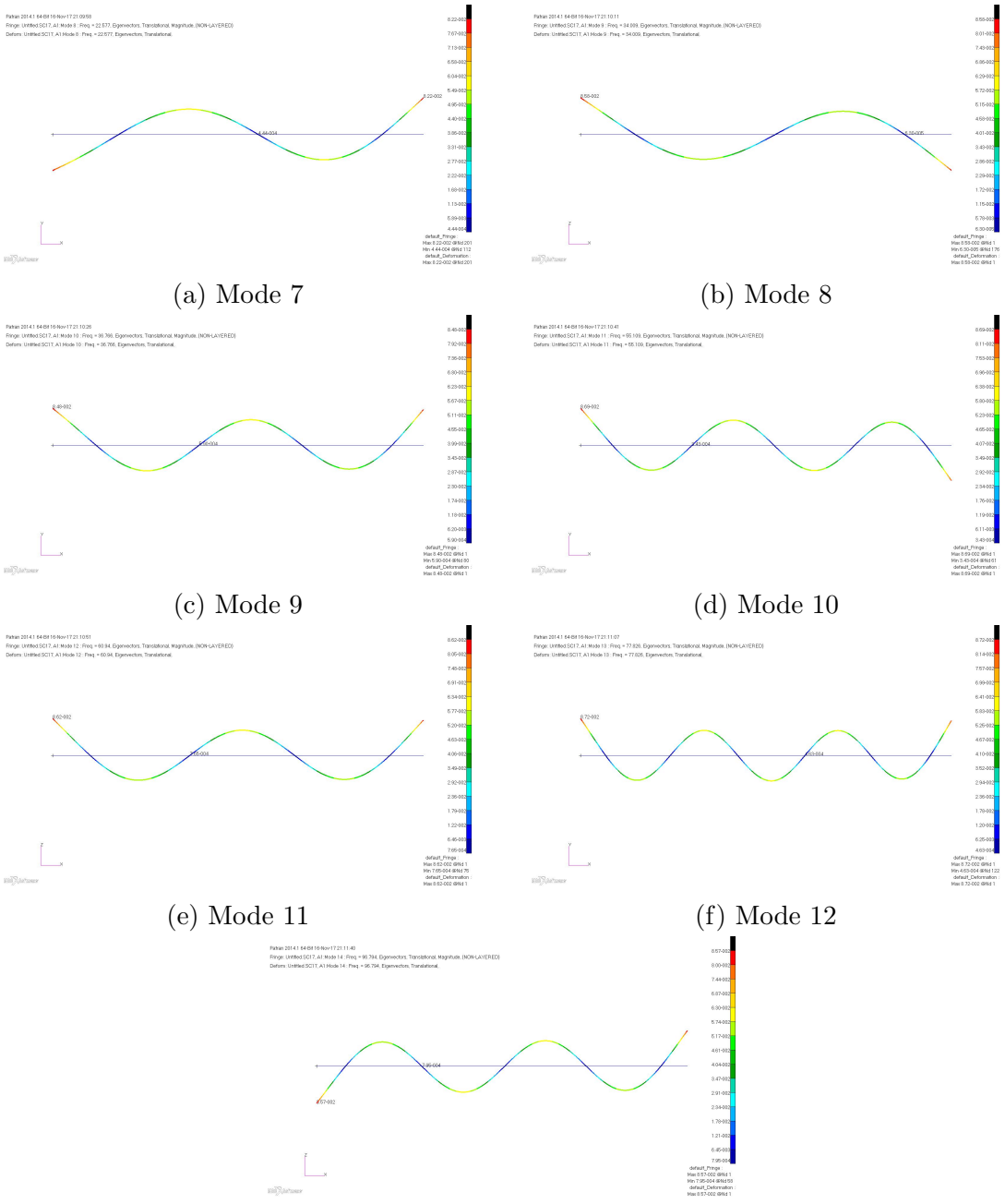

(a) Mode 7

(b) Mode 8

(c) Mode 9

(d) Mode 10

(e) Mode 11

(f) Mode 12

(g) Mode 12

Figure A.6: Mode shapes for the Modes 8 to 14 of a Uniform F-F Rotating Beam with $\eta = 7$

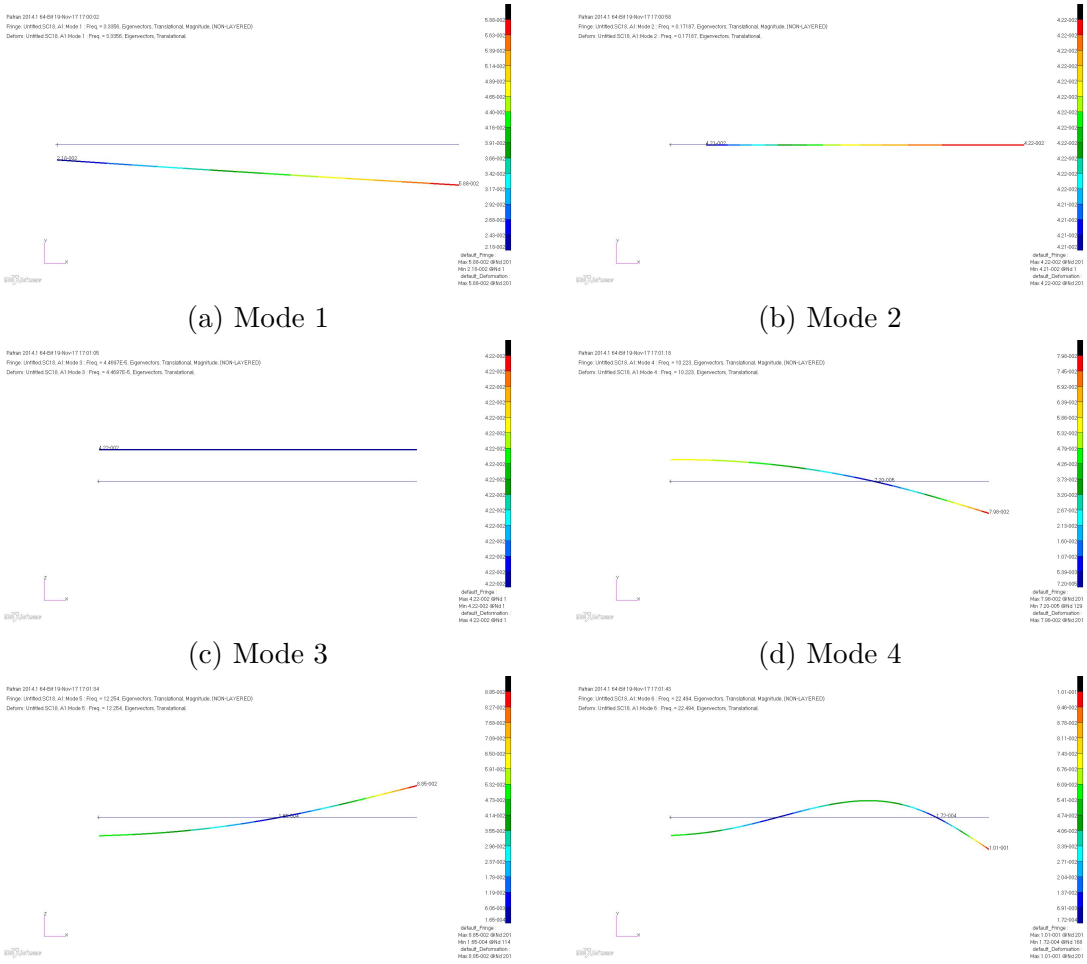

(a) Mode 1

(b) Mode 2

(c) Mode 3

(d) Mode 4

(e) Mode 5

(f) Mode 6

Figure A.7: Mode shapes for the Modes 1 to 6 of a Uniform F-F Rotating Beam with $\eta = 15$

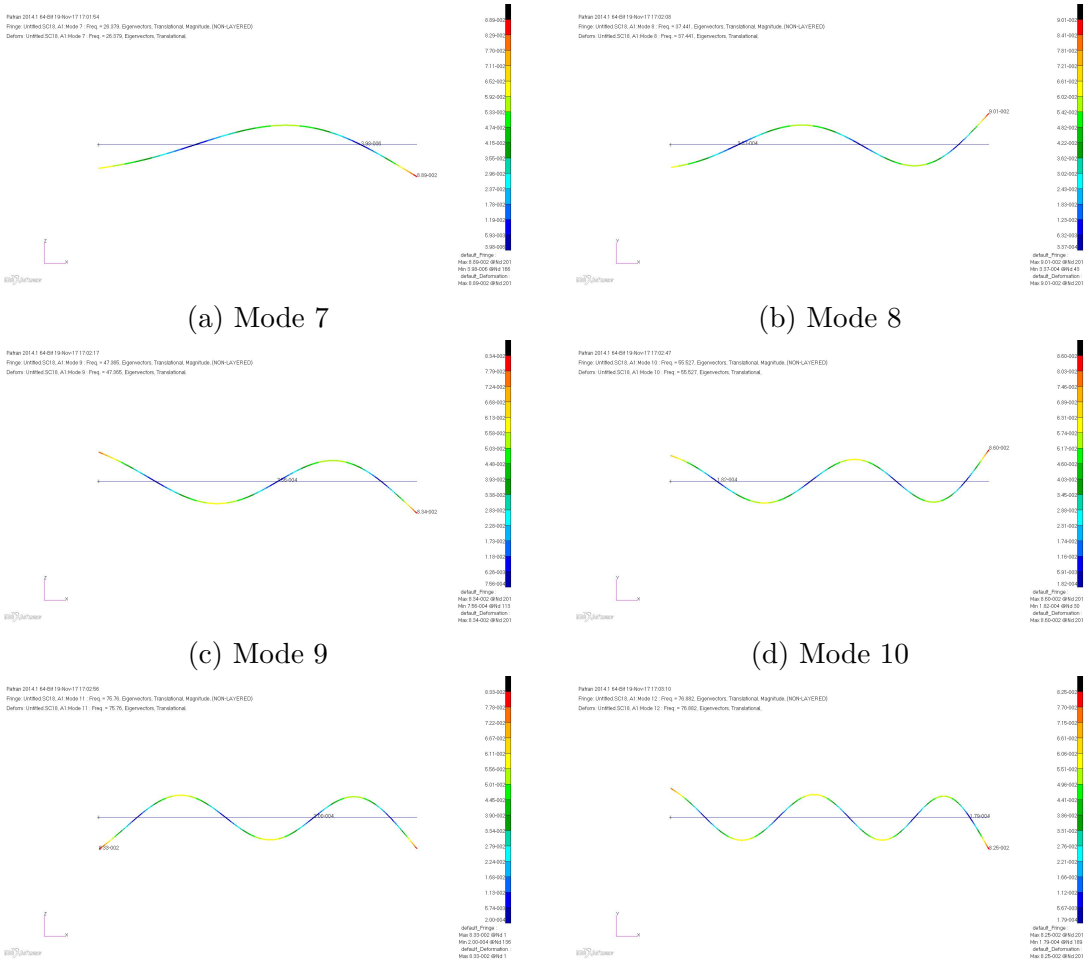

(a) Mode 7

(b) Mode 8

(c) Mode 9

(d) Mode 10

(e) Mode 11

(f) Mode 12

Figure A.8: Mode shapes for the Modes 7 to 12 of a Uniform F-F Rotating Beam with $\eta = 15$

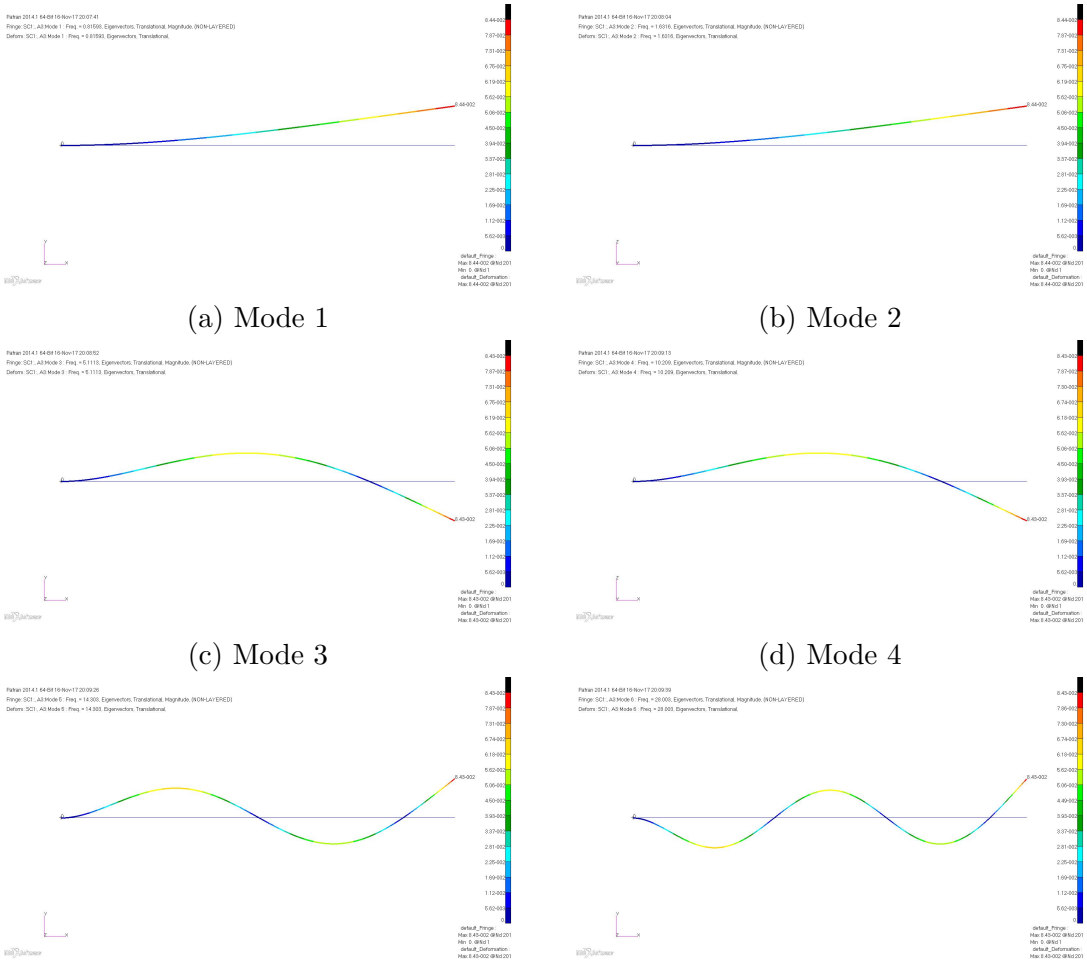

(a) Mode 1

(b) Mode 2

(c) Mode 3

(d) Mode 4

(e) Mode 5

(f) Mode 6

Figure A.9: Mode shapes for the Modes 1 to 6 of a Uniform C-F Beam

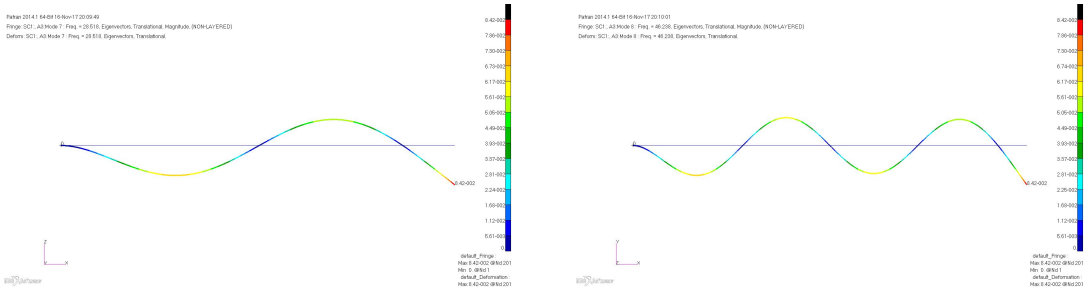

(a) Mode 7 (b) Mode 8

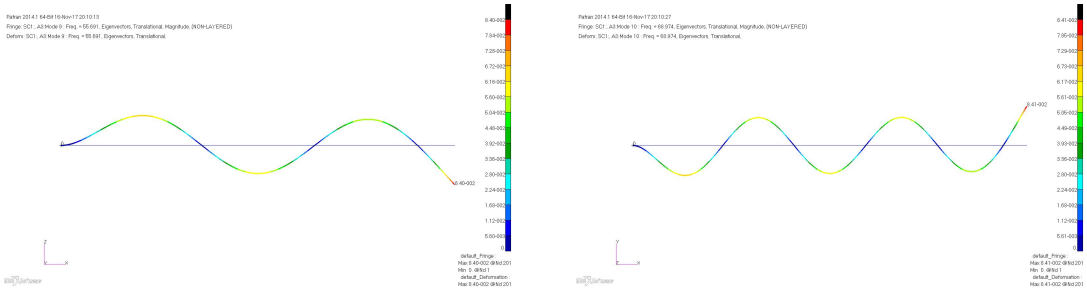

(c) Mode 9 (d) Mode 10

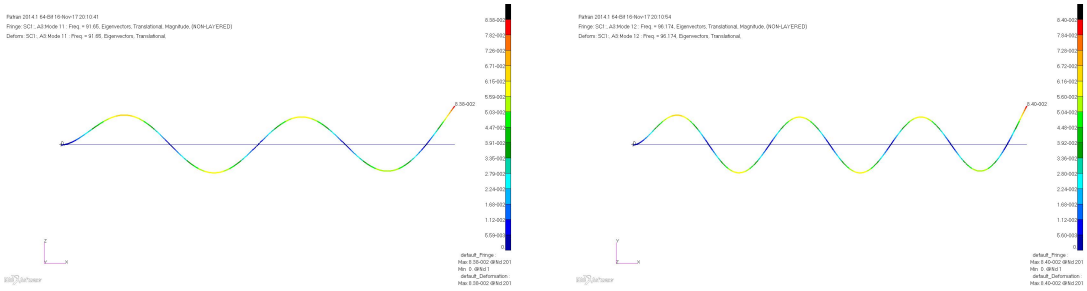

(e) Mode 11 (f) Mode 12

Figure A.10: Mode shapes for the Modes 7 to 12 of a Uniform C-F Beam

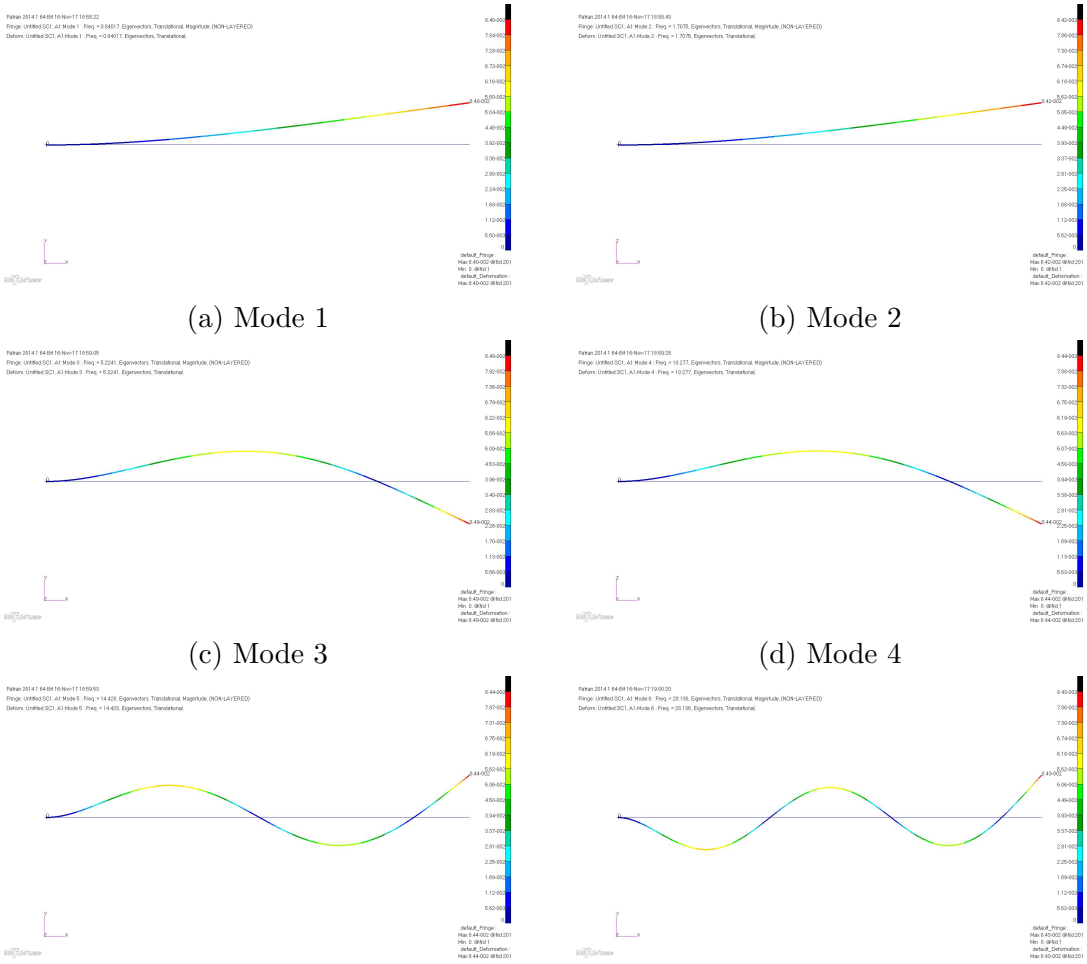

(a) Mode 1

(b) Mode 2

(c) Mode 3

(d) Mode 4

(e) Mode 5

(f) Mode 6

Figure A.11: Mode shapes for the Modes 1 to 6 of a Uniform C-F Rotating Beam with $\eta = 1$

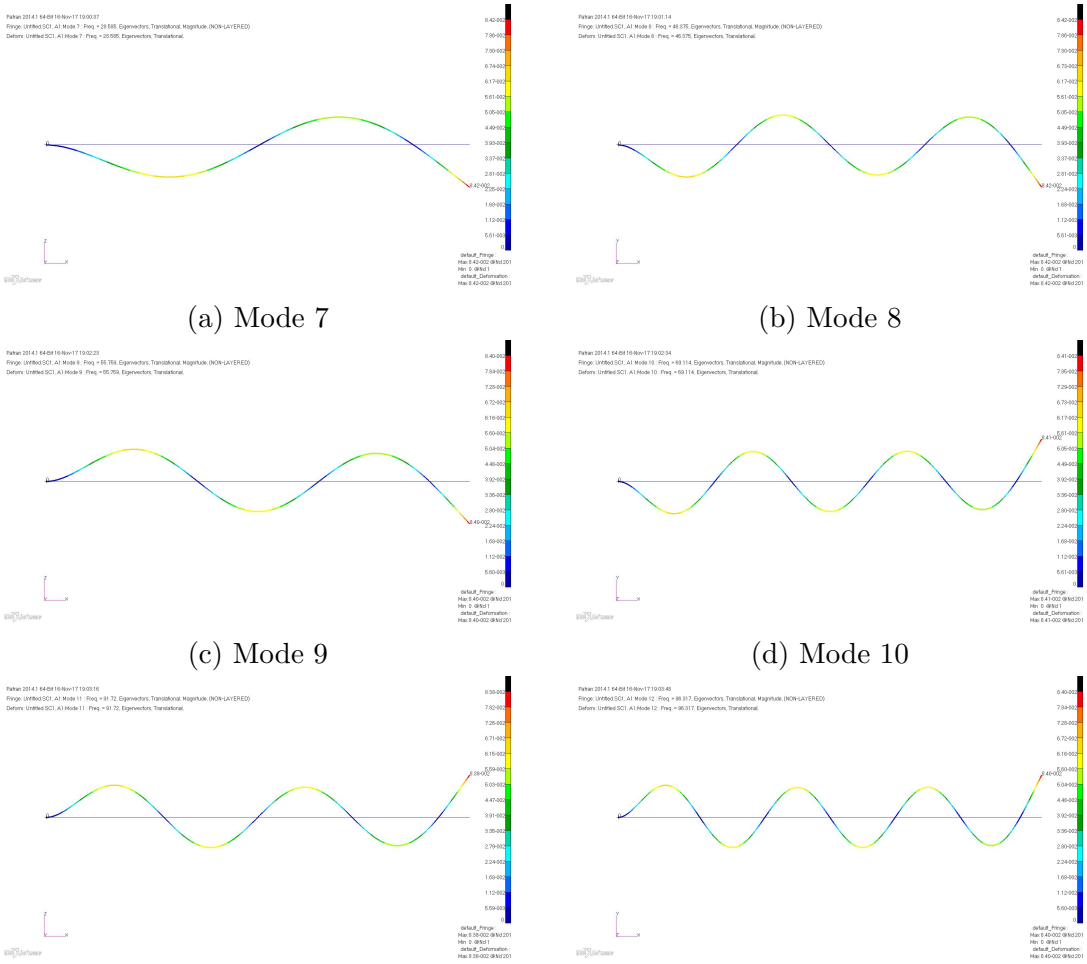

(a) Mode 7

(b) Mode 8

(c) Mode 9

(d) Mode 10

(e) Mode 11

(f) Mode 12

Figure A.12: Mode shapes for the Modes 7 to 12 of a Uniform C-F Rotating Beam with $\eta = 1$

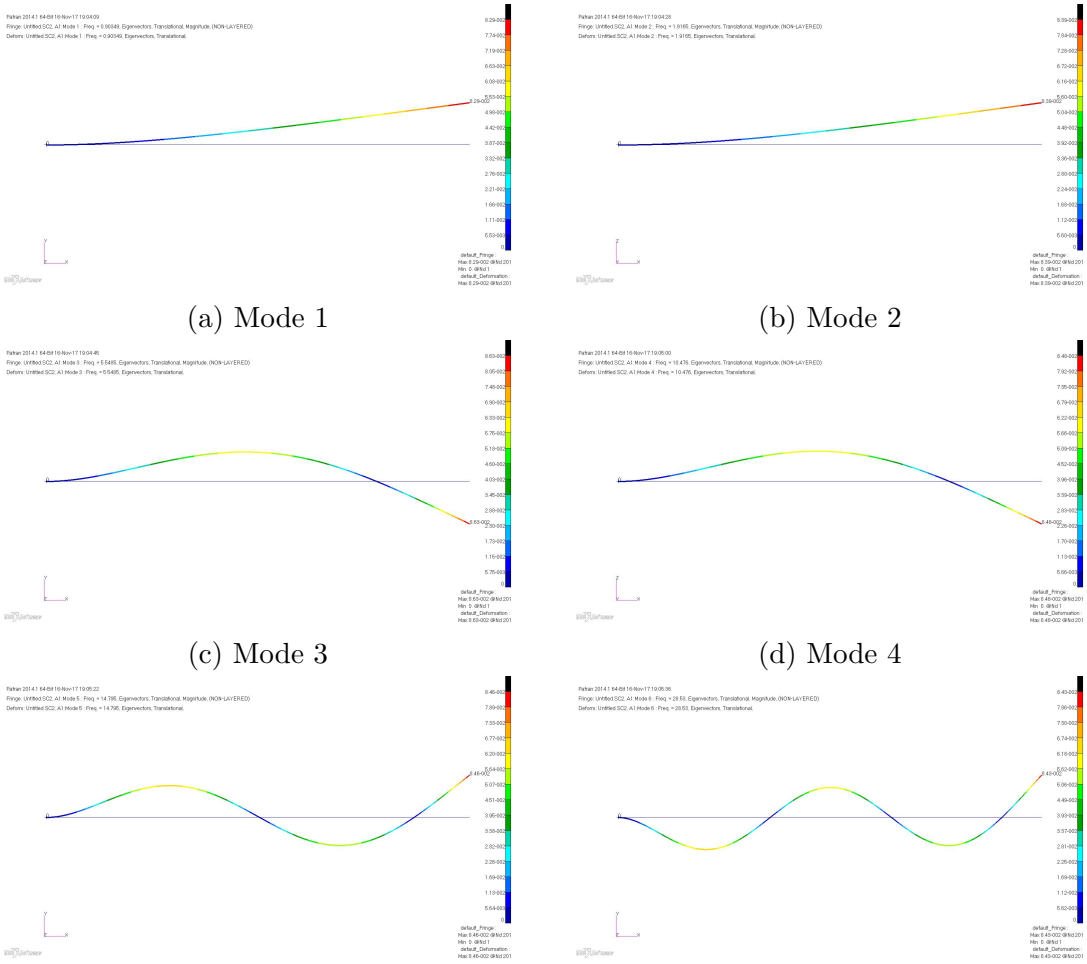

(a) Mode 1

(b) Mode 2

(c) Mode 3

(d) Mode 4

(e) Mode 5

(f) Mode 6

Figure A.13: Mode shapes for the Modes 1 to 6 of a Uniform C-F Rotating Beam with $\eta = 1$

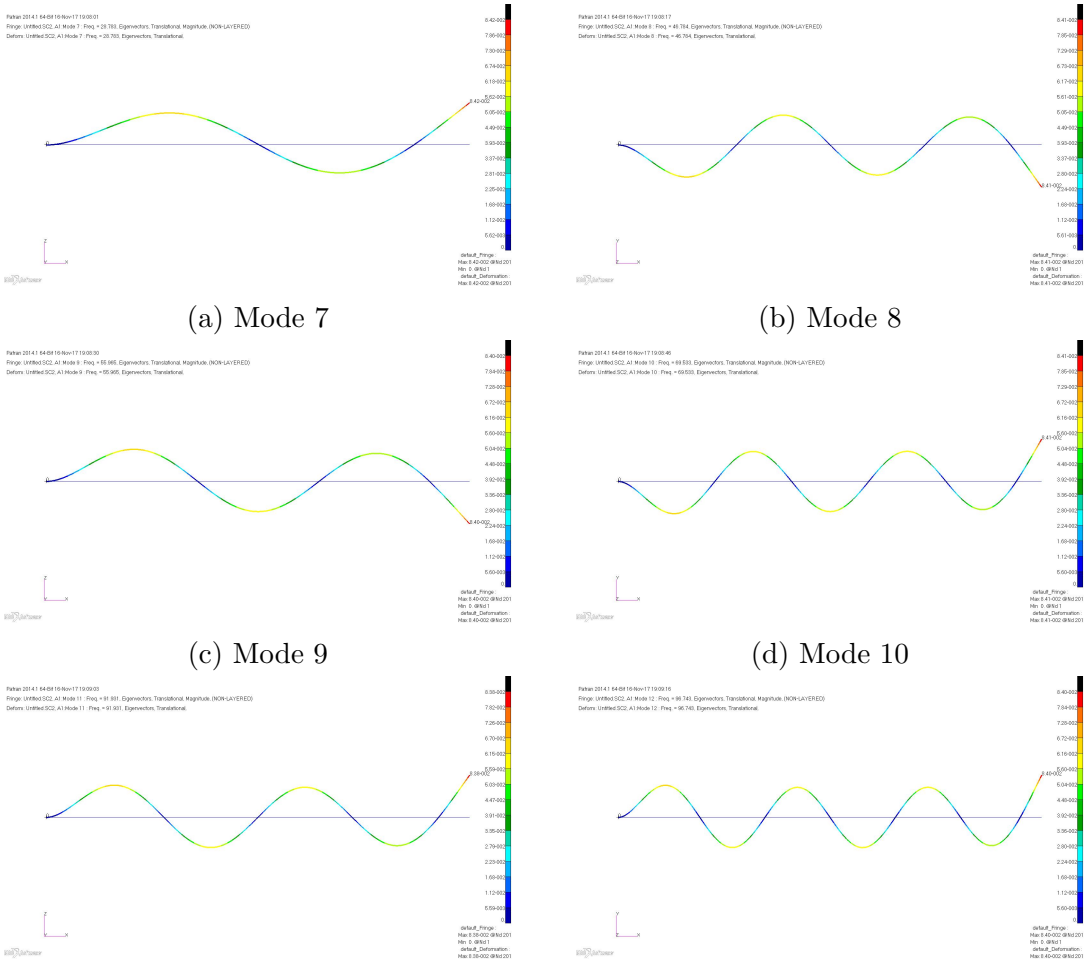

(a) Mode 7

(b) Mode 8

(c) Mode 9

(d) Mode 10

(e) Mode 11

(f) Mode 12

Figure A.14: Mode shapes for the Modes 7 to 12 of a Uniform C-F Rotating Beam with $\eta = 2$

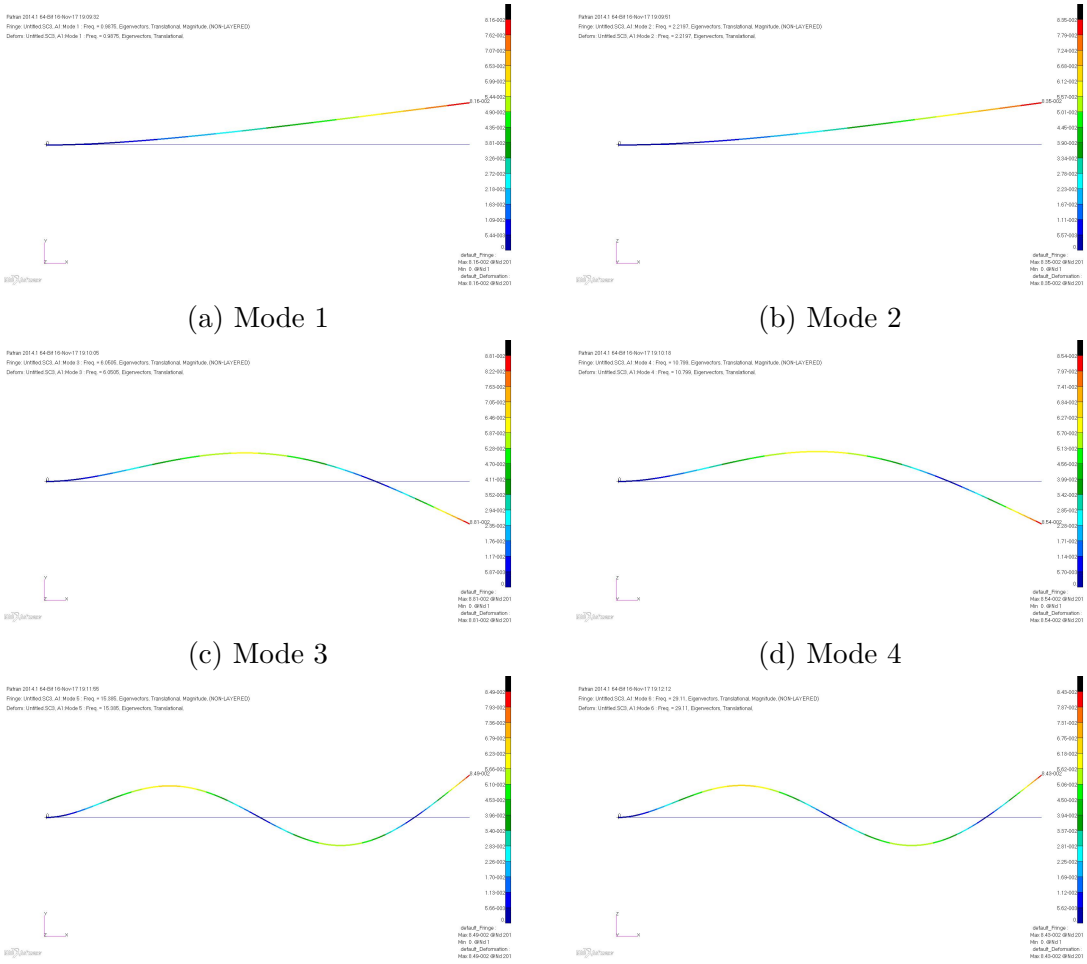

(a) Mode 1

(b) Mode 2

(c) Mode 3

(d) Mode 4

(e) Mode 5

(f) Mode 6

Figure A.15: Mode shapes for the Modes 1 to 6 of a Uniform C-F Rotating Beam with $\eta = 3$

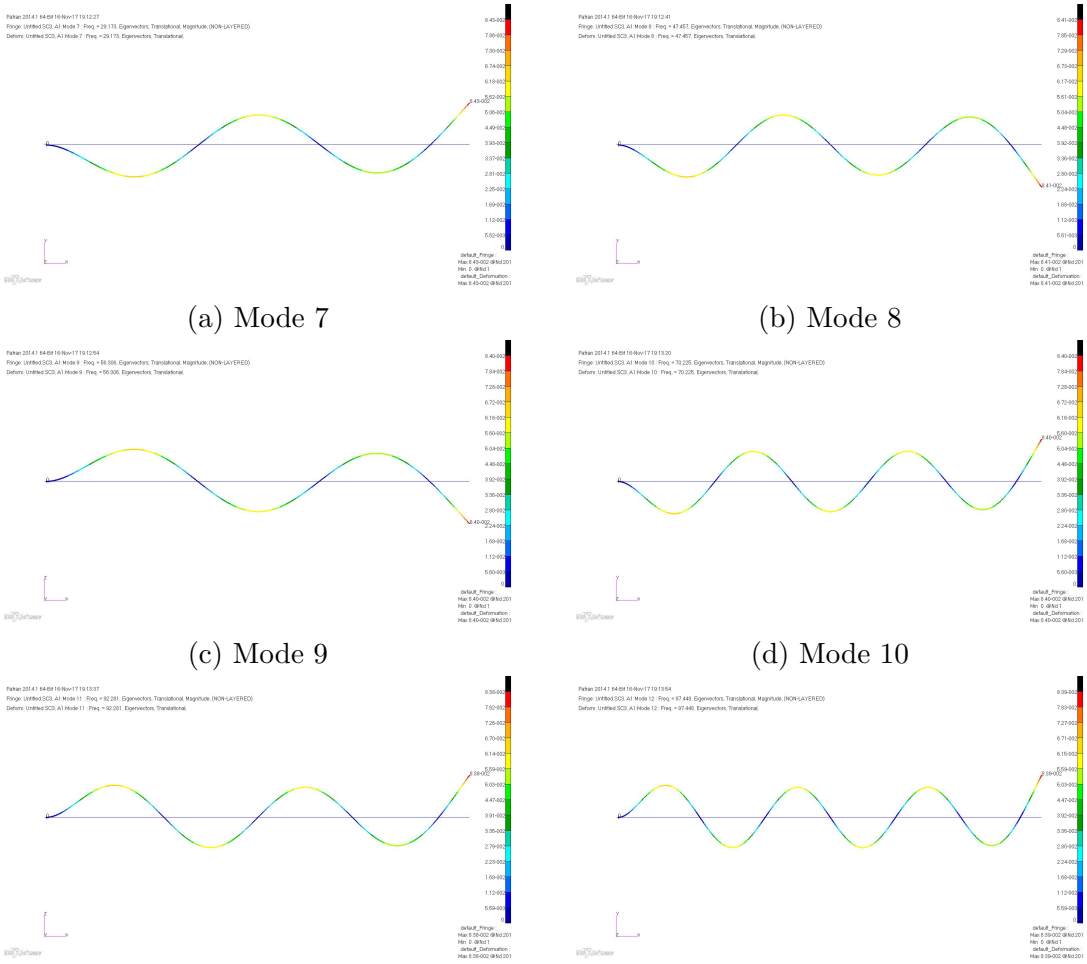

(a) Mode 7

(b) Mode 8

(c) Mode 9

(d) Mode 10

(e) Mode 11

(f) Mode 12

Figure A.16: Mode shapes for the Modes 7 to 12 of a Uniform C-F Rotating Beam with $\eta = 3$

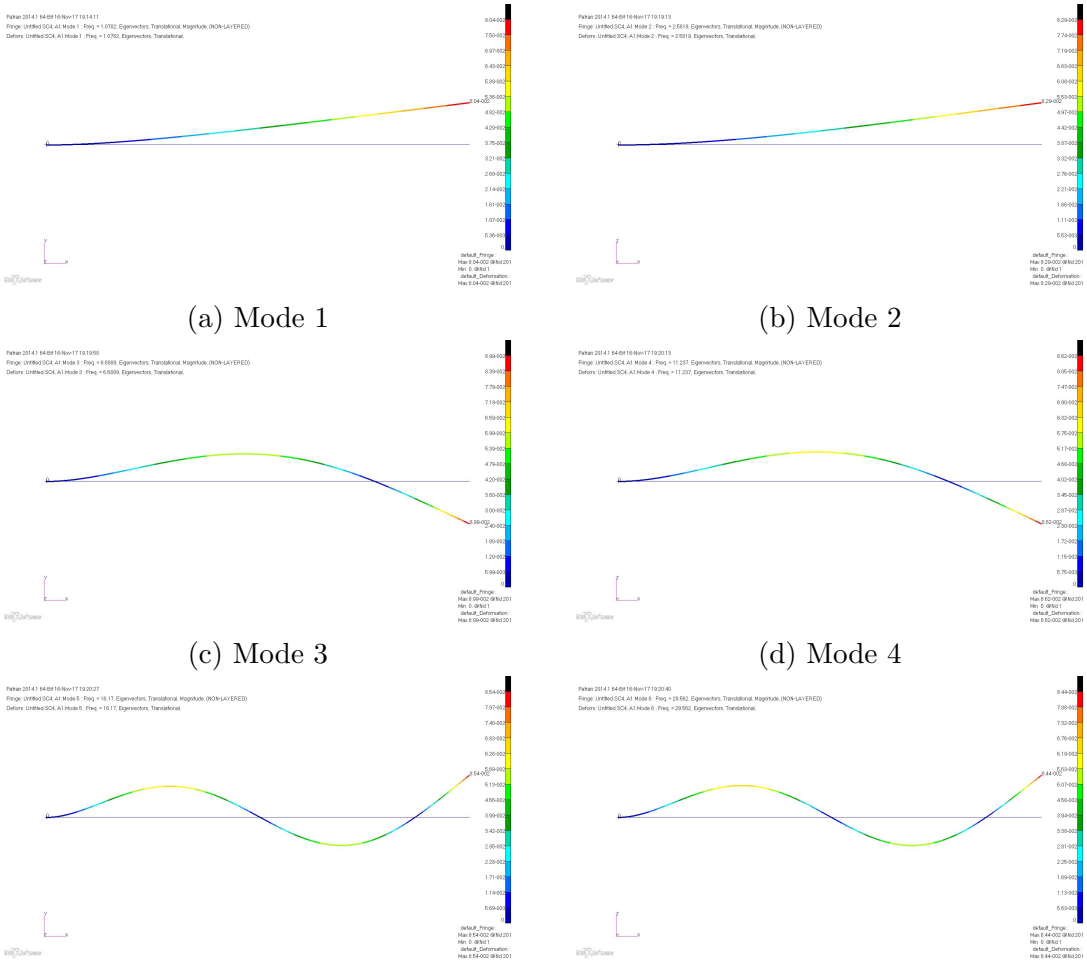

(a) Mode 1

(b) Mode 2

(c) Mode 3

(d) Mode 4

(e) Mode 5

(f) Mode 6

Figure A.17: Mode shapes for the Modes 1 to 6 of a Uniform C-F Rotating Beam with $\eta = 4$

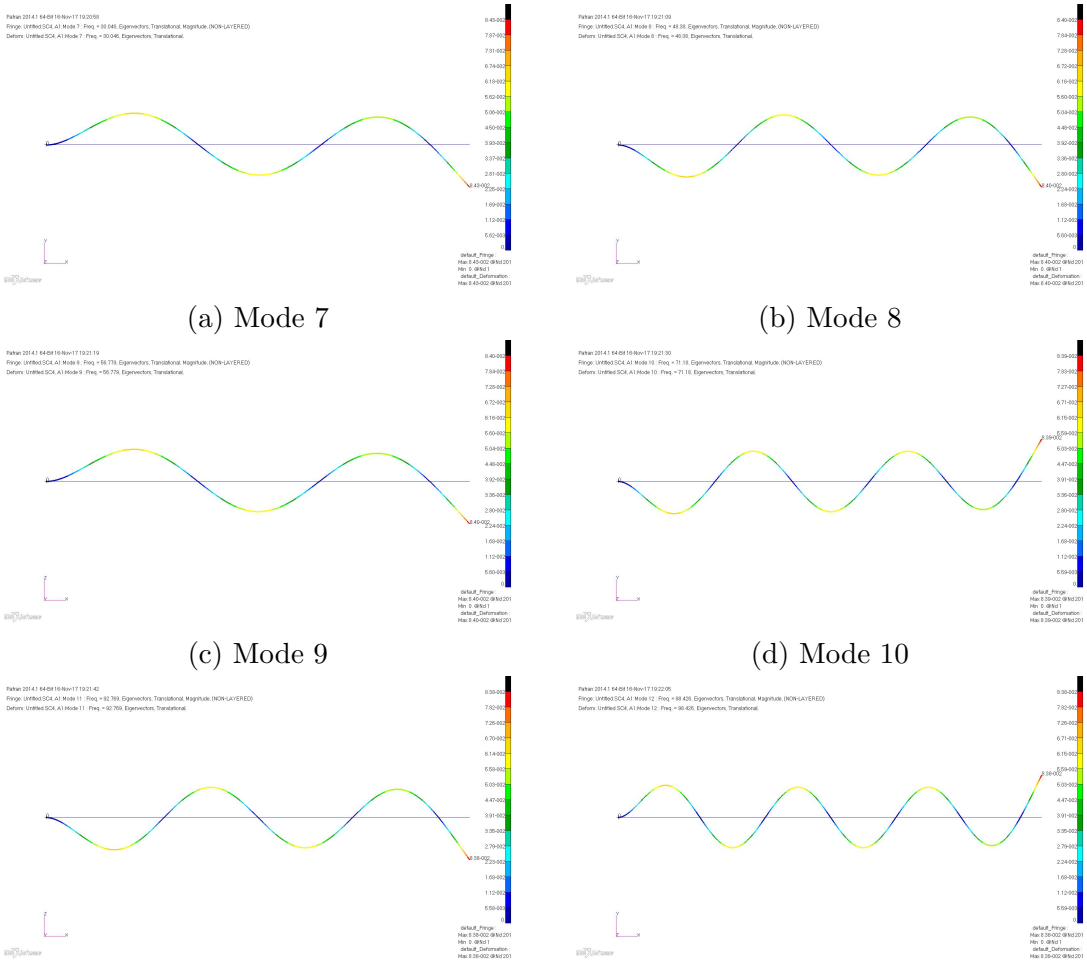

(a) Mode 7

(b) Mode 8

(c) Mode 9

(d) Mode 10

(e) Mode 11

(f) Mode 12

Figure A.18: Mode shapes for the Modes 7 to 12 of a uniform C-F Rotating Beam with $\eta = 4$

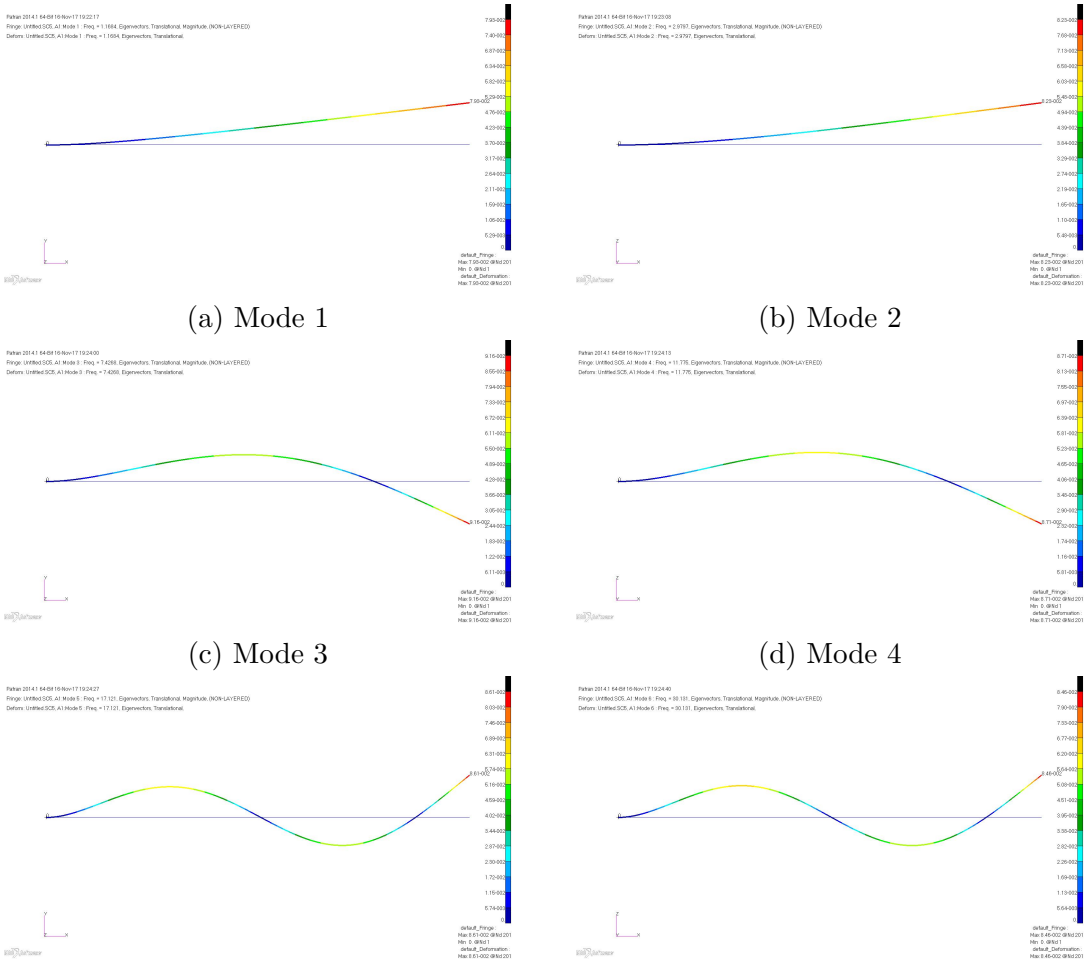

(a) Mode 1

(b) Mode 2

(c) Mode 3

(d) Mode 4

(e) Mode 5

(f) Mode 6

Figure A.19: Mode shapes for the Modes 1 to 6 of a Uniform C-F Rotating Beam with $\eta = 5$

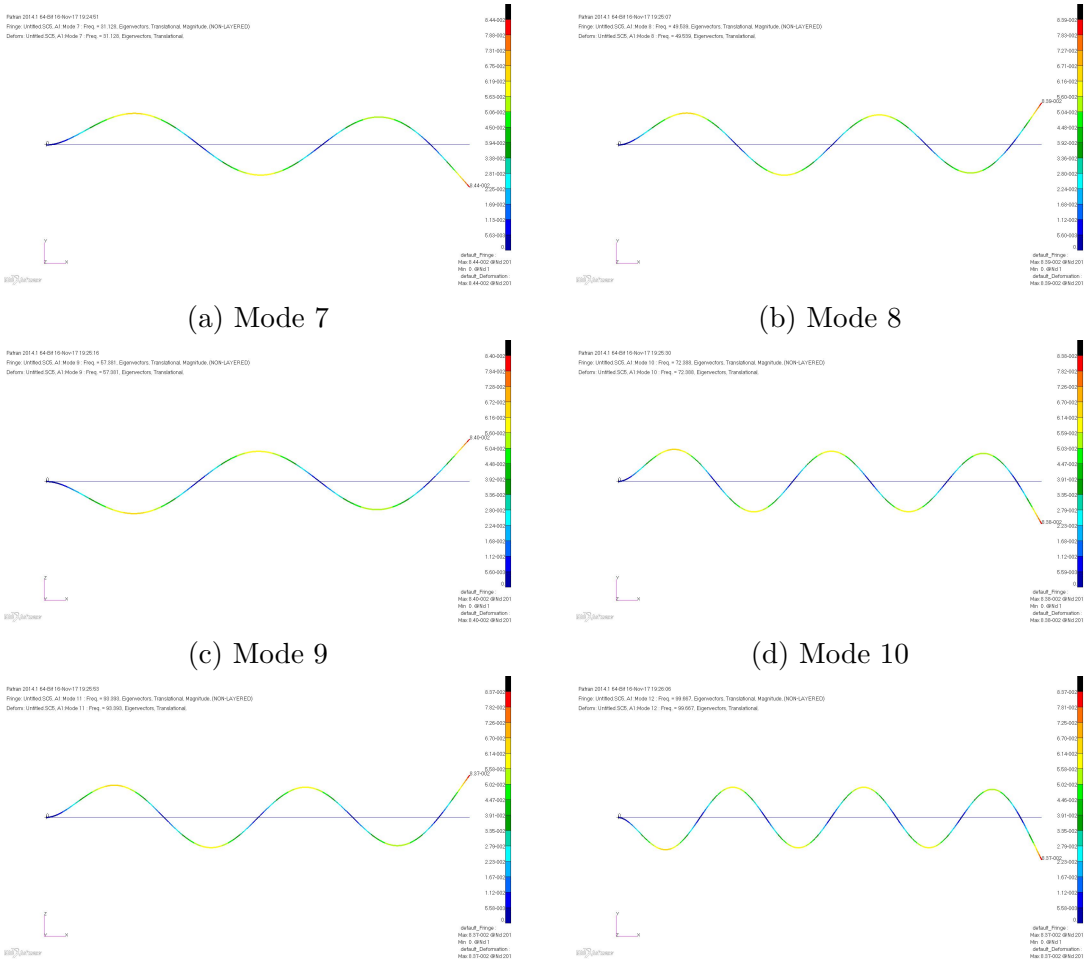

(a) Mode 7

(b) Mode 8

(c) Mode 9

(d) Mode 10

(e) Mode 11

(f) Mode 12

Figure A.20: Mode shapes for the Modes 7 to 12 of a Uniform C-F Rotating Beam with $\eta = 5$

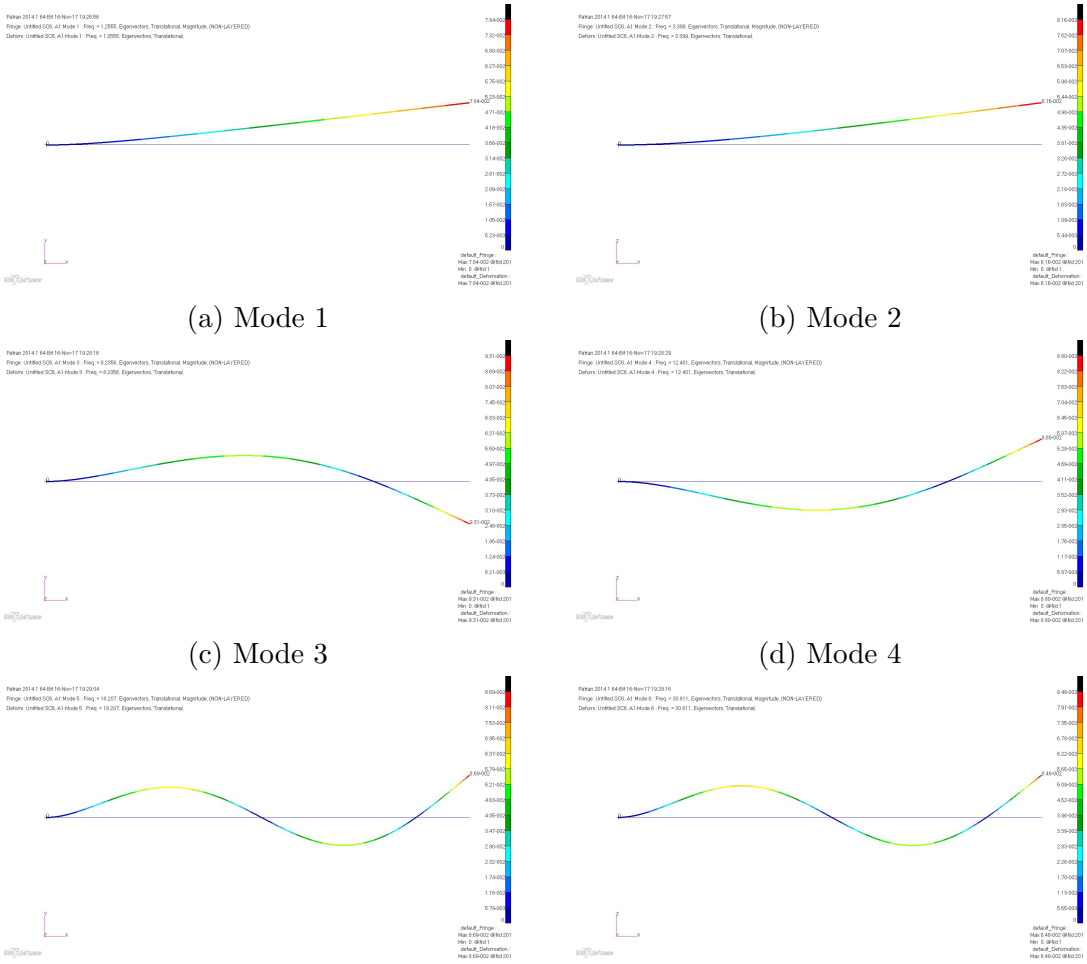

(a) Mode 1

(b) Mode 2

(c) Mode 3

(d) Mode 4

(e) Mode 5

(f) Mode 6

Figure A.21: Mode shapes for the Modes 1 to 6 of a Uniform C-F Rotating Beam with $\eta = 6$

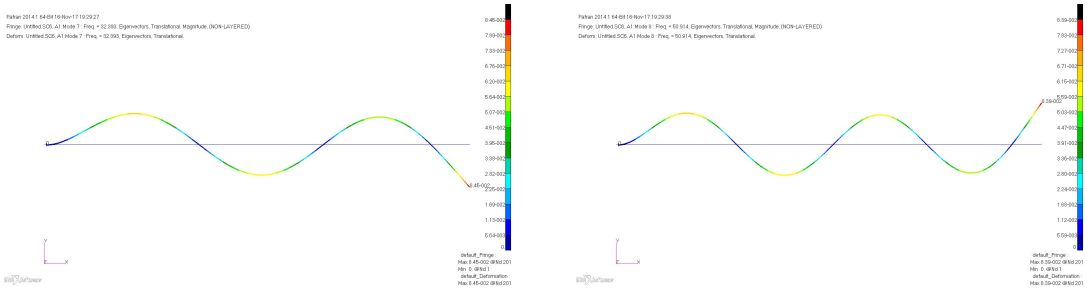

(a) Mode 7

(b) Mode 8

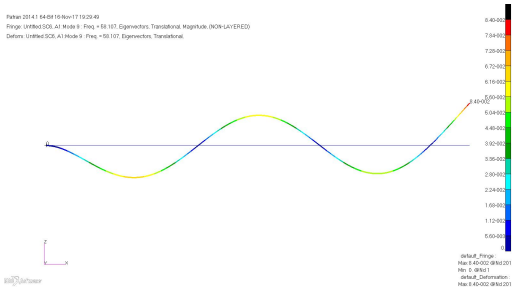

(c) Mode 9

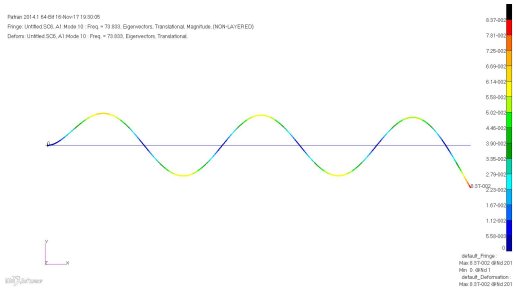

(d) Mode 10

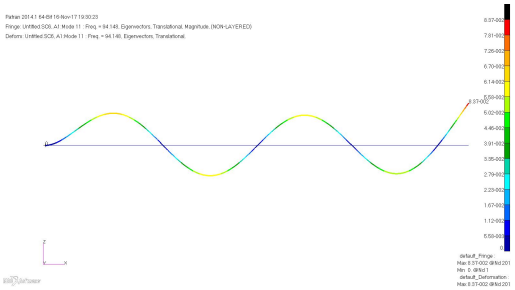

(e) Mode 11

Figure A.22: Mode shapes for the Modes 7 to 11 of a Uniform C-F Rotating Beam with $\eta = 6$

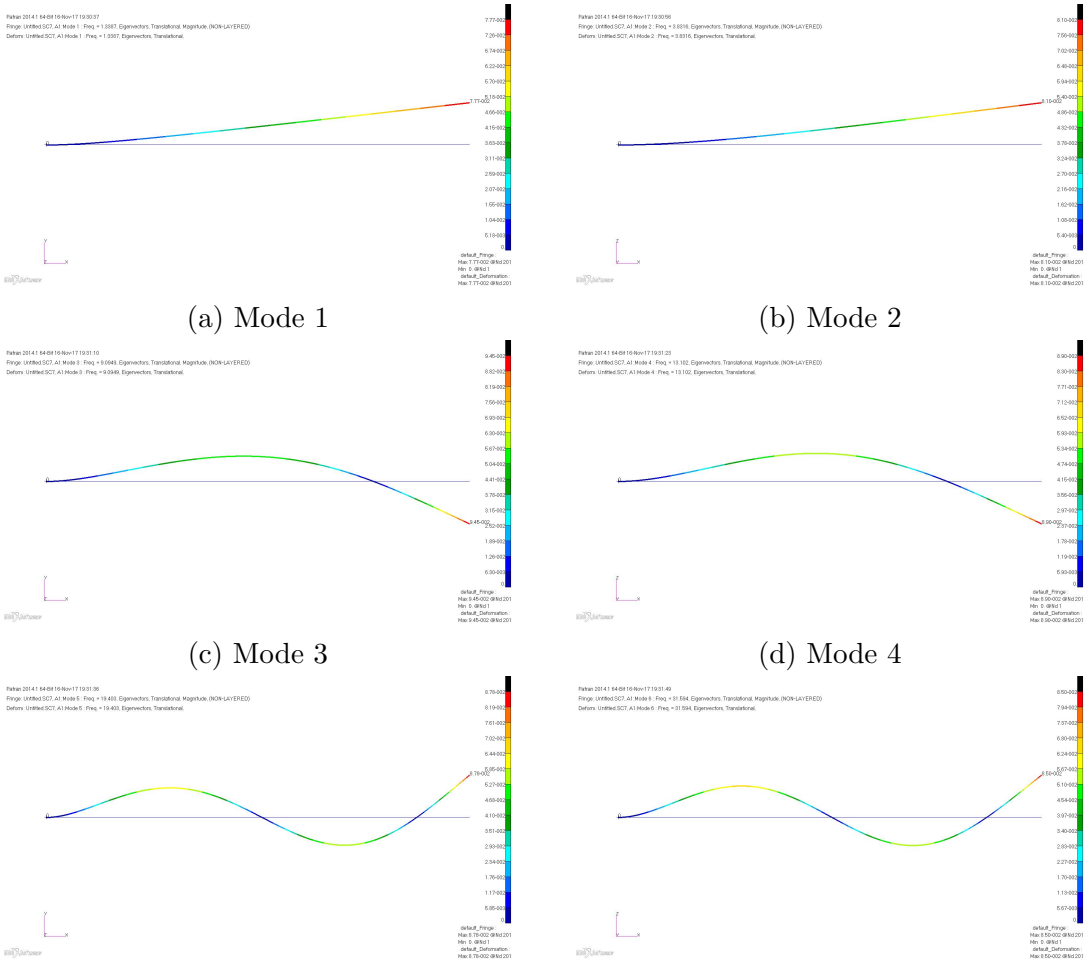

(a) Mode 1

(b) Mode 2

(c) Mode 3

(d) Mode 4

(e) Mode 5

(f) Mode 6

Figure A.23: Mode shapes for the Modes 1 to 6 of a Uniform C-F Rotating Beam with $\eta = 7$

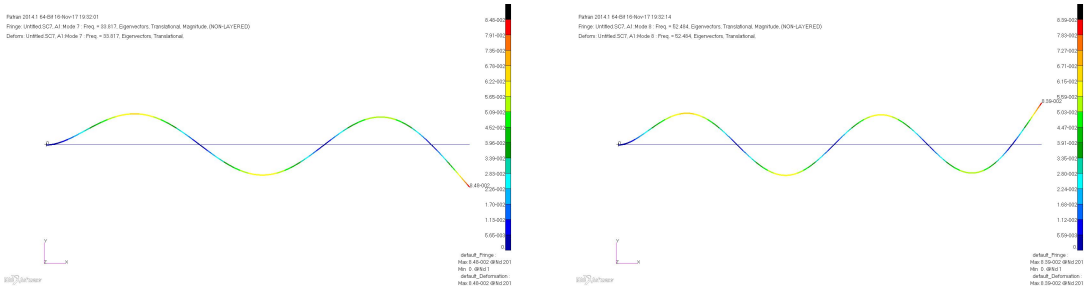

(a) Mode 7

(b) Mode 8

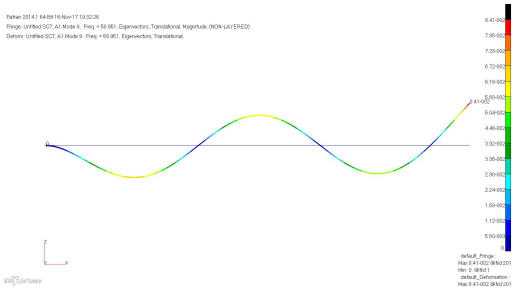

(c) Mode 9

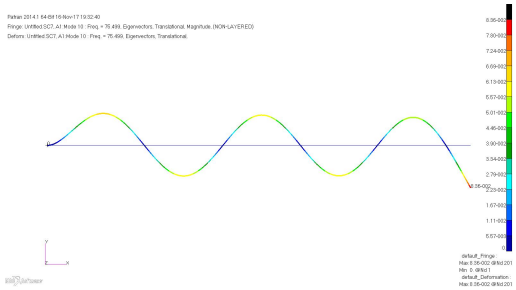

(d) Mode 10

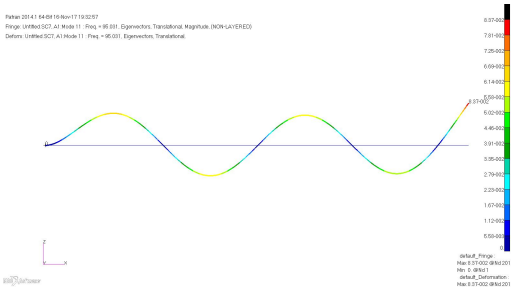

(e) Mode 11

Figure A.24: Mode shapes for the Modes 7 to 11 of a Uniform C-F Rotating Beam with $\eta = 7$

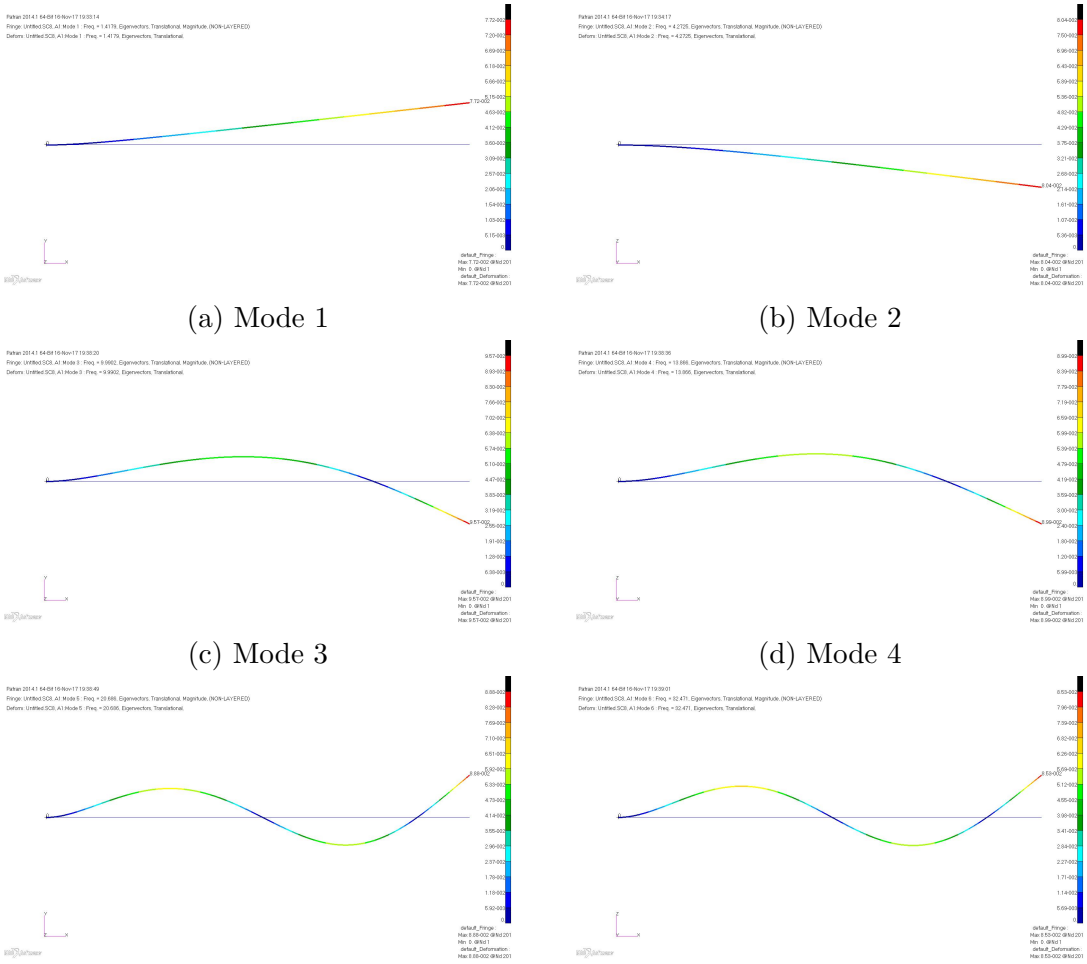

(a) Mode 1

(b) Mode 2

(c) Mode 3

(d) Mode 4

(e) Mode 5

(f) Mode 6

Figure A.25: Mode shapes for the modes 1 to 6 of a Uniform C-F Rotating Beam with $\eta = 8$

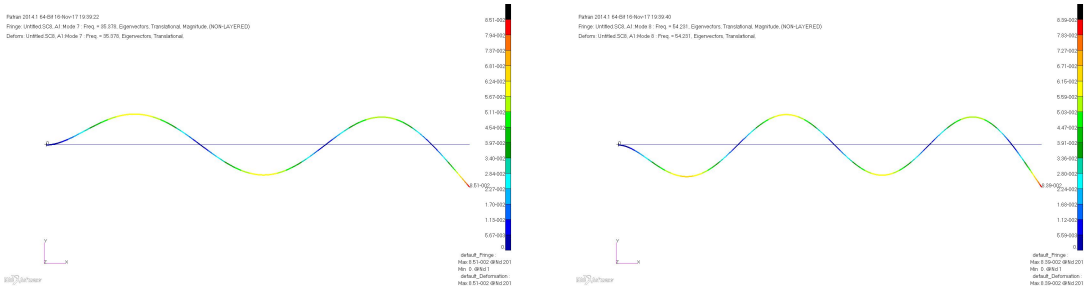

(a) Mode 7

(b) Mode 8

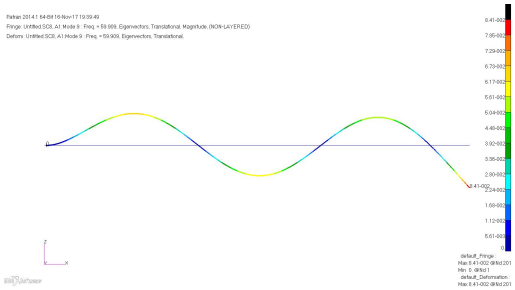

(c) Mode 9

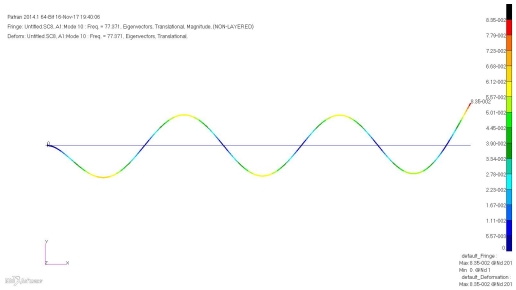

(d) Mode 10

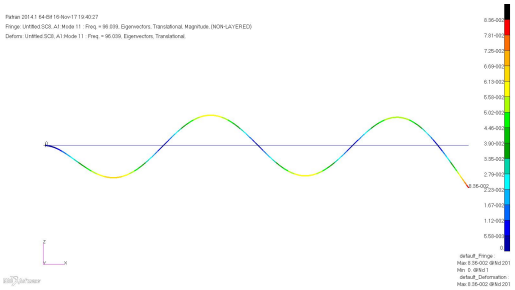

(e) Mode 11

Figure A.26: Mode shapes for the Modes 7 to 11 of a Uniform C-F Rotating Beam with $\eta = 8$

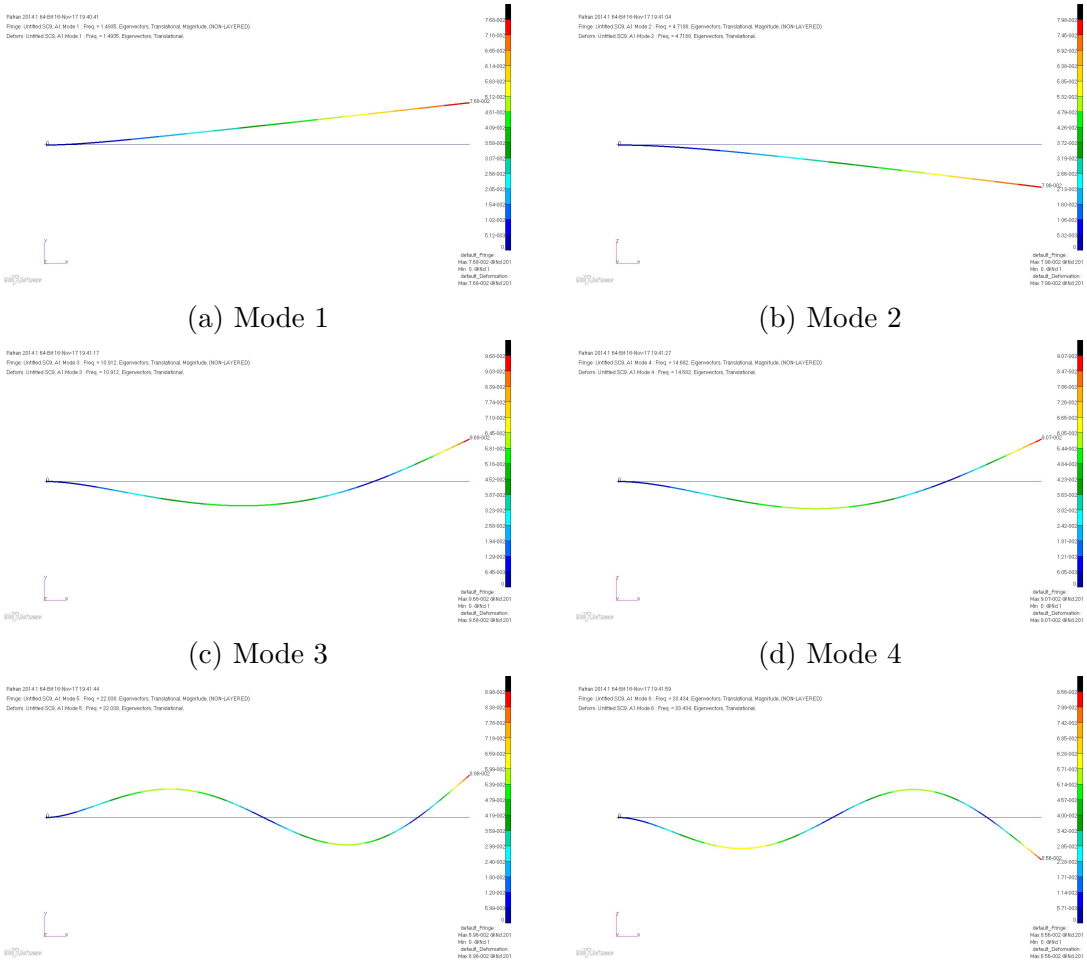

(a) Mode 1

(b) Mode 2

(c) Mode 3

(d) Mode 4

(e) Mode 5

(f) Mode 6

Figure A.27: Mode shapes for the modes 1 to 6 of a Uniform C-F Rotating Beam with $\eta = 9$

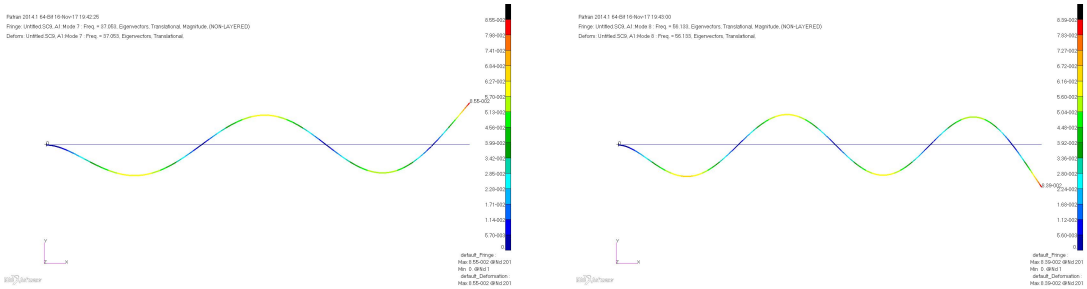

(a) Mode 7

(b) Mode 8

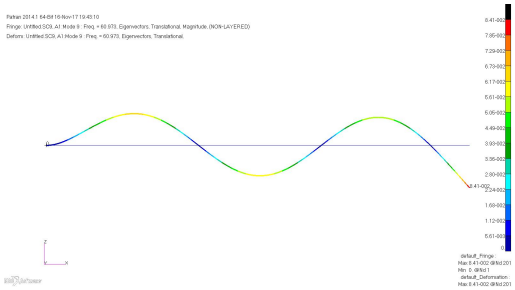

(c) Mode 9

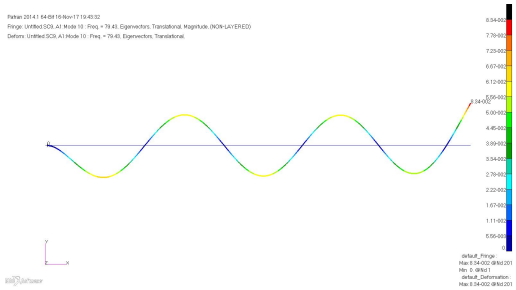

(d) Mode 10

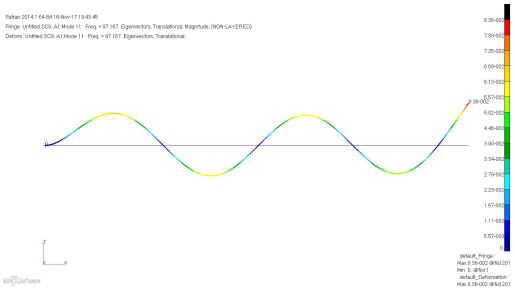

(e) Mode 11

Figure A.28: Mode shapes for the modes 7 to 12 of a Uniform C-F Rotating Beam with $\eta = 9$

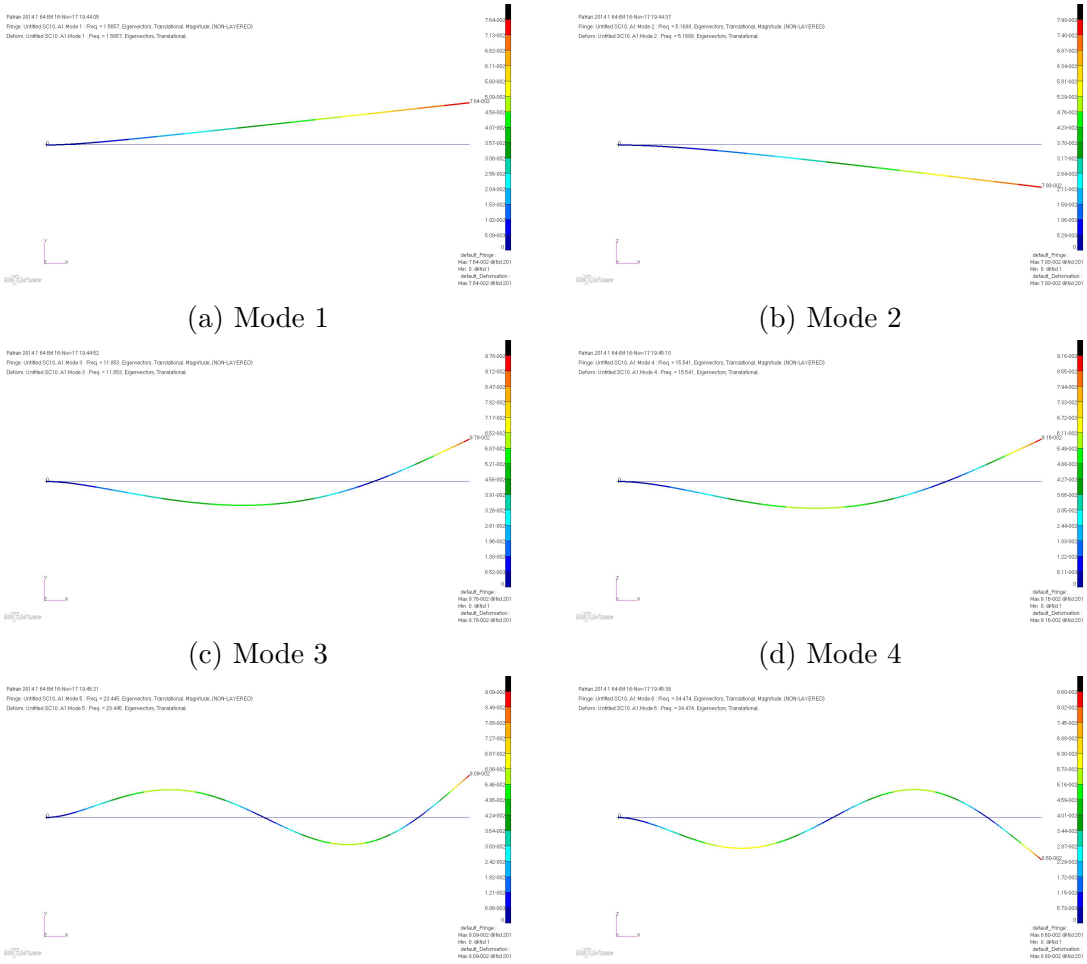

(a) Mode 1

(b) Mode 2

(c) Mode 3

(d) Mode 4

(e) Mode 5

(f) Mode 6

Figure A.29: Mode shapes for the Modes 1 to 6 of a Uniform C-F Rotating Beam with $\eta = 10$

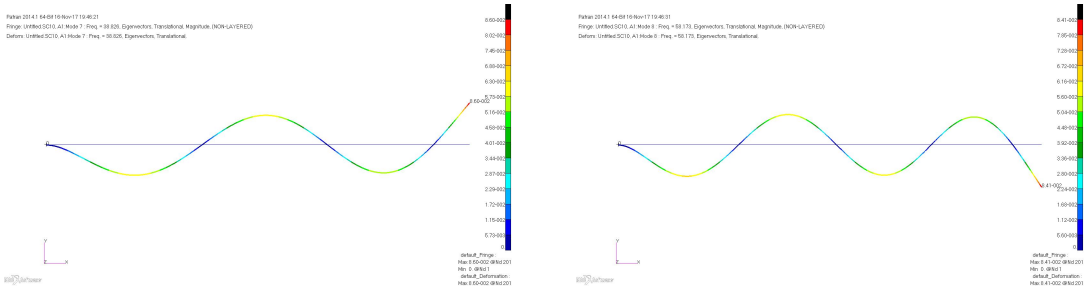

(a) Mode 7

(b) Mode 8

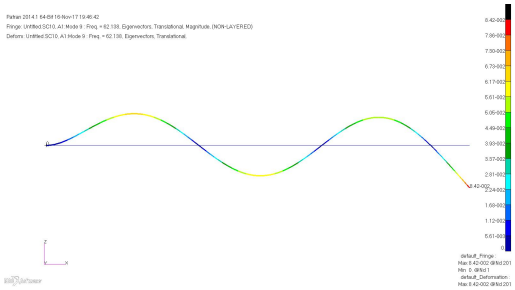

(c) Mode 9

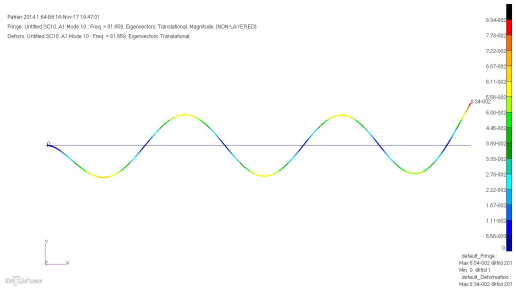

(d) Mode 10

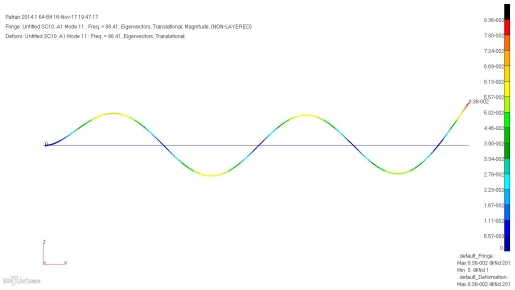

(e) Mode 11

Figure A.30: Mode shapes for the Modes 7 to 11 of a Uniform C-F Rotating Beam with $\eta = 10$

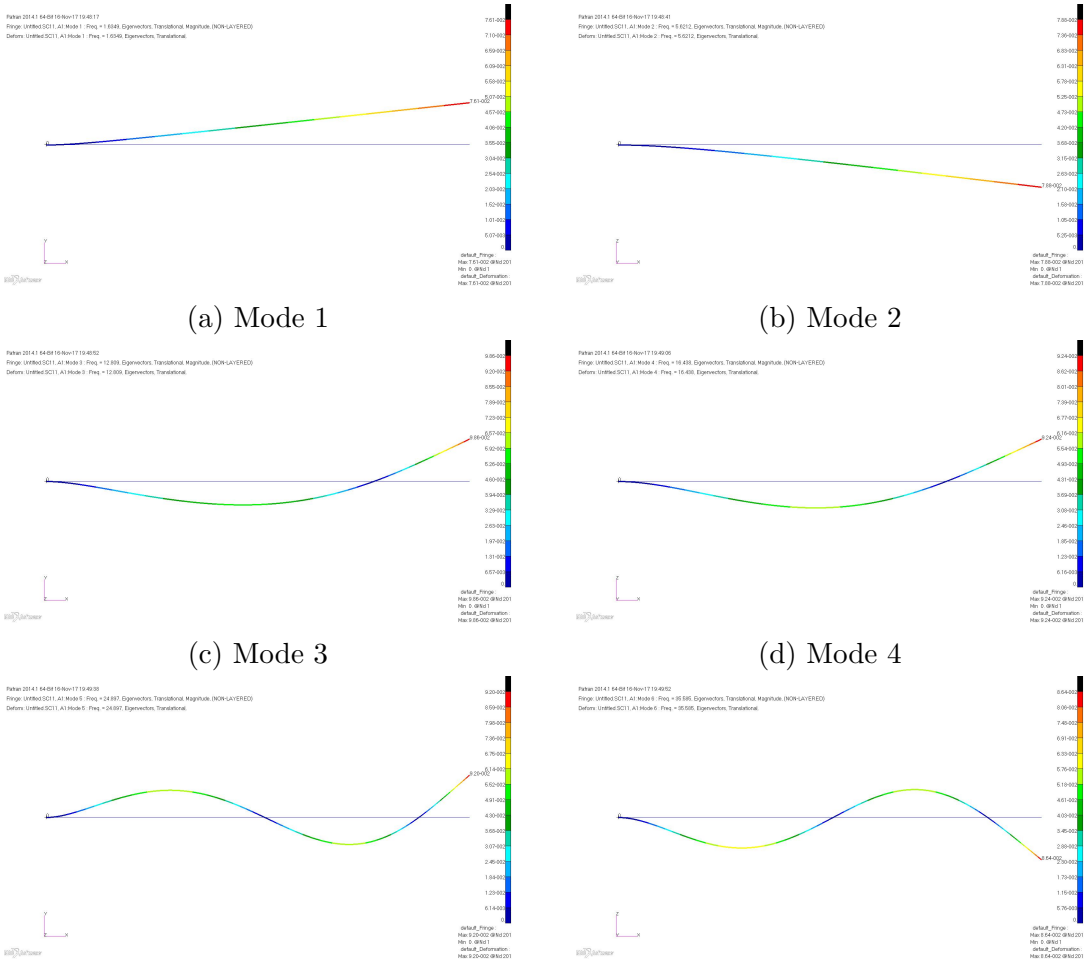

(a) Mode 1

(b) Mode 2

(c) Mode 3

(d) Mode 4

(e) Mode 5

(f) Mode 6

Figure A.31: Mode shapes for the Modes 1 to 6 of a Uniform C-F Rotating Beam with $\eta = 11$

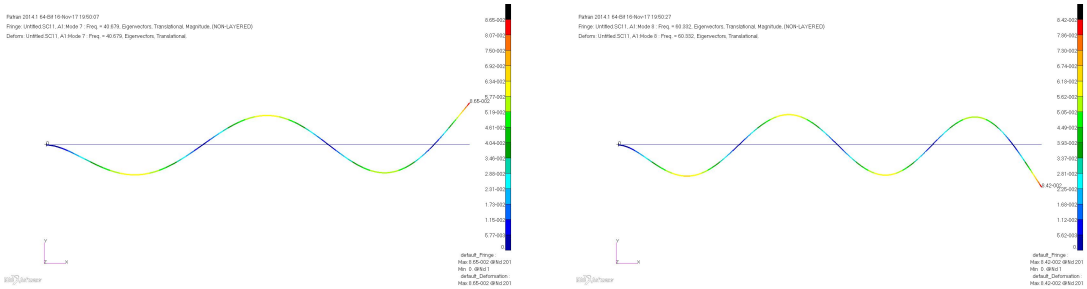

(a) Mode 7

(b) Mode 8

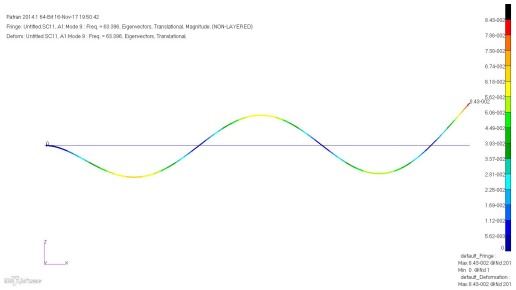

(c) Mode 9

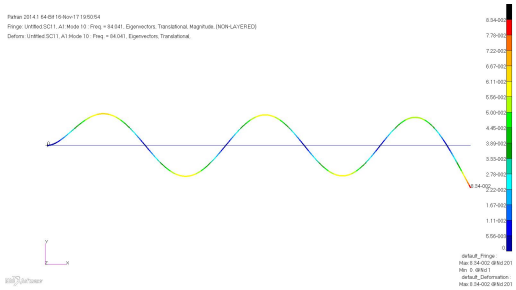

(d) Mode 10

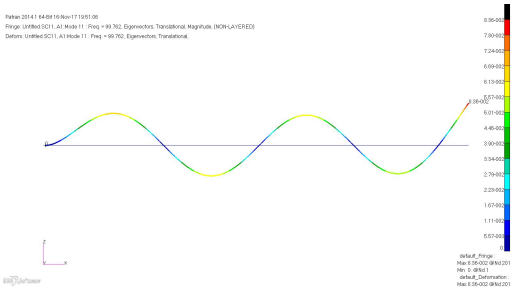

(e) Mode 11

Figure A.32: Mode shapes for the Modes 7 to 11 of a Uniform C-F Rotating Beam with $\eta = 11$

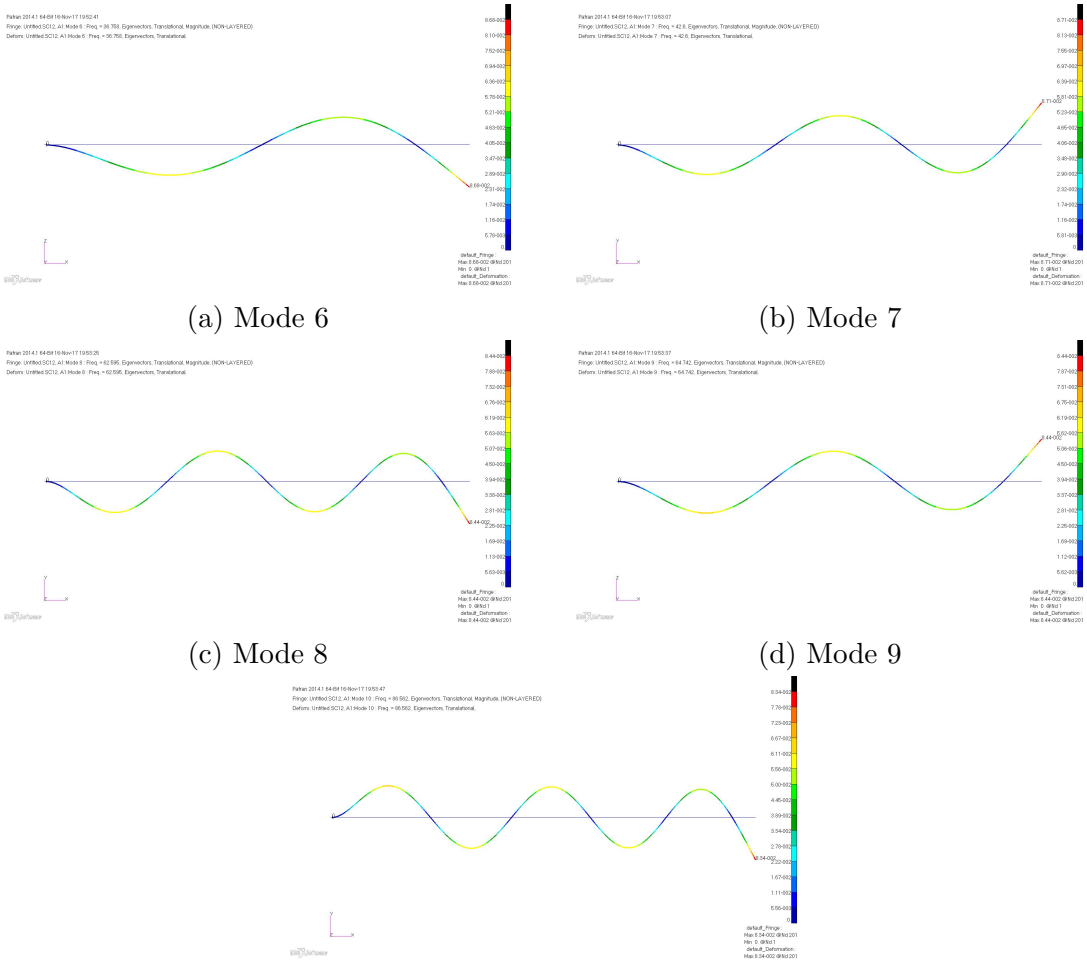

(a) Mode 6

(b) Mode 7

(c) Mode 8

(d) Mode 9

(e) Mode 10

Figure A.33: Mode shapes for the Modes 6 to 10 of a Uniform C-F Rotating Beam with η = 12

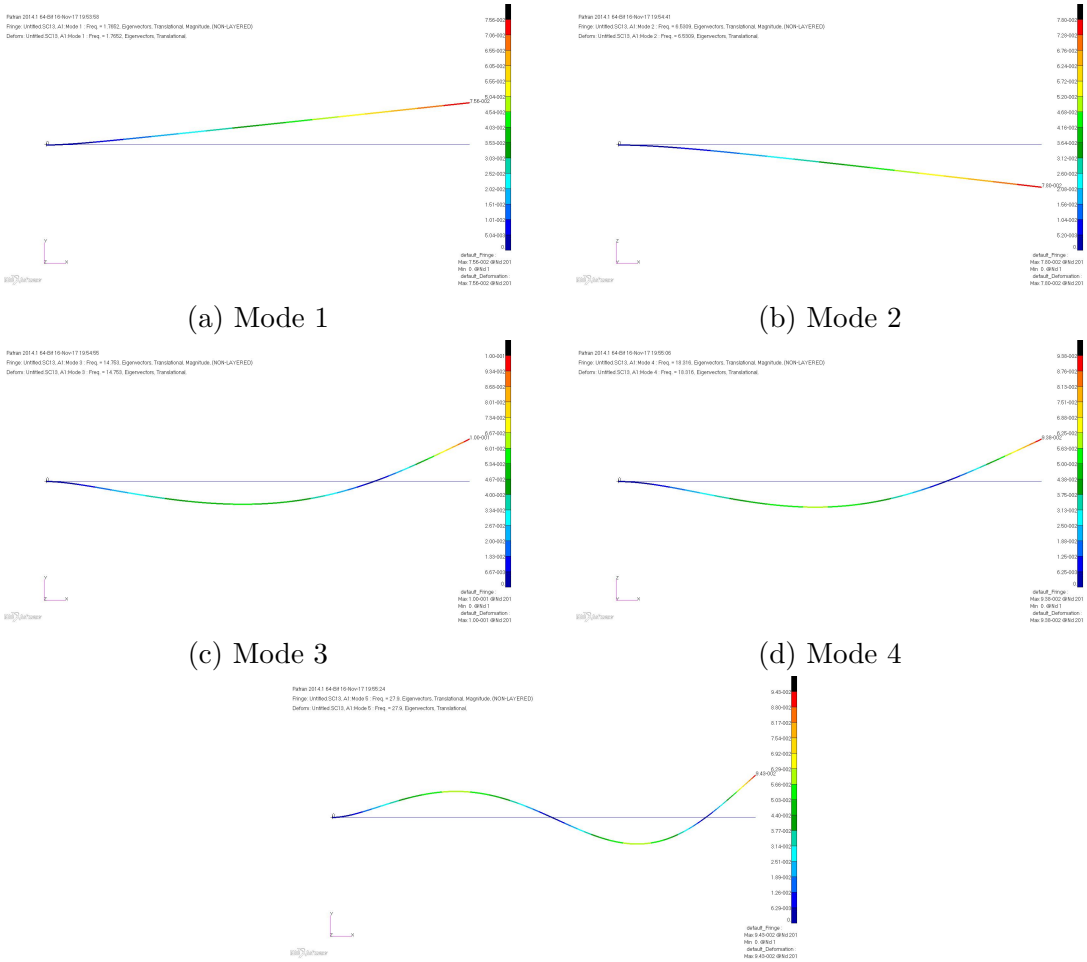

(a) Mode 1

(b) Mode 2

(c) Mode 3

(d) Mode 4

(e) Mode 5

Figure A.34: Mode shapes for the modes 1 to 5 of a Uniform C-F Rotating Beam with $\eta = 13$

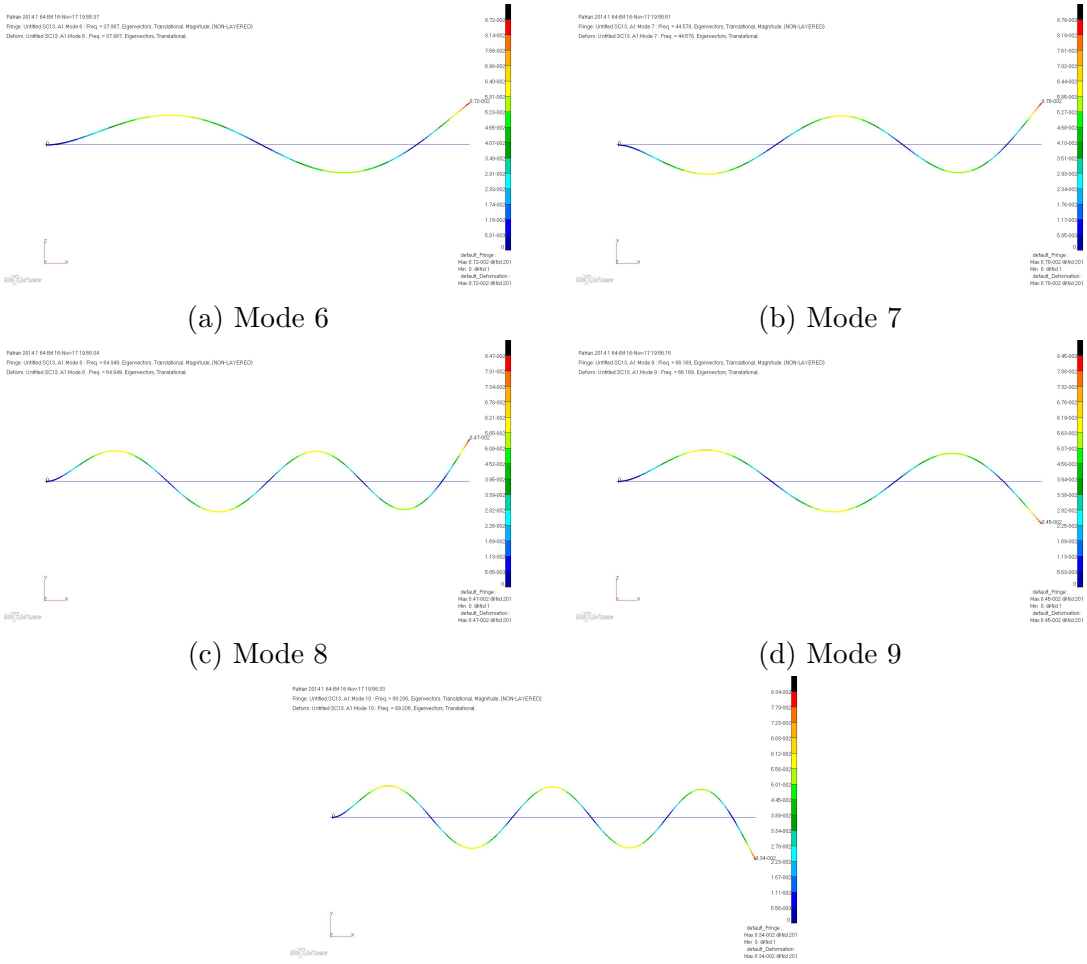

(a) Mode 6

(b) Mode 7

(c) Mode 8

(d) Mode 9

(e) Mode 10

Figure A.35: Mode shapes for the modes 6 to 10 of a Uniform C-F Rotating Beam with η = 13

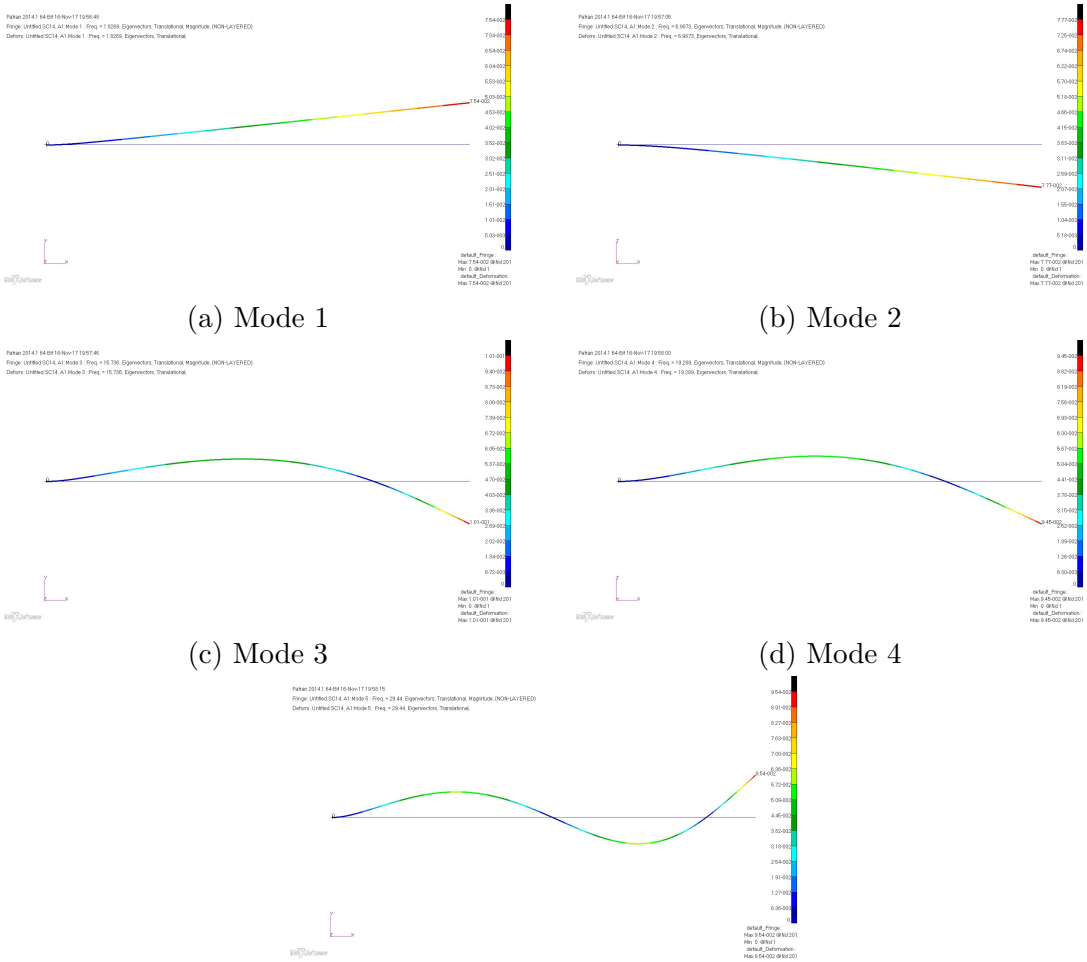

(a) Mode 1

(b) Mode 2

(c) Mode 3

(d) Mode 4

(e) Mode 5

Figure A.36: Mode shapes for the Modes 1 to 5 of a Uniform C-F Rotating Beam with $\eta = 14$

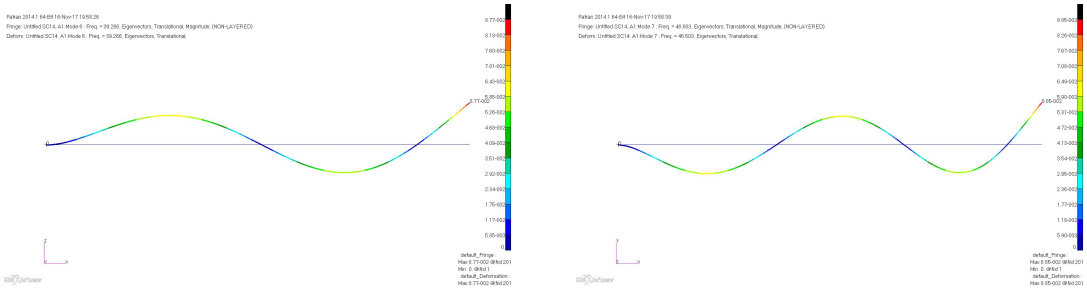

(a) Mode 6

(b) Mode 7

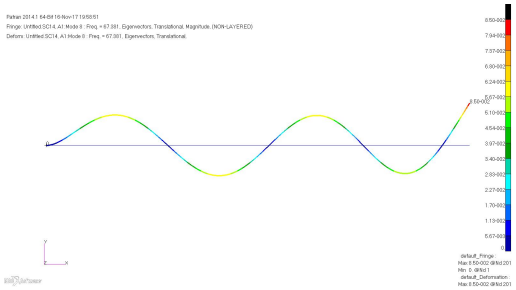

(c) Mode 8

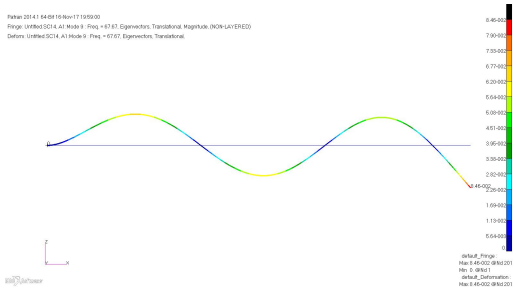

(d) Mode 9

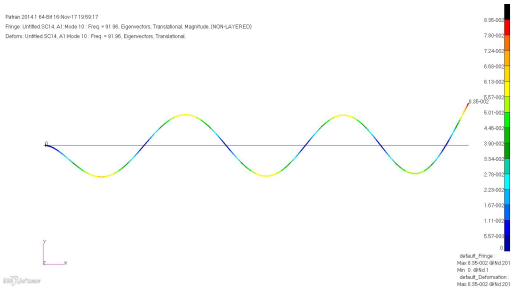

(e) Mode 10

Figure A.37: Mode shapes for the Modes 6 to 10 of a Uniform C-F Rotating Beam with $\eta = 14$

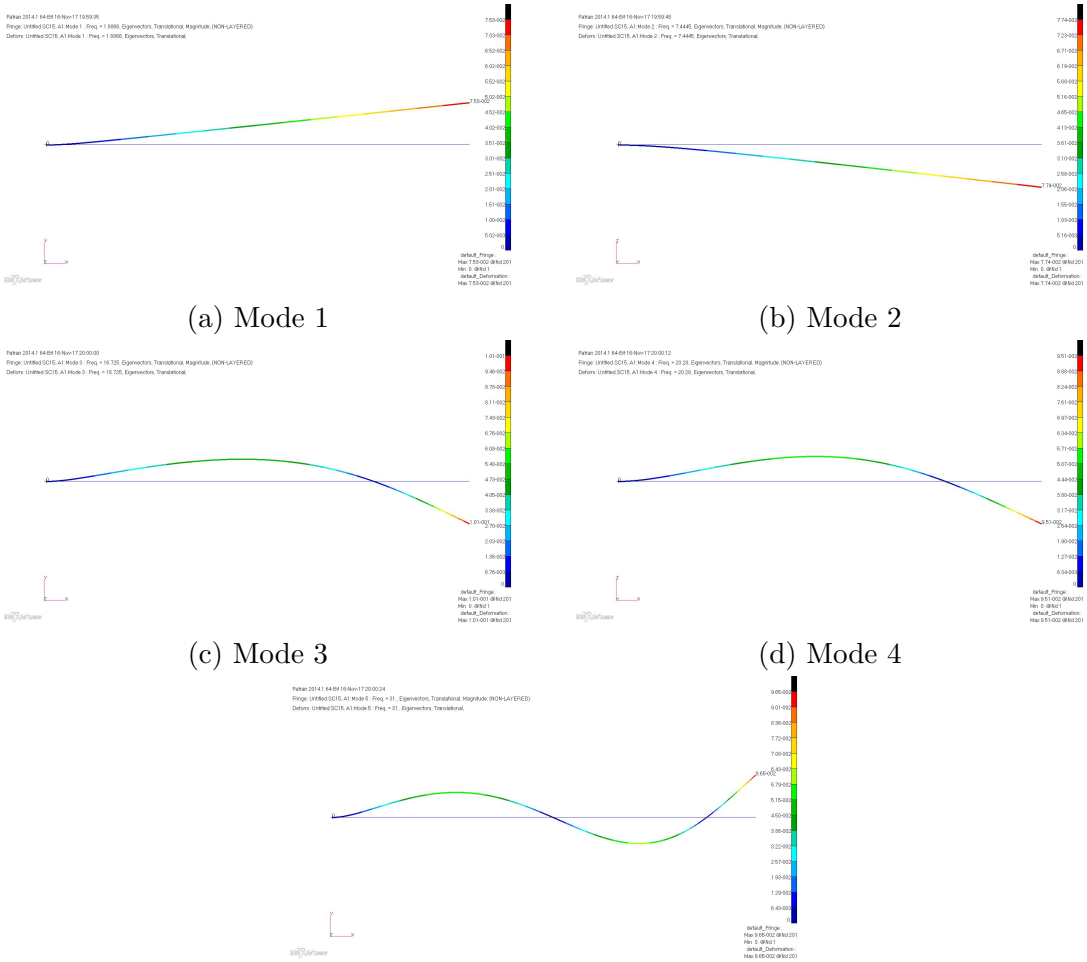

(a) Mode 1

(b) Mode 2

(c) Mode 3

(d) Mode 4

(e) Mode 5

Figure A.38: Mode shapes for the Modes 1 to 5 of a Uniform C-F Rotating Beam with $\eta = 15$

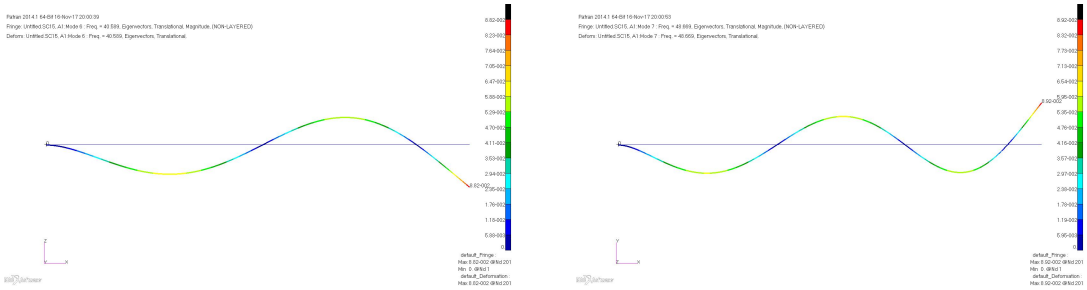

(a) Mode 6

(b) Mode 7

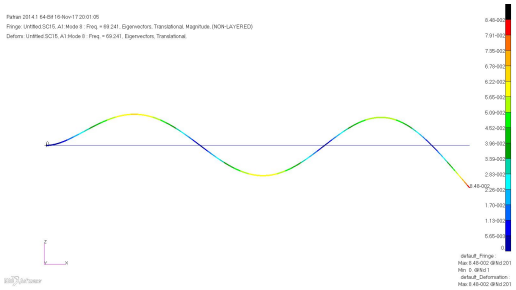

(c) Mode 8

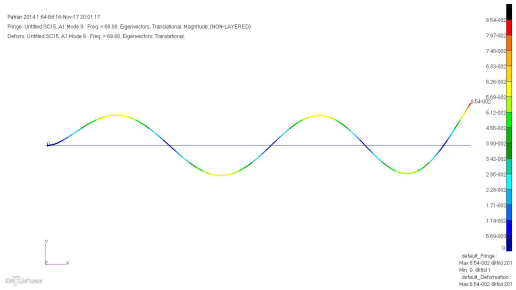

(d) Mode 9

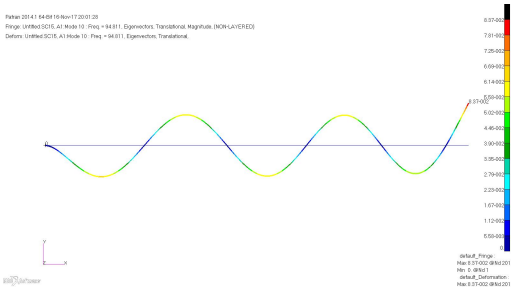

(e) Mode 10

Figure A.39: Mode shapes for the Modes 6 to 10 of a Uniform C-F Rotating Beam with $\eta = 15$

Appendix B

B.1 Mode shapes of Non-rotating C-F Tapered Beam

B.2 Mode shapes of Rotating C-F Tapered Beam

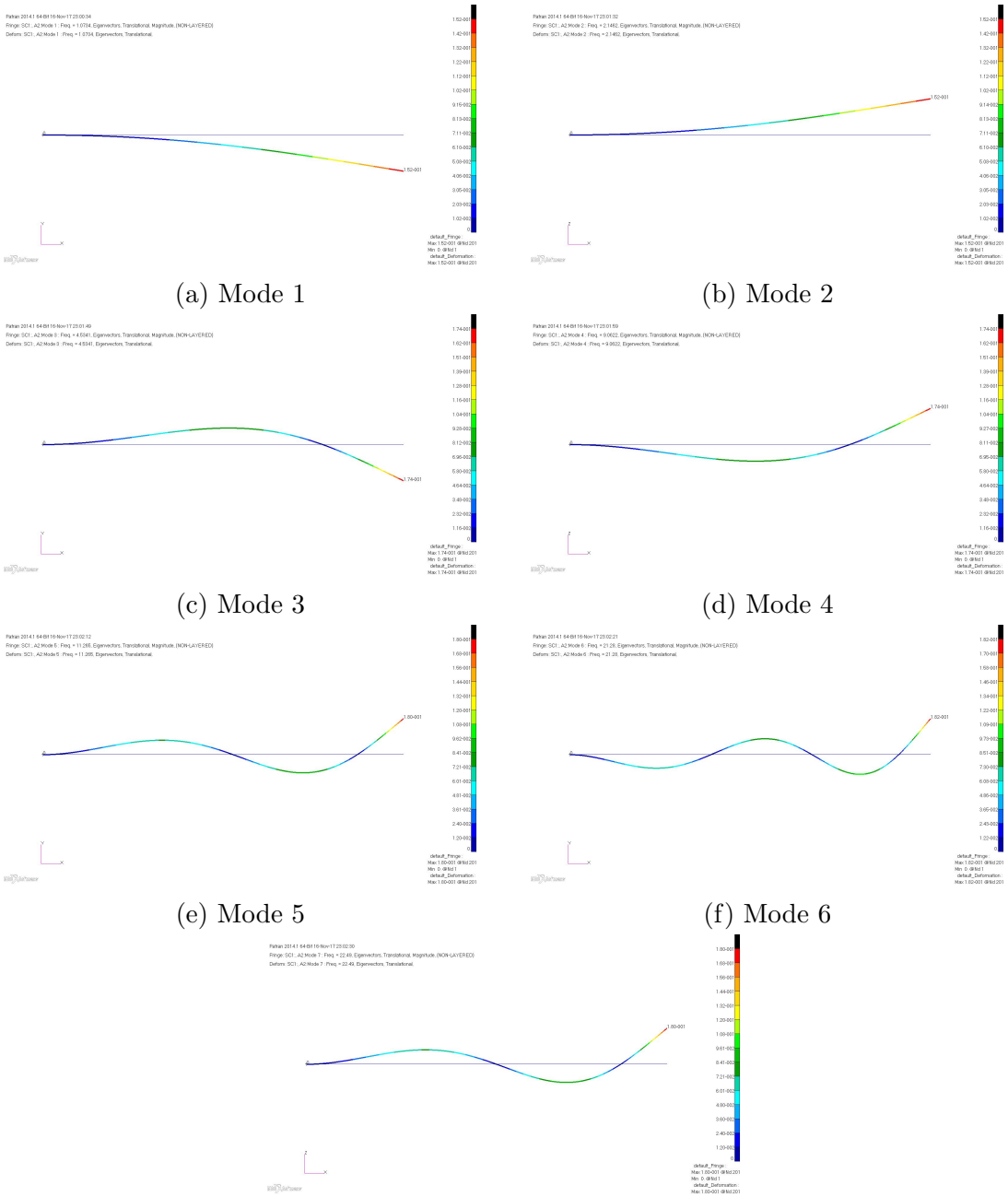

(a) Mode 1

(b) Mode 2

(c) Mode 3

(d) Mode 4

(e) Mode 5

(f) Mode 6

(g) Mode 7

Figure B.1: Mode shapes for the Modes 1 to 7 of a Non-rotating C-F Tapered Beam

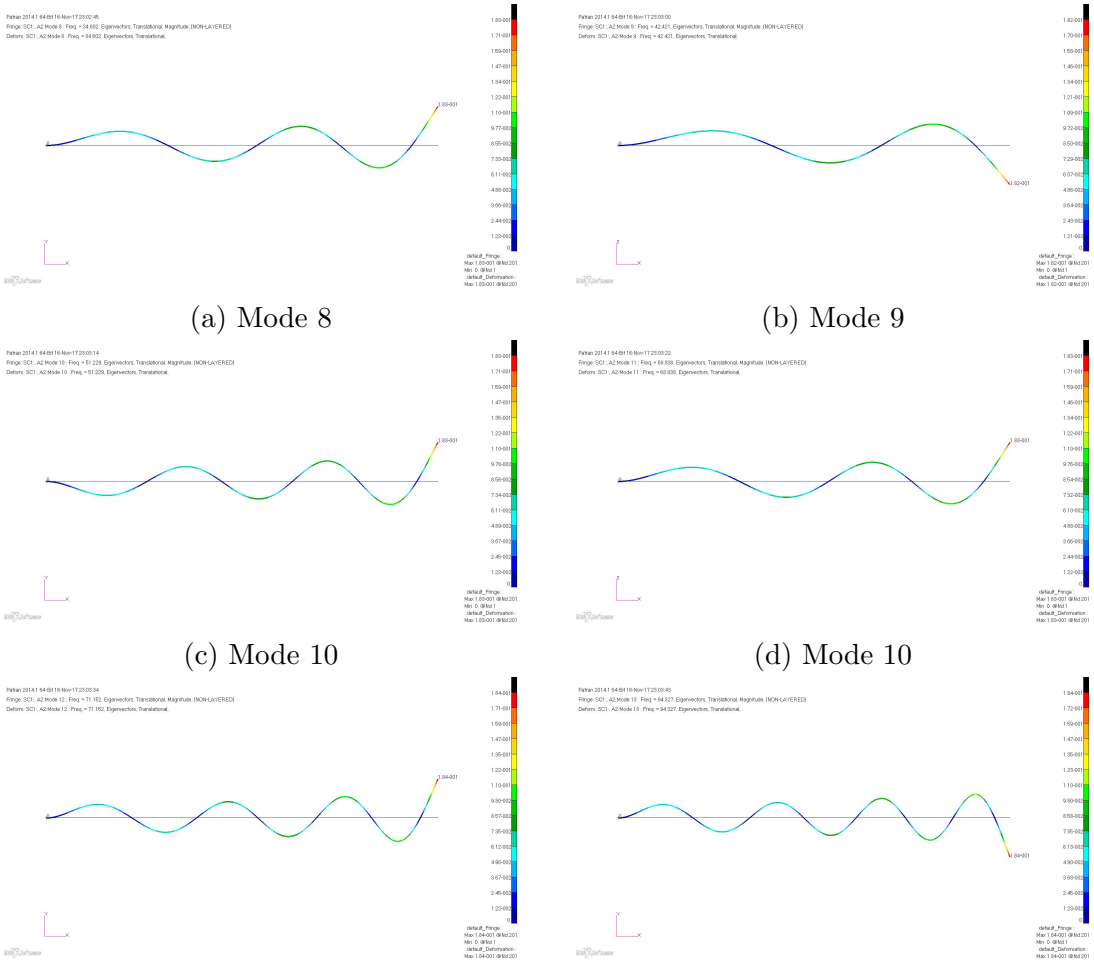

(a) Mode 8

(b) Mode 9

(c) Mode 10

(d) Mode 10

(e) Mode 10

(f) Mode 10

Figure B.2: Mode shapes for the Modes 8 to 13 of a Non-rotating C-F Tapered Beam

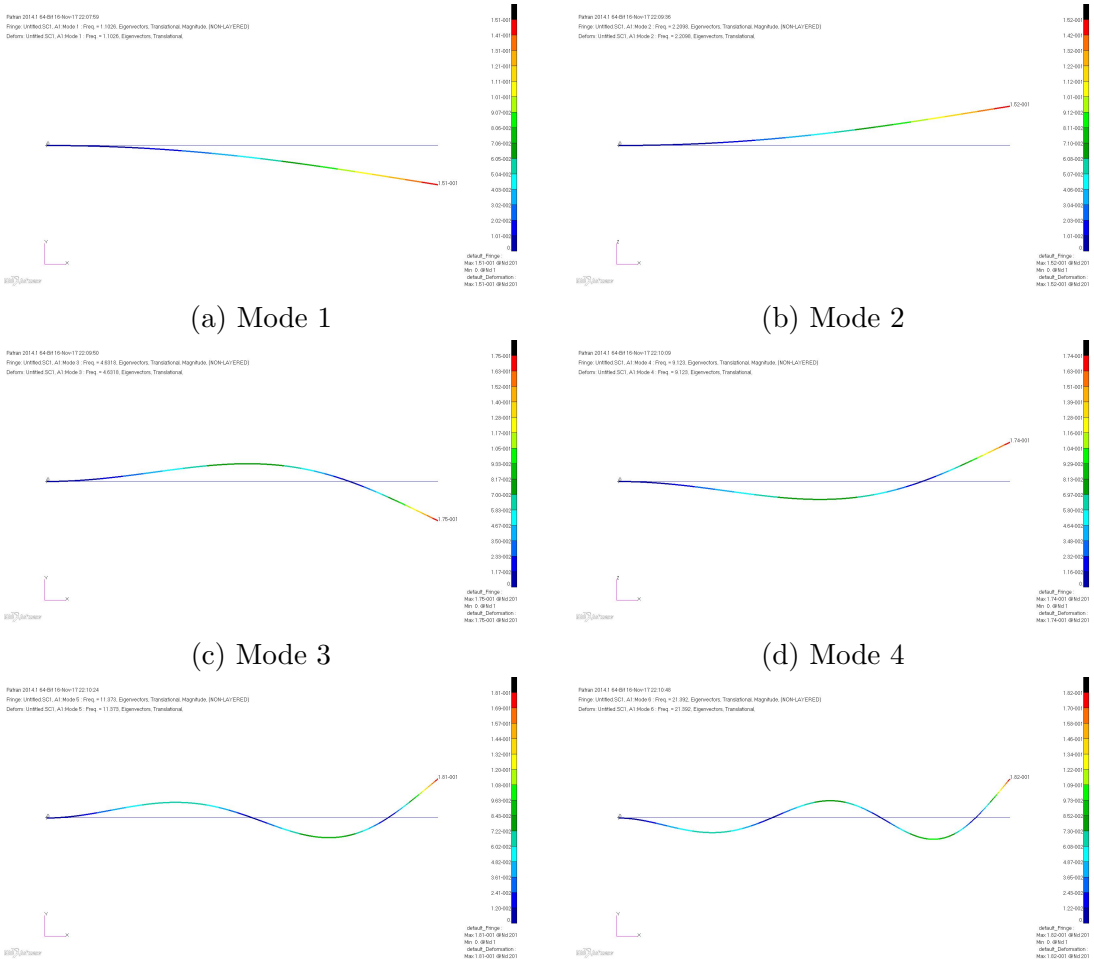

(a) Mode 1 (b) Mode 2

(c) Mode 3 (d) Mode 4

(e) Mode 5 (f) Mode 6

Figure B.3: Mode shapes for the Modes 1 to 6 of a C-F Rotating Tapered Beam with $\eta = 1$

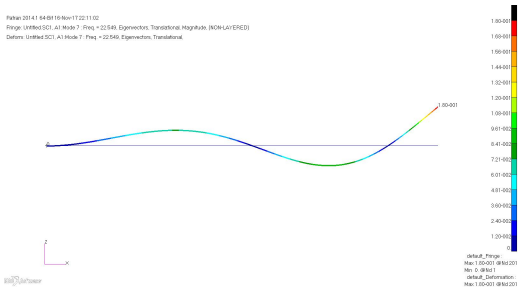

(a) Mode 7

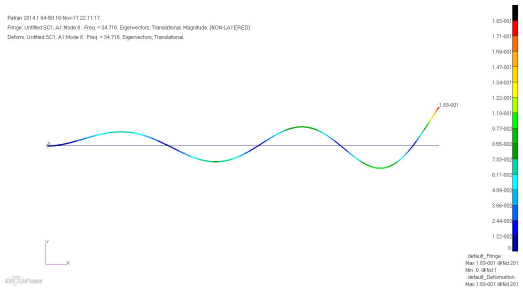

(b) Mode 8

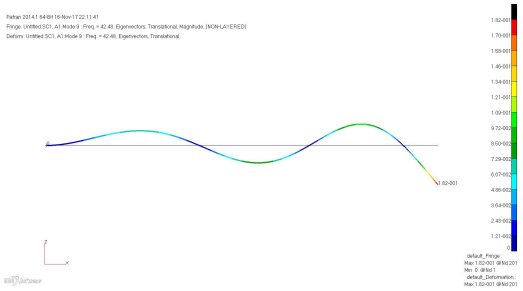

(c) Mode 9

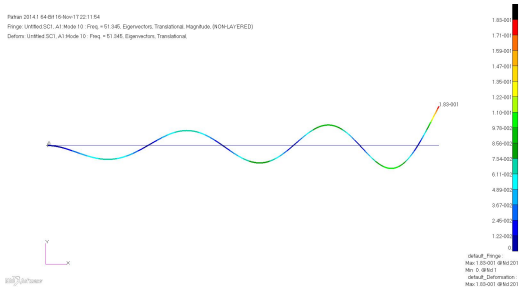

(d) Mode 10

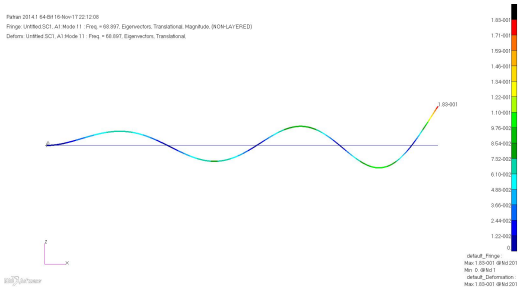

(e) Mode 9

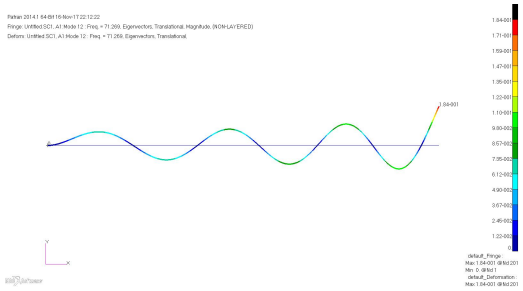

(f) Mode 10

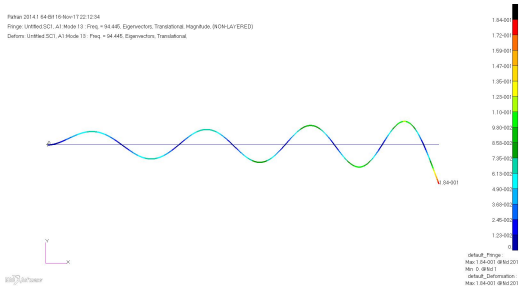

(g) Mode 10

Figure B.4: Mode shapes for the Modes 7 to 13 of a C-F Rotating Tapered Beam with $\eta = 1$

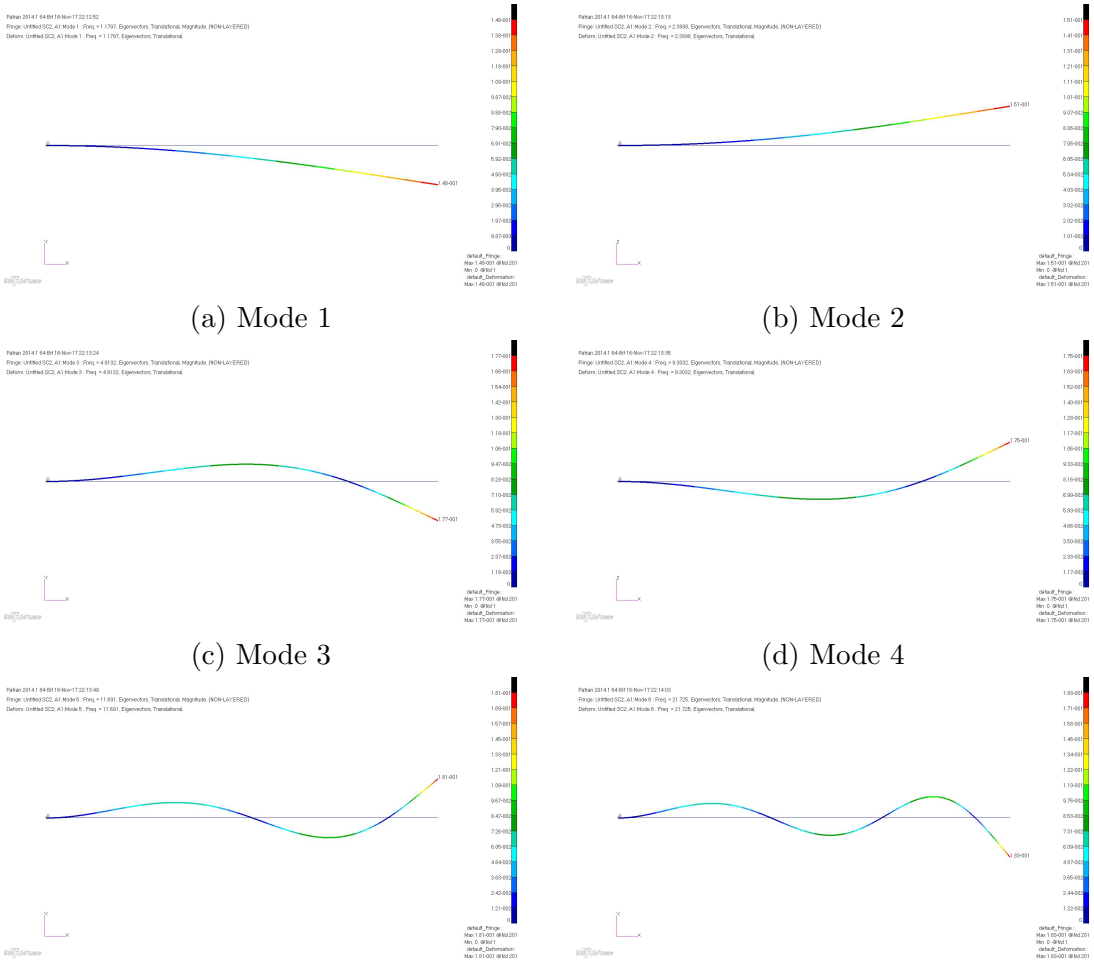

(a) Mode 1

(b) Mode 2

(c) Mode 3

(d) Mode 4

(e) Mode 5

(f) Mode 6

Figure B.5: Mode shapes for the Modes 1 to 6 of a C-F Rotating Tapered Beam with $\eta = 2$

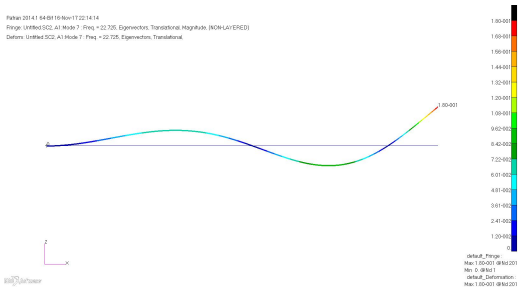

(a) Mode 7

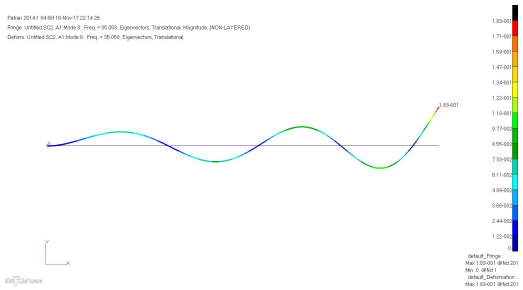

(b) Mode 8

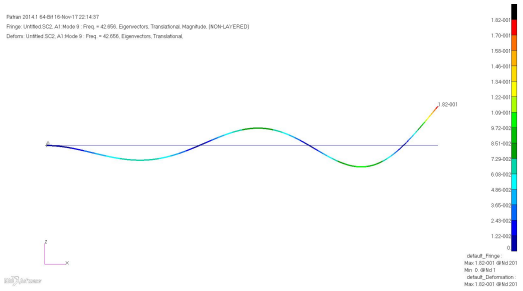

(c) Mode 9

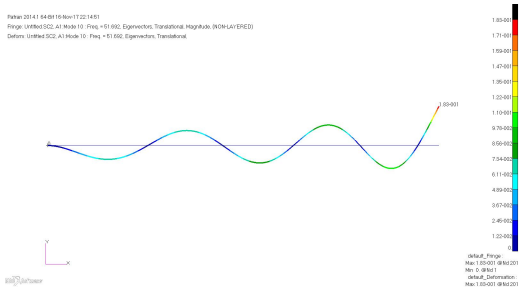

(d) Mode 10

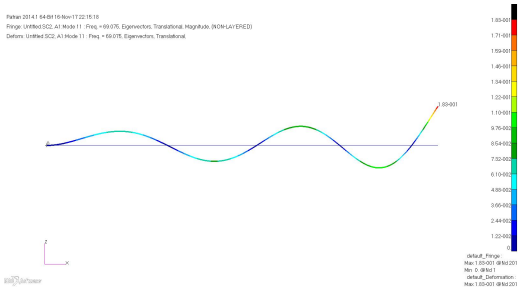

(e) Mode 9

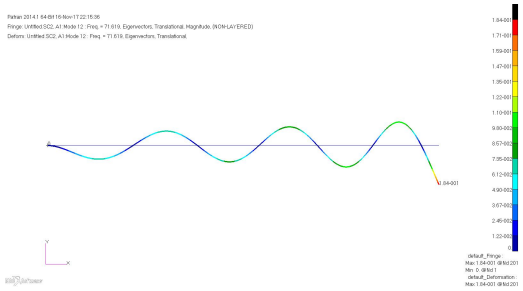

(f) Mode 10

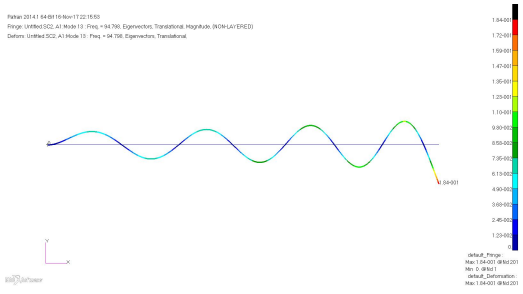

(g) Mode 10

Figure B.6: Mode shapes for the Modes 7 to 13 of a C-F Rotating Tapered Beam with $\eta = 2$

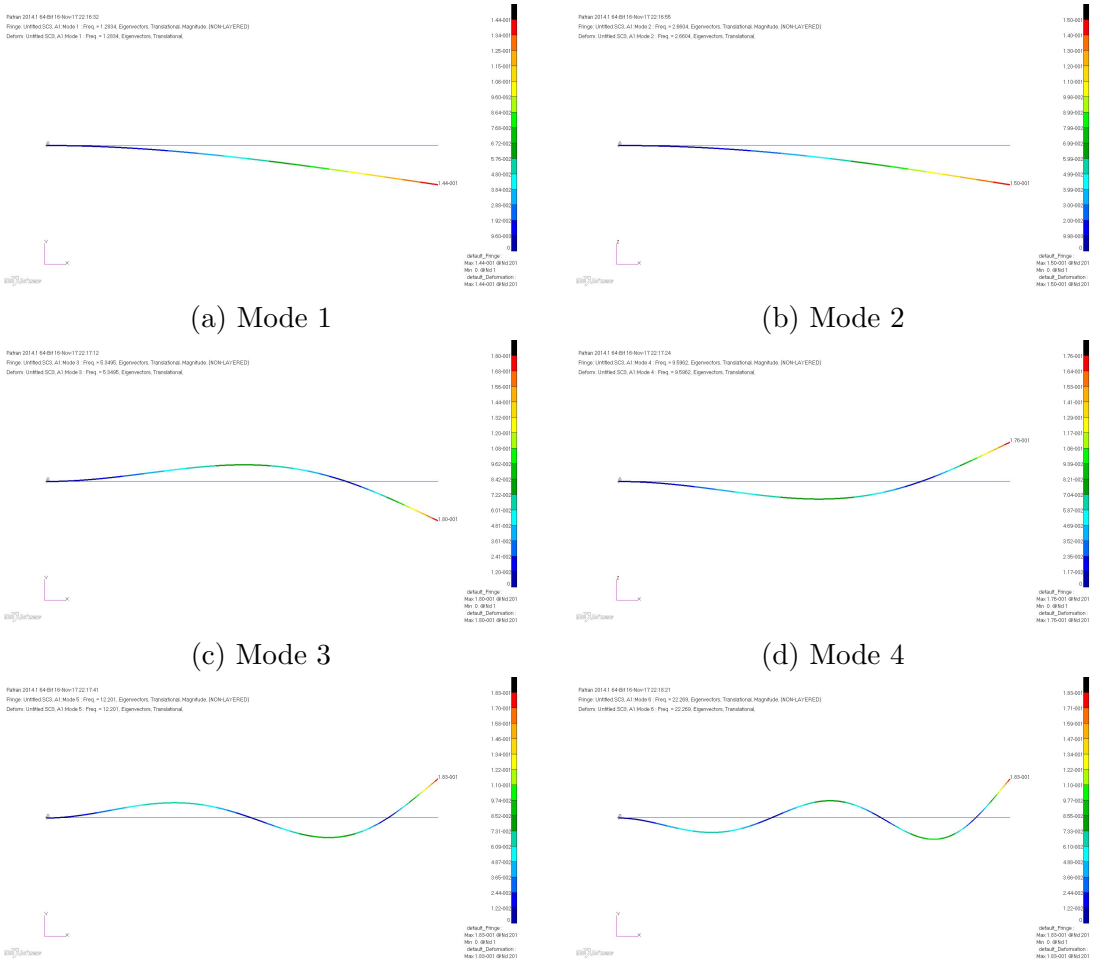

(a) Mode 1

(b) Mode 2

(c) Mode 3

(d) Mode 4

(e) Mode 5

(f) Mode 6

Figure B.7: Mode shapes for the modes 1 to 6 of a C-F Rotating Tapered Beam with $\eta = 3$

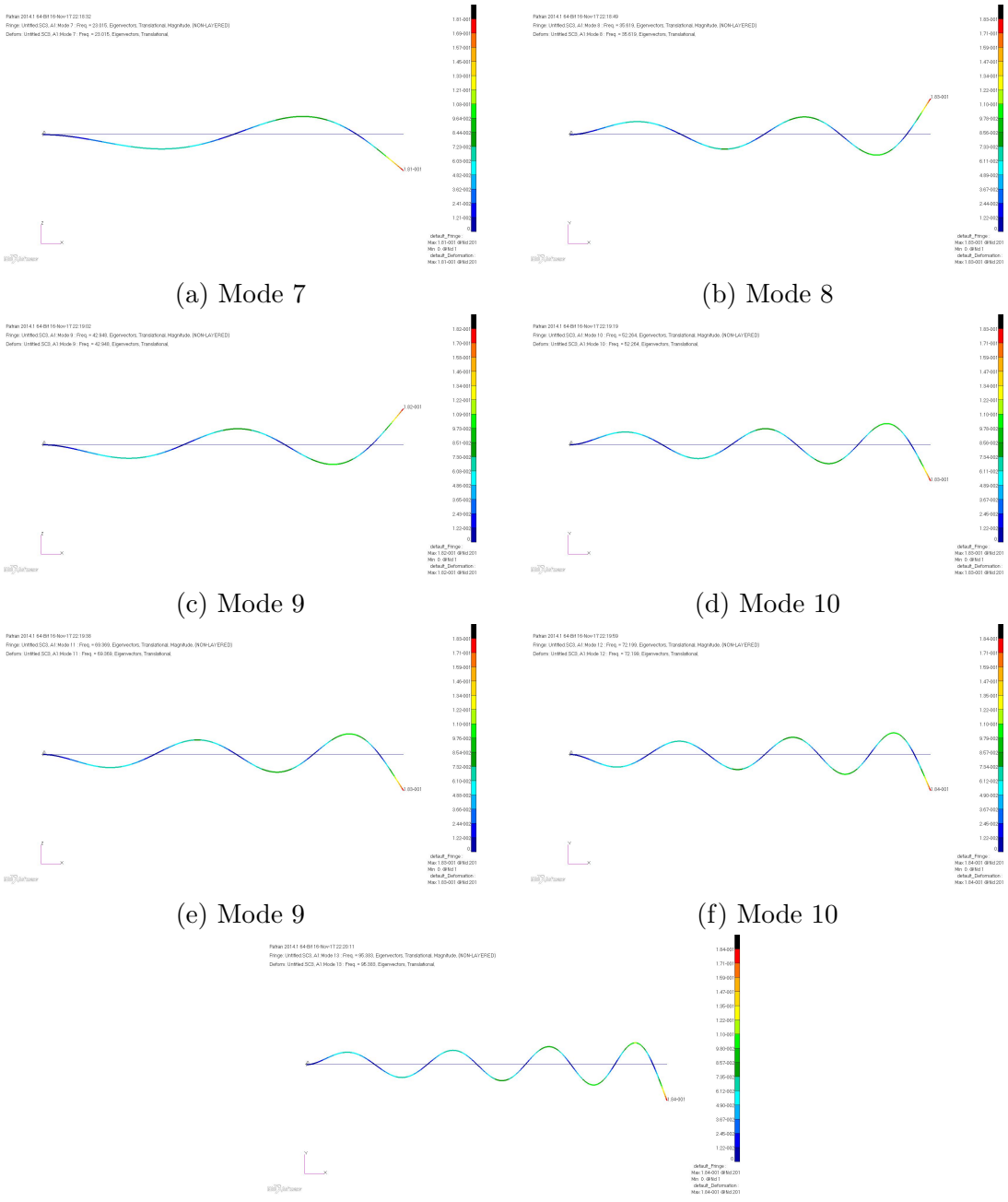

(a) Mode 7

(b) Mode 8

(c) Mode 9

(d) Mode 10

(e) Mode 9

(f) Mode 10

(g) Mode 10

Figure B.8: Mode shapes for the Modes 7 to 13 of a C-F Rotating Tapered Beam with $\eta = 3$

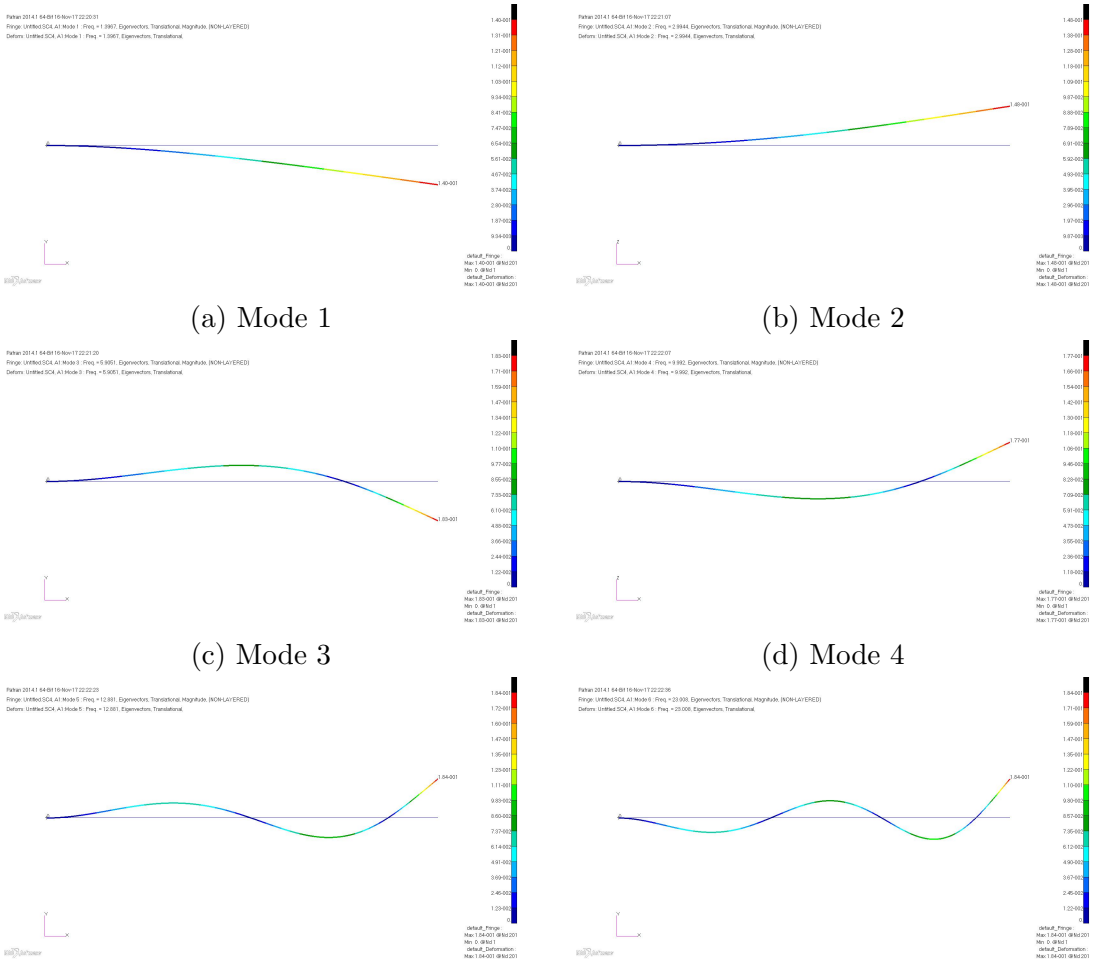

(a) Mode 1

(b) Mode 2

(c) Mode 3

(d) Mode 4

(e) Mode 5

(f) Mode 6

Figure B.9: Mode shapes for the Modes 1 to 6 of a C-F Rotating Tapered Beam with $\eta = 4$

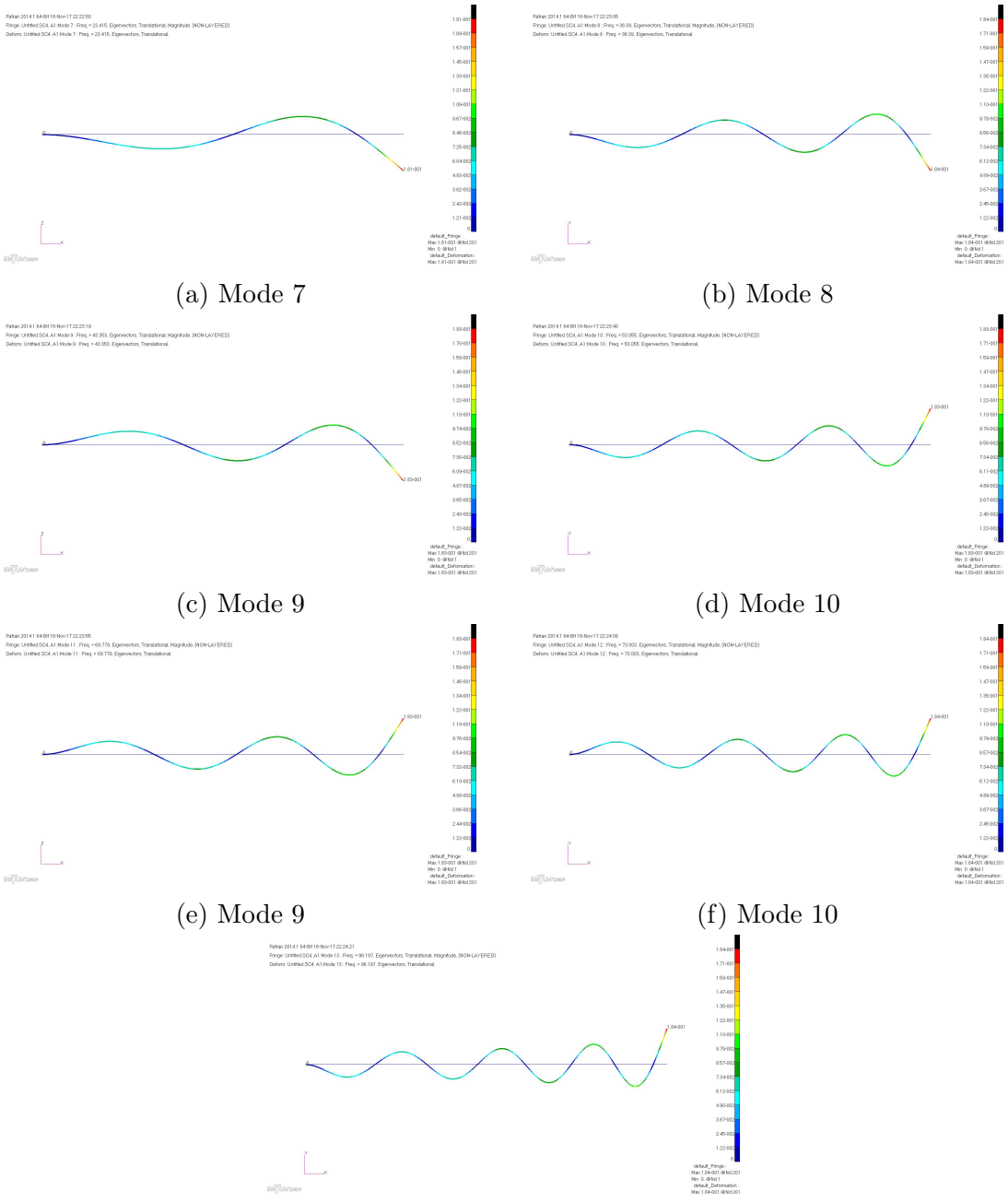

(a) Mode 7

(b) Mode 8

(c) Mode 9

(d) Mode 10

(e) Mode 9

(f) Mode 10

(g) Mode 10

Figure B.10: Mode shapes for the Modes 7 to 13 of a C-F Rotating Tapered Beam with $\eta = 4$

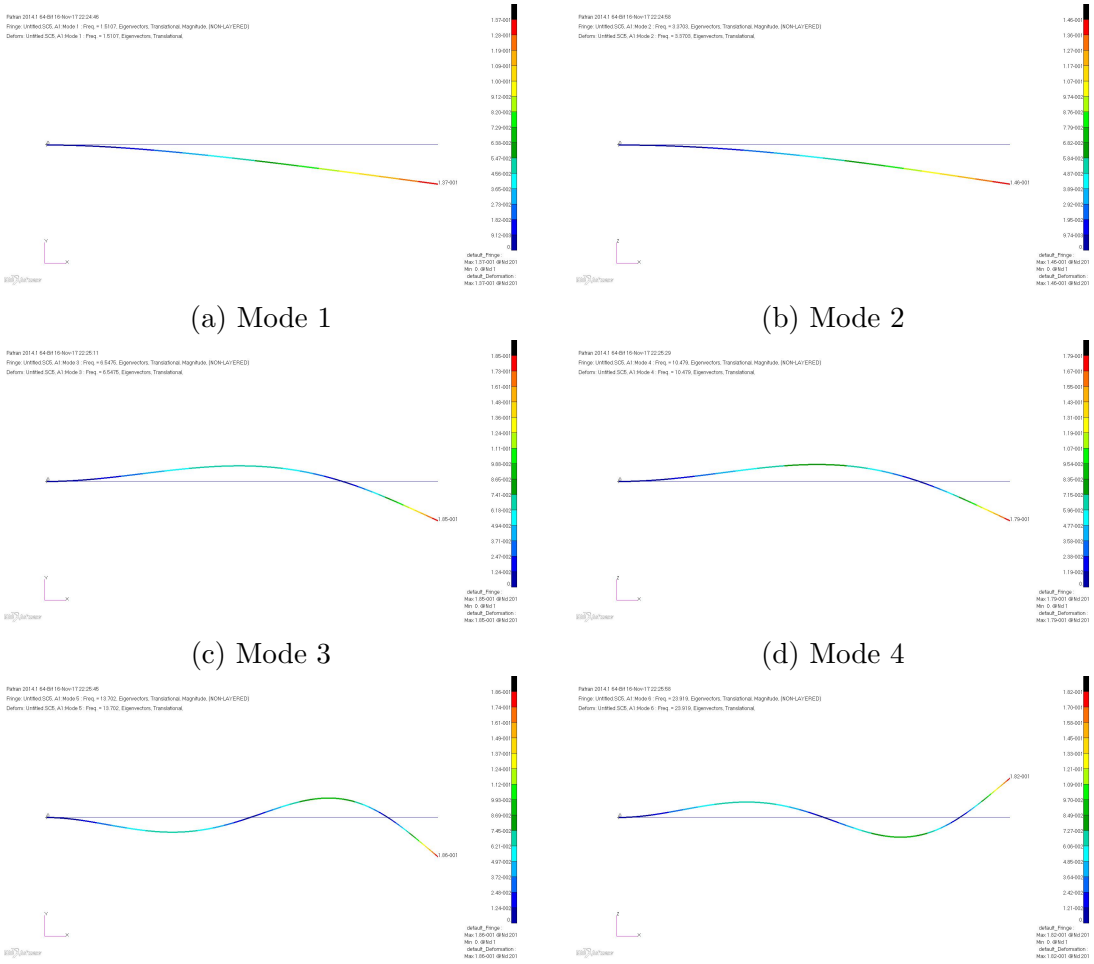

(a) Mode 1

(b) Mode 2

(c) Mode 3

(d) Mode 4

(e) Mode 5

(f) Mode 6

Figure B.11: Mode shapes for the Modes 1 to 6 of a C-F Rotating Tapered Beam with $\eta = 5$

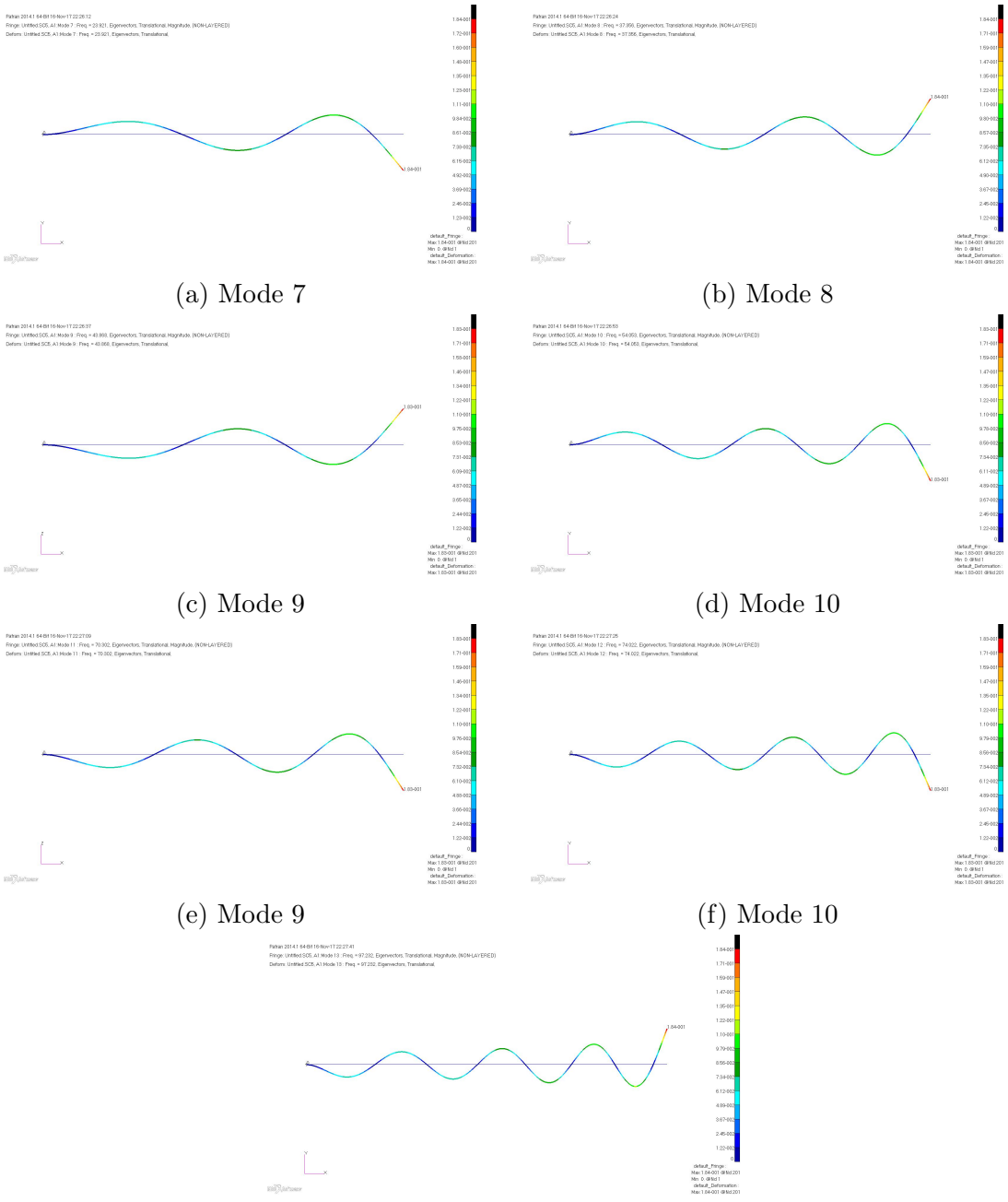

(a) Mode 7

(b) Mode 8

(c) Mode 9

(d) Mode 10

(e) Mode 9

(f) Mode 10

(g) Mode 10

Figure B.12: Mode shapes for the Modes 7 to 13 of a C-F Rotating Tapered Beam with $\eta = 5$

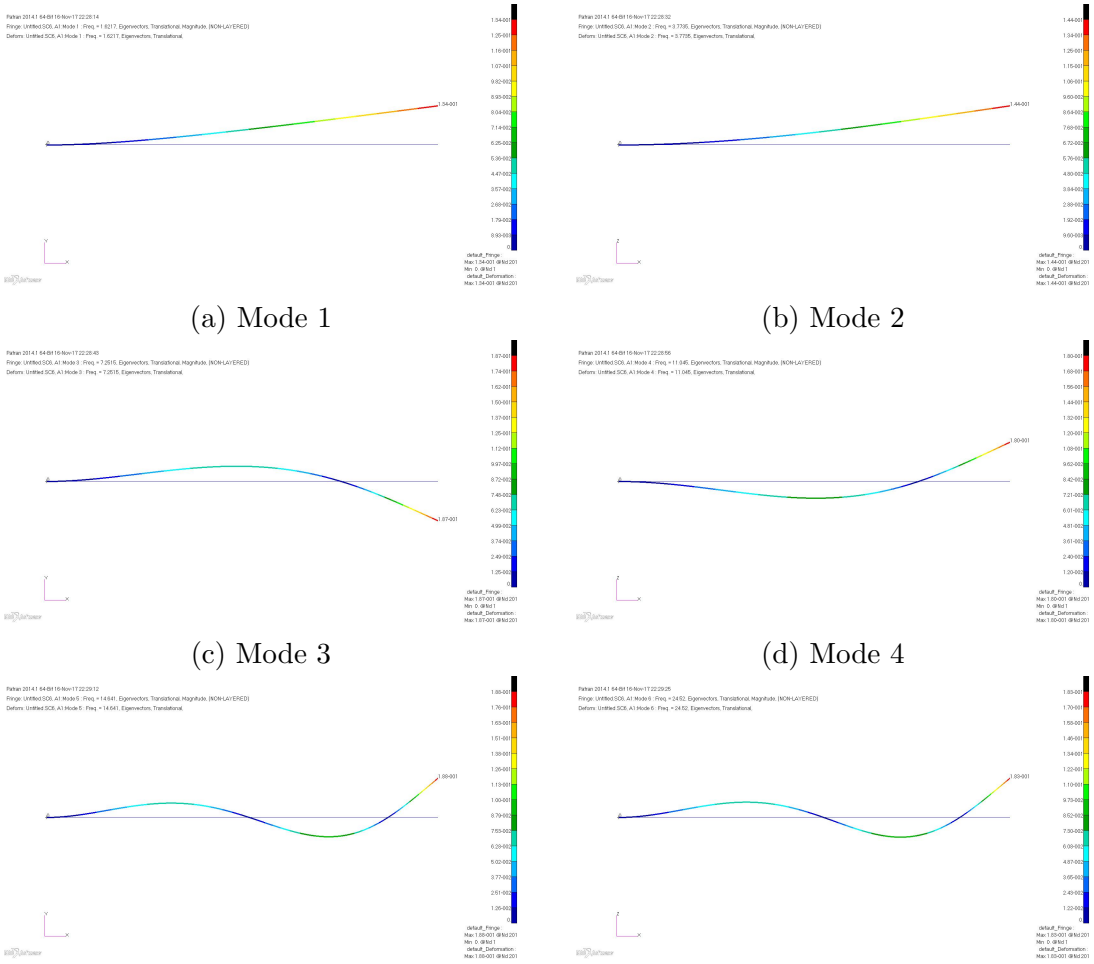

(a) Mode 1

(b) Mode 2

(c) Mode 3

(d) Mode 4

(e) Mode 5

(f) Mode 6

Figure B.13: Mode shapes for the Modes 1 to 6 of a C-F Rotating Tapered Beam with $\eta = 6$

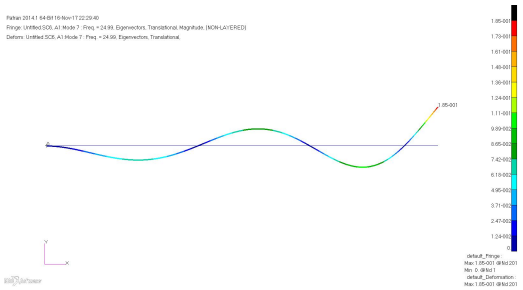

(a) Mode 7

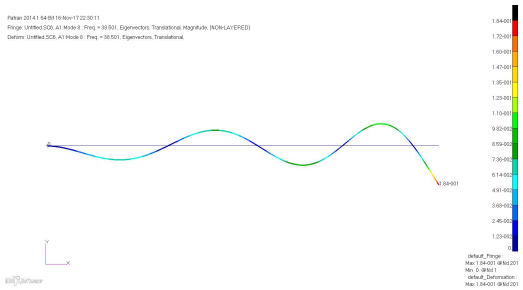

(b) Mode 8

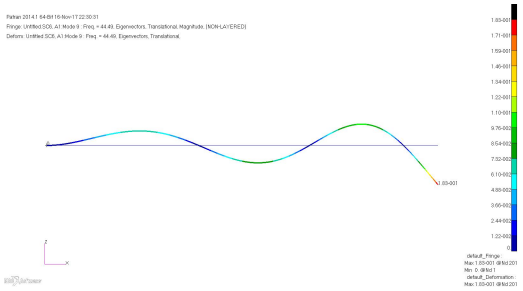

(c) Mode 9

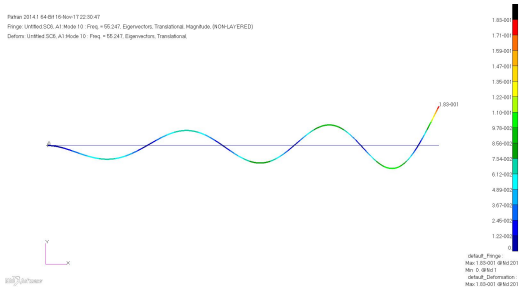

(d) Mode 10

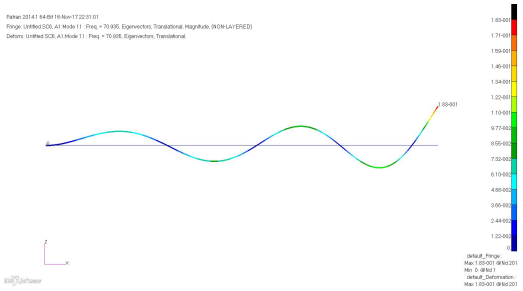

(e) Mode 9

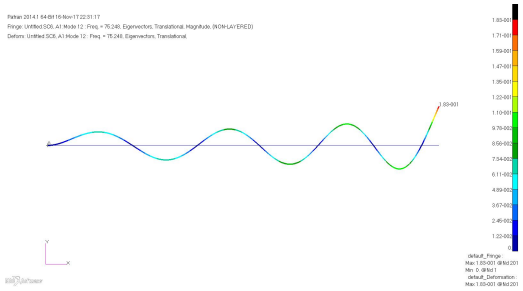

(f) Mode 10

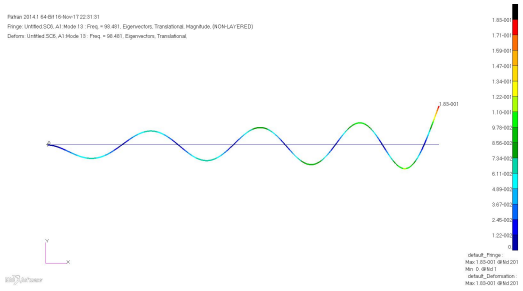

(g) Mode 10

Figure B.14: Mode shapes for the Modes 7 to 13 of a C-F Rotating Tapered Beam with $\eta = 6$

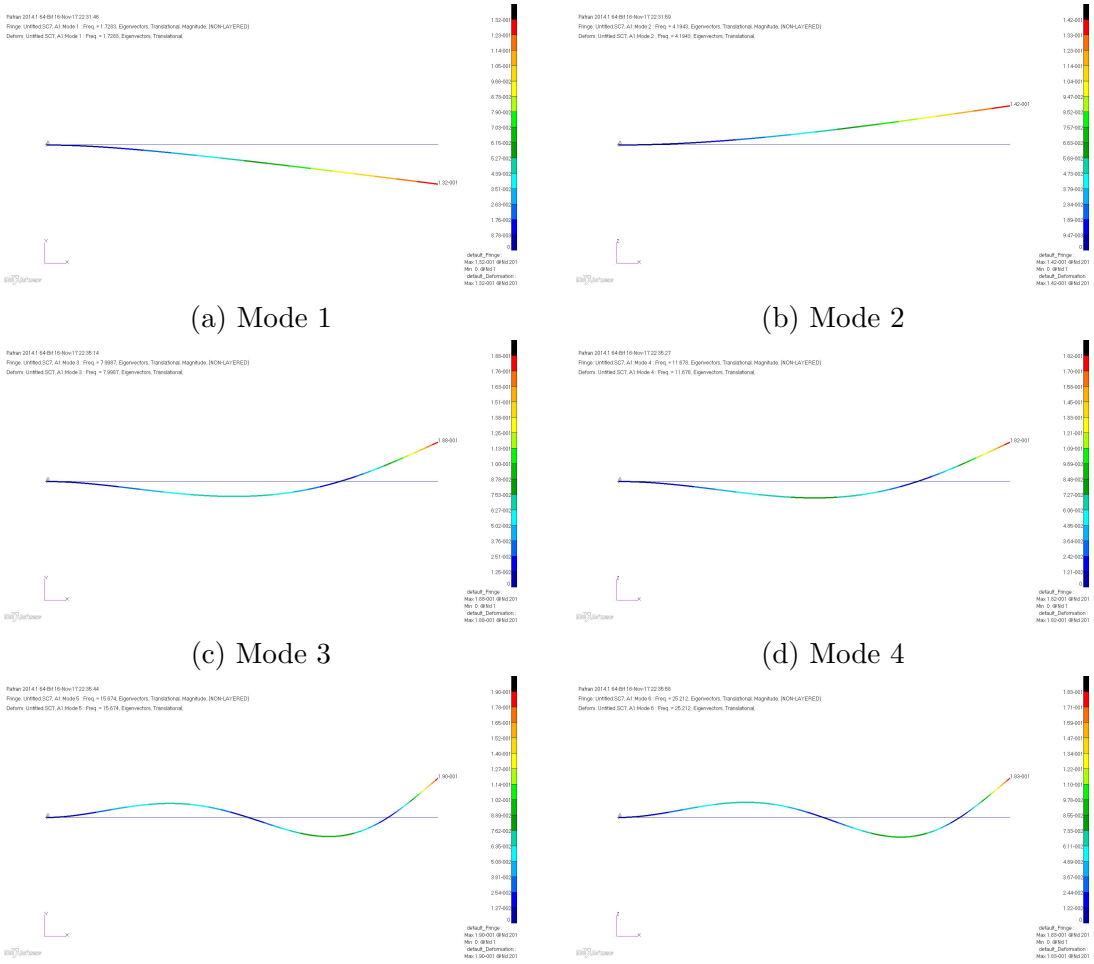

(a) Mode 1

(b) Mode 2

(c) Mode 3

(d) Mode 4

(e) Mode 5

(f) Mode 6

Figure B.15: Mode shapes for the Modes 1 to 6 of a C-F Rotating Tapered Beam with $\eta = 7$

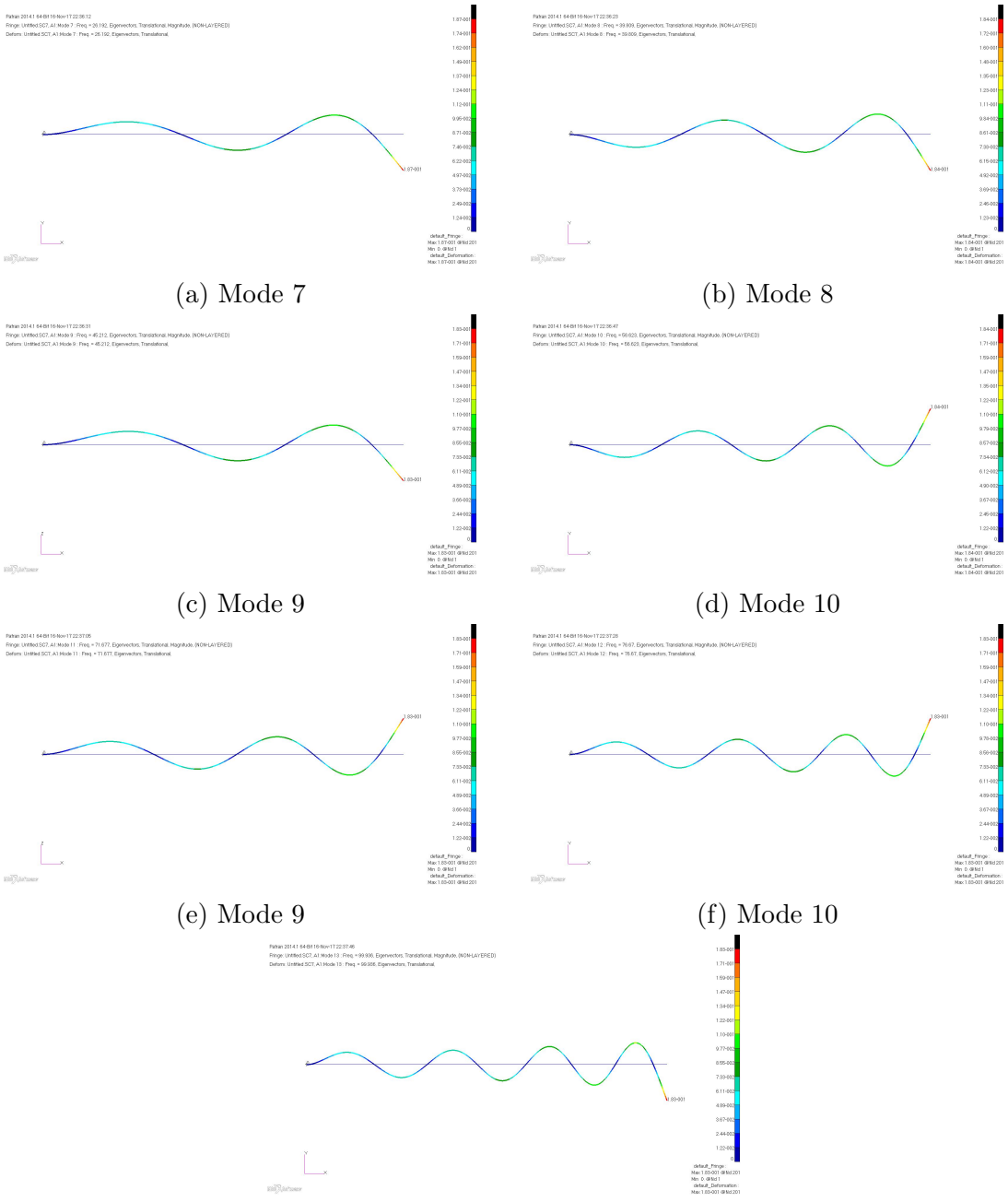

(a) Mode 7

(b) Mode 8

(c) Mode 9

(d) Mode 10

(e) Mode 9

(f) Mode 10

(g) Mode 10

Figure B.16: Mode shapes for the Modes 7 to 13 of a C-F Rotating Tapered Beam with $\eta = 7$

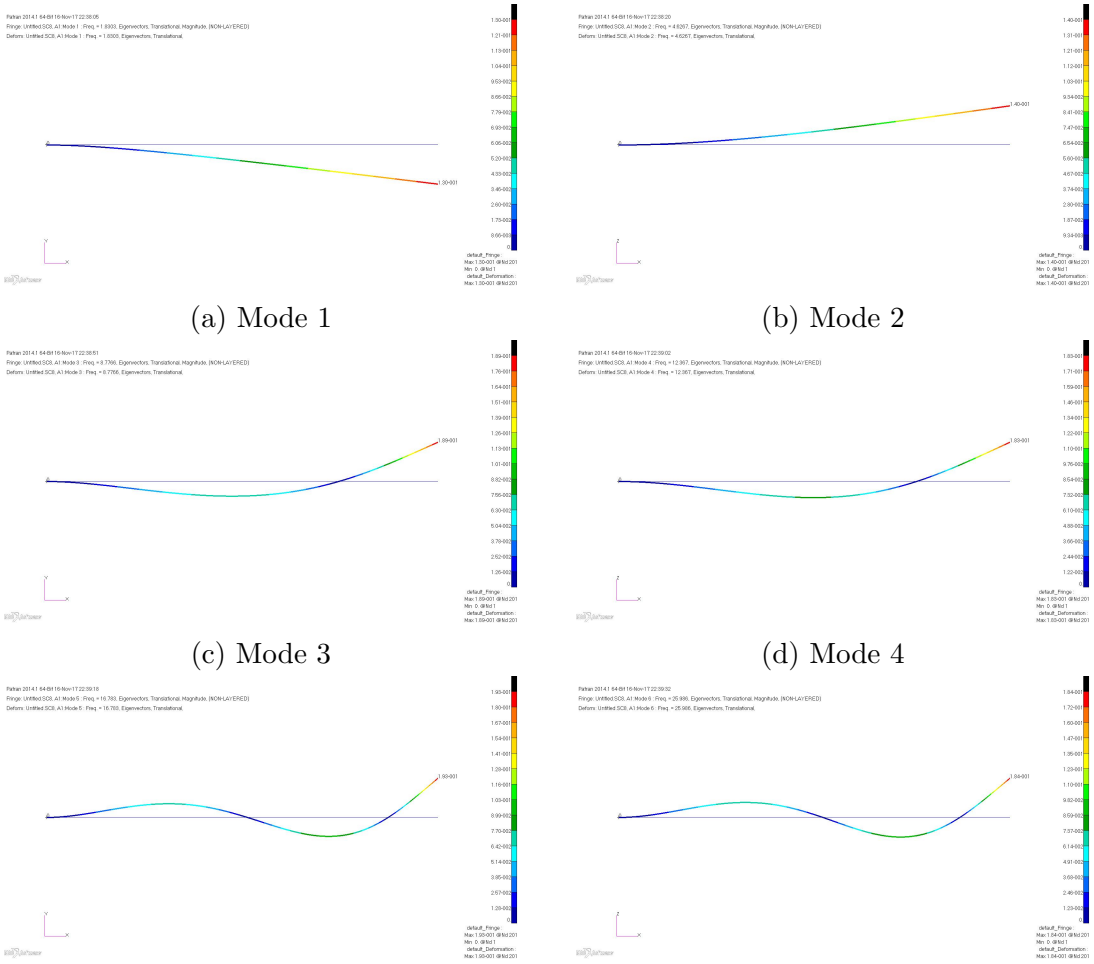

(a) Mode 1

(b) Mode 2

(c) Mode 3

(d) Mode 4

(e) Mode 5

(f) Mode 6

Figure B.17: Mode shapes for the Modes 1 to 6 of a C-F Rotating Tapered Beam with $\eta = 8$

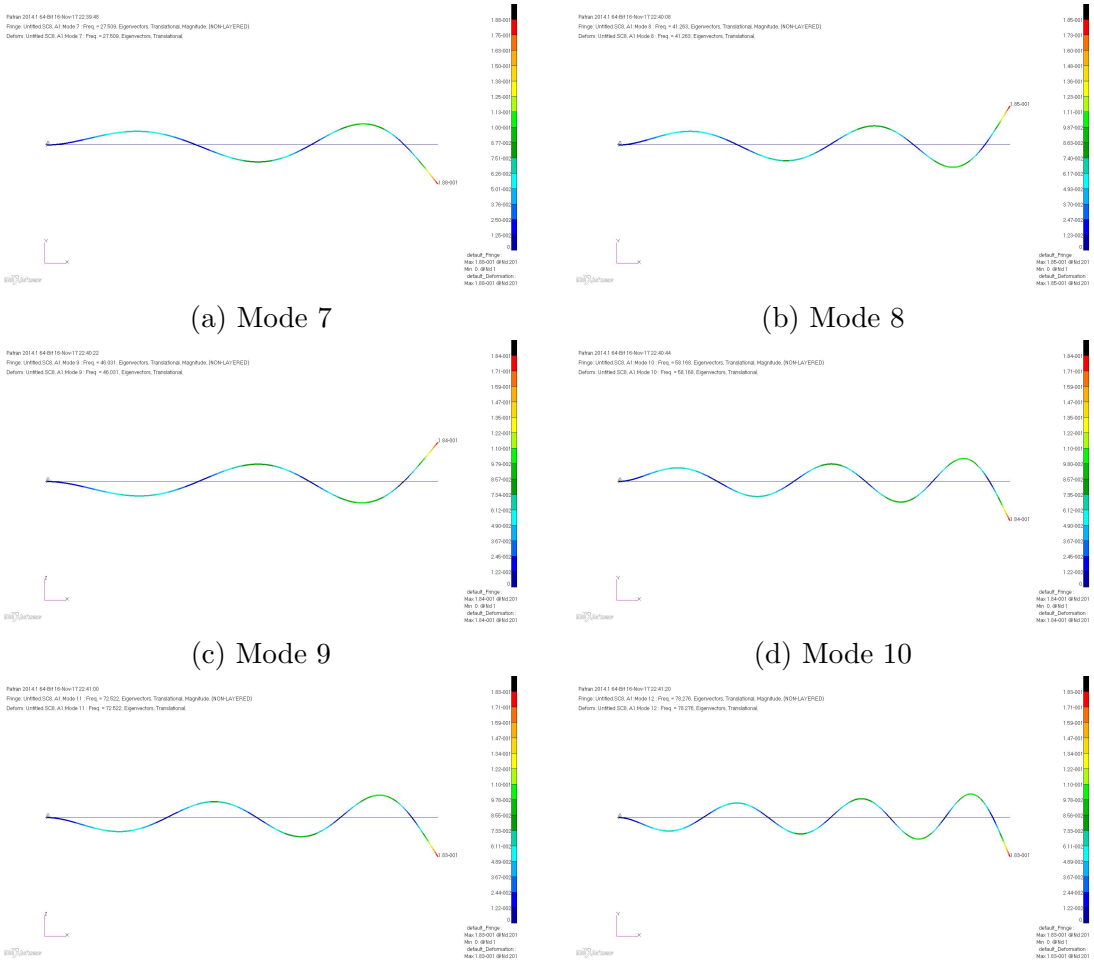

(a) Mode 7

(b) Mode 8

(c) Mode 9

(d) Mode 10

(e) Mode 9

(f) Mode 10

Figure B.18: Mode shapes for the Modes 7 to 12 of a C-F Rotating Tapered Beam with $\eta = 8$

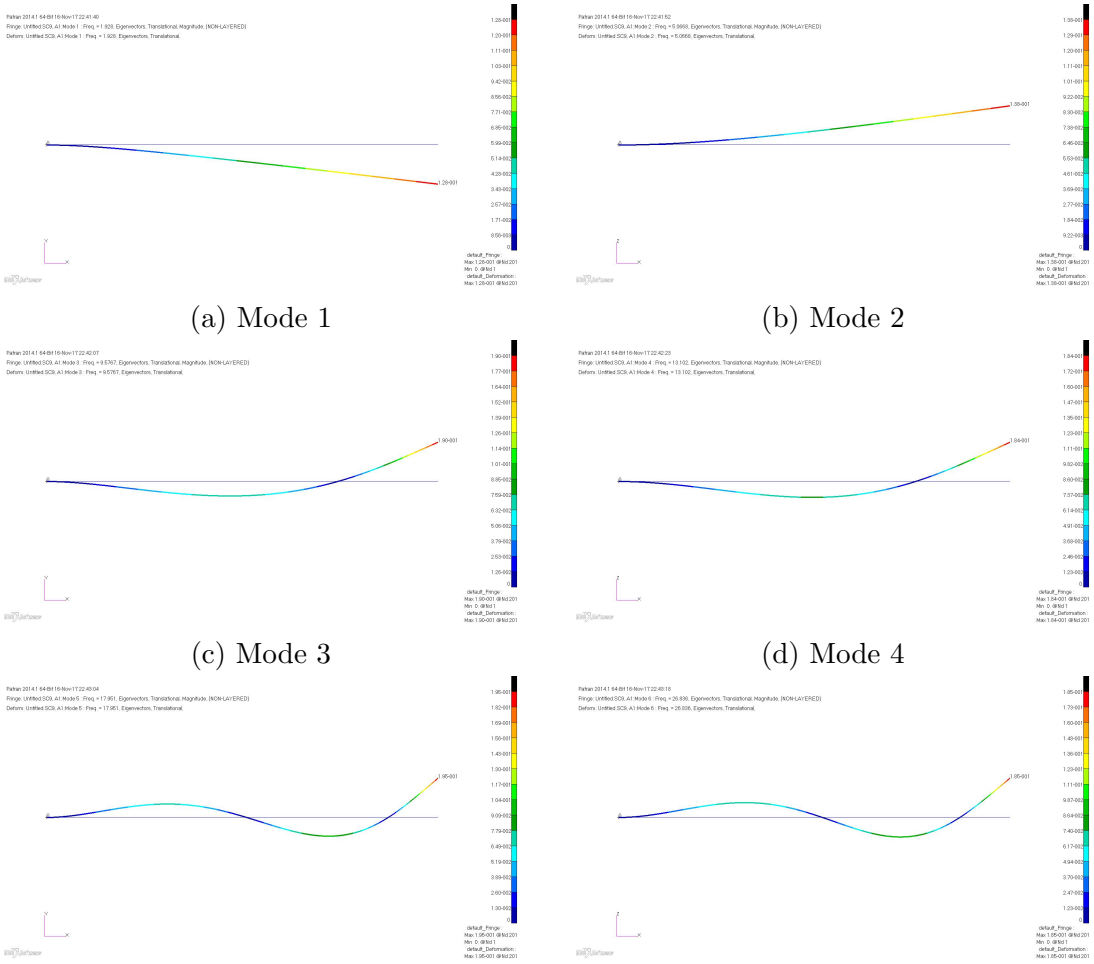

(a) Mode 1

(b) Mode 2

(c) Mode 3

(d) Mode 4

(e) Mode 5

(f) Mode 6

Figure B.19: Mode shapes for the Modes 1 to 6 of a C-F Rotating Tapered Beam with $\eta = 9$

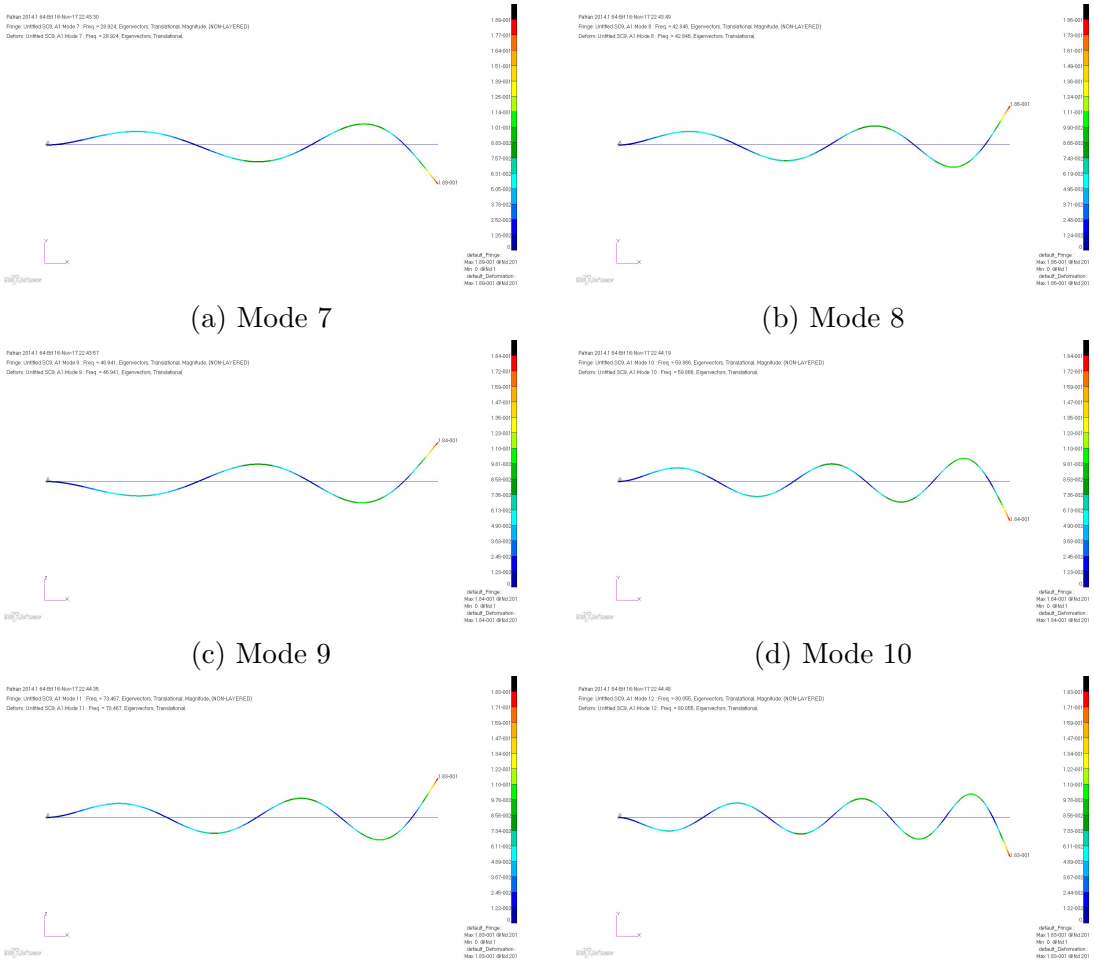

(a) Mode 7

(b) Mode 8

(c) Mode 9

(d) Mode 10

(e) Mode 9

(f) Mode 10

Figure B.20: Mode shapes for the Modes 7 to 12 of a C-F Rotating Tapered Beam with $\eta = 9$

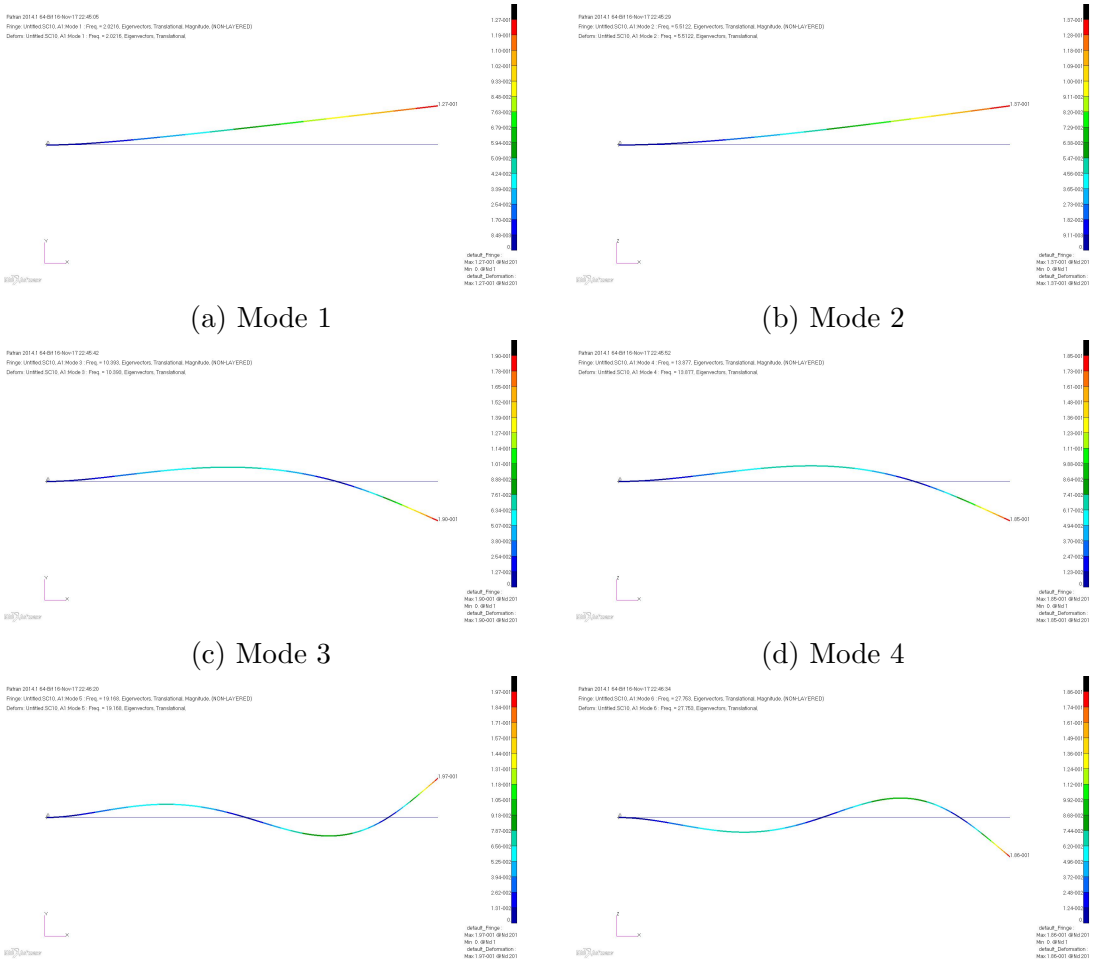

(a) Mode 1

(b) Mode 2

(c) Mode 3

(d) Mode 4

(e) Mode 5

(f) Mode 6

Figure B.21: Mode shapes for the Modes 1 to 6 of a C-F Rotating Tapered Beam with $\eta = 10$

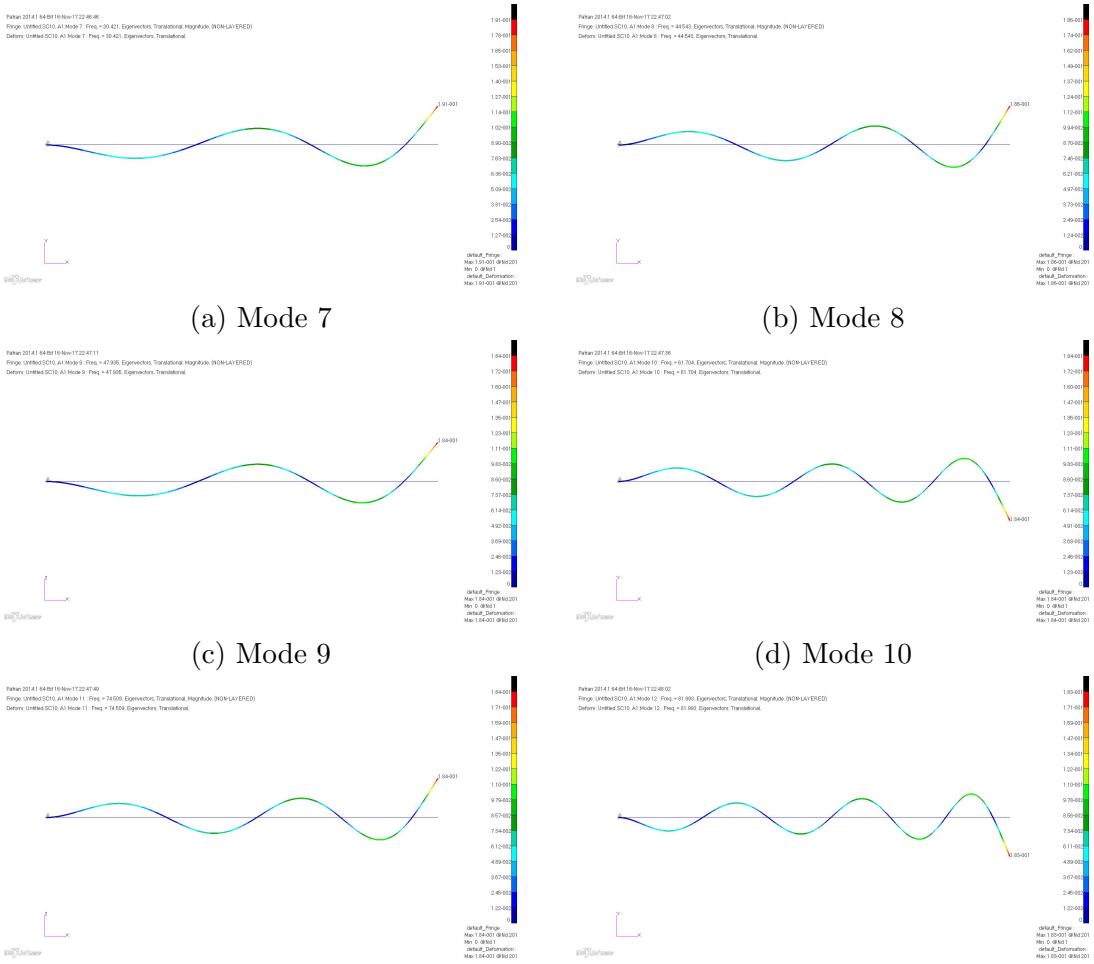

(a) Mode 7

(b) Mode 8

(c) Mode 9

(d) Mode 10

(e) Mode 9

(f) Mode 10

Figure B.22: Mode shapes for the Modes 7 to 12 of a C-F Rotating Tapered Beam with $\eta = 10$

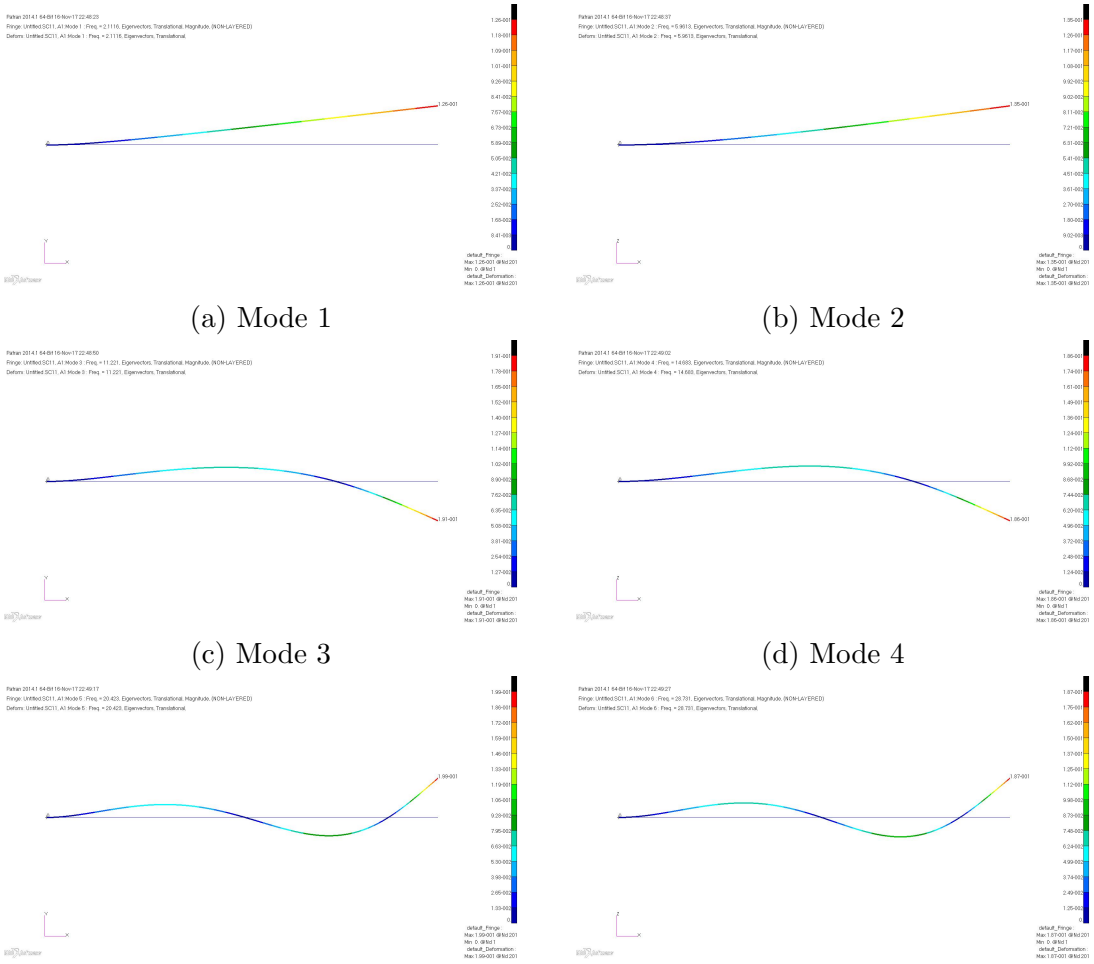

(a) Mode 1

(b) Mode 2

(c) Mode 3

(d) Mode 4

(e) Mode 5

(f) Mode 6

Figure B.23: Mode shapes for the Modes 1 to 6 of a C-F Rotating Tapered Beam with $\eta = 11$

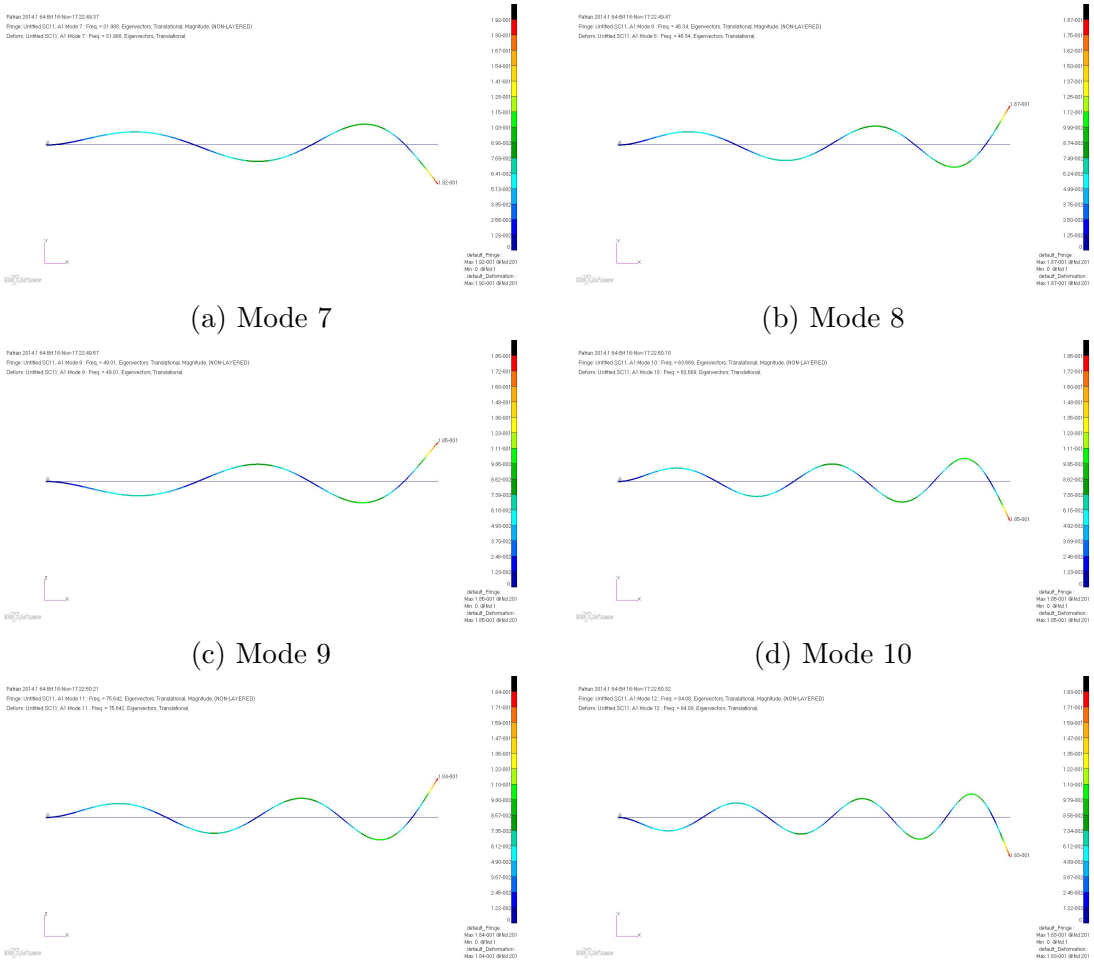

(a) Mode 7

(b) Mode 8

(c) Mode 9

(d) Mode 10

(e) Mode 9

(f) Mode 10

Figure B.24: Mode shapes for the Modes 7 to 12 of a C-F Rotating Tapered Beam with $\eta = 11$

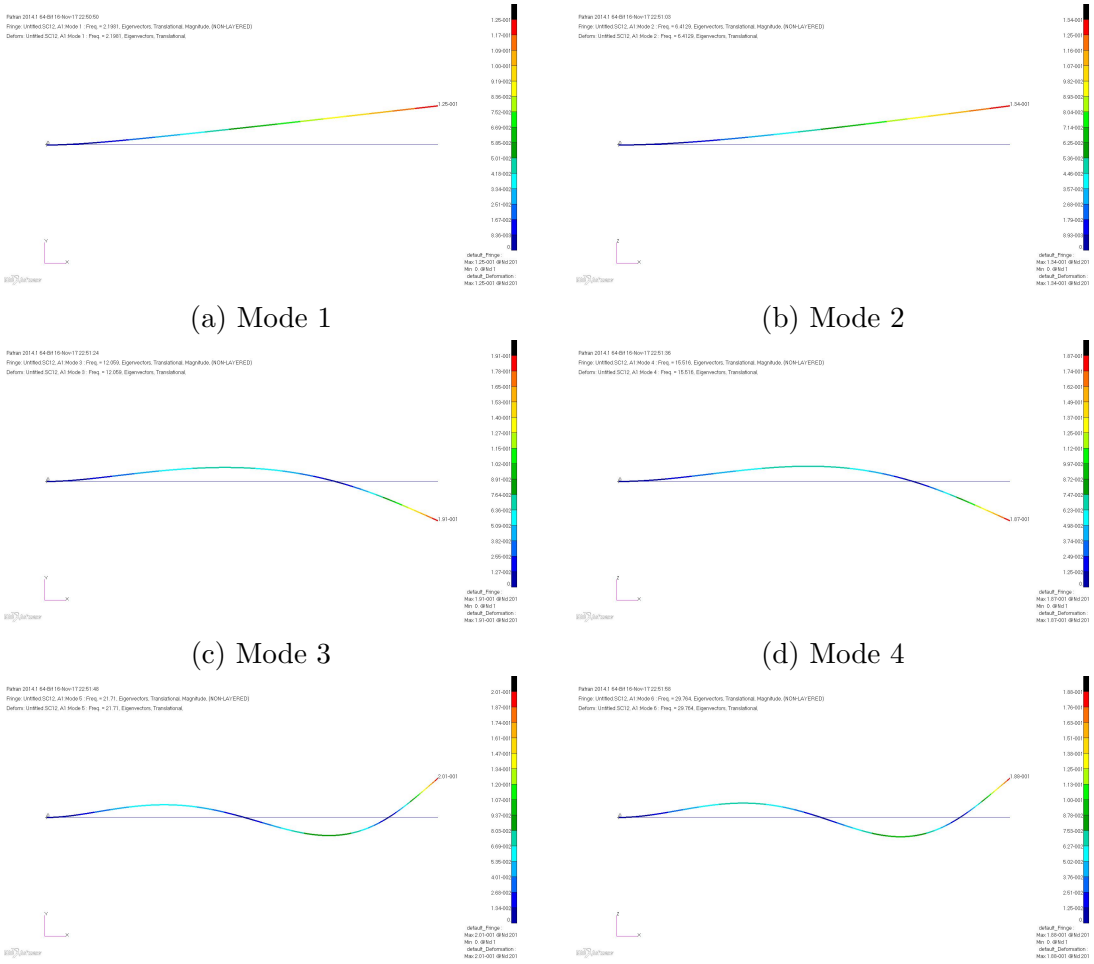

(a) Mode 1

(b) Mode 2

(c) Mode 3

(d) Mode 4

(e) Mode 5

(f) Mode 6

Figure B.25: Mode shapes for the Modes 1 to 6 of a C-F Rotating Tapered Beam with $\eta = 12$

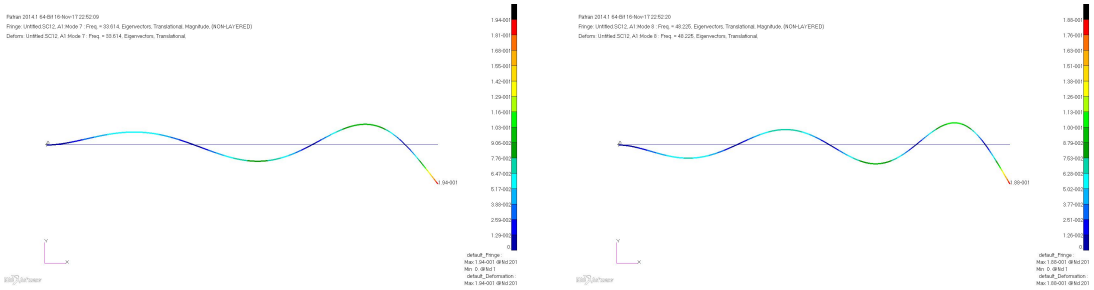

(a) Mode 7

(b) Mode 8

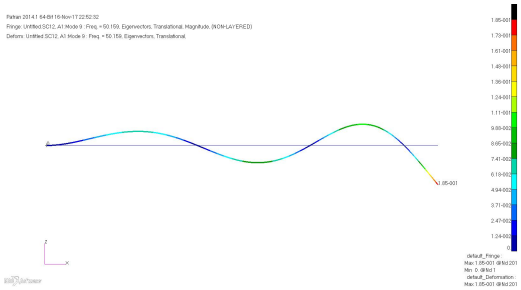

(c) Mode 9

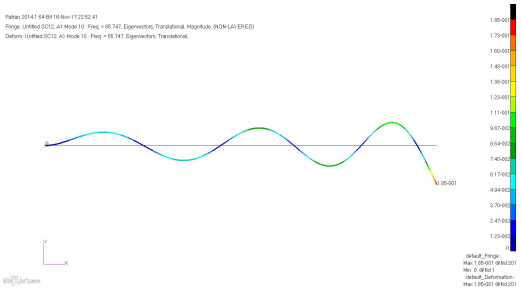

(d) Mode 10

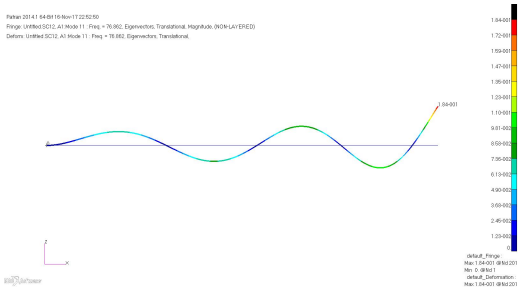

(e) Mode 9

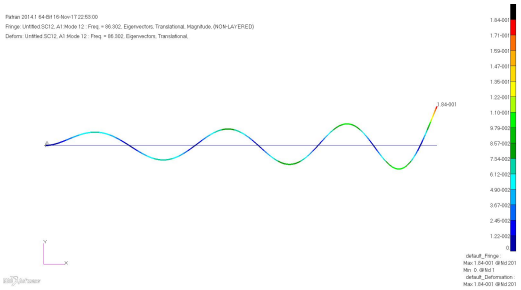

(f) Mode 10

Figure B.26: Mode shapes for the Modes 7 to 12 of a C-F Rotating Tapered Beam with $\eta = 12$

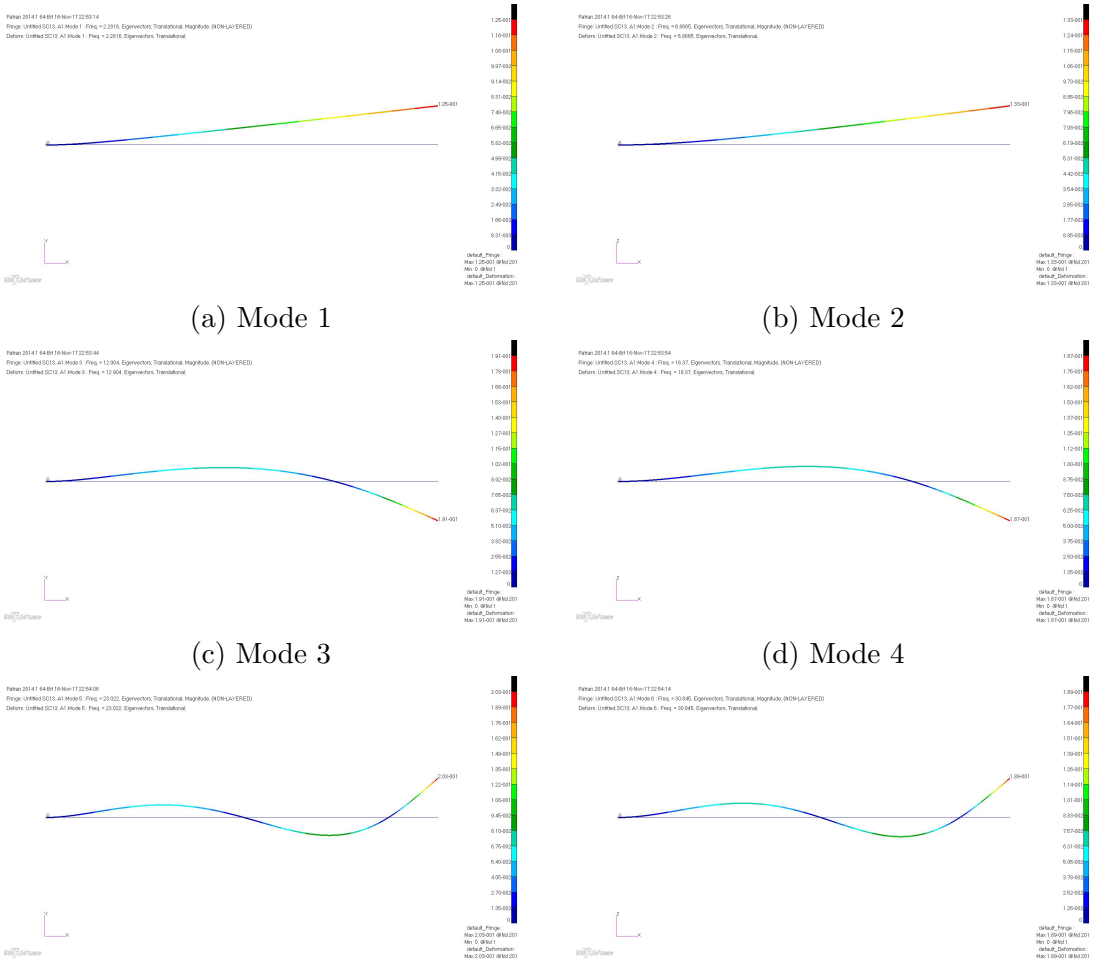

(a) Mode 1

(b) Mode 2

(c) Mode 3

(d) Mode 4

(e) Mode 5

(f) Mode 6

Figure B.27: Mode shapes for the Modes 1 to 6 of a C-F Rotating Tapered Beam with $\eta = 13$

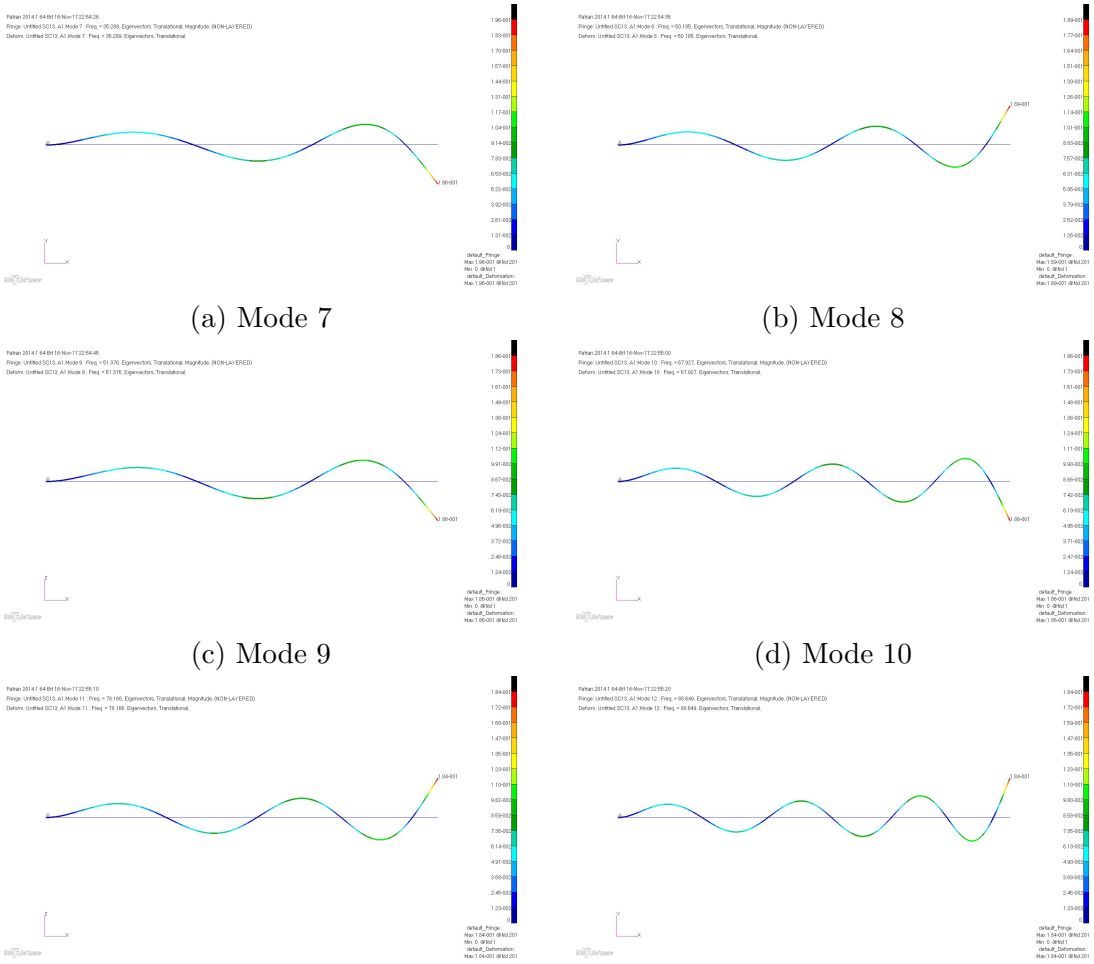

(a) Mode 7

(b) Mode 8

(c) Mode 9

(d) Mode 10

(e) Mode 9

(f) Mode 10

Figure B.28: Mode shapes for the Modes 7 to 12 of a C-F Rotating Tapered Beam with η = 13

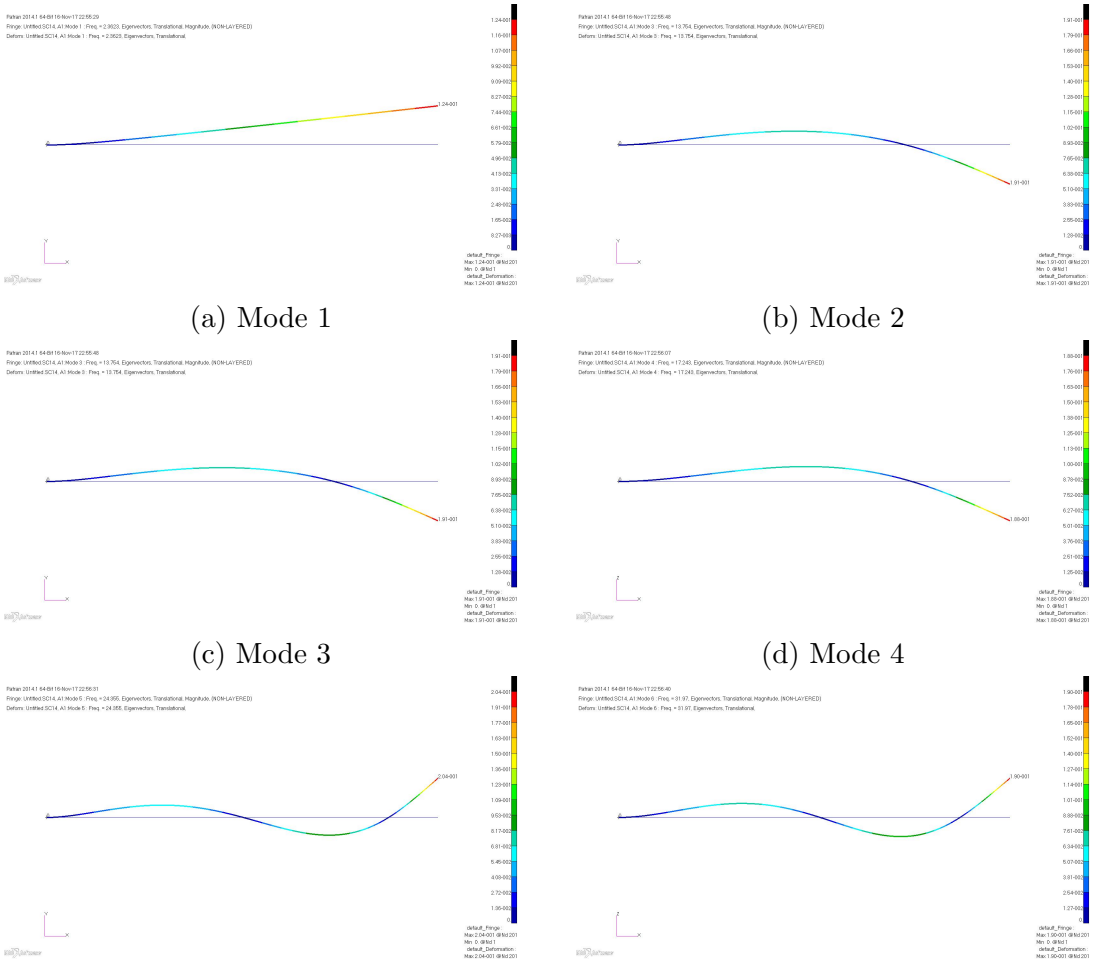

(a) Mode 1

(b) Mode 2

(c) Mode 3

(d) Mode 4

(e) Mode 5

(f) Mode 6

Figure B.29: Mode shapes for the Modes 1 to 6 of a C-F Rotating Tapered Beam with $\eta = 14$

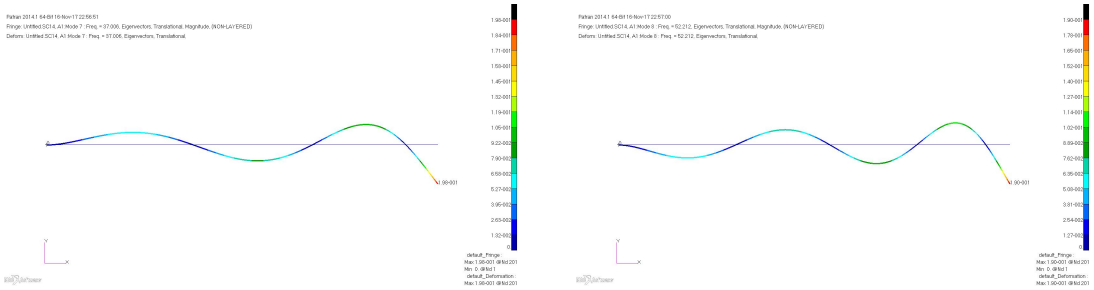

(a) Mode 7

(b) Mode 8

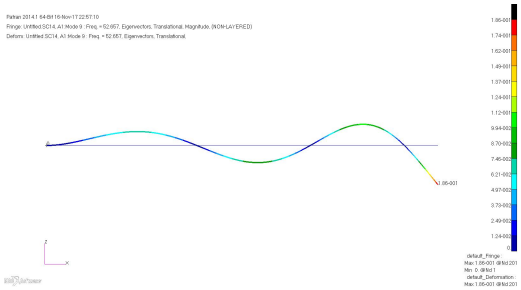

(c) Mode 9

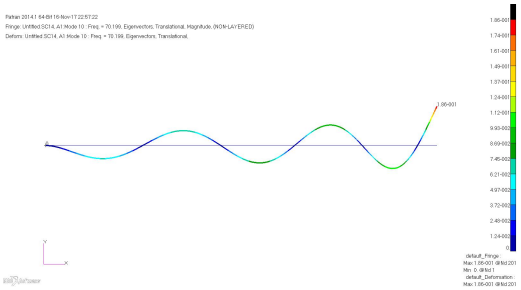

(d) Mode 10

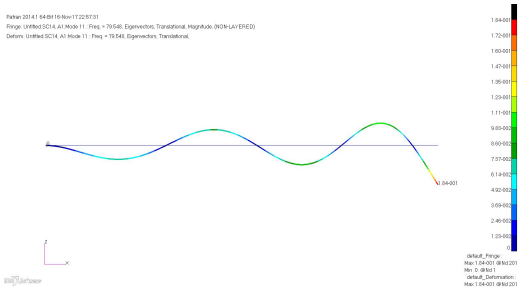

(e) Mode 9

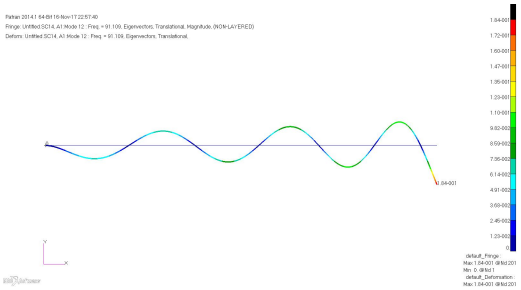

(f) Mode 10

Figure B.30: Mode shapes for the Modes 7 to 12 of a C-F Rotating Tapered Beam with $\eta = 14$

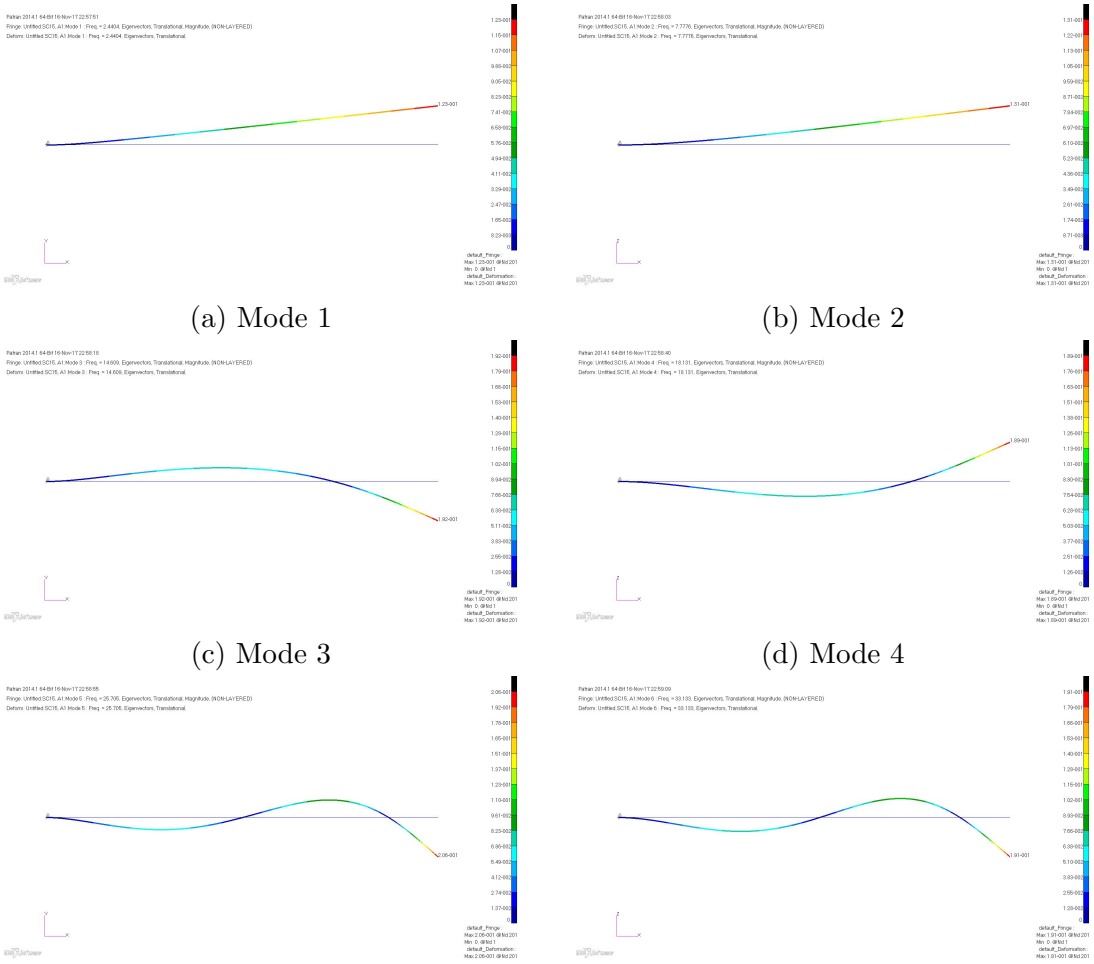

(a) Mode 1

(b) Mode 2

(c) Mode 3

(d) Mode 4

(e) Mode 5

(f) Mode 6

Figure B.31: Mode shapes for the Modes 1 to 6 of a C-F Rotating Tapered Beam with $\eta = 15$

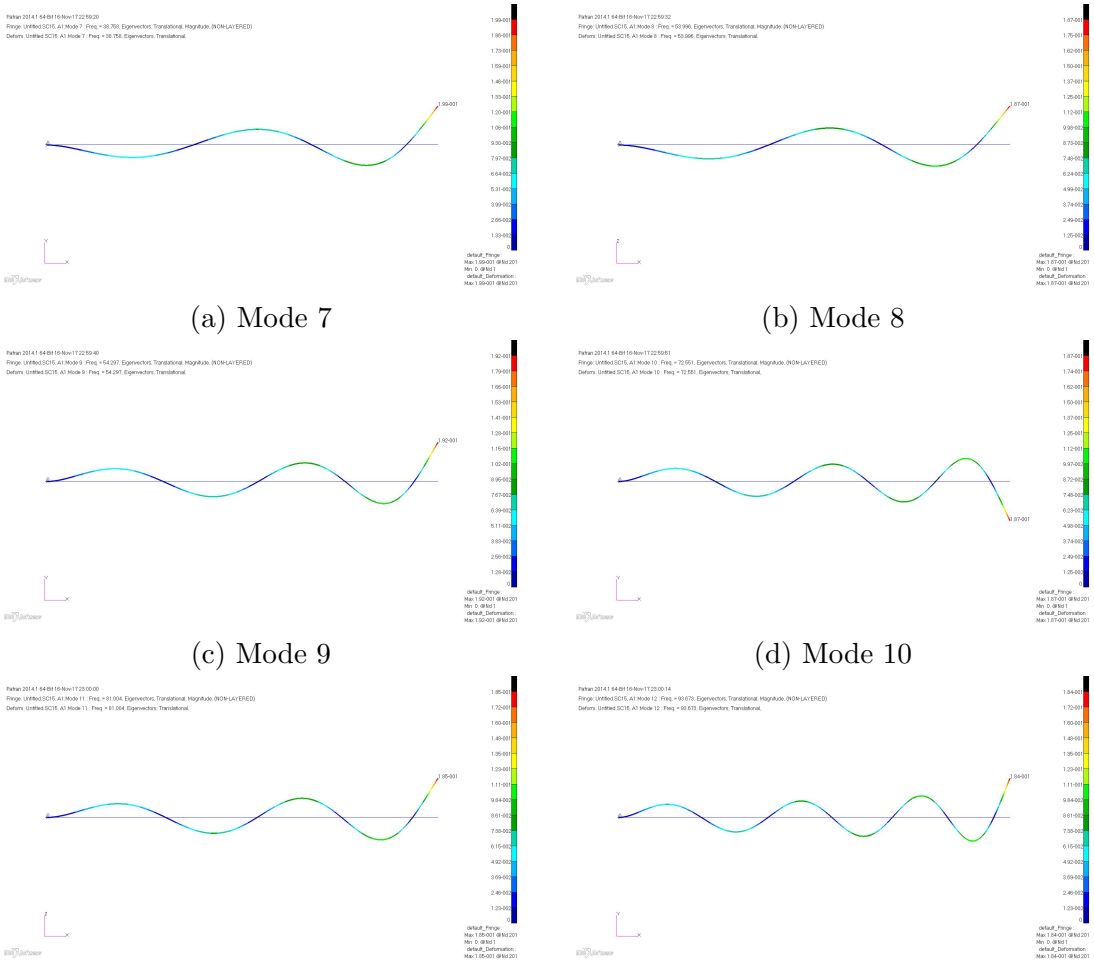

(a) Mode 7

(b) Mode 8

(c) Mode 9

(d) Mode 10

(e) Mode 9

(f) Mode 10

Figure B.32: Mode shapes for the Modes 7 to 12 of a C-F Rotating Tapered Beam with η = 15

Appendix C

C.1 Mode shapes of a C-F Non-rotating Beam with Added Mass

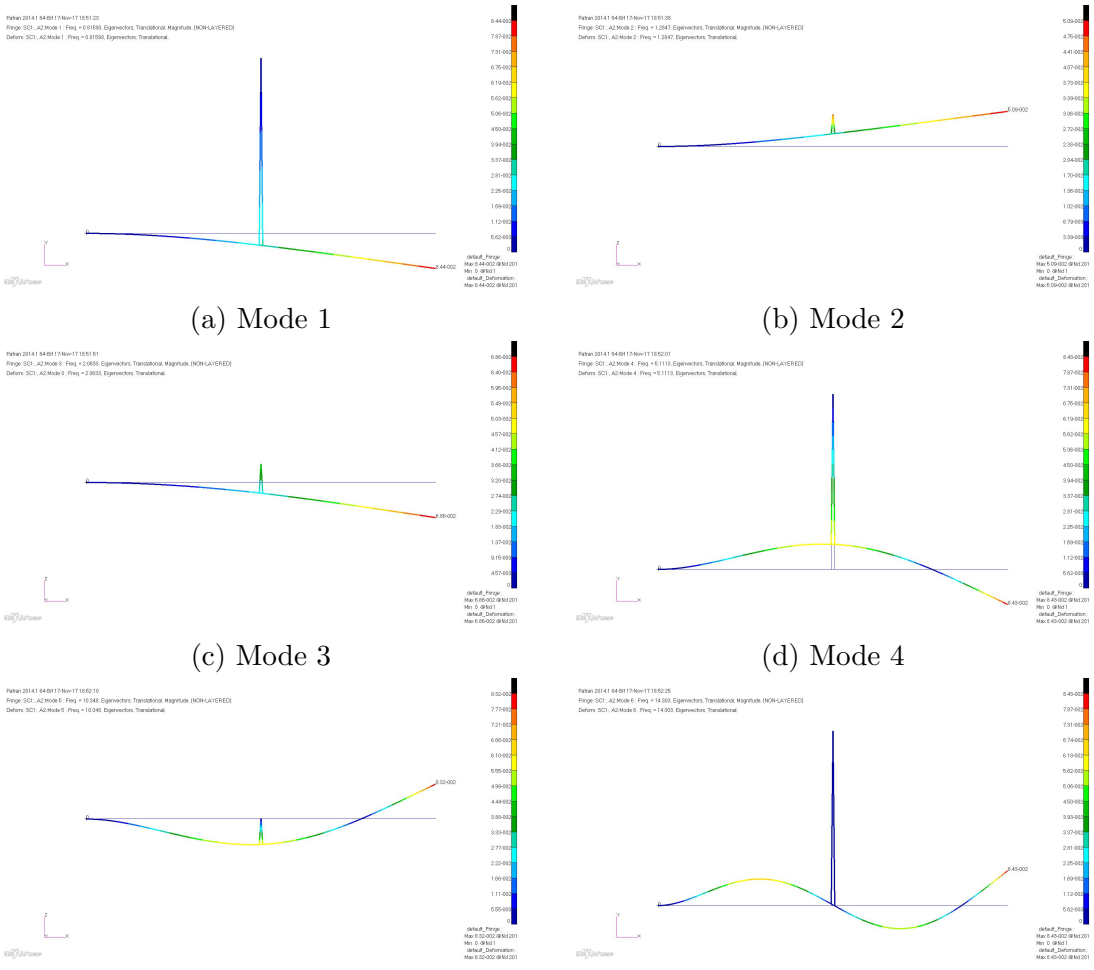

(a) Mode 1

(b) Mode 2

(c) Mode 3

(d) Mode 4

(e) Mode 5

(f) Mode 6

Figure C.1: Mode shapes for the Modes 1 to 6 of a C-F Non-rotating Beam with Added Mass

C.2 Mode shapes of a C-F Rotating Beam with Added Mass for $\eta = 1$ to 15

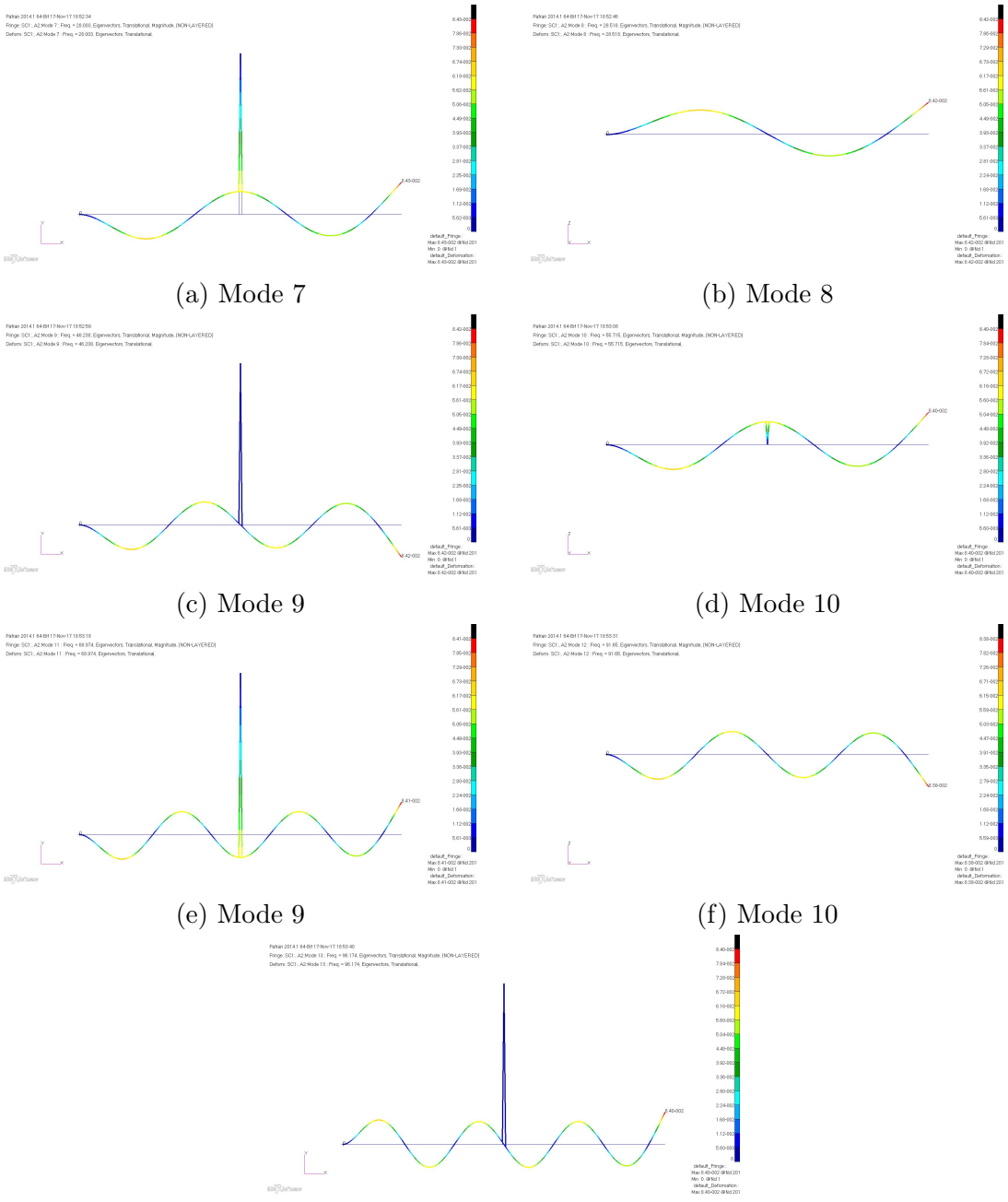

(a) Mode 7

(b) Mode 8

(c) Mode 9

(d) Mode 10

(e) Mode 9

(f) Mode 10

(g) Mode 10

Figure C.2: Mode shapes for the Modes 7 to 13 of a C-F Non-rotating Beam with Added Mass

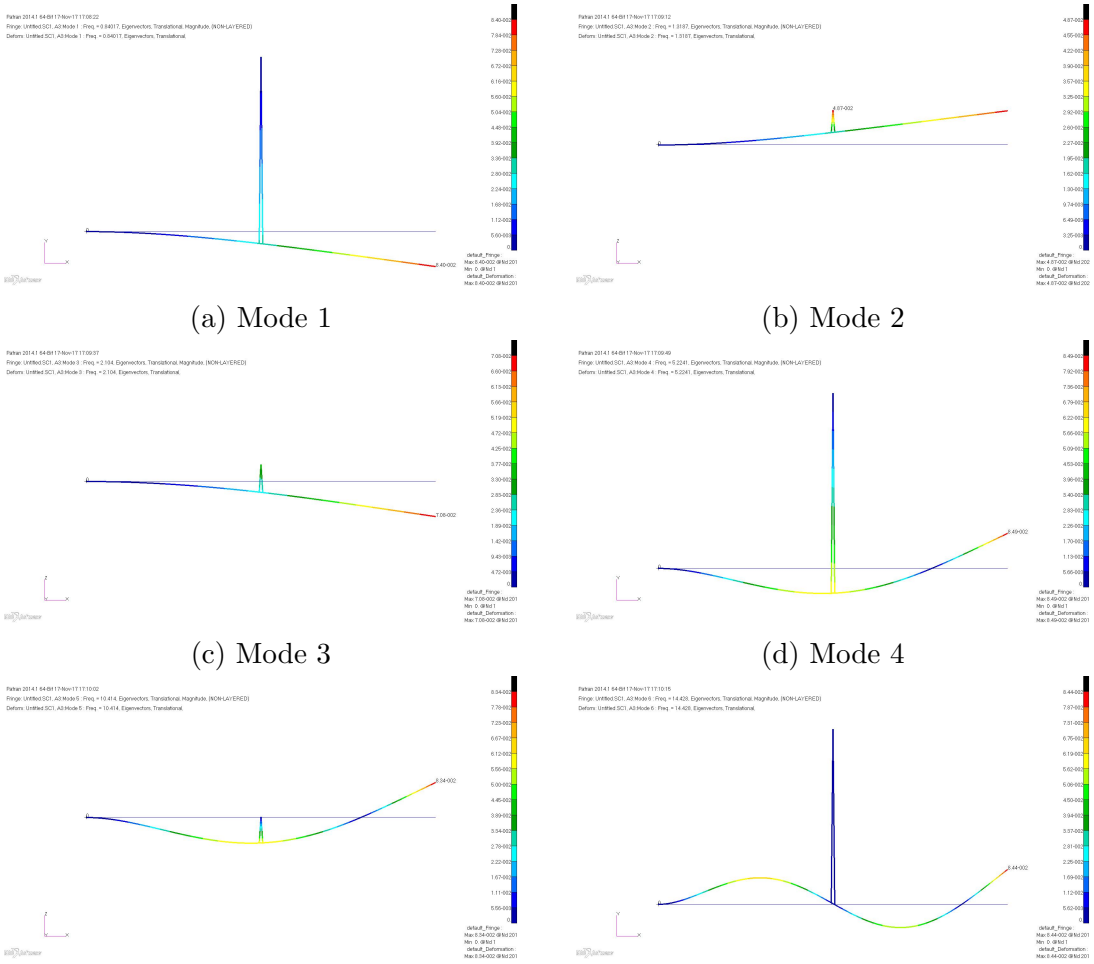

(a) Mode 1

(b) Mode 2

(c) Mode 3

(d) Mode 4

(e) Mode 5

(f) Mode 6

Figure C.3: Mode shapes for the Modes 1 to 6 of a C-F Rotating Beam with Added Mass $\eta = 1$

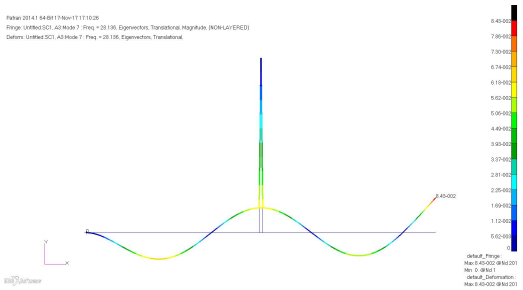

(a) Mode 7

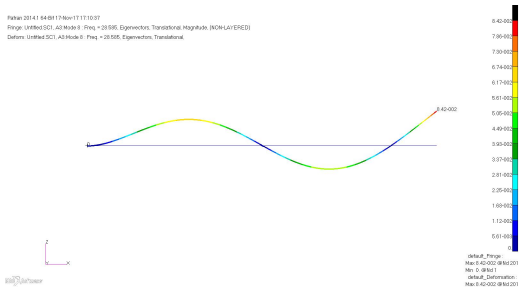

(b) Mode 8

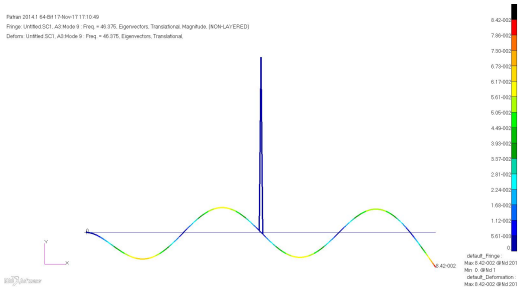

(c) Mode 9

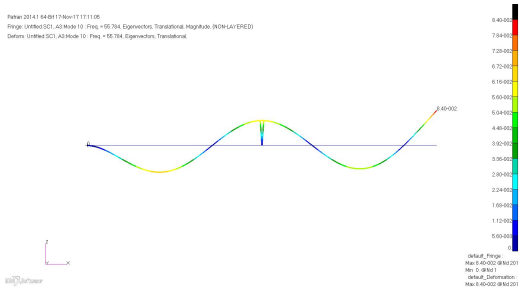

(d) Mode 10

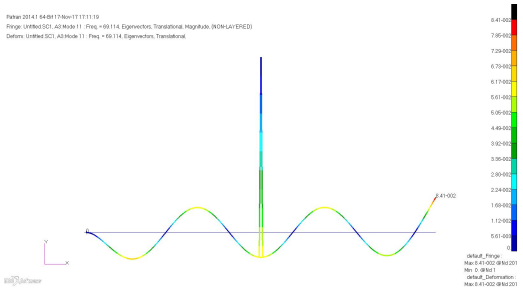

(e) Mode 11

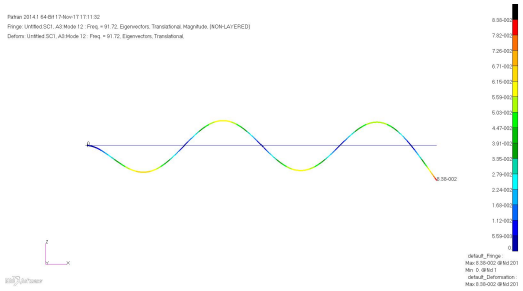

(f) Mode 12

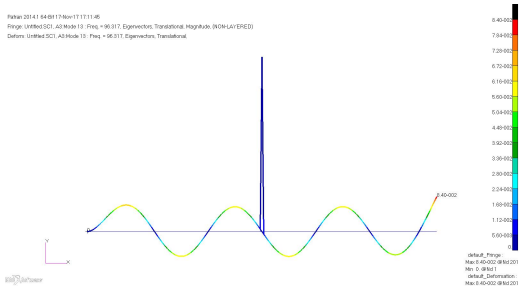

(g) Mode 13

Figure C.4: Mode shapes for the Modes 7 to 13 of a C-F Rotating Beam with Added Mass $\eta = 1$

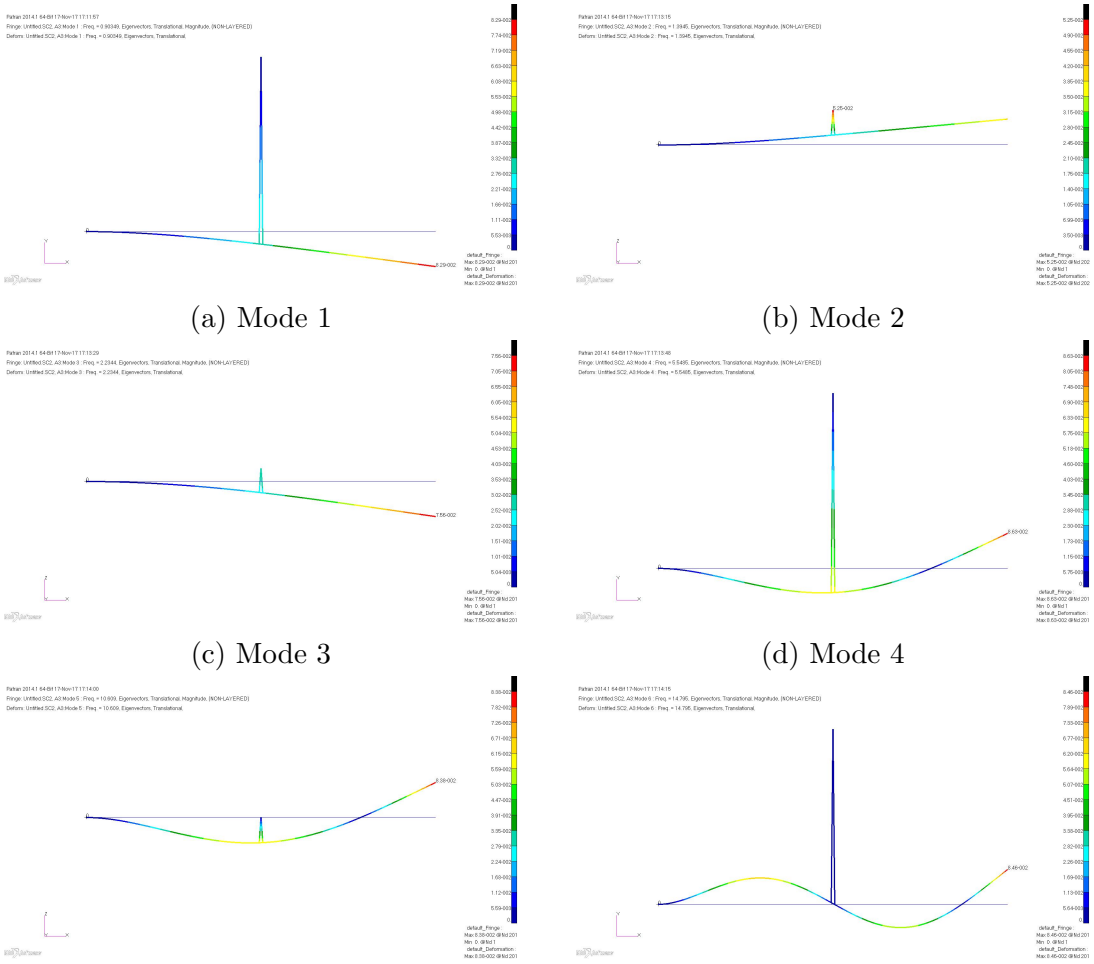

(a) Mode 1

(b) Mode 2

(c) Mode 3

(d) Mode 4

(e) Mode 5

(f) Mode 6

Figure C.5: Mode shapes for the Modes 1 to 6 of a C-F Rotating Beam with Added Mass $\eta = 2$

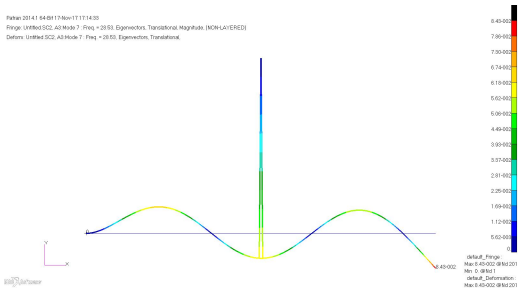

(a) Mode 7

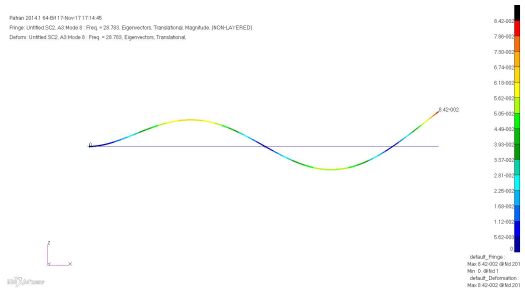

(b) Mode 8

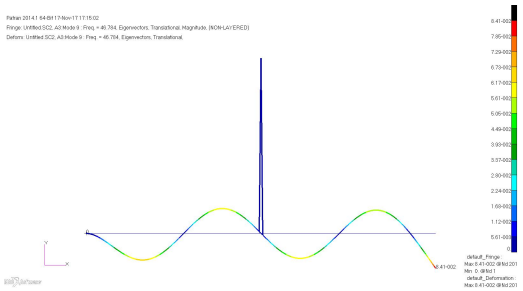

(c) Mode 9

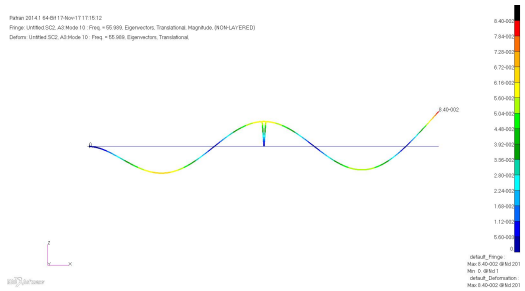

(d) Mode 10

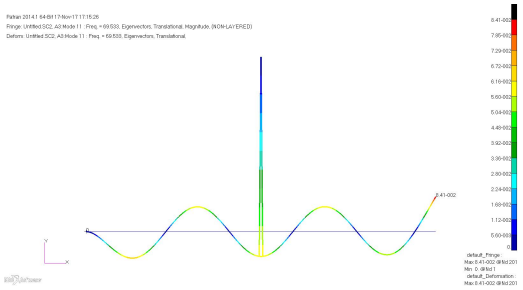

(e) Mode 11

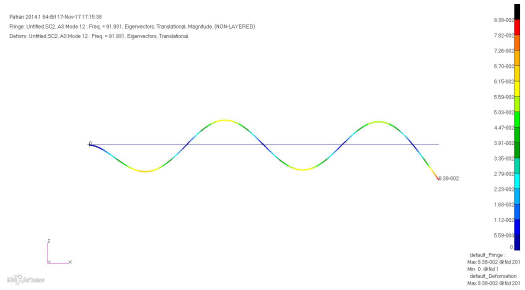

(f) Mode 12

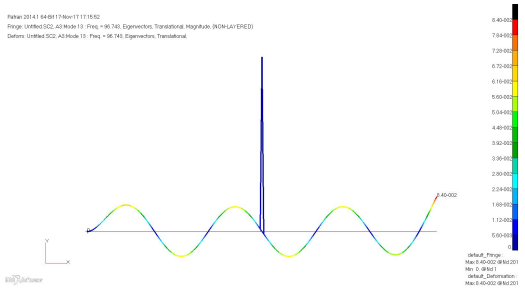

(g) Mode 13

Figure C.6: Mode shapes for the Modes 7 to 13 of a C-F Beam with Added Mass $\eta = 2$

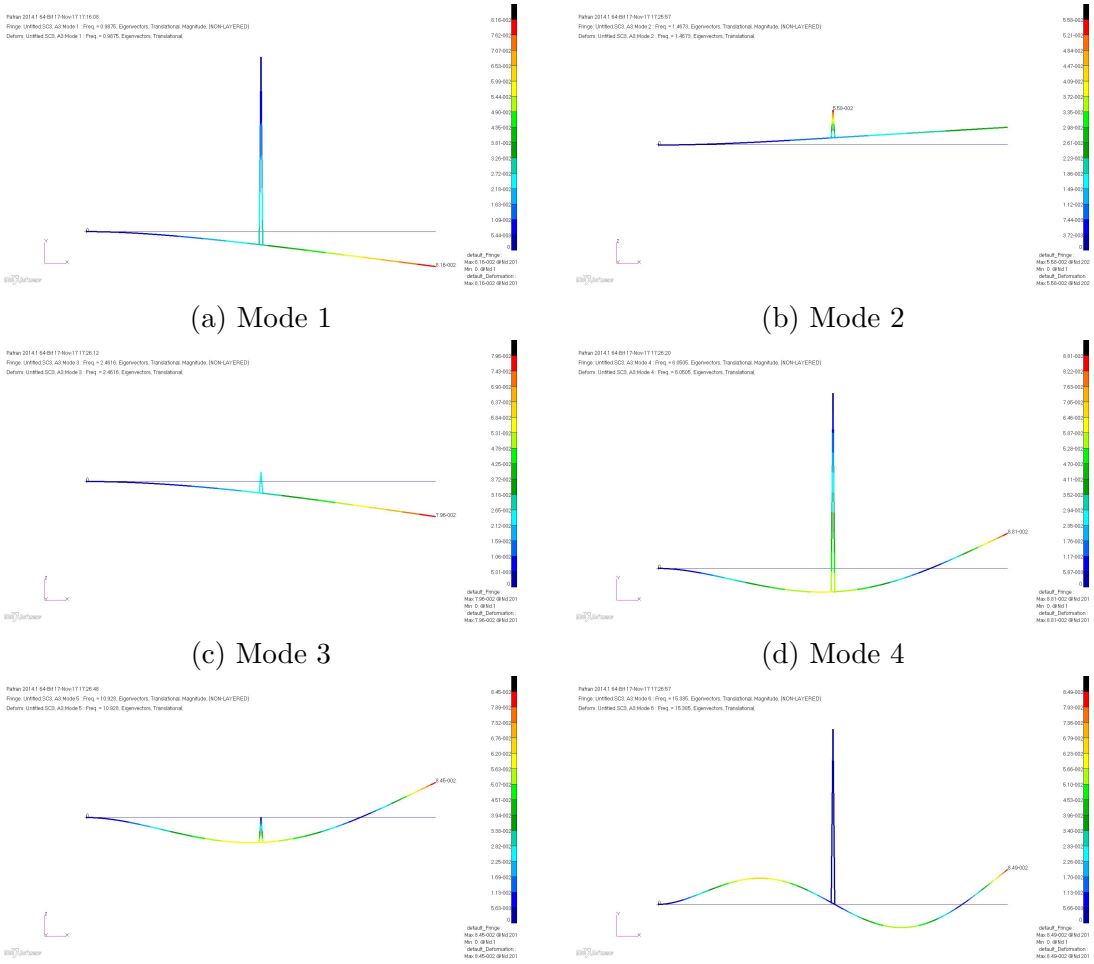

(a) Mode 1

(b) Mode 2

(c) Mode 3

(d) Mode 4

(e) Mode 5

(f) Mode 6

Figure C.7: Mode shapes for the Modes 1 to 6 of a C-F Rotating Beam with Added Mass $\eta = 3$

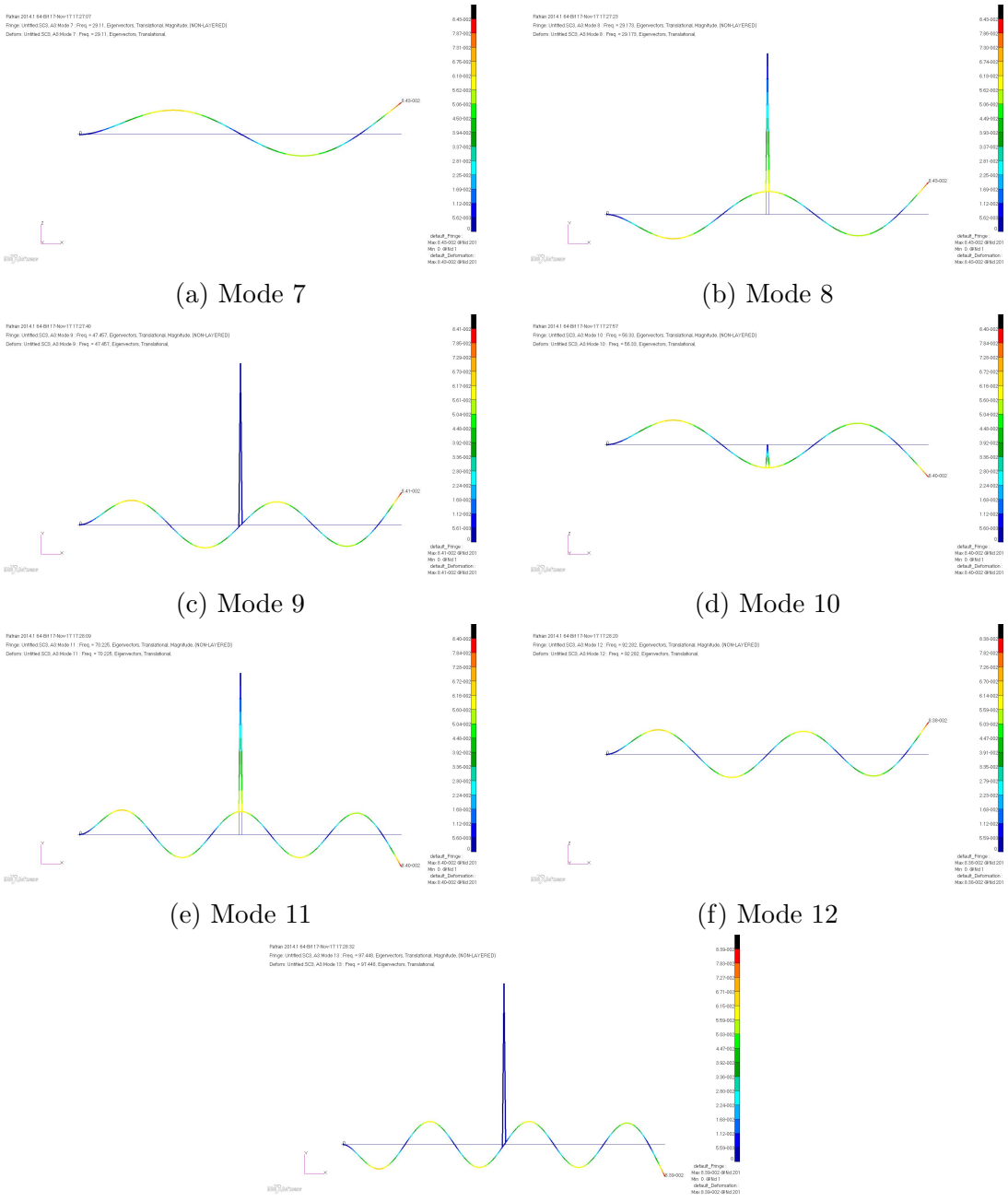

(a) Mode 7

(b) Mode 8

(c) Mode 9

(d) Mode 10

(e) Mode 11

(f) Mode 12

(g) Mode 13

Figure C.8: Mode shapes for the Modes 7 to 13 of a C-F Rotating Beam with Added Mass $\eta = 3$

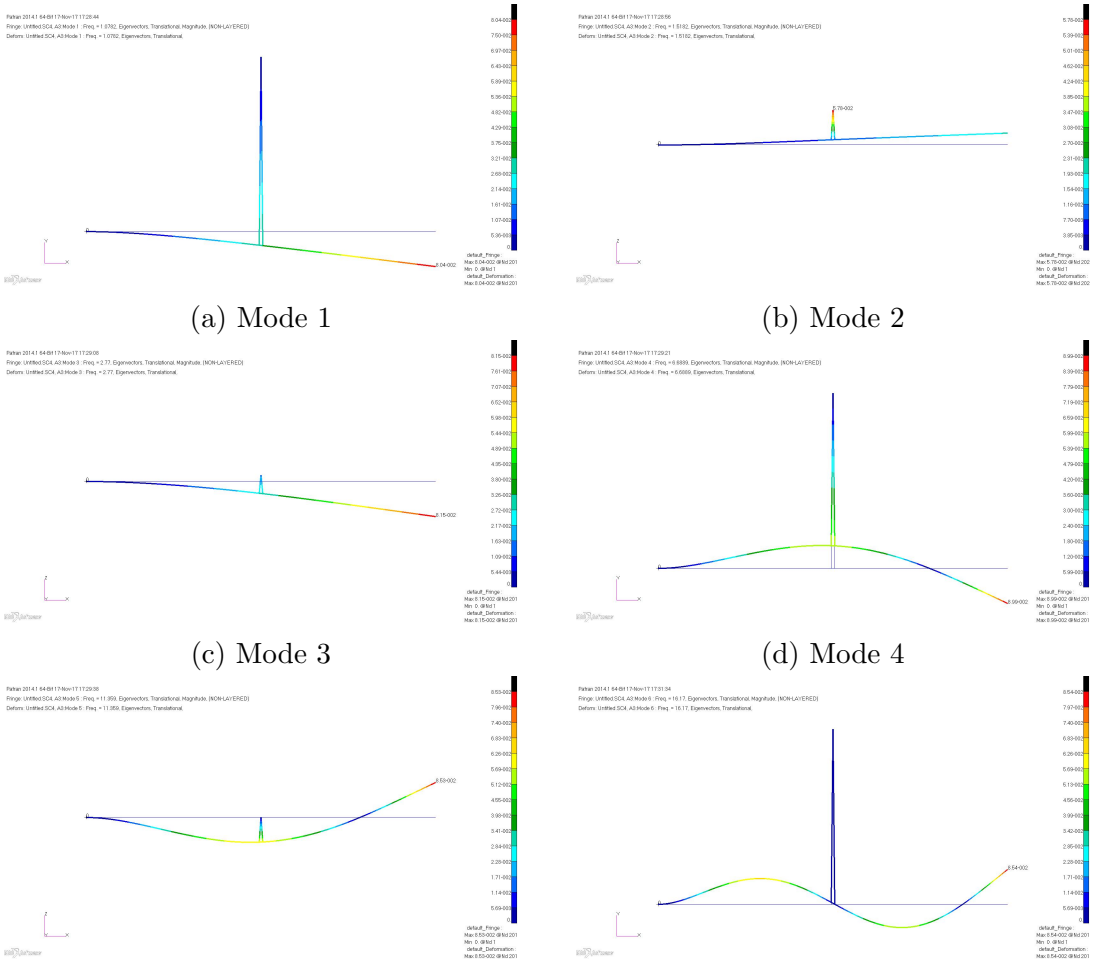

(a) Mode 1

(b) Mode 2

(c) Mode 3

(d) Mode 4

(e) Mode 5

(f) Mode 6

Figure C.9: Mode shapes for the Modes 1 to 6 of a C-F Rotating Beam with Added Mass $\eta = 4$

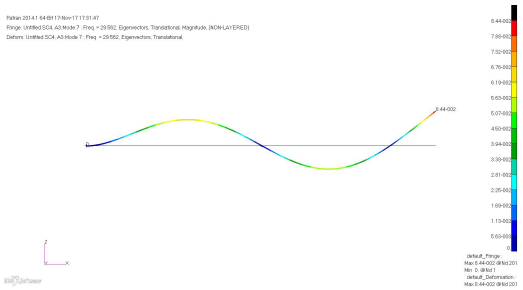

(a) Mode 7

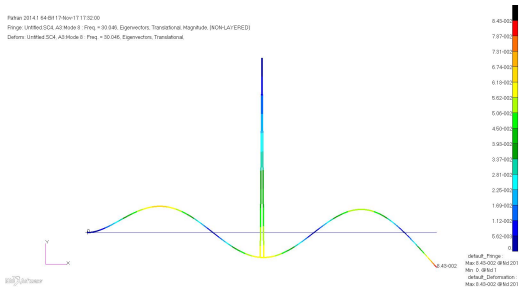

(b) Mode 8

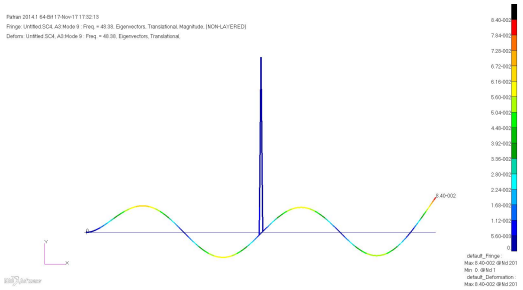

(c) Mode 9

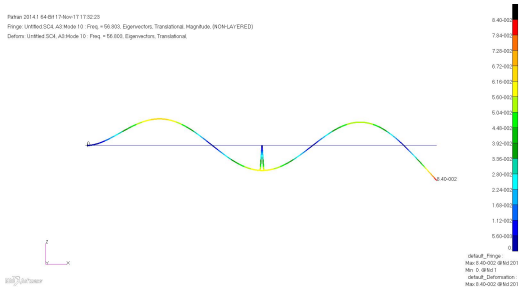

(d) Mode 10

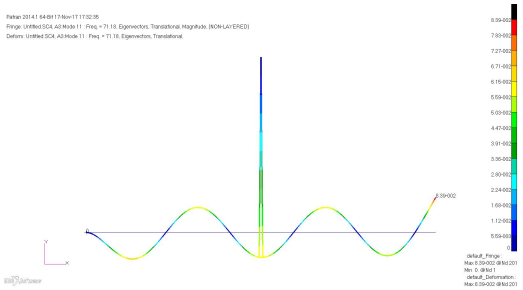

(e) Mode 11

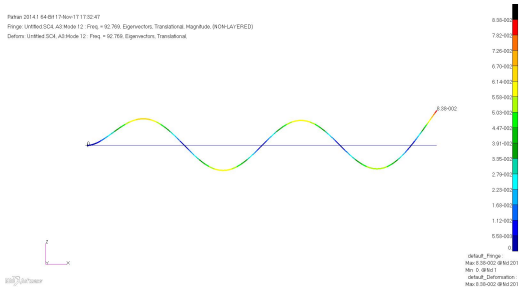

(f) Mode 12

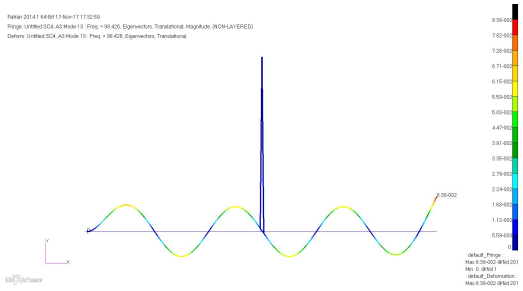

(g) Mode 13

Figure C.10: Mode shapes for the Modes 7 to 13 of a C-F Rotating Beam with Added Mass $\eta = 4$

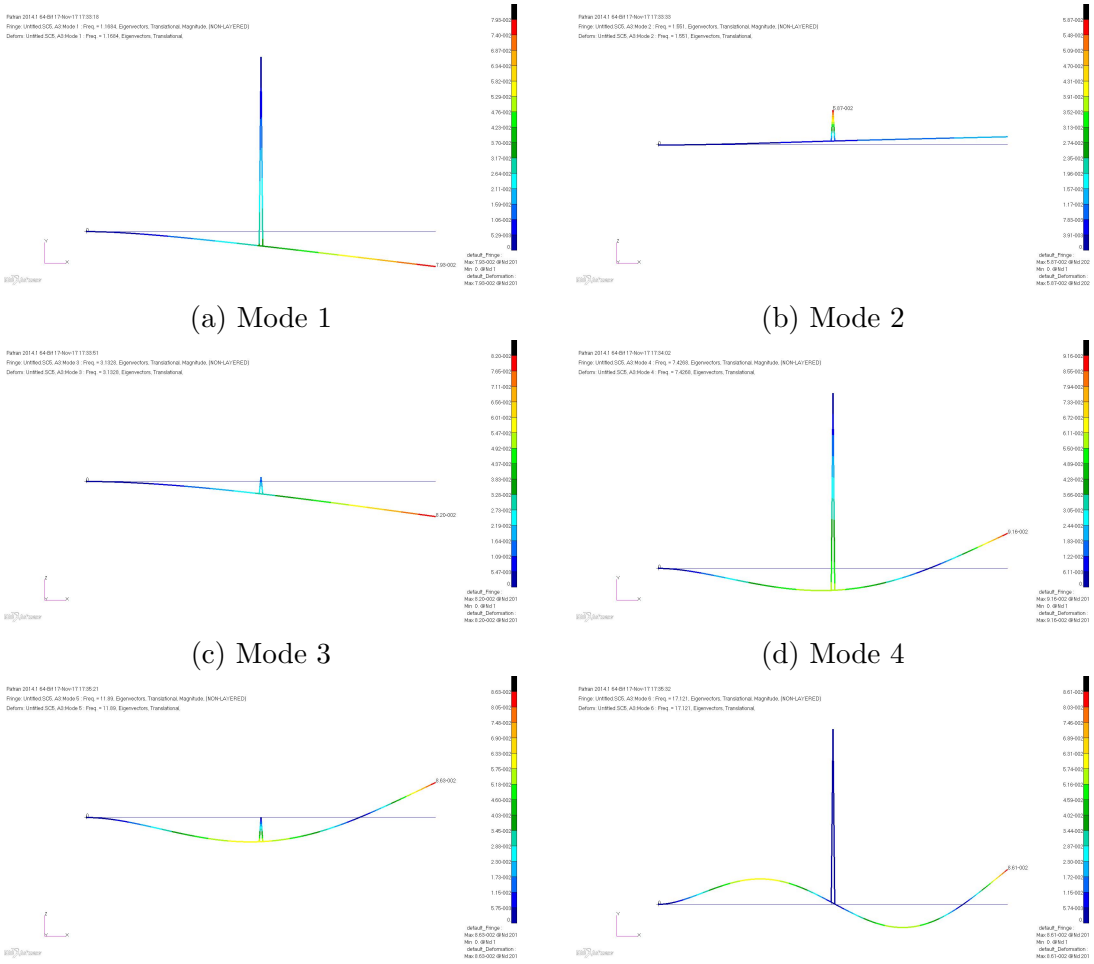

(a) Mode 1

(b) Mode 2

(c) Mode 3

(d) Mode 4

(e) Mode 5

(f) Mode 6

Figure C.11: Mode shapes for the Modes 1 to 6 of a C-F Rotating Beam with Added Mass $\eta = 5$

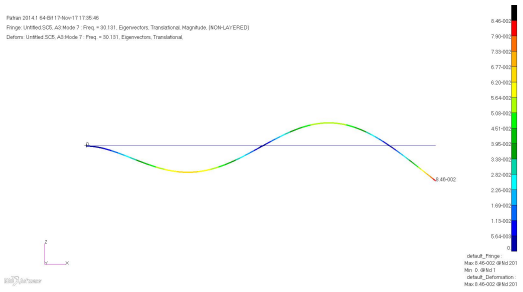

(a) Mode 7

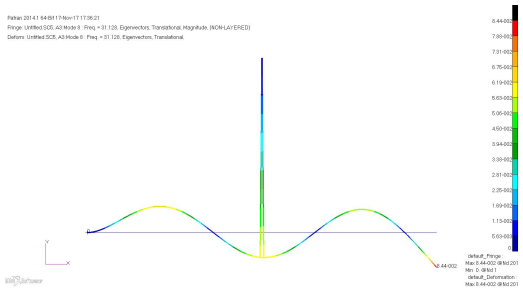

(b) Mode 8

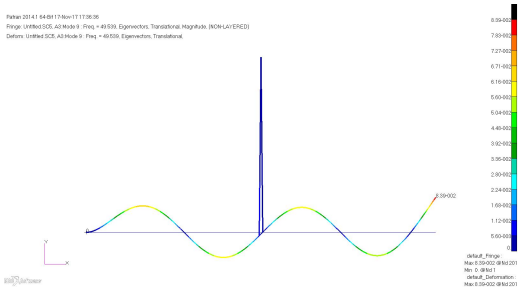

(c) Mode 9

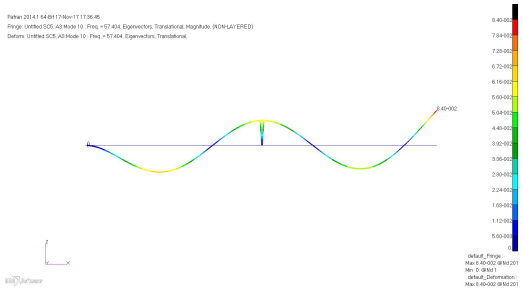

(d) Mode 10

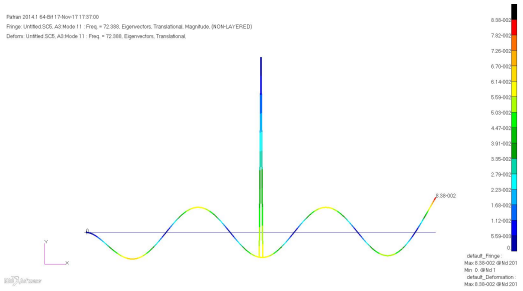

(e) Mode 11

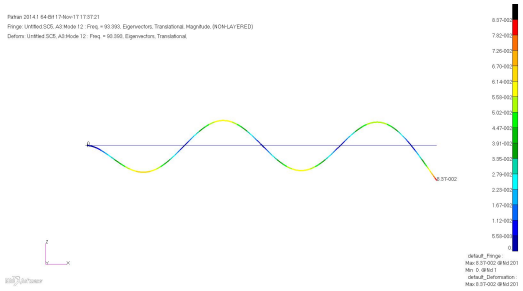

(f) Mode 12

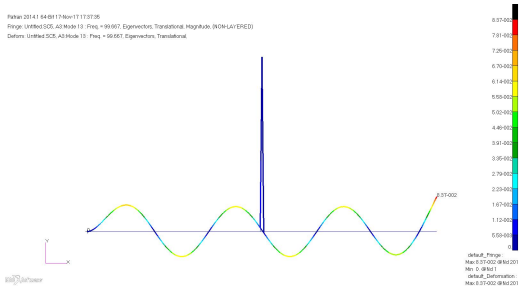

(g) Mode 13

Figure C.12: Mode shapes for the Modes 7 to 13 of a C-F Rotating Beam with Added Mass $\eta = 5$

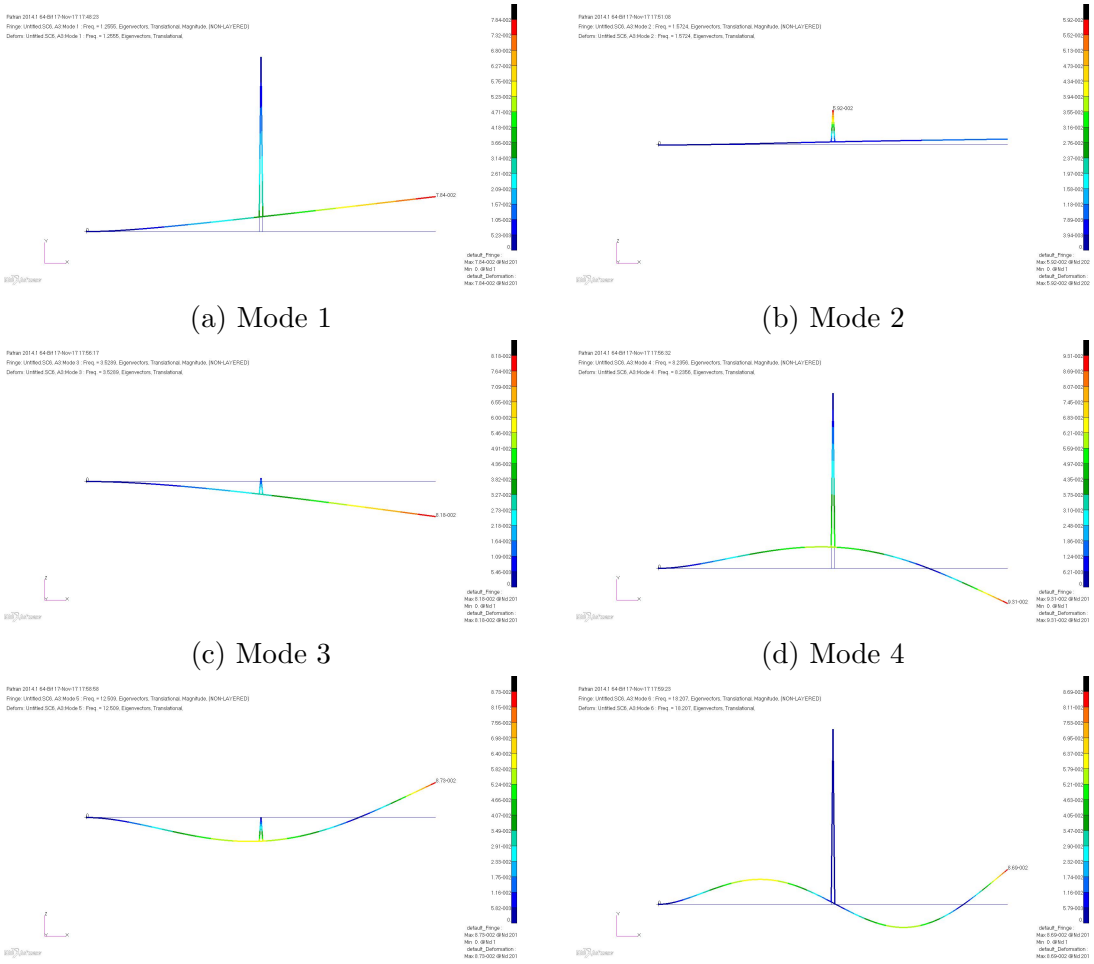

(a) Mode 1

(b) Mode 2

(c) Mode 3

(d) Mode 4

(e) Mode 5

(f) Mode 6

Figure C.13: Mode shapes for the Modes 1 to 6 of a C-F Rotating Beam with Added Mass $\eta = 6$

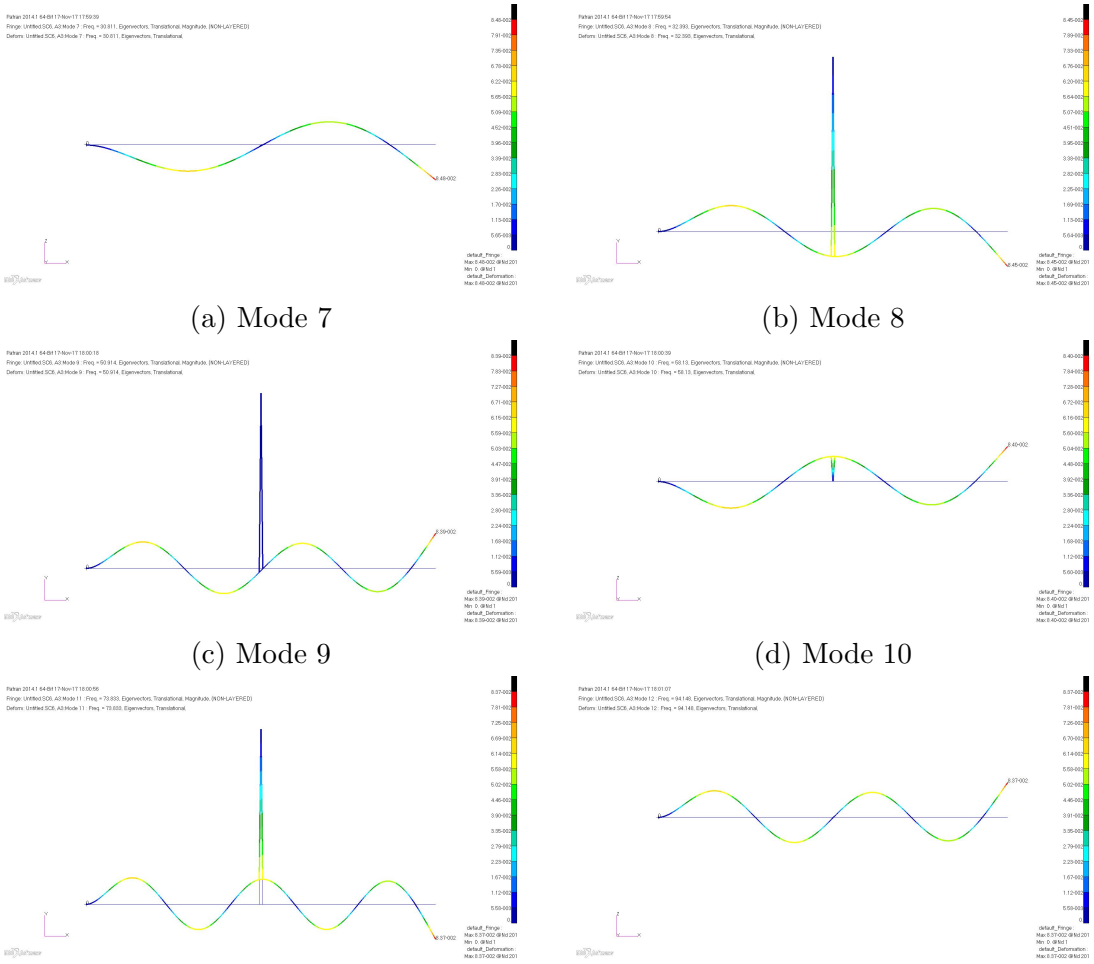

(a) Mode 7

(b) Mode 8

(c) Mode 9

(d) Mode 10

(e) Mode 11

(f) Mode 12

Figure C.14: Mode shapes for the Modes 7 to 12 of a C-F Rotating Beam with Added Mass $\eta = 6$

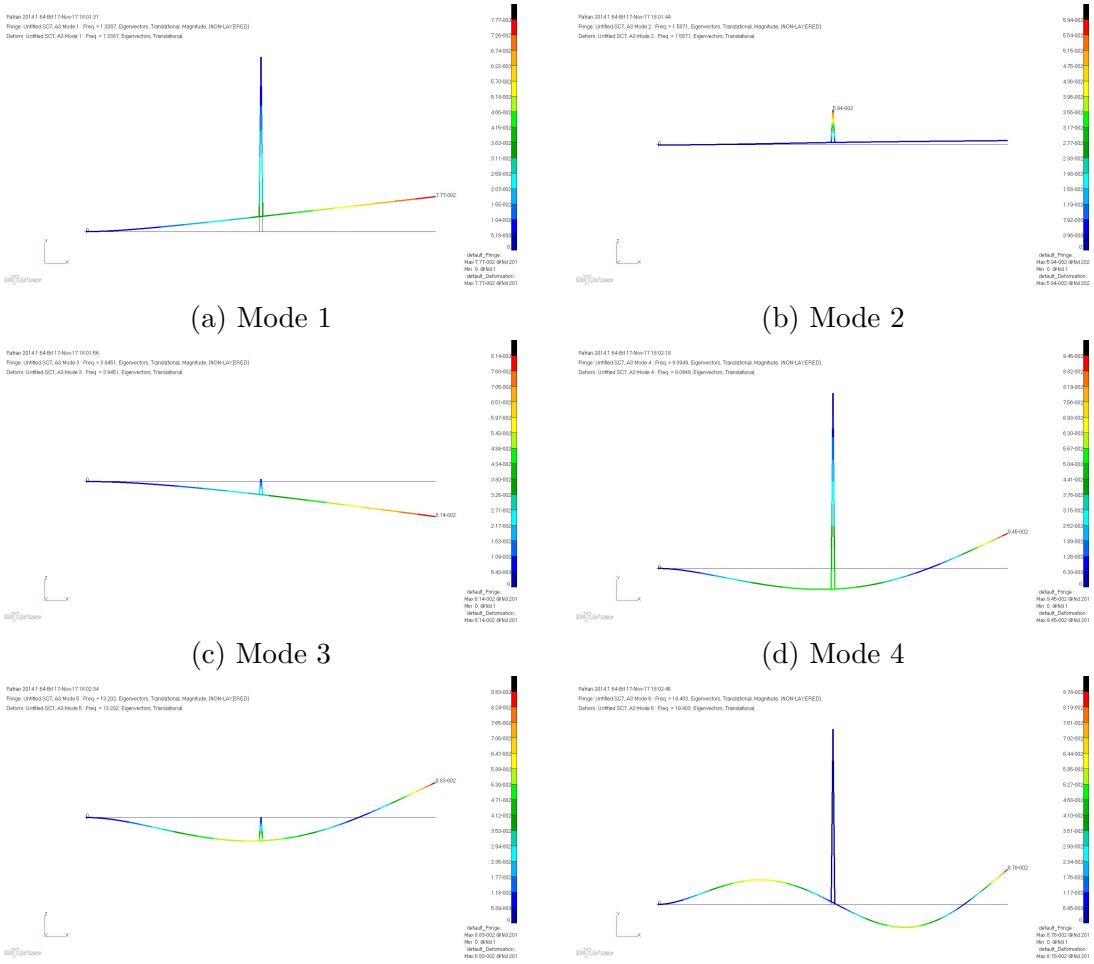

(a) Mode 1

(b) Mode 2

(c) Mode 3

(d) Mode 4

(e) Mode 5

(f) Mode 6

Figure C.15: Mode shapes for the Modes 1 to 6 of a C-F Rotating Beam with Added Mass $\eta = 7$

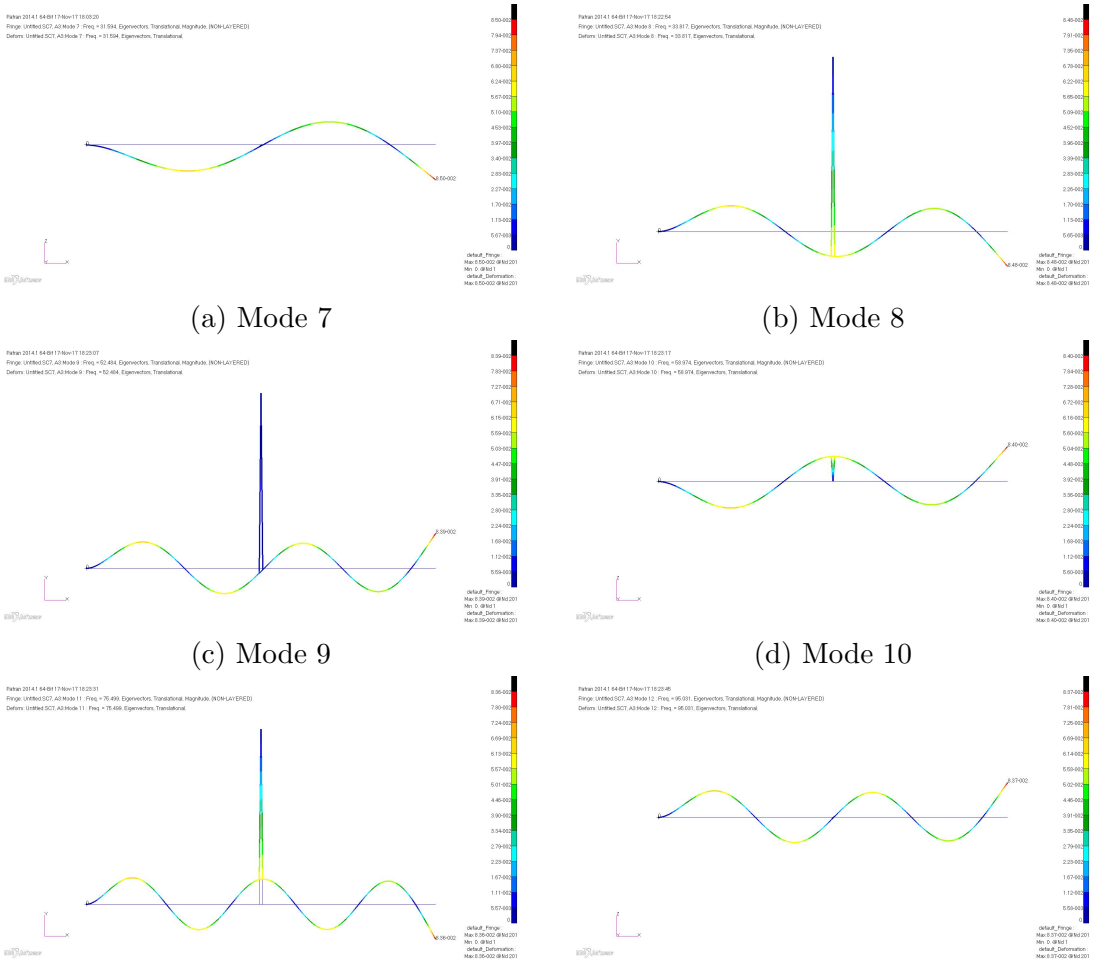

(a) Mode 7

(b) Mode 8

(c) Mode 9

(d) Mode 10

(e) Mode 11

(f) Mode 12

Figure C.16: Mode shapes for the Modes 7 to 12 of a C-F Rotating Beam with Added Mass $\eta = 7$

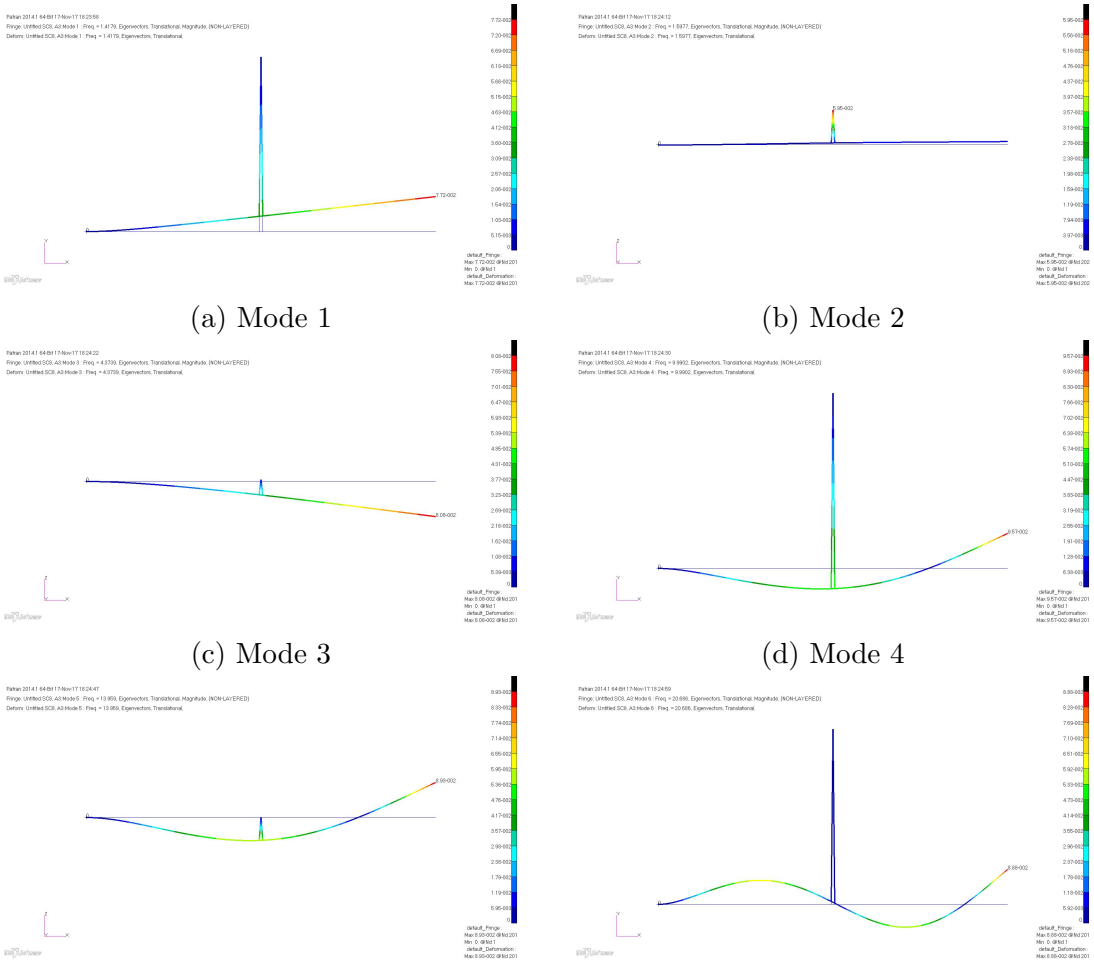

(a) Mode 1

(b) Mode 2

(c) Mode 3

(d) Mode 4

(e) Mode 5

(f) Mode 6

Figure C.17: Mode shapes for the Modes 1 to 6 of a C-F Rotating Beam with Added Mass $\eta = 8$

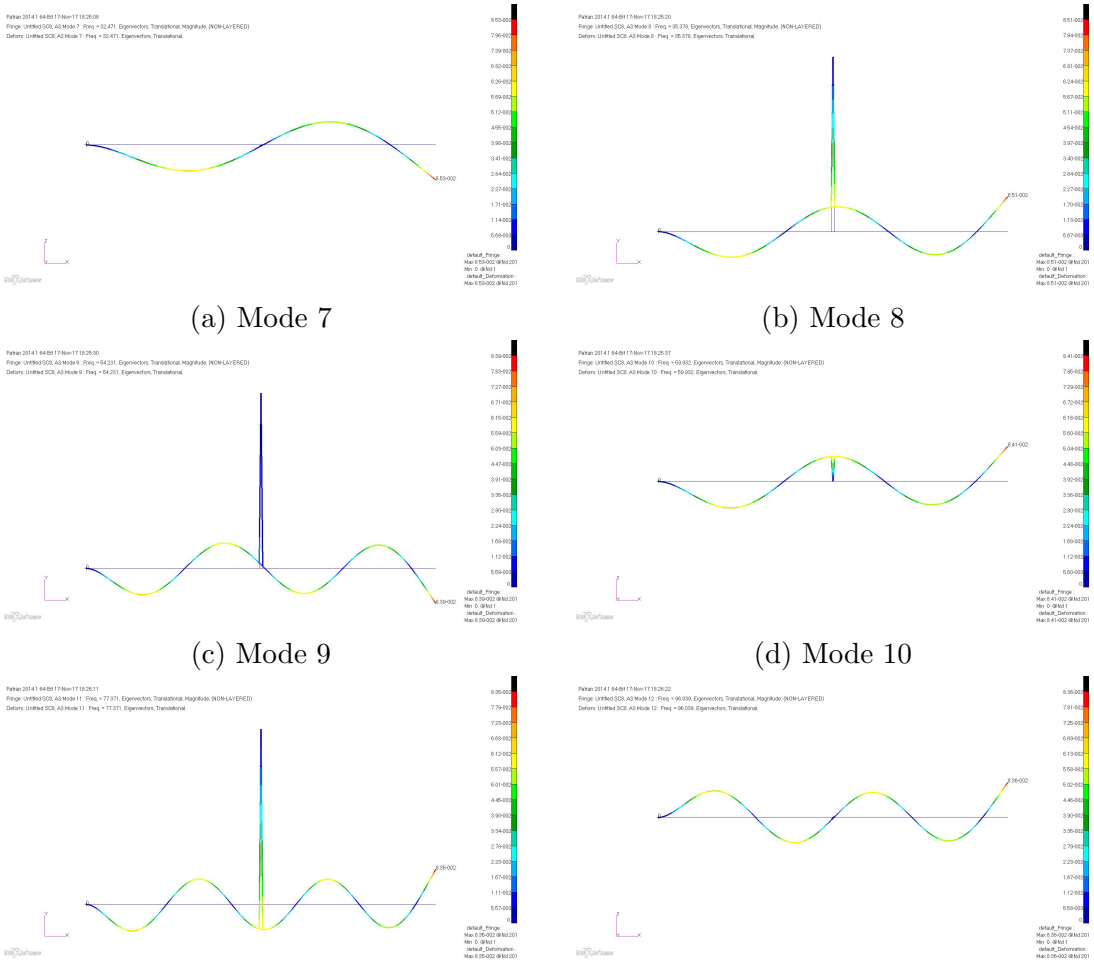

(a) Mode 7

(b) Mode 8

(c) Mode 9

(d) Mode 10

(e) Mode 11

(f) Mode 12

Figure C.18: Mode shapes for the Modes 7 to 12 of a C-F Rotating Beam with Added Mass $\eta = 8$

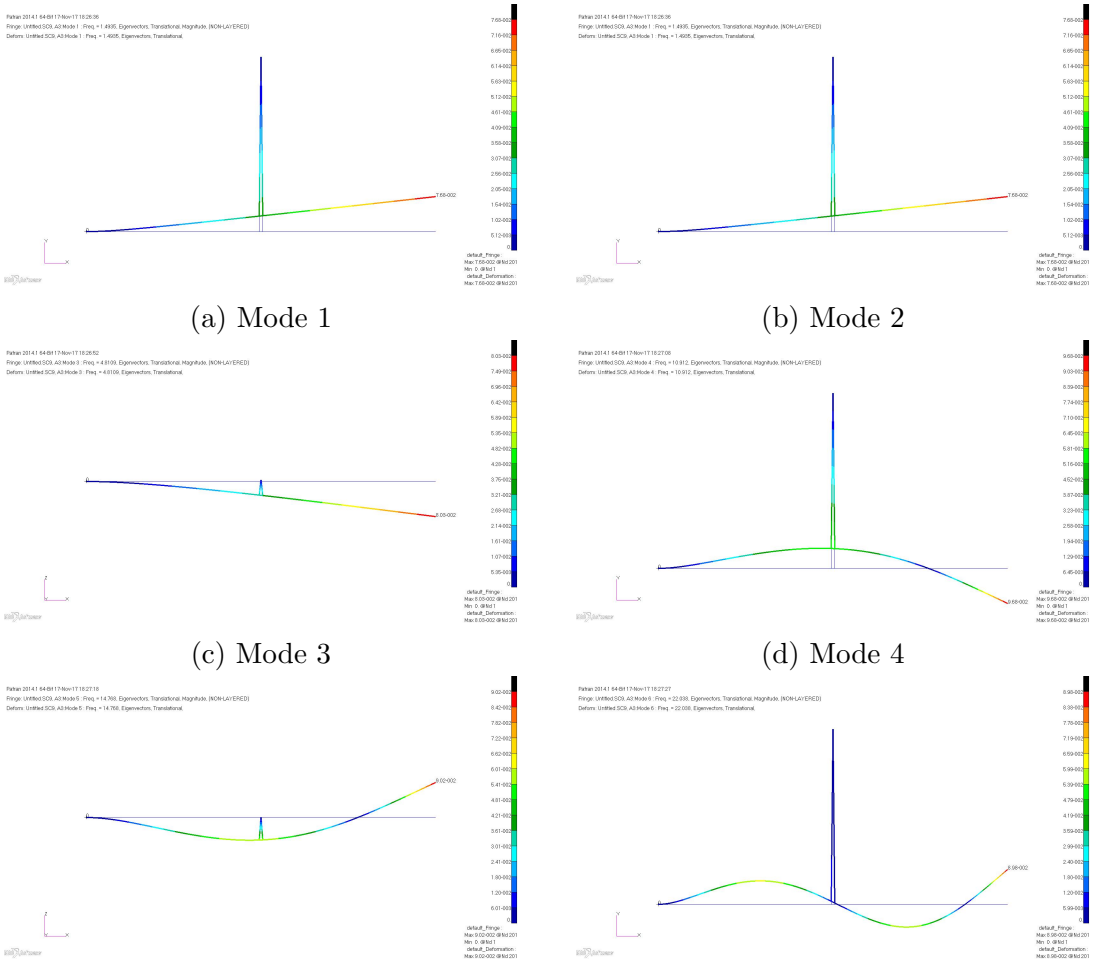

(a) Mode 1

(b) Mode 2

(c) Mode 3

(d) Mode 4

(e) Mode 5

(f) Mode 6

Figure C.19: Mode shapes for the Modes 1 to 6 of a C-F Rotating Beam with Added Mass $\eta = 9$

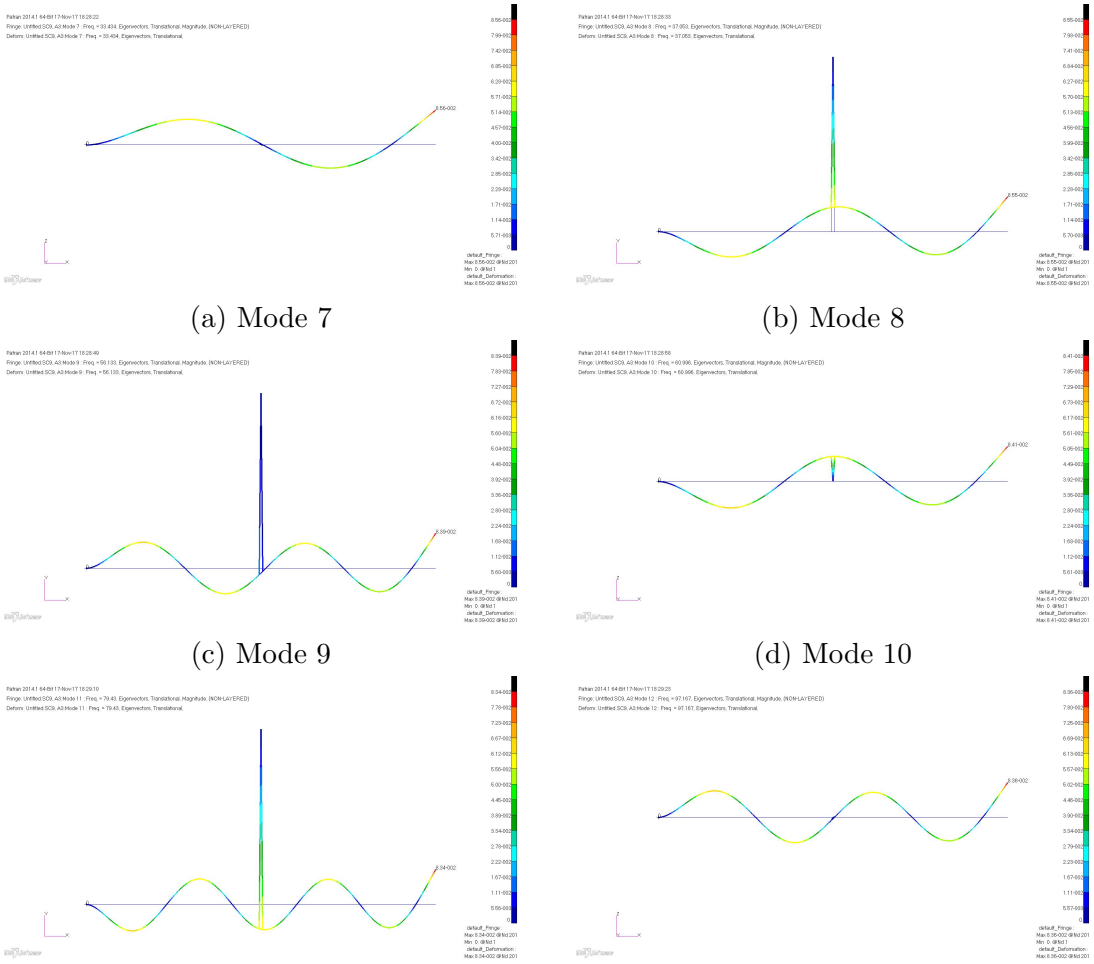

(a) Mode 7

(b) Mode 8

(c) Mode 9

(d) Mode 10

(e) Mode 11

(f) Mode 12

Figure C.20: Mode shapes for the Modes 7 to 12 of a C-F Rotating Beam with Added Mass $\eta = 9$

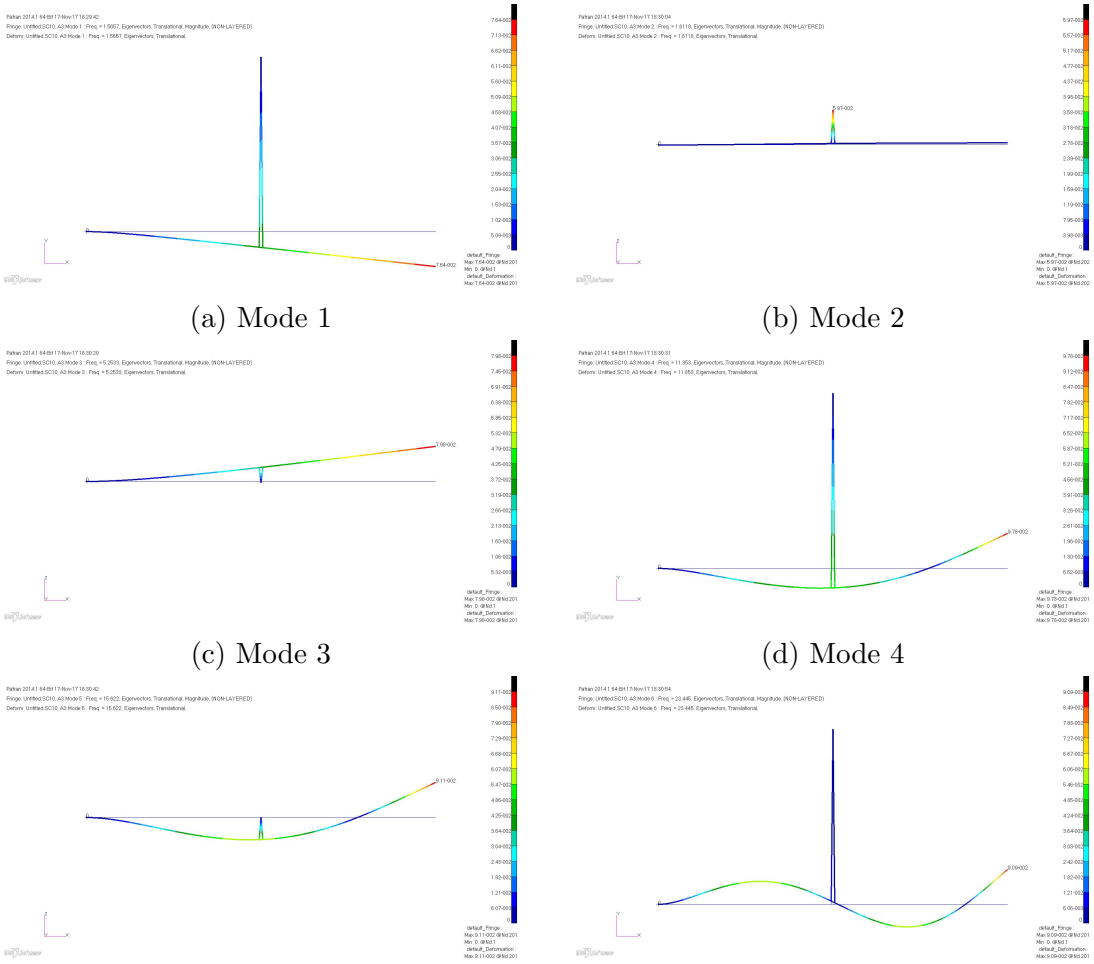

(a) Mode 1

(b) Mode 2

(c) Mode 3

(d) Mode 4

(e) Mode 5

(f) Mode 6

Figure C.21: Mode shapes for the Modes 1 to 6 of a C-F Rotating Beam with Added Mass $\eta = 10$

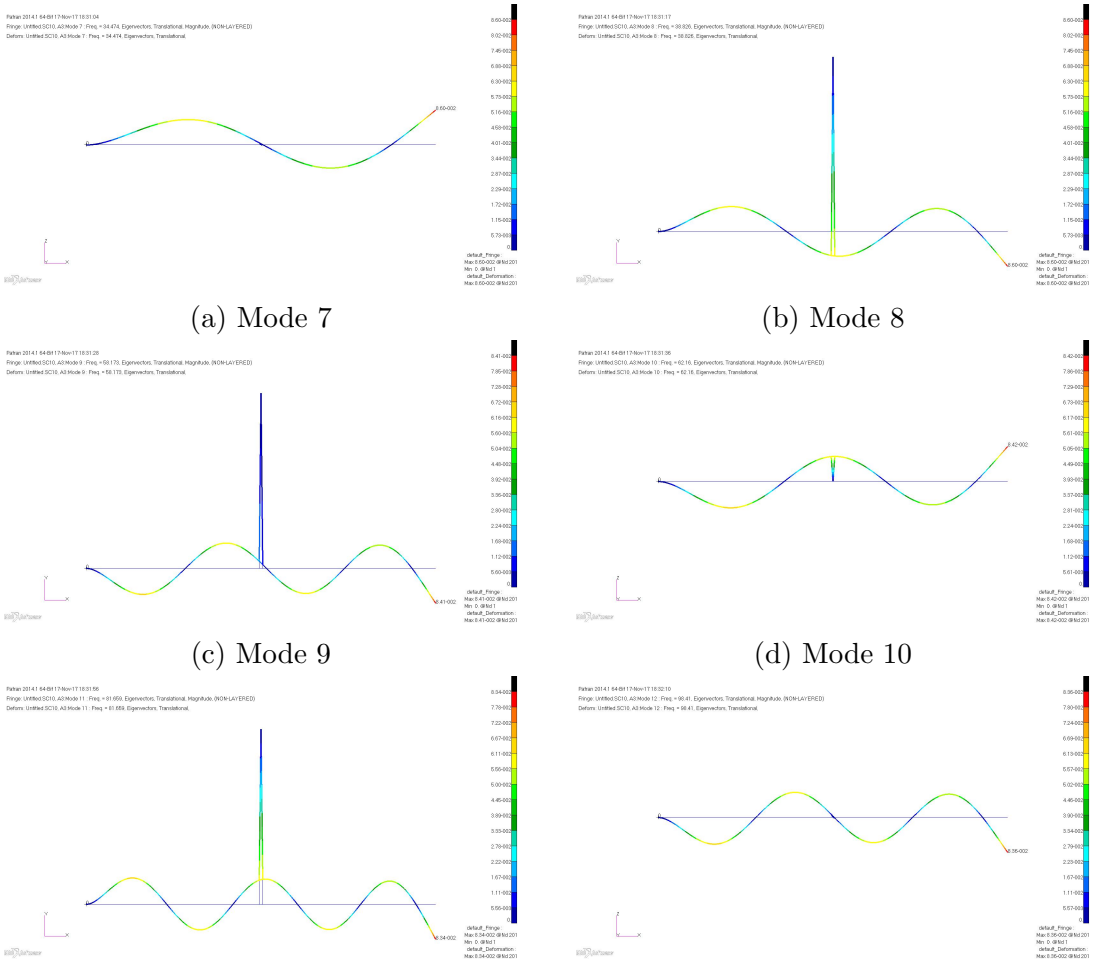

(a) Mode 7

(b) Mode 8

(c) Mode 9

(d) Mode 10

(e) Mode 11

(f) Mode 12

Figure C.22: Mode shapes for the Modes 7 to 12 of a C-F Rotating Beam with Added Mass $\eta = 10$

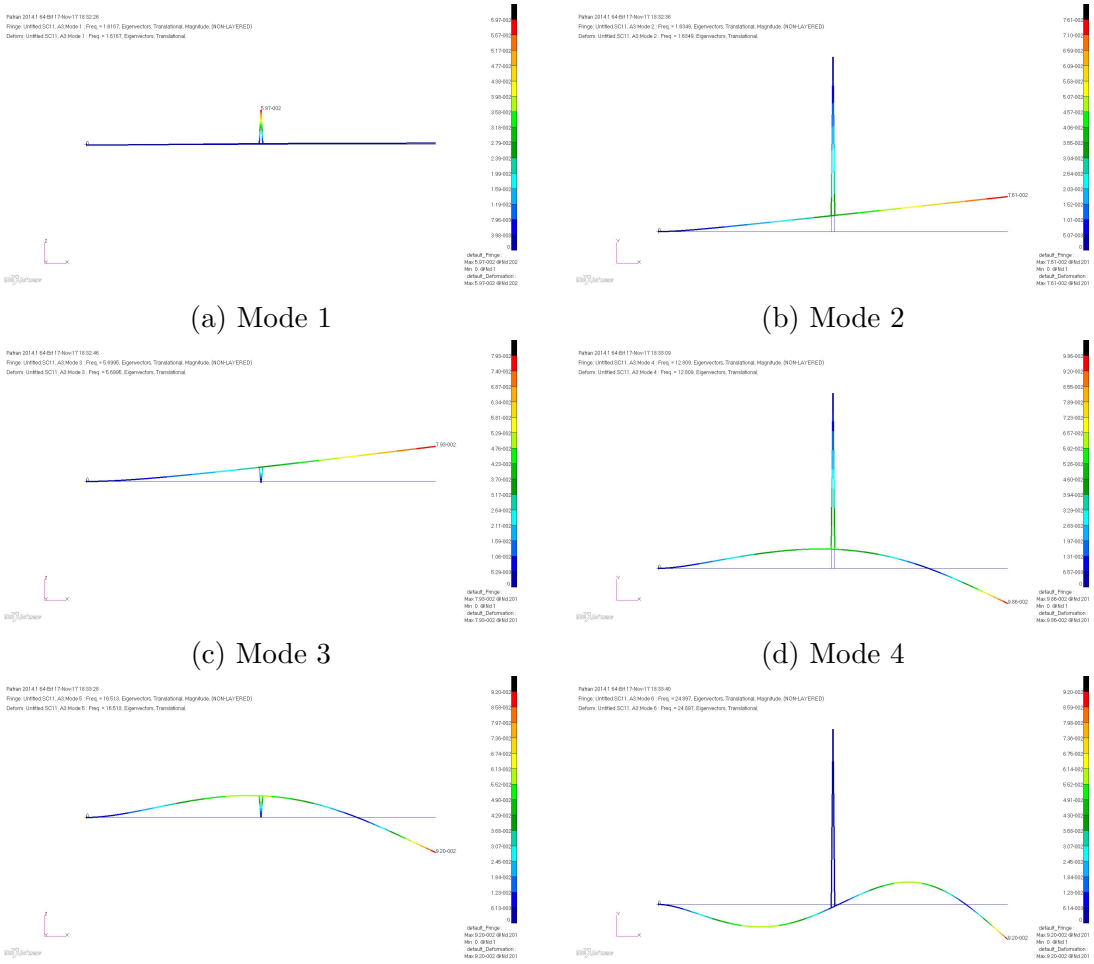

(a) Mode 1

(b) Mode 2

(c) Mode 3

(d) Mode 4

(e) Mode 5

(f) Mode 6

Figure C.23: Mode shapes for the Modes 1 to 6 of a C-F Rotating Beam with Added Mass $\eta = 11$

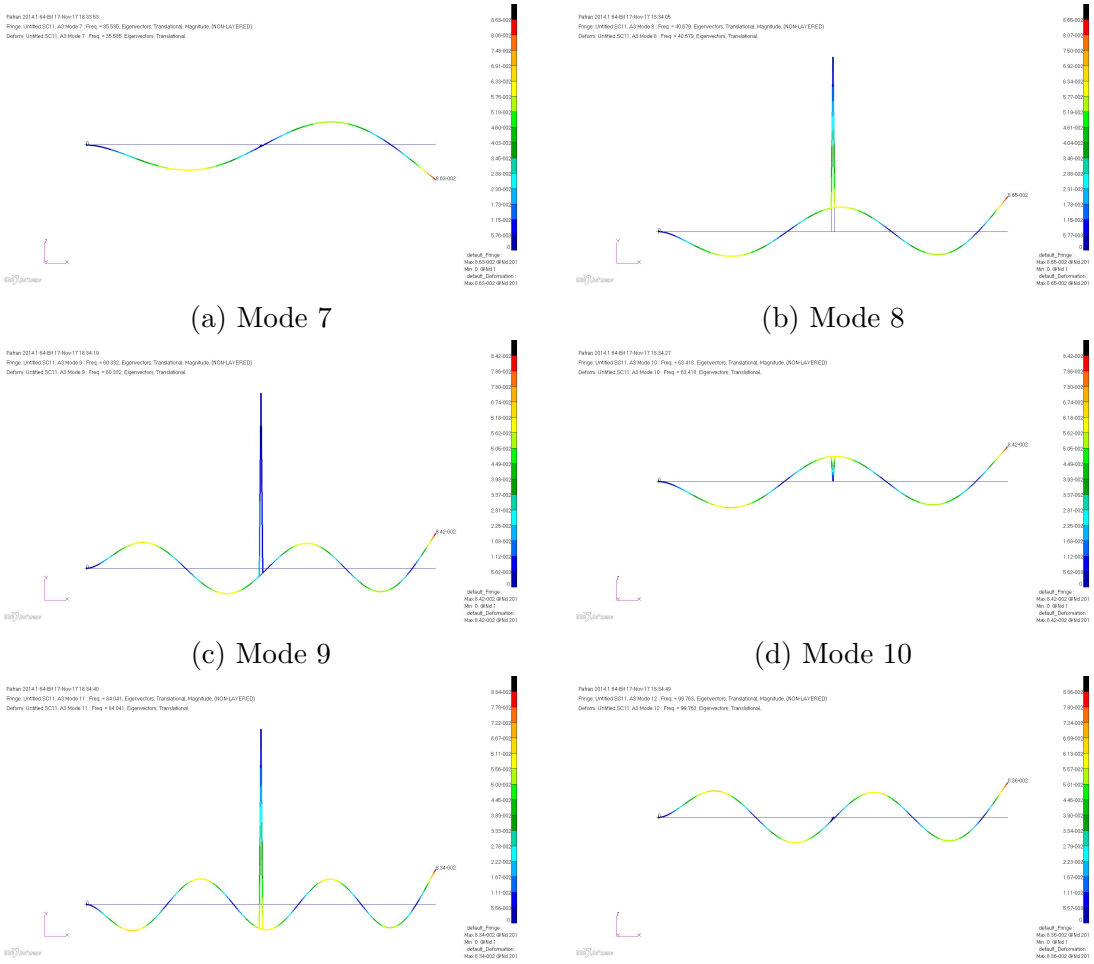

(a) Mode 7

(b) Mode 8

(c) Mode 9

(d) Mode 10

(e) Mode 11

(f) Mode 12

Figure C.24: Mode shapes for the Modes 7 to 12 of a C-F Rotating Beam with Added Mass $\eta = 11$

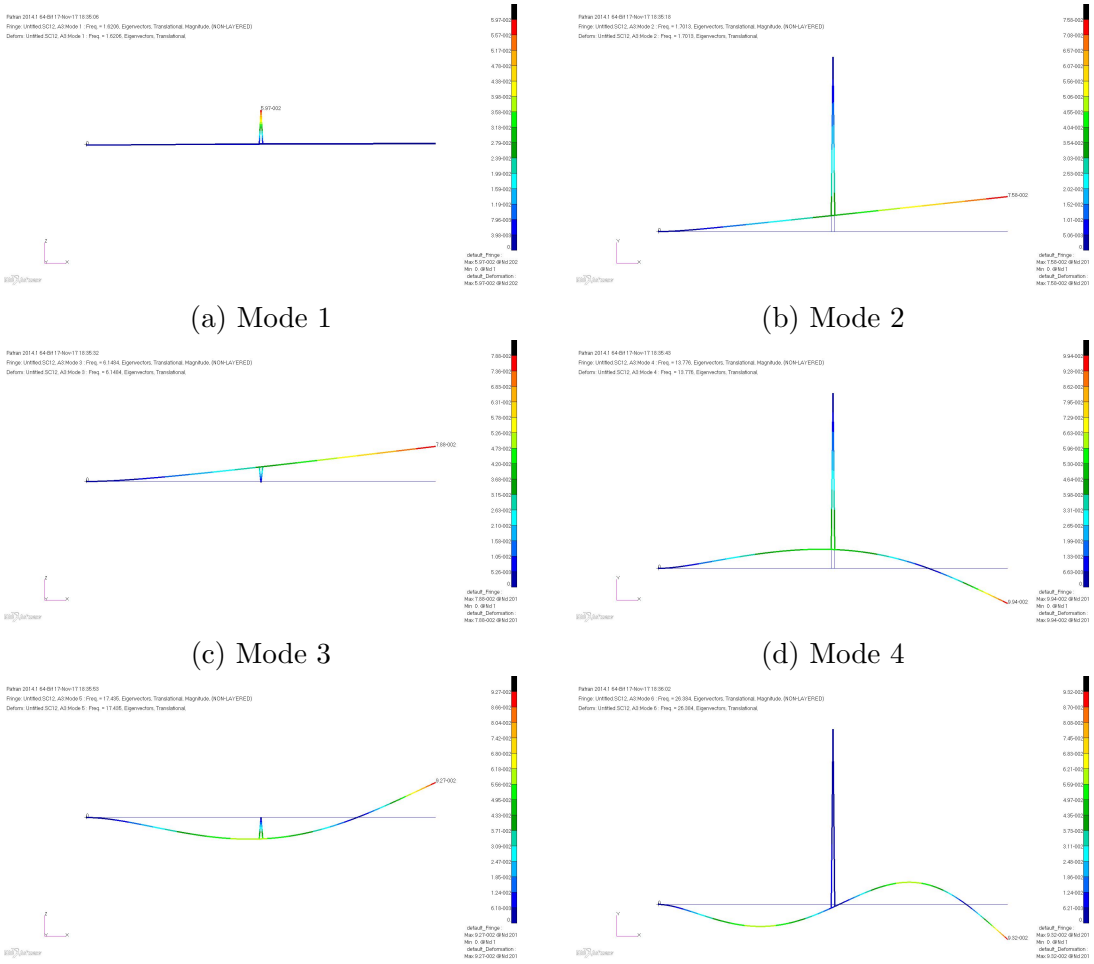

(a) Mode 1

(b) Mode 2

(c) Mode 3

(d) Mode 4

(e) Mode 5

(f) Mode 6

Figure C.25: Mode shapes for the Modes 1 to 6 of a C-F Rotating Beam with Added Mass $\eta = 12$

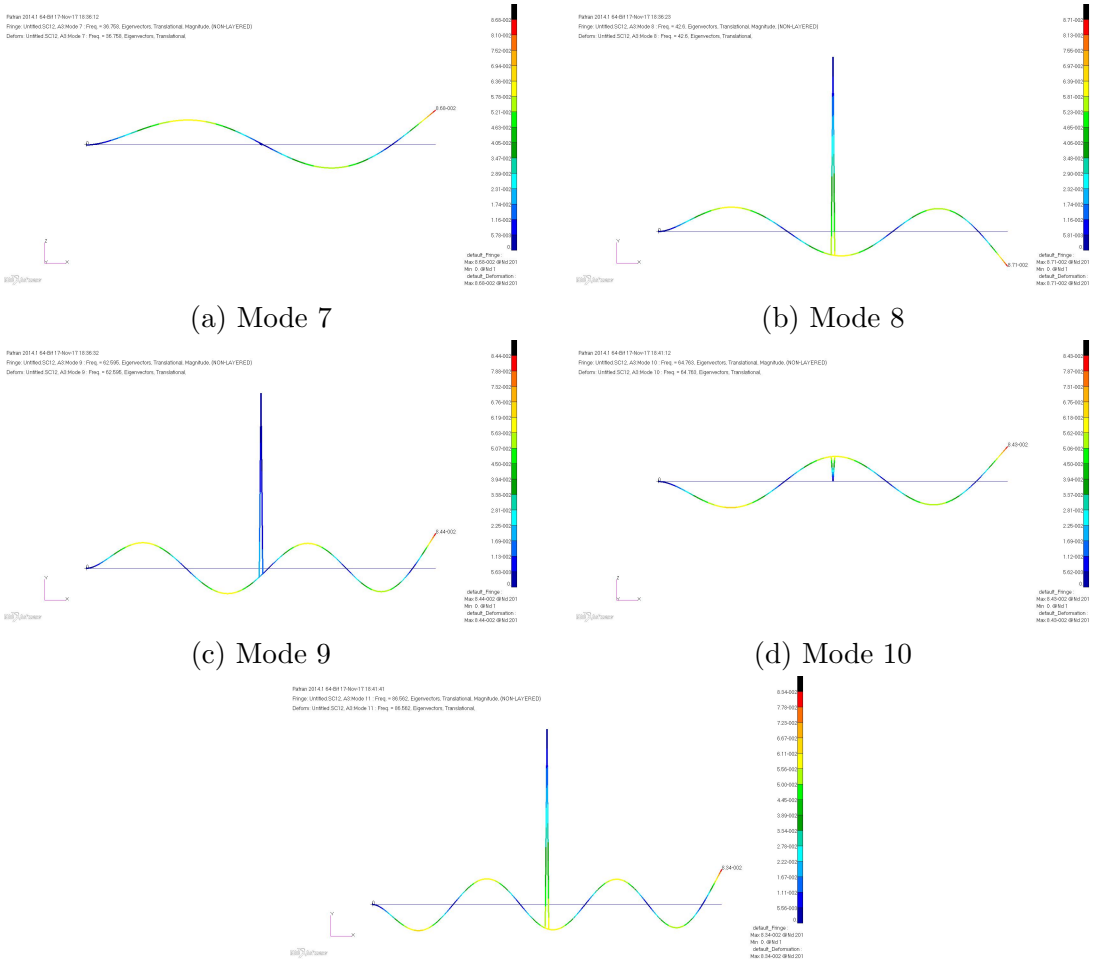

(a) Mode 7

(b) Mode 8

(c) Mode 9

(d) Mode 10

(e) Mode 11

Figure C.26: Mode shapes for the Modes 7 to 11 of a C-F Rotating Beam with Added Mass $\eta = 12$

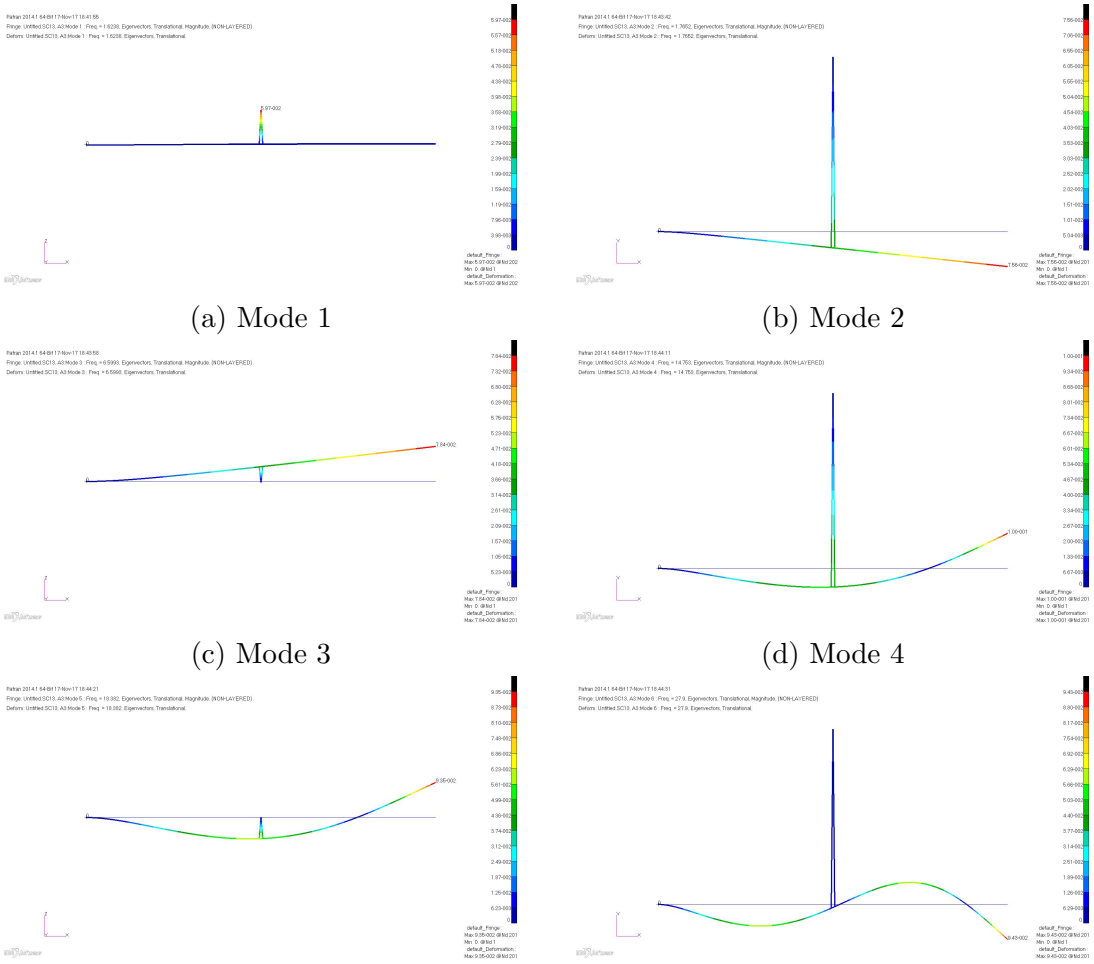

(a) Mode 1

(b) Mode 2

(c) Mode 3

(d) Mode 4

(e) Mode 5

(f) Mode 6

Figure C.27: Mode shapes for the Modes 1 to 6 of a C-F Rotating Beam with Added Mass $\eta = 13$

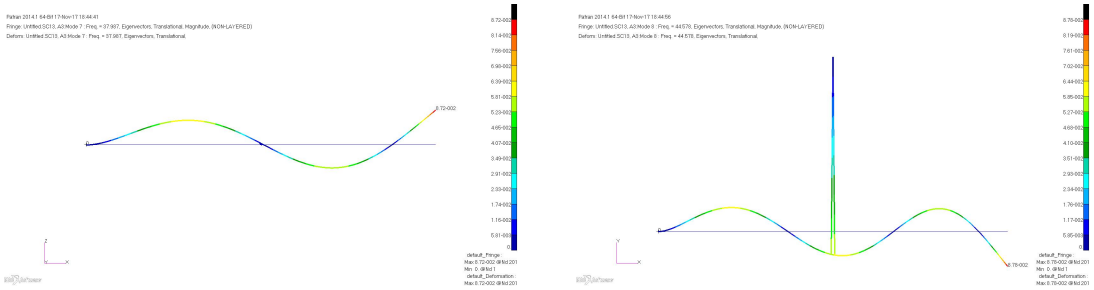

(a) Mode 7

(b) Mode 8

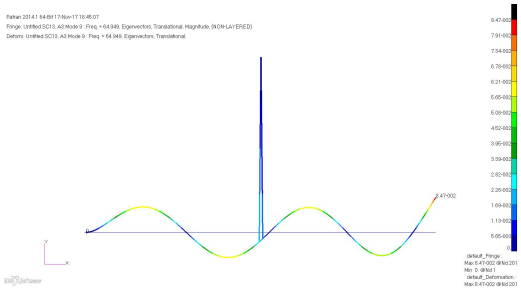

(c) Mode 9

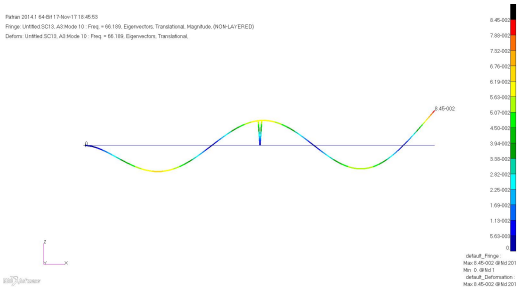

(d) Mode 10

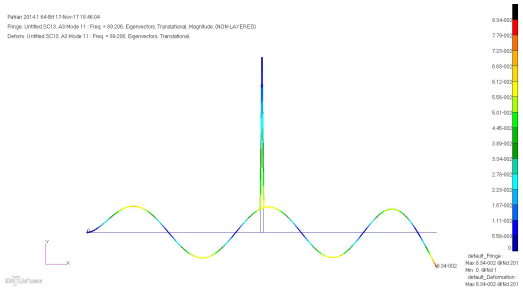

(e) Mode 11

Figure C.28: Mode shapes for the Modes 7 to 11 of a C-F Rotating Beam with Added Mass $\eta = 13$

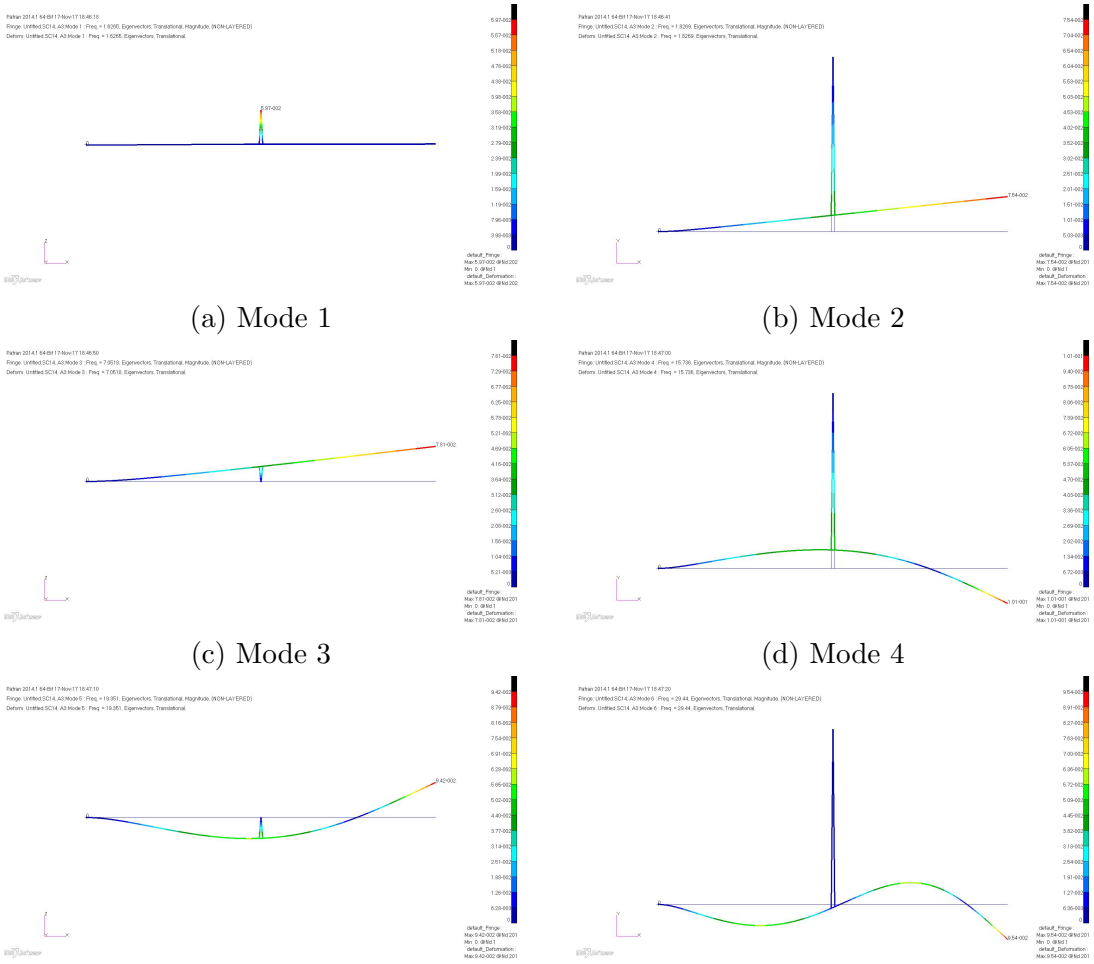

(a) Mode 1

(b) Mode 2

(c) Mode 3

(d) Mode 4

(e) Mode 5

(f) Mode 6

Figure C.29: Mode shapes for the Modes 1 to 6 of a C-F Rotating Beam with Added Mass $\eta = 14$

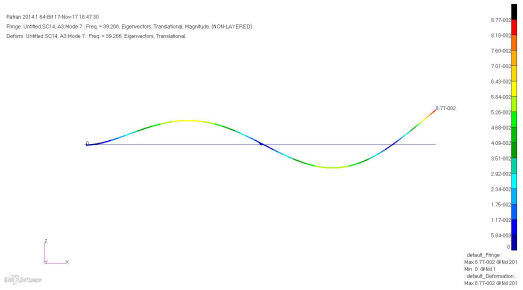

(a) Mode 7

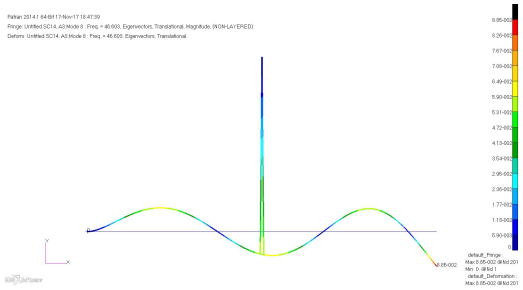

(b) Mode 8

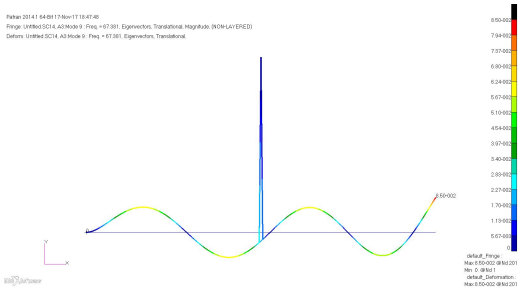

(c) Mode 9

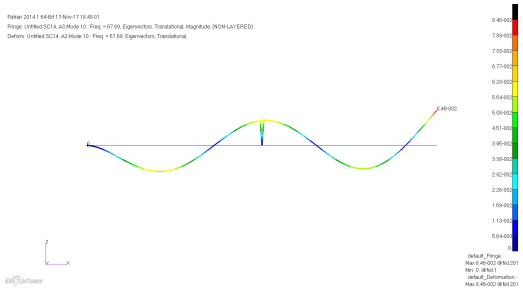

(d) Mode 10

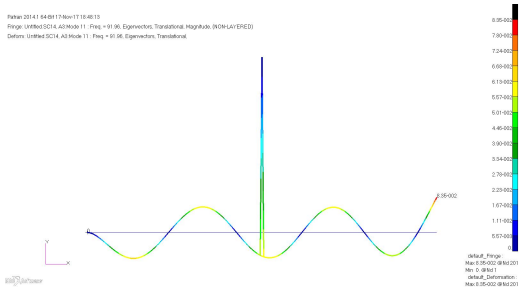

(e) Mode 11

Figure C.30: Mode shapes for the Modes 7 to 11 of a C-F Rotating Beam with Added Mass for $\eta = 14$

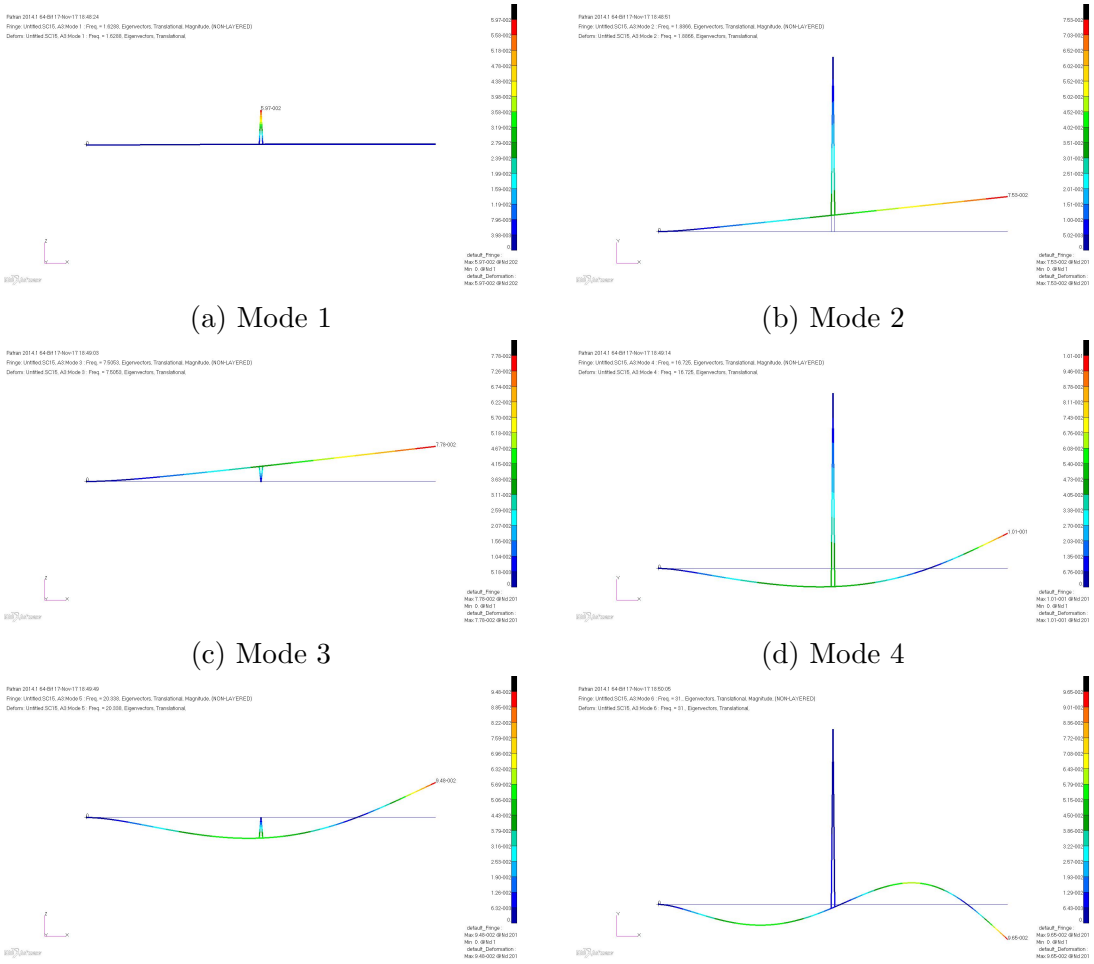

(a) Mode 1

(b) Mode 2

(c) Mode 3

(d) Mode 4

(e) Mode 5

(f) Mode 6

Figure C.31: Mode shapes for the Modes 1 to 6 of a C-F Rotating Beam with added mass for $\eta = 15$

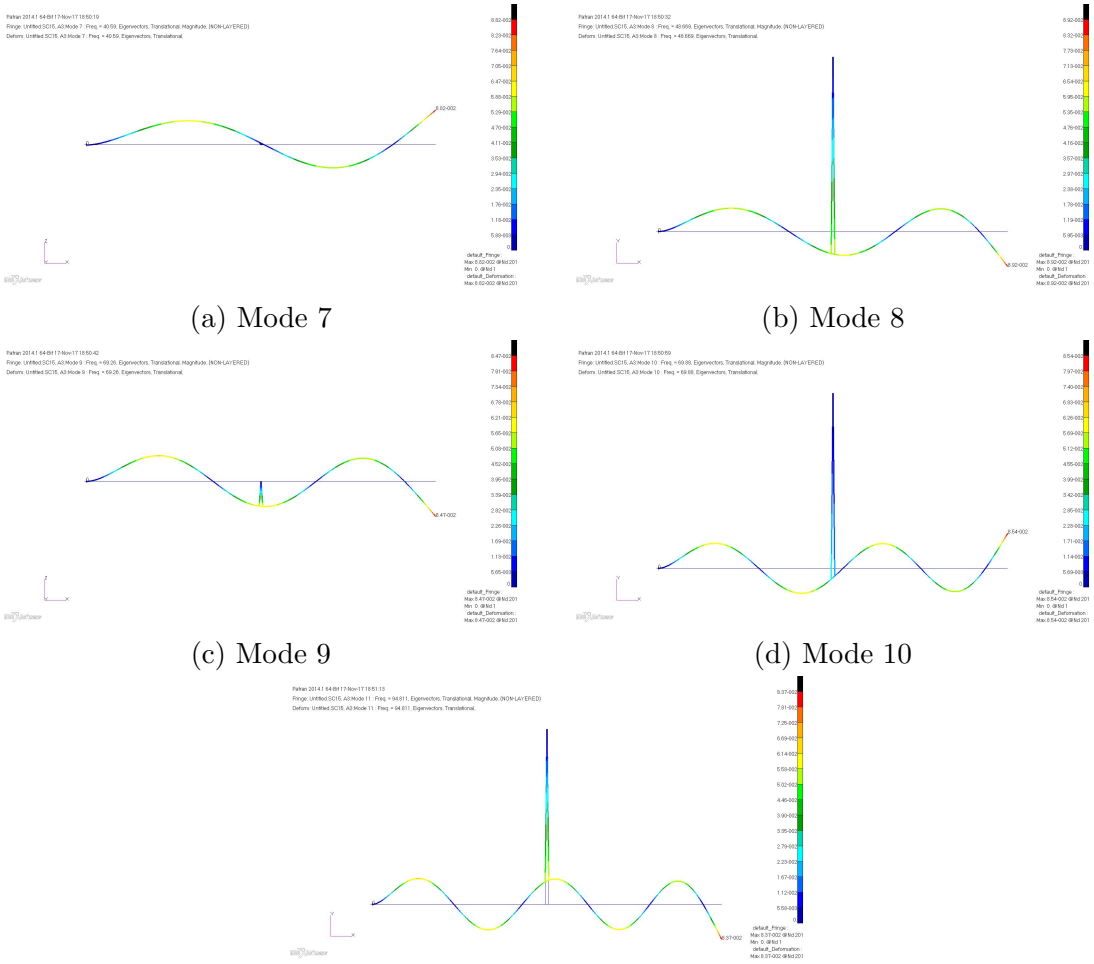

(a) Mode 7

(b) Mode 8

(c) Mode 9

(d) Mode 10

(e) Mode 11

Figure C.32: Mode shapes for the Modes 7 to 11 of a C-F Rotating Beam with Added Mass for $\eta = 15$

Appendix D

D.1 Mode shapes of v1.1 mAEWing2 for AoA 2°, 4°, 6°, and 8° and Zero Roll Rate

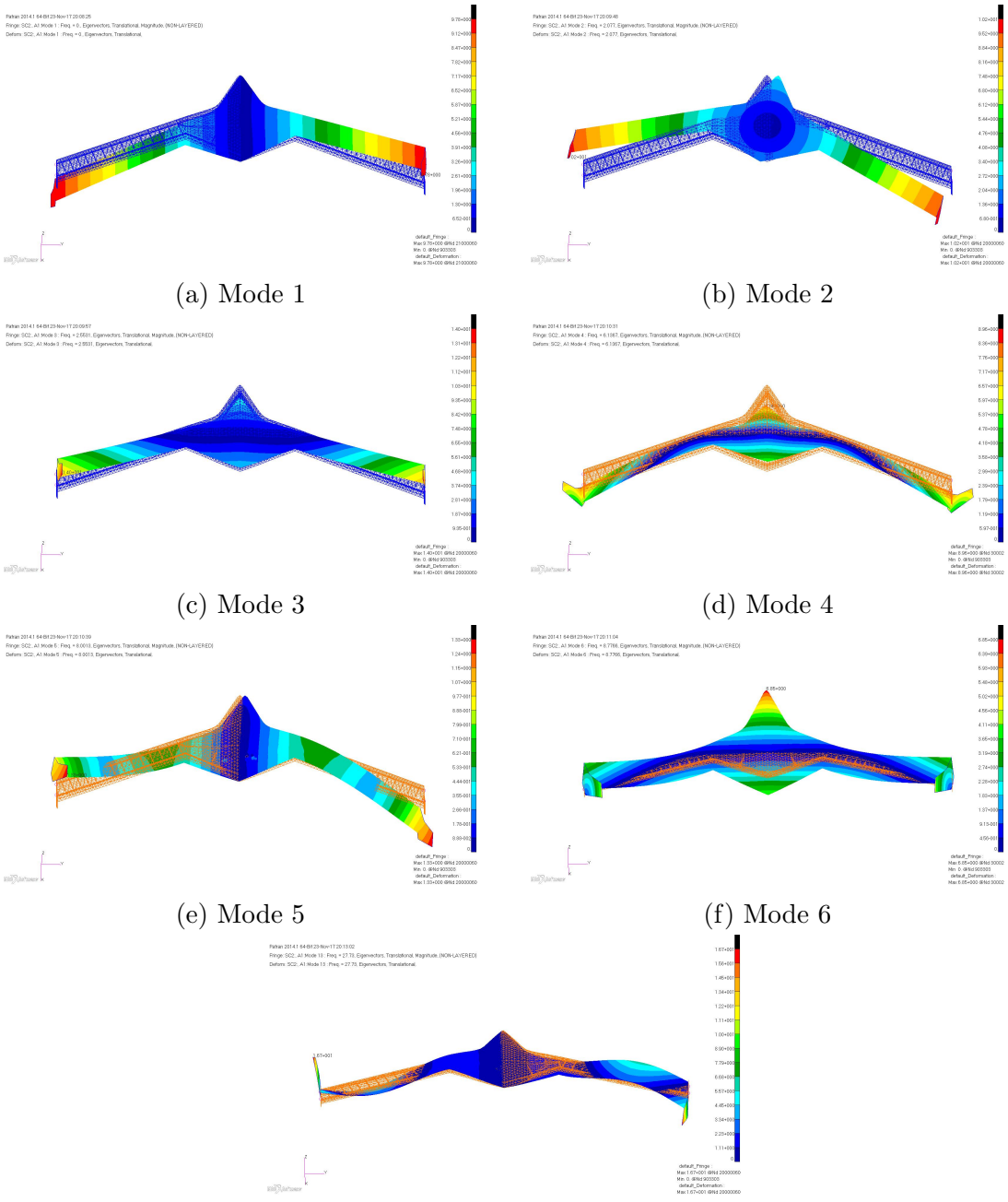

(a) Mode 1

(b) Mode 2

(c) Mode 3

(d) Mode 4

(e) Mode 5

(f) Mode 6

(g) Mode 13

Figure D.1: Mode shapes for the Seven Modes of mAEWing2 v1.1 for AoA 2°

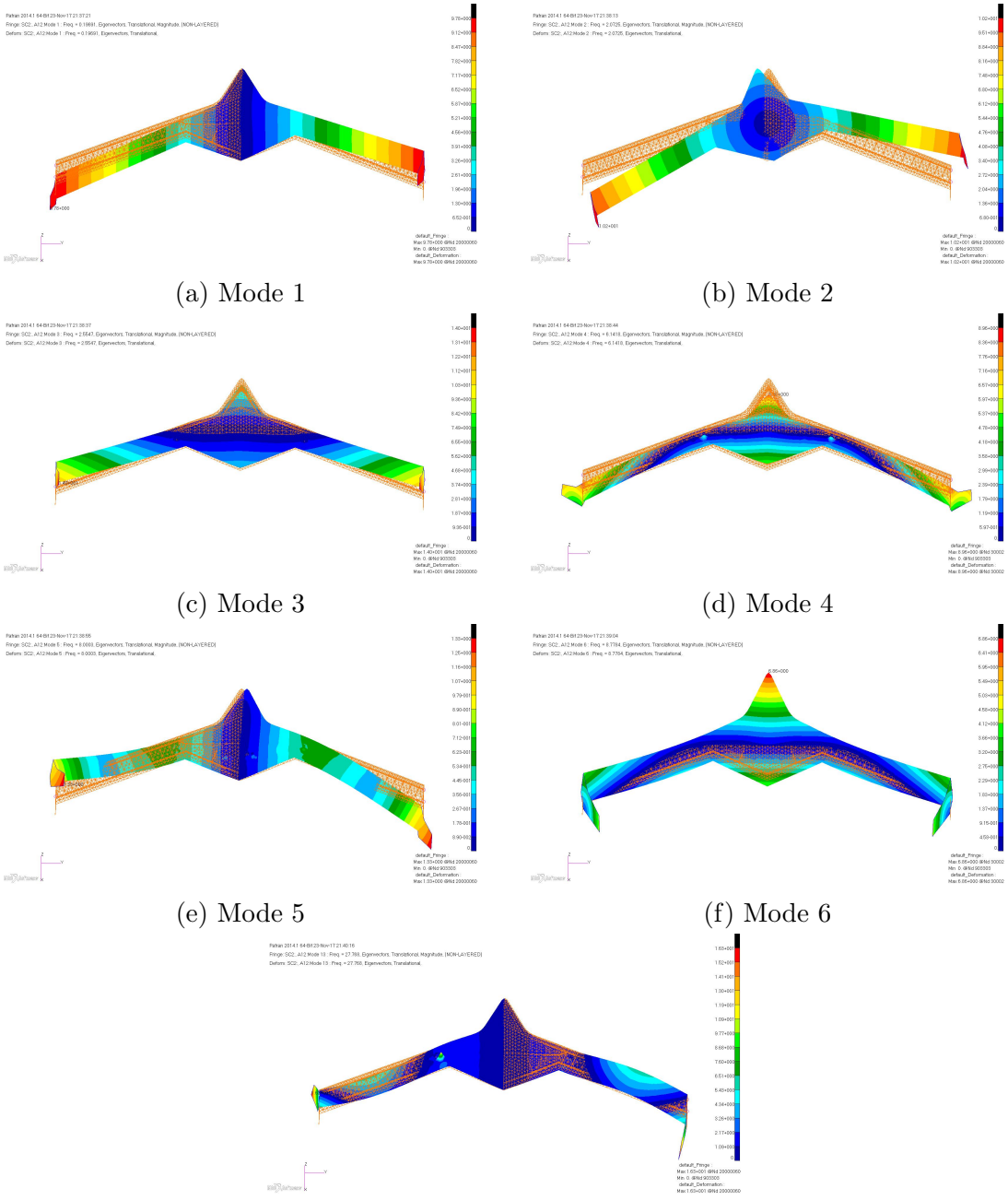

(a) Mode 1

(b) Mode 2

(c) Mode 3

(d) Mode 4

(e) Mode 5

(f) Mode 6

(g) Mode 13

Figure D.2: Mode shapes for the Seven Modes of mAEWing2 v1.1 for AoA 4°

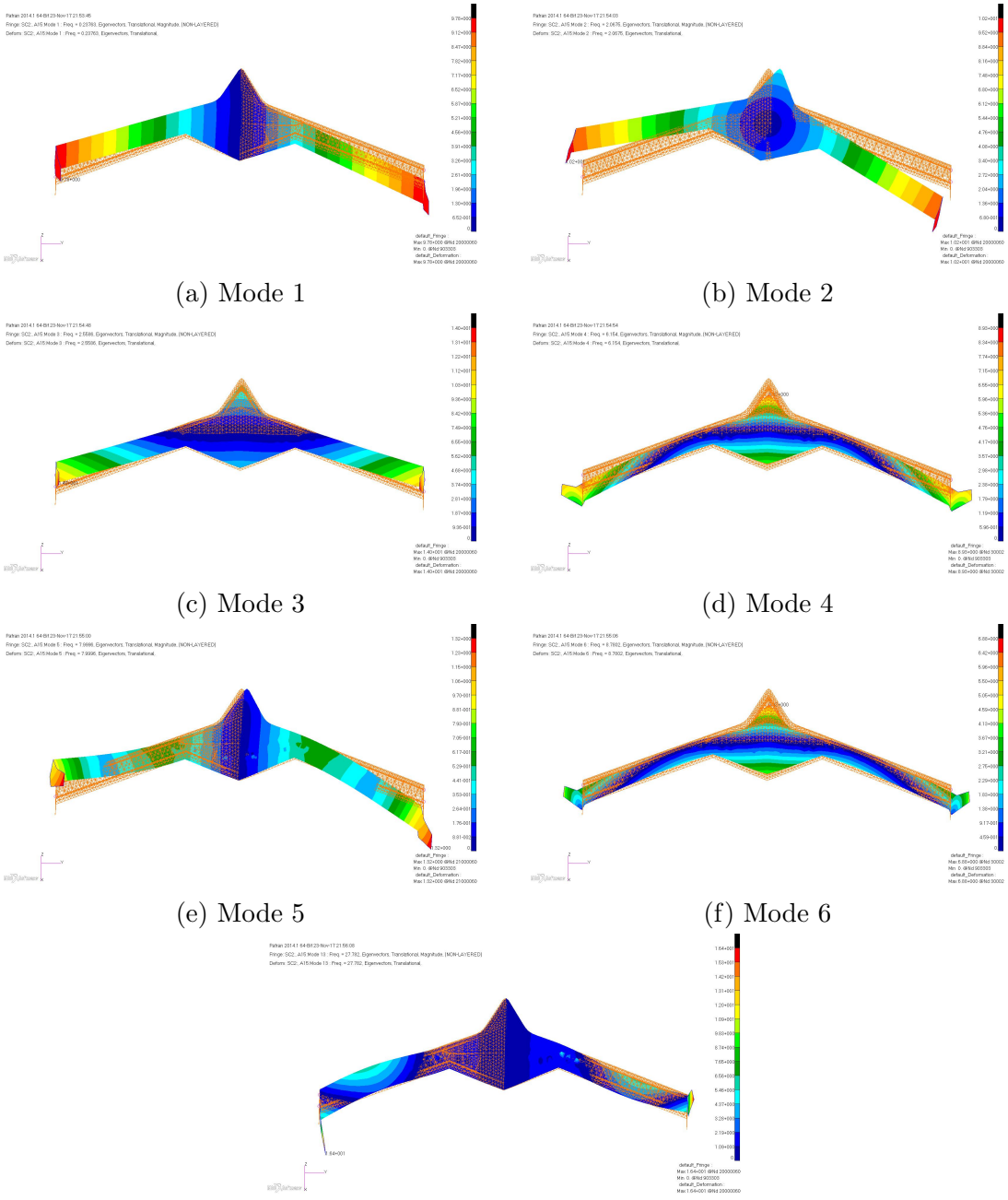

(a) Mode 1

(b) Mode 2

(c) Mode 3

(d) Mode 4

(e) Mode 5

(f) Mode 6

(g) Mode 13

Figure D.3: Mode shapes for the Seven Modes of mAEWing2 v1.1 for AoA 6°

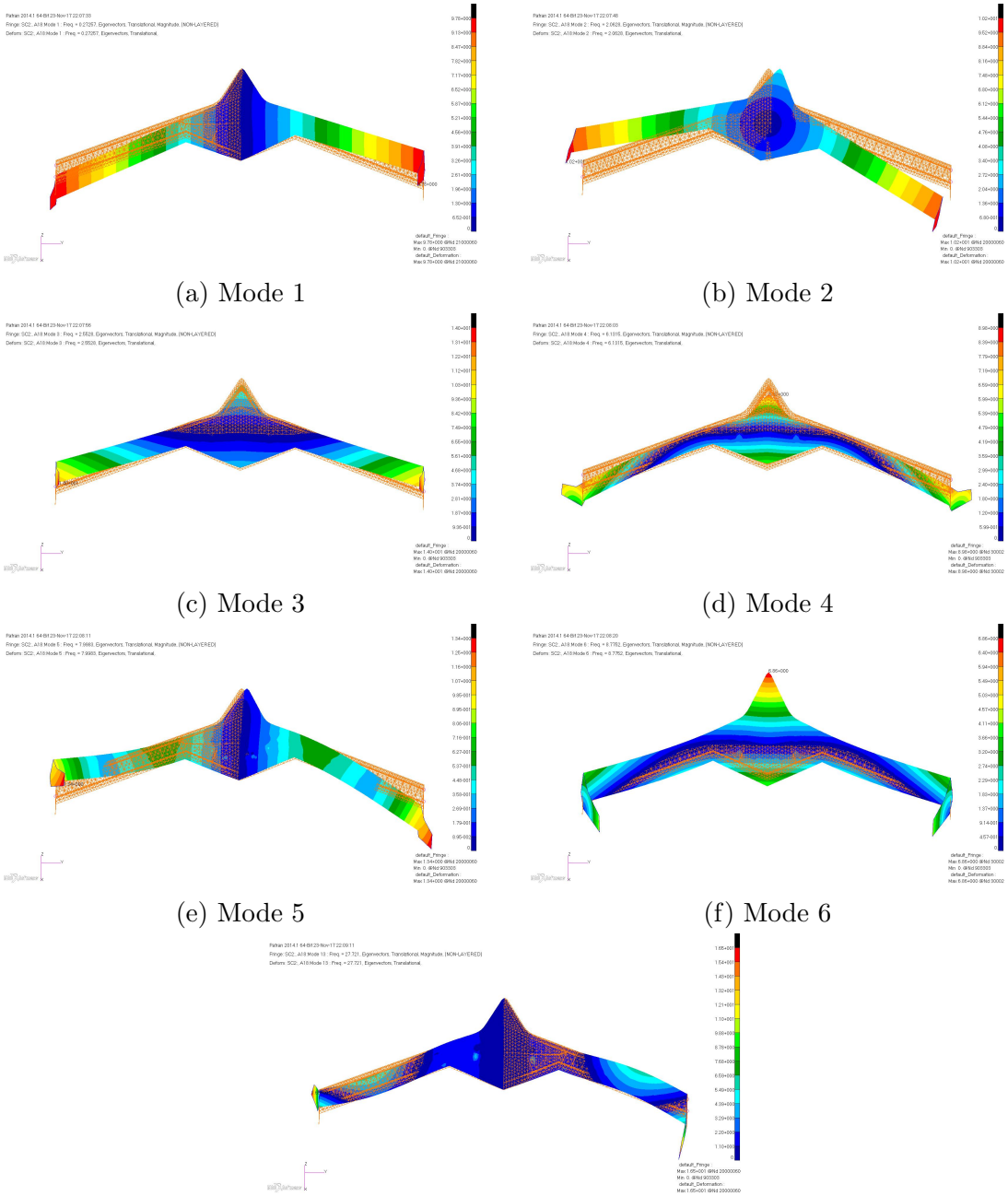

(a) Mode 1

(b) Mode 2

(c) Mode 3

(d) Mode 4

(e) Mode 5

(f) Mode 6

(g) Mode 13

Figure D.4: Mode shapes for the Seven Modes of mAEWing2 v1.1 for AoA 8°

Appendix E

E.1 Mode shapes of v1.1 mAEWing2 for AoA 2°, 4°, 6°, 8° and Roll Rates 0.5 rad/sec and 1 rad/sec

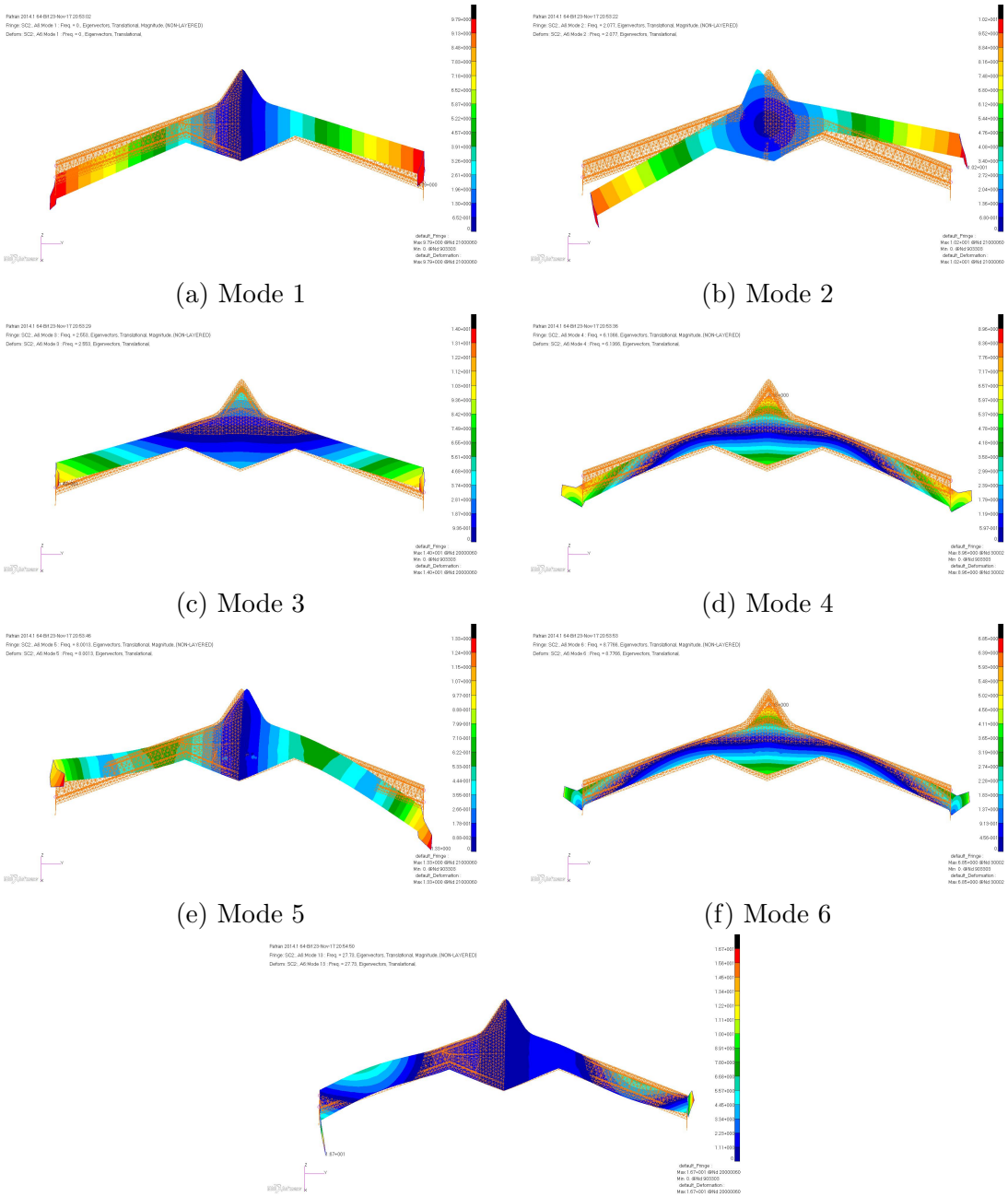

(a) Mode 1

(b) Mode 2

(c) Mode 3

(d) Mode 4

(e) Mode 5

(f) Mode 6

(g) Mode 13

Figure E.1: Mode shapes for the Seven Modes of mAEWing2 v1.1 for AoA 2° for Roll Rate 0.5 rad/sec

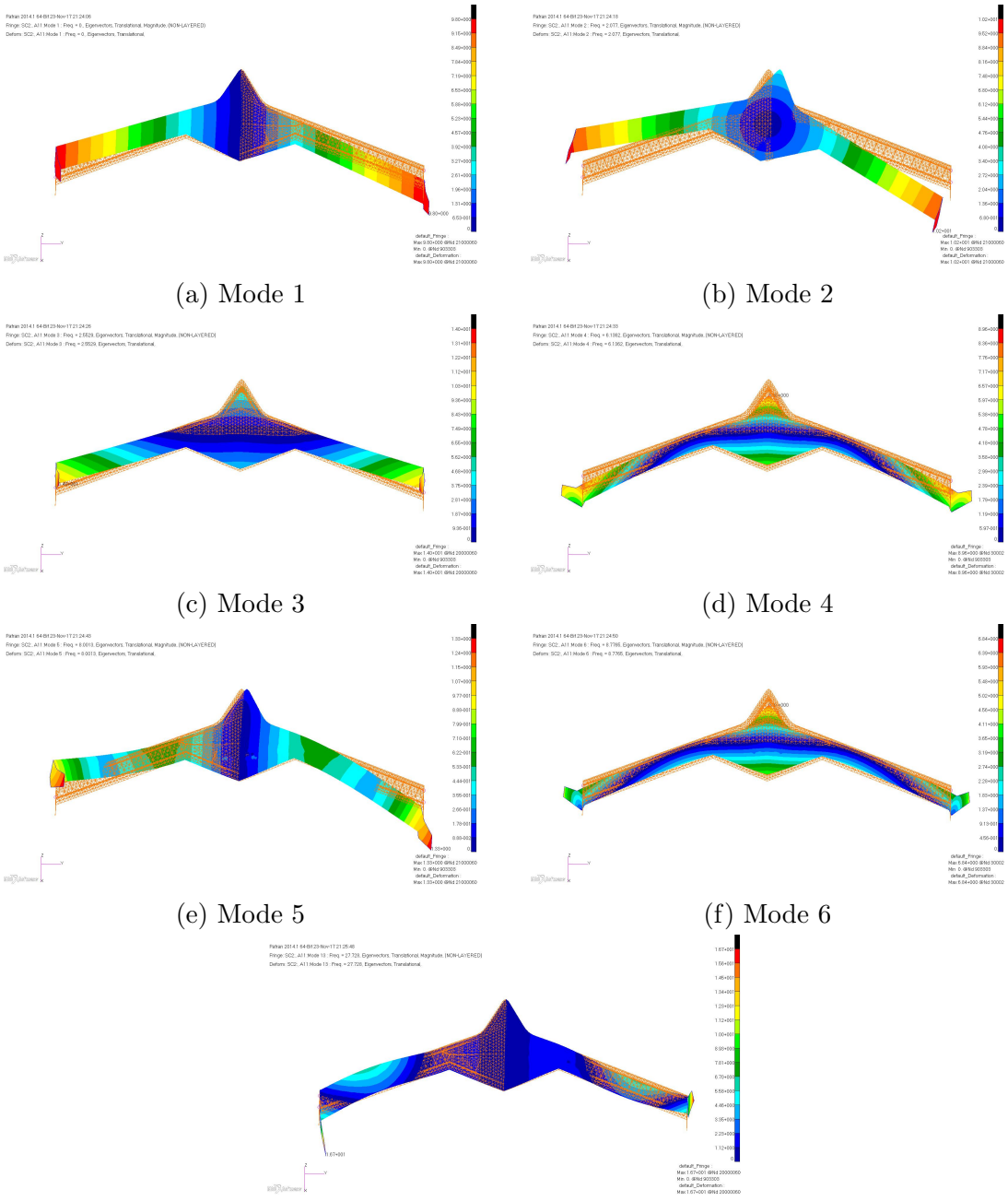

(a) Mode 1

(b) Mode 2

(c) Mode 3

(d) Mode 4

(e) Mode 5

(f) Mode 6

(g) Mode 13

Figure E.2: Mode shapes for the Seven Modes of mAEWing2 v1.1 for AoA 2° for Roll Rate 1 rad/sec

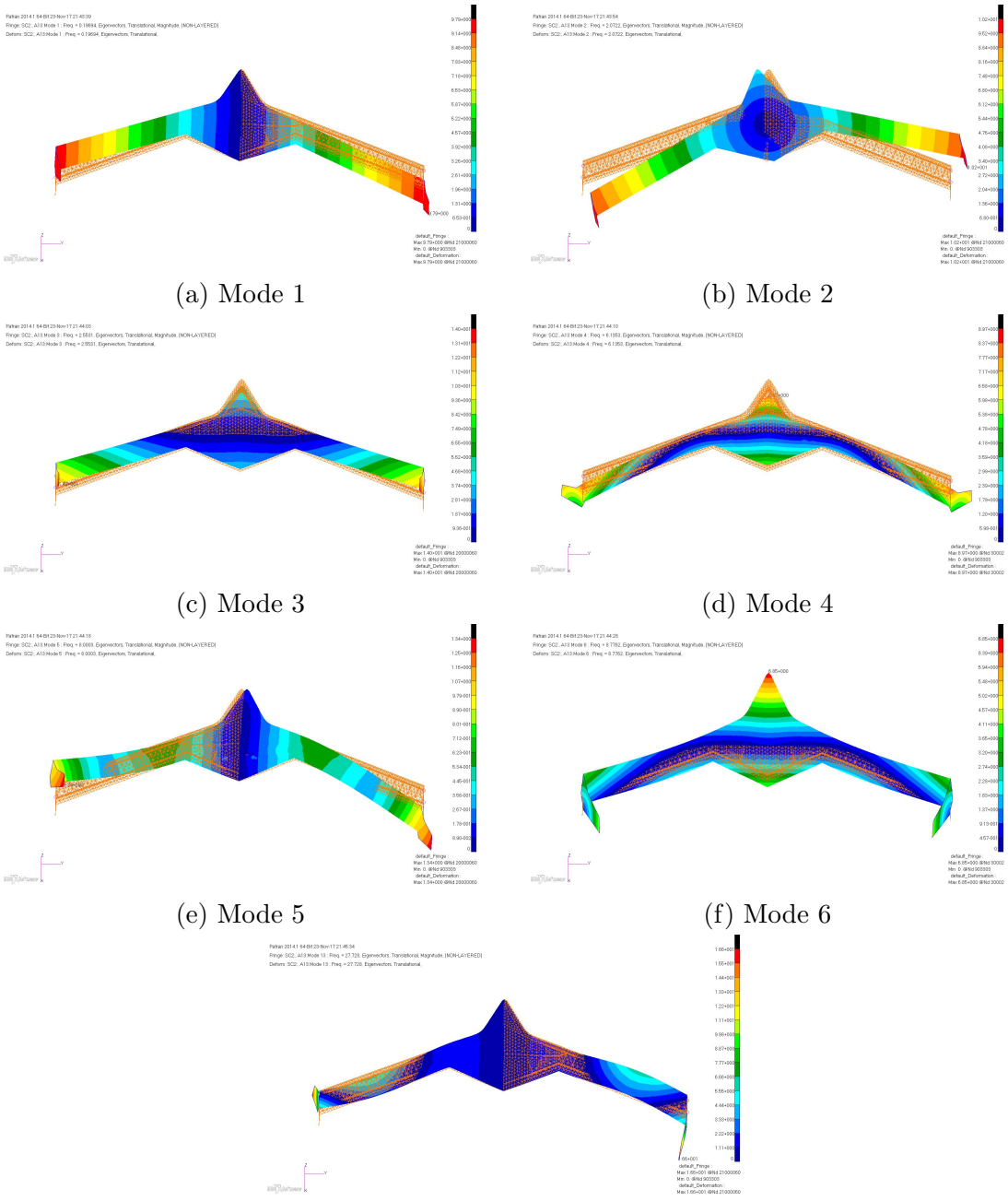

(a) Mode 1

(b) Mode 2

(c) Mode 3

(d) Mode 4

(e) Mode 5

(f) Mode 6

(g) Mode 7

Figure E.3: Mode shapes for the Seven Modes of mAEWing2 v1.1 for AoA 4° for Roll Rate 0.5 rad/sec

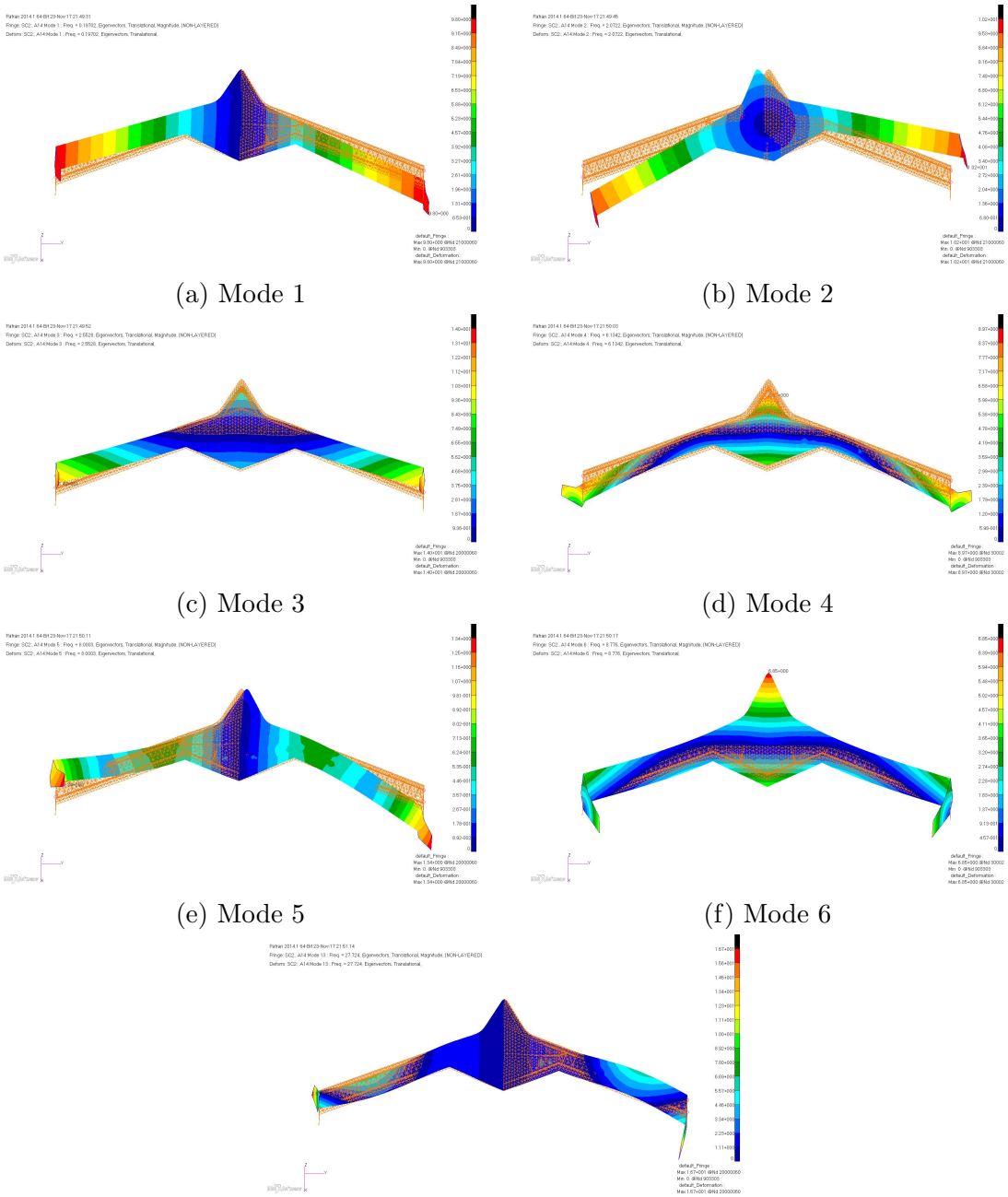

(a) Mode 1

(b) Mode 2

(c) Mode 3

(d) Mode 4

(e) Mode 5

(f) Mode 6

(g) Mode 13

Figure E.4: Mode shapes for the Seven Modes of mAEWing2 v1.1 for AoA 4° for Roll Rate 1 rad/sec

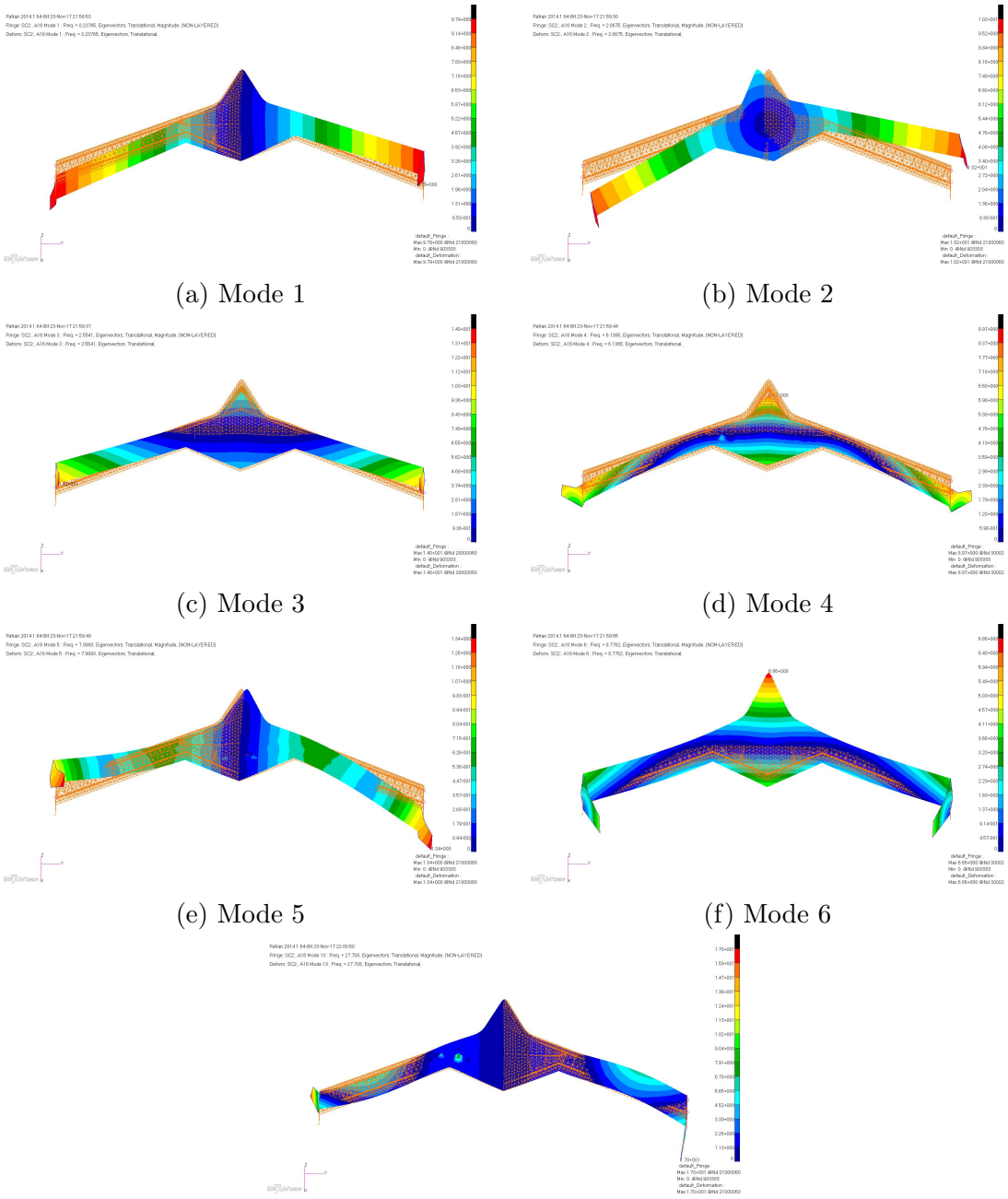

(a) Mode 1

(b) Mode 2

(c) Mode 3

(d) Mode 4

(e) Mode 5

(f) Mode 6

(g) Mode 7

Figure E.5: Mode shapes for the Seven Modes of mAEWing2 v1.1 for AoA 6° for Roll Rate 0.5 rad/sec

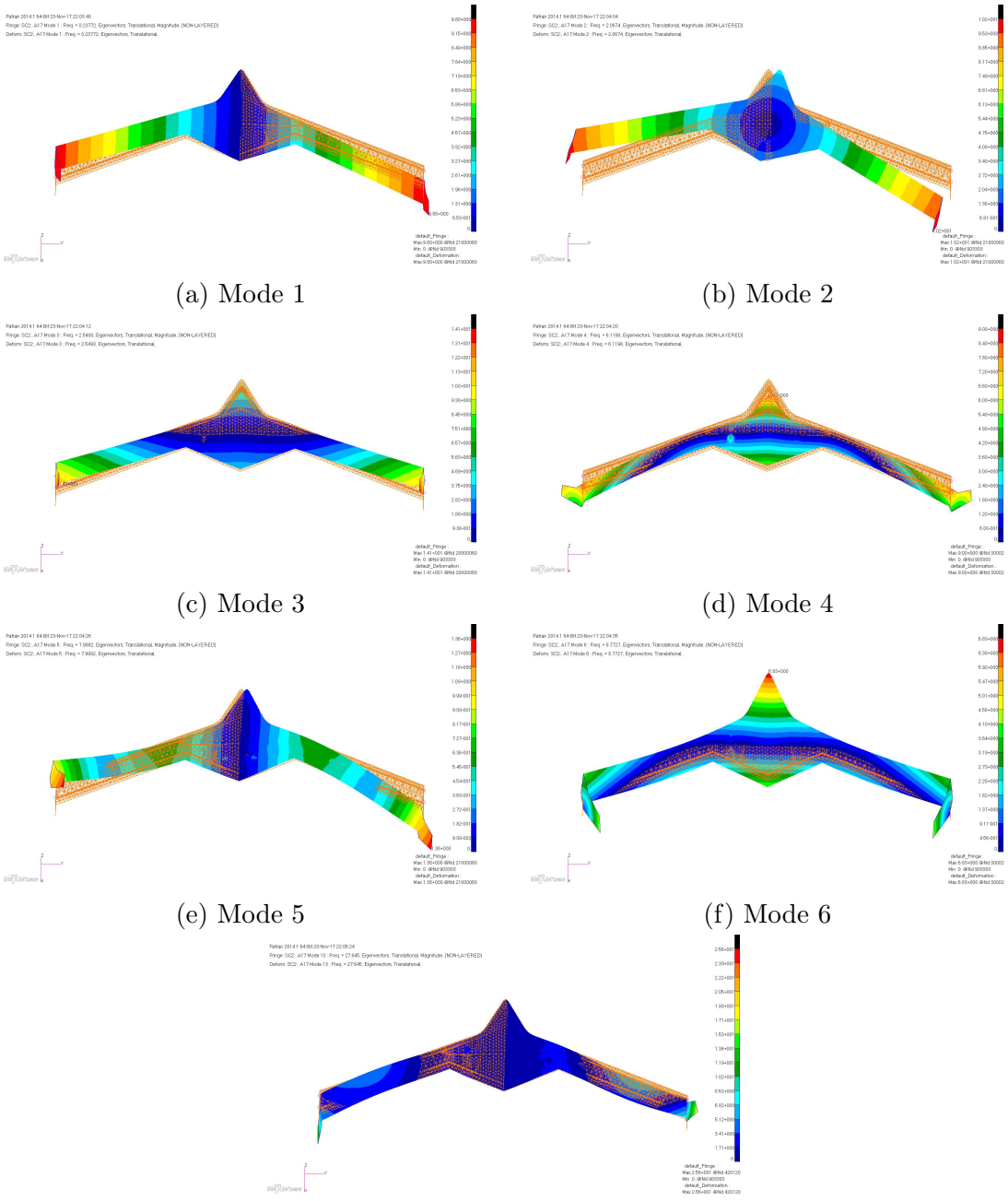

(a) Mode 1

(b) Mode 2

(c) Mode 3

(d) Mode 4

(e) Mode 5

(f) Mode 6

(g) Mode 13

Figure E.6: Mode shapes for the Seven Modes of mAEWing2 v1.1 for AoA 6° for Roll Rate 1 rad/sec

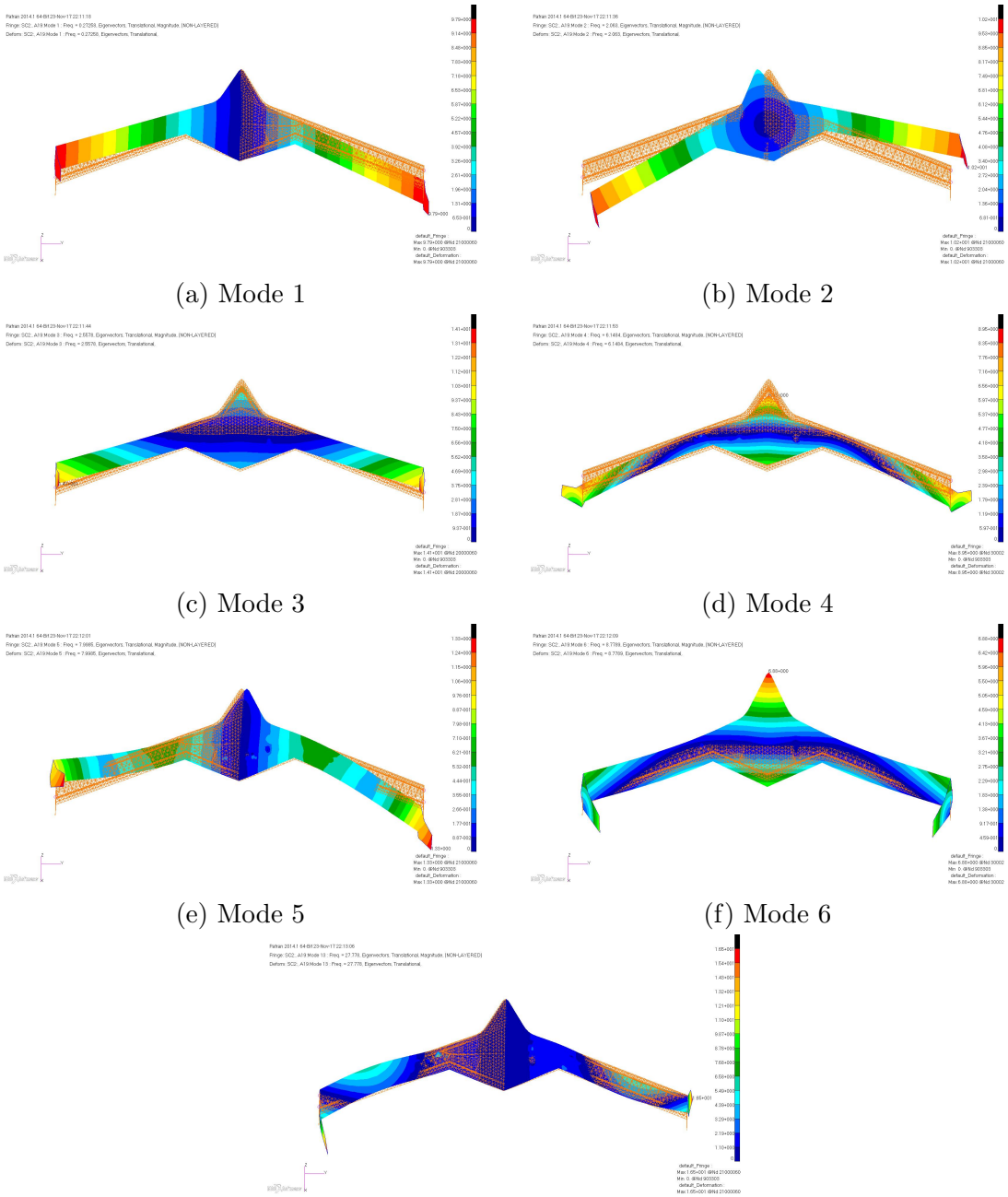

(a) Mode 1

(b) Mode 2

(c) Mode 3

(d) Mode 4

(e) Mode 5

(f) Mode 6

(g) Mode 13

Figure E.7: Mode shapes for the Modes 1 - 8 of mAEWing2 v1.1 for AoA 8° for Roll Rate 0.5 rad/sec

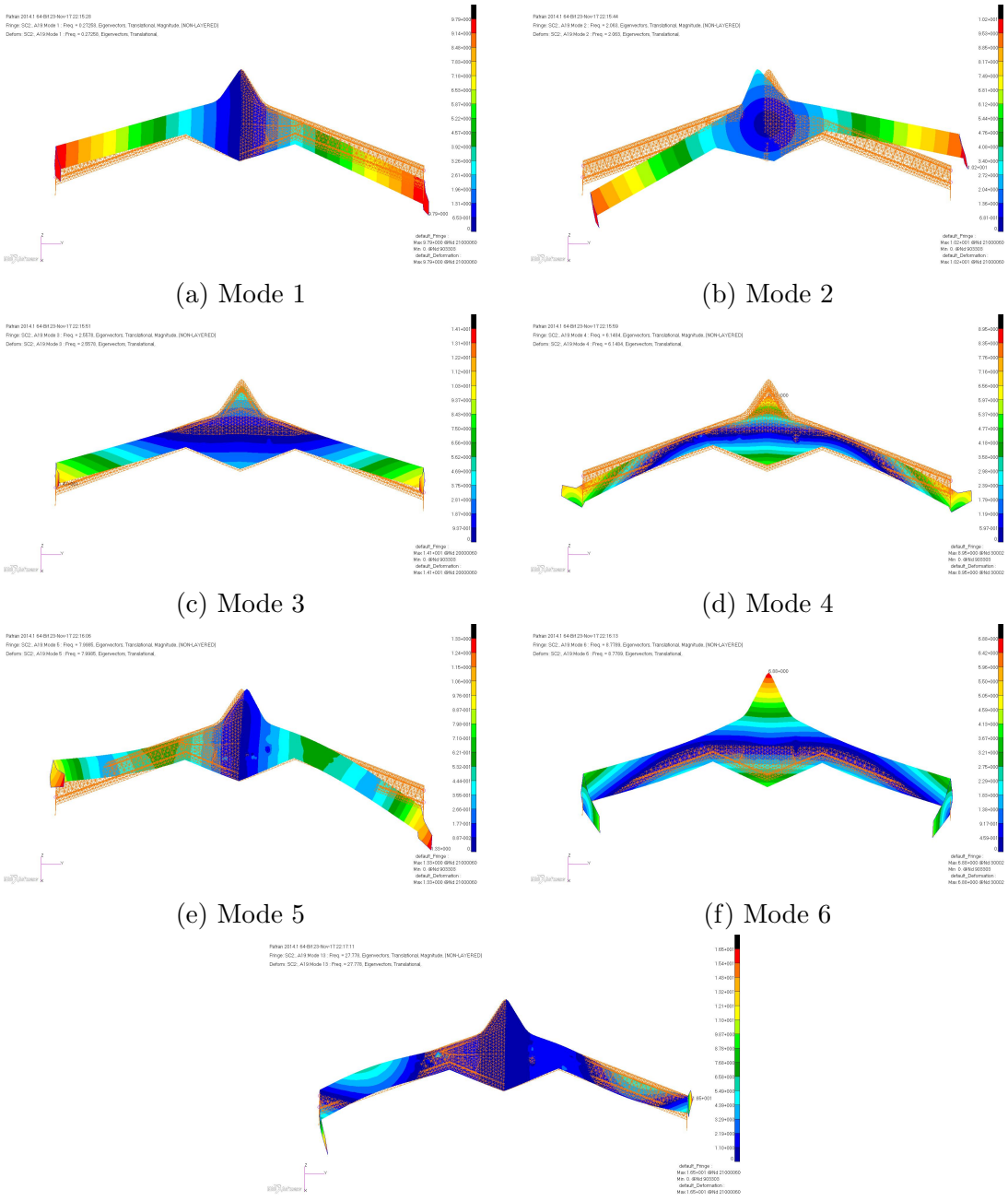

(a) Mode 1

(b) Mode 2

(c) Mode 3

(d) Mode 4

(e) Mode 5

(f) Mode 6

(g) Mode 13

Figure E.8: Mode shapes for the Seven Modes of mAEWing2 v1.1 for AoA 8° for Roll Rate 1 rad/sec